DOI 10.1007/s10958-017-3590-2
Journal of Mathematical Sciences, Vol. 227, No. 3, December, 2017

TOPOLOGICAL ATLAS OF THE KOVALEVSKAYA–YEHIA GYROSTAT

M. P. Kharlamov, P. E. Ryabov, and I. I. Kharlamova UDC 517.93

Abstract. This paper is a review of results obtained during the last fifty years on the problem of the motion of a heavy gyrostat under the conditions of S. V. Kovalevskaya.

Key words and phrases: gyrostat, Kovalevskaya conditions, Yehia integral, exact solutions, phase topology.

AMS Subject Classification: 70E17, 70G40

CONTENTS

Translated from Itogi Nauki i Tekhniki, Seriya Sovremennaya Matematika i Ee Prilozheniya. Tematicheskie Obzory, Vol. 128, Dynamical Systems, 2016.

Introduction

The report about the fact that the Kovalevskaya case of the dynamics of a rigid body can be generalized to a gyrostat was made by Yehia at Demin's seminar and Kozlov's seminar at the Moscow State University in 1985. At the same time, Yehia presented an article in *Journal de Mechanique Theoretique et Applique* which, for unknown reasons, was not published. In this regard, the official opening date of this integrable cases is 1986 when the paper [69] was published. The Russian version of this paper [54] was presented much later, in April 1986. In fact, in [69], the Kovalevskaya integral was generalized in two ways: to a gyrostat and to a double field, which simulates the action of the gravity and a constant magnetic field. Earlier, an analogue of the Kovalevskaya integral for a double field was found by Bogoyavlensky [5]; however, Yehia's generalization turned out to be crucial: the introduction of the gyrostatic moment violated the classical structure of the integral (the sum of squares) and its homogeneity: the new summand, proportional to the gyrostatic moment, has the third degree in the angular velocity, similarly to the Goryachev–Chaplygin integral. In 1987, the papers [59, 64] appear; they contain a generalization of the the Kovalevskaya integral to a gyrostat in a uniform field that simulates the gravity force, but these publications cannot be considered original.

Since, in the general case, the introduction of a double field breaks the symmetry of the problem (the area integral becomes invalid), Yehia noted the following two cases of complete integrability: a gyrostat of the Kovalevskaya type in the gravity field and a gyrostat in the double field of a specific structure that admits a singular symmetry. In the present review, we we consider the first problem. Until now, it has not been reduced to quadratures. However, it surprisingly turned out that all motions on critical manifolds of the integral mapping that play a key role in the topological analysis of the problem had been detected and integrated long before the paper [69] and the emergence of the modern approach to the study of integrable Hamiltonian systems. In 1991, scientists began a systematic study of the phase topology of the Kovalevskaya–Yehia case. The first step of the study is the examination of singularities of the integral mapping (in modern literature, it is usually called the moment mapping). These singularities are trajectories on the phase space on which the first integrals are dependent in the sense of the linear dependence of differentials. The corresponding solutions of the Euler–Poisson equations are either fixed points (from the physical standpoint, they correspond to uniform rotations of the body) or periodic trajectories of a special nature, on which the rank of the moment mapping decreases. This subset of the phase space is a critical set of the moment mapping. In [25], a system of equations that determines the critical set was obtained; considering sections of this set and taking into account obvious symmetries, one can obtain the parametric equations of the surfaces that contain critical values of the moment mapping (the bifurcation diagram of the problem). We emphasize the connection of the bifurcation diagram with Appelrot classes of the classical Kovalevskaya top (see [4]). It turned out that surfaces in the space of constants of first integrals corresponding to the four Appelrot classes in the Kovalevskaya case are transformed into two surfaces in the Yehia case at nonzero gyrostatic moment; one of these surfaces consists of two connected components. At the same time, in the paper [11], all solutions of the Euler–Poisson equations that lie in the preimage of the first surface have been reduced to quadratures.

It was stated in [12] that solutions that correspond to singular periodic solutions (i.e., consist of critical points of the moment mapping, see [25]) have been obtained and studied earlier in [36] as a part of the class of motions of a heavy gyrostat (this class is a generalization of the Bobylev–Steklov solution). Further, in [13, 26] the exhaustive study of the structure of the bifurcation set was proposed; It was noted in [13] that the equations of critical points in the preimage of the second surface coincide with the invariant relations that describe a particular solution detected in [37]. A more accurate analysis shows that to describe all critical motions in the preimage of the second bifurcation surface, it is necessary to consider the set of solutions found in [37, 51]. Thus, the whole set of critical motions of the Kovalevskaya–Yehia top is an open set described by quadratures in [36, 37, 51] without analogs of the Kovalevskaya integral that were unknown at that time.

Note that the bifurcation diagram of the moment mapping depends on a significant physical parameter (namely, the gyrostatic moment), and, therefore, the reduced systems with two degrees of freedom, obtained by the reduction of the order, depend on two parameters (the gyrostatic moment and the area constant). In [27, 28], the classification problem for bifurcation diagrams for reduced systems was solved and the separating set in the plane of these parameters was constructed. Possible variants of classification of topological invariants (Fomenko graphs), still without complete analytical classification, were considered in [14, 46].

In the present paper, we make an attempt of systematic treatment (from the modern point of view) of existing analytical and qualitative results. The idea of the work belongs to M. P. Kharlamov who devised it in 2011 as a review article for the 25th anniversary of the discovery of this integrable case. However, it was found that numerous papers treating these topics contain a lot of discrepancies, errors, and gaps in proofs. Therefore, we continued our work as an analytical research with the aim of giving an exhaustive description of the phase topology with a complete argumentation. This leads us to another series of publications supported by the Russian Foundation for Basic Research in 2011–2015. All these results are presented below. A. Yu. Savushkin and E. G. Shvedov participated in the research and development of computer visualization programs of the objects considered; they created a software package in the Mathematica system, which can be called a constructor of topological invariants.

The research has been continued for several years under the support of the Russian Foundation for Basic Research (project Nos. 10-01-00043, 10-01-97001, 13-01-97025, 14-01-00119, and 15-41-02049).

We do not include a detailed presentation of results regarding the two problems that can be considered as degenerate cases of the general case. First, this is the classic Kovalevskaya problem (with zero gyrostatic moment) and, second, the Kovalevskaya–Yehia gyrostat in the case where the constant cyclic integral (the are constant) vanishes. The rough topology of the first problem is completely described in [38–40]. In [23], the sequence of bifurcations described in [39] was combined in Fomenko graphs on isoenergetic levels and a complete list of these graphs was found (i.e., a classification of graphs in the energy-momentum plane was proposed). Marks on graphs (fine topological invariants or Fomenko–Zischang invariants) are calculated in the paper [7], which also contains a consistent presentation of the method of loop molecules in subtle topological analysis. Topological analysis of a family of systems that occur for the zero area constant (the free parameter is the value of the gyrostatic moment) is described in a series of papers [25–29]. Marks on graphs (fine topological invariants or Fomenko–Zischang invariants) have also been calculated in [20, 21], where a number of general assertions important for applications of the method of loop molecules were proved. We appeal to these problems only when necessary, if we want to generalize any facts.

1. Analytic Results

1.1. Equations and integrals. In the general case, the Euler–Poisson equations of motion of a gyrostat in the gravitational field have the form

$$\dot{\mathbf{M}} = \mathbf{M} \times \boldsymbol{\omega} + \mathbf{c} \times \boldsymbol{\alpha}, \quad \dot{\boldsymbol{\alpha}} = \boldsymbol{\alpha} \times \boldsymbol{\omega}, \tag{1.1}$$

where $\boldsymbol{\omega}$ is the angular velocity, $\boldsymbol{\alpha}$ is the unit vector of the direction of the gravitation force (it is called the vertical), and $\mathbf{c}$ is the vector connecting the immovable point O of the body and its center of mass whose magnitude is equal to the product of the weight of the system "body+rotor" by the distance between O and the center of mass. All objects are assigned to the movable axes. The vector of kinetic moment $\mathbf{M}$ is related with the angular velocity by the formula

$$\mathbf{M} = \mathbf{I}\boldsymbol{\omega} + \boldsymbol{\lambda}, \tag{1.2}$$

where $\mathbf{I}$ and $\boldsymbol{\lambda}$ are the tensor of inertia at the point O and the vector of gyrostatic moment, respectively; they are constant in the movable coordinate system. For brevity, objects that are constant in the movable coordinate system are said to be "constant in the body." The system (1.1) is obtained from the mechanical system with the configuration space $SO(3)$ (a Hamiltonian system with three degrees

of freedom) by factorization with respect to the action of the group of rotations about a fixed (in the inertial space) vertical direction; the phase space of this system is the five-dimensional manifold $P^5 = \mathbb{R}^3(\boldsymbol{\omega}) \times S^2(\boldsymbol{\alpha})$.

Here and below, we denote by $\mathbb{R}^n(u_1, \ldots, u_n)$ the space $\mathbb{R}^n$ with a fixed system of coordinate functions $u_1, \ldots, u_n$. We denote by $S^2(\boldsymbol{\alpha})$ the unit sphere in $\mathbb{R}^3(\boldsymbol{\alpha}) = \mathbb{R}^3(\alpha_1, \alpha_2, \alpha_3)$.

The definitions above imply the relation

$$\Gamma = 1 \tag{1.3}$$

called the geometric integral, where

$$\Gamma = \alpha_1^2 + \alpha_2^2 + \alpha_3^2.$$

Other general integrals are the Hamiltonian (the total energy)

$$H = \frac{1}{2}\mathbf{I}\boldsymbol{\omega} \cdot \boldsymbol{\omega} - \mathbf{c} \cdot \boldsymbol{\alpha} \tag{1.4}$$

and the cyclic integral (the area integral)

$$L = \frac{1}{2}\mathbf{M} \cdot \boldsymbol{\alpha}. \tag{1.5}$$

The coefficient 1/2 is introduced following by S. V. Kovalevskaya. The Poisson bracket of this mechanical system on the space $\{(\mathbf{M}, \boldsymbol{\alpha})\}$ can be represented by its values on pairs of the coordinate functions (see, e.g., [5]):

$$\{M_i, M_j\} = \varepsilon_{ijk} M_k, \quad \{M_i, \alpha_j\} = \varepsilon_{ijk}\alpha_k, \quad \{\alpha_i, \alpha_j\} = 0. \tag{1.6}$$

The functions Γ and L are Casimir functions of the bracket (1.6). Therefore, on each level of the area integral fixed in P^5,

$$P^4_\ell = \{L = \ell\} \subset P^5, \tag{1.7}$$

this bracket induces a symplectic structure, whereas the restriction of the dynamical system of the Euler–Poisson equations is a Hamiltonian system with two degrees of freedom. This restriction corresponds to the reduction of order in the Routh sense in the system with three degrees of freedom on the phase space $TSO(3)$. For the complete integrability, we need one more general integral independent with H and L almost everywhere on P^5. (Here the independence of functions at a point means the linear independence of their differentials.) The independence of two functions almost everywhere is sometimes called the functional independence [8]. Cases where one can indicate submanifolds in P^5 of positive codimension that are distinct from P^4_ℓ and are invariant for the system (1.1), on which this system is integrable in quadratures, are called particular cases of integrability.

The following assumptions are called the Kovalevskaya–Yehia conditions. As a movable coordinate system, we take the orthonormal trihedron $O\mathbf{e}_1\mathbf{e}_2\mathbf{e}_3$ of the principal axes of the tensor of inertia. Assume that the corresponding principal moments of inertia are in ratio 2:2:1, the center of mass lies in the equatorial plane $\mathbf{c} \cdot \mathbf{e}_3 = 0$, and the gyrostatic moment is directed along the axis of dynamical symmetry: $\boldsymbol{\lambda} = \lambda\mathbf{e}_3$. Then, using the remaining freedom of the choice of movable axes and appropriately taking measurement units, we can achieve that

$$\mathbf{c} = \{1, 0, 0\}, \quad \mathbf{I} = \operatorname{diag}\{2, 2, 1\}, \quad \lambda > 0; \tag{1.8}$$

then Eqs. (1.1) take the form

$$\begin{aligned} 2\dot\omega_1 &= \omega_2(\omega_3 - \lambda), & 2\dot\omega_2 &= -\omega_1(\omega_3 - \lambda) - \alpha_3, & \dot\omega_3 &= \alpha_2, \\ \dot\alpha_1 &= \alpha_2\omega_3 - \alpha_3\omega_2, & \dot\alpha_2 &= \alpha_3\omega_1 - \alpha_1\omega_3, & \dot\alpha_3 &= \alpha_1\omega_2 - \alpha_2\omega_1. \end{aligned} \tag{1.9}$$

This system possesses an additional Kovalevskaya–Yehia integral, which we denote by K. Thus, there exists a complete involutive set of integrals

$$\begin{gathered} H = \omega_1^2 + \omega_2^2 + \frac{1}{2}\omega_3^2 - \alpha_1, \quad L = \omega_1\alpha_1 + \omega_2\alpha_2 + \frac{1}{2}(\omega_3 + \lambda)\alpha_3, \\ K = (\omega_1^2 - \omega_2^2 + \alpha_1)^2 + (2\omega_1\omega_2 + \alpha_2)^2 + 2\lambda\left[(\omega_3 - \lambda)(\omega_1^2 + \omega_2^2) + 2\omega_1\alpha_3\right]. \end{gathered} \tag{1.10}$$

We note another important aspect of terminology, which sometimes leads to a false sense of the presence of more general problems than the problem described by the last formulas. Since the center of mass lies in the equatorial plane of the ellipsoid of inertia, each orthonormal basis in this plane is a basis of principal axes of inertia. Taking into account the arbitrariness of the choice of measurement units, we can write conditions (1.8) in the form

$$\mathbf{c} = \{c_1, c_2, 0\}, \quad \mathbf{I} = \operatorname{diag}\{2C, 2C, C\}, \quad \lambda \in \mathbb{R}.$$

In the literature, systems determined by these conditions are called "Kovalevskaya–Yehia-type systems." We emphasize that each of these systems is completely equivalent to the system with conditions (1.8), i.e., can be obtained from it by a *global nondegenerate linear* change of variables. Therefore, in our opinion, the use if this term is incorrect.

1.2. Exact solutions. Before the paper [69], the following three general cases of integrability for $\boldsymbol{\lambda} \neq 0$ were known: the generalization of the Euler case proposed by N. E. Zhukovsky ($\mathbf{c} = 0$), the generalization of the Lagrange case ($\boldsymbol{\lambda} \times \mathbf{c} = 0$), and the generalization of the Goryachev–Chaplygin proposed by L. N. Sretensky. A series of particular cases of integrability of a heavy gyrostat ($\mathbf{c} \neq 0$) was indicated in the papers of P. V. Kharlamov and E. I. Kharlamova. As was noted above, two of them are fundamentally important for the study of the system (1.9). Let us dwell on them in detail.

1.2.1. Solution of P. V. Kharlamov. The first exact solution[1] was published in [36]. Assume that in system (1.1), (1.2)

$$\boldsymbol{\omega} = \boldsymbol{\omega}_0 + r(t)\mathbf{e}, \quad r \neq \text{const}, \tag{1.11}$$

where $\boldsymbol{\omega}_0$ and $\mathbf{e}$ are constant in the body. Without loss of generality, we set $|\mathbf{e}| = 1$ and $\boldsymbol{\omega}_0 \cdot \mathbf{e} = 0$. The representation (1.11) is a most general for solutions that admit two particular integrals that are linear with respect to the angular velocity. It is well known that all solutions of the system (1.1) are defined and bounded for all t since all levels of the energy integral are compact. This implies that if a function $r(t)$ satisfies an equation of the form

$$b\,\dot{r} = \sum_{i=0}^{k} a_i\, r^i \tag{1.12}$$

with constant coefficients b and a_i, then all these coefficients are equal to zero.

Theorem 1 (P. V. Kharlamov [36])**.** *For each motion of the form* (1.11)*, the following conditions hold*:

(1) *the axis* $O\mathbf{e}$ *is a principal axis of inertia at the immovable point*;

(2) *the center of mass lies in the plane passing through the immovable point perpendicularly* $O\mathbf{e}$*, i.e.,*

$$\mathbf{c} \cdot \mathbf{e} = 0;$$

(3) *the total kinetic moment of the system is coplanar to the vectors* $\mathbf{c}$ *and* $\mathbf{e}$.

Proof. We multiply the first vector equation (1.1) (the Euler equation) scalarly by a nonzero constant vector $\mathbf{c}$. Then we obtain an equation of the form (1.12) in which $k = 2$ and $b = \mathbf{c} \cdot \mathbf{I}\mathbf{e}$, $a_2 = \mathbf{c} \cdot (\mathbf{I}\mathbf{e} \times \mathbf{e})$. Thus,

$$\mathbf{c} \cdot \mathbf{I}\mathbf{e} = 0, \quad \mathbf{c} \cdot (\mathbf{I}\mathbf{e} \times \mathbf{e}) = 0. \tag{1.13}$$

We write the following geometric identity:

$$\boldsymbol{\alpha} = \frac{1}{\mathbf{c}^2}[(\mathbf{c} \cdot \boldsymbol{\alpha})\mathbf{c} + (\mathbf{c} \times \boldsymbol{\alpha}) \times \mathbf{c}]. \tag{1.14}$$

We denote by h the constant of the integral (1.4); then from (1.1) and (1.4) we obtain the expressions

$$\mathbf{c} \times \boldsymbol{\alpha} = \mathbf{I}\dot{\boldsymbol{\omega}} - (\mathbf{I}\boldsymbol{\omega} + \boldsymbol{\lambda}) \times \boldsymbol{\omega}, \quad \mathbf{c} \cdot \boldsymbol{\alpha} = h - \frac{1}{2}\mathbf{I}\boldsymbol{\omega} \cdot \boldsymbol{\omega}.$$

[1] An exact solution is a general or particular case of integrability explicitly reduced to quadratures.

Substitute them on the right-hand side of (1.14); then the relation $L = \ell$ and the area integral (1.5) yield an equation of the form (1.12) in which $k = 3$ and

$$b = (\mathbf{I}\boldsymbol{\omega} + \boldsymbol{\lambda}) \cdot (\mathbf{I}\mathbf{e} \times \mathbf{c}), \quad a_3 = 2(\mathbf{c} \cdot \mathbf{e})(\mathbf{I}\mathbf{e} \cdot \mathbf{I}\mathbf{e}) - (\mathbf{c} \cdot \mathbf{I}\mathbf{e})(\mathbf{I}\mathbf{e} \times \mathbf{e}).$$

Therefore, taking into account (1.13), we have

$$\mathbf{c} \cdot \mathbf{e} = 0, \quad \mathbf{M} \cdot (\mathbf{I}\mathbf{e} \times \mathbf{c}) = 0. \tag{1.15}$$

For nonzero $\mathbf{c}$, the first of these relations together with (1.13) imply $\mathbf{I}\mathbf{e} \times \mathbf{e} = 0$; therefore, the axis $O\mathbf{e}$ is a principal axis of the tensor $\mathbf{I}$. Then the relation (1.15) express the remaining assertions of the theorem. □

Note that we do not impose any requirements for the vector $\boldsymbol{\omega}_0$, which is constant in the body. In particular, for $\boldsymbol{\omega}_0 = 0$ we see that the theorem is valid for all pendulum motions of a gyrostat in the gravitational field.

In accordance with the above, we introduce a movable coordinate system so that $\mathbf{e}_3 = \mathbf{e}$ and the following notation for the components of the constant vectors and the tensor of inertia:

$$\boldsymbol{\omega}_0 = p\,\mathbf{e}_1 + q\,\mathbf{e}_2, \quad \boldsymbol{\lambda} = \lambda_1\mathbf{e}_1 + \lambda_2\mathbf{e}_2 + \lambda_3\mathbf{e}_3, \quad \mathbf{I} = \operatorname{diag}\{A, B, C\}.$$

Let $\mathbf{M}_0$ be the projection of the vector $\mathbf{M}$ on the plane $O\mathbf{e}_1\mathbf{e}_2$. By Theorem 1,

$$\mathbf{M}_0 = m\mathbf{c}, \quad m = \text{const}\,. \tag{1.16}$$

The projection of the Euler equation on the plane $O\mathbf{e}_1\mathbf{e}_2$ takes the form

$$r\,(m\mathbf{c} - C\boldsymbol{\omega}_0) + \alpha_3\mathbf{c} - \lambda_3\boldsymbol{\omega}_0 = 0.$$

Since, by the assumption, $\mathbf{c} \neq 0$ and $r \neq \text{const}$, we see that

$$\boldsymbol{\omega}_0 = \varepsilon\mathbf{c}, \tag{1.17}$$

$$(m - \varepsilon C)r + \alpha_3 - \lambda_3\varepsilon = 0. \tag{1.18}$$

From (1.16) and (1.17) we obtain $\mathbf{M}_0 \times \boldsymbol{\omega}_0 = 0$; therefore, the projection of the Euler equation on the axis $O\mathbf{e}_3$ has the form

$$C\dot{r} + c_2\alpha_1 - c_1\alpha_2 = 0. \tag{1.19}$$

At the same time, differentiating (1.18) and taking into account (1.17), we obtain

$$(m - \varepsilon C)\dot{r} + \varepsilon(c_2\alpha_1 - c_1\alpha_2) = 0. \tag{1.20}$$

The compatibility condition for (1.19) and (1.20) yields

$$m = 2C\varepsilon. \tag{1.21}$$

Finally, taking arbitrarily the constants A, B, C, c_1, c_2, λ_3, ε, and h, we obtain a solution in the form

$$\begin{aligned}
&\omega_1 = \varepsilon c_1, \quad \omega_2 = \varepsilon c_2, \quad \omega_3 = r,\\
&\alpha_1 = \frac{1}{c_1^2 + c_2^2}\left[\left(\frac{1}{2}Cr^2 + h_*\right)c_1 - C\sqrt{R(r)}c_2\right],\\
&\alpha_2 = \frac{1}{c_1^2 + c_2^2}\left[\left(\frac{1}{2}Cr^2 + h_*\right)c_2 + C\sqrt{R(r)}c_1\right],\\
&\alpha_3 = \varepsilon(\lambda_3 - Cr),
\end{aligned} \tag{1.22}$$

where the following notation is used:

$$h_* = \frac{\varepsilon^2}{2}(Ac_1^2 + Bc_2^2) - h, \quad R(r) = \frac{1}{C}\left\{\left(c_1^2 + c_2^2\right)\left[1 - \varepsilon^2(\lambda_3 - Cr)^2\right] - \left(\frac{1}{2}Cr^2 + h_*\right)^2\right\}.$$

The two components of the gyrostatic moment, by (1.16) and (1.21), are defined by the relations

$$\lambda_1 = (2C - A)\varepsilon c_1, \quad \lambda_2 = (2C - B)\varepsilon c_2, \tag{1.23}$$

and the evolution of the variable r, which has been chosen as the principal variable, is described by the equation

$$\dot r = \sqrt{R(r)}. \tag{1.24}$$

Due to the arbitrariness of the choice of the measurement units, only three physical parameters among A, B, C, c_1, c_2, and λ_3 are substantial. The parameters ε and h related to the choice of an initial point are arbitrary. Therefore, formulas (1.22) and (1.24), for fixed physical parameters, describe a three-dimensional invariant submanifold of the phase space stratified into periodic trajectories (with possible bifurcations). This solution generalizes the classical Bobylev–Steklov case.

Now we consider a gyrostat under the Kovalevskaya conditions (i.e., $A = B = 2C$ and the center of mass lies in the equatorial plane) and write the solutions (1.22), where the axis of dynamical symmetry is the axis $O\mathbf{e}$ (which is a principal axis by Theorem 1). From (1.23) we see that $\lambda_1 = \lambda_2 = 0$. An arbitrary axis lying in the equatorial plane is principal; therefore, without loss of generality, we assume that $c_2 = 0$ and hence $\omega_2 \equiv 0$. We choose measurement units so that $C = 1$ and $c_1 = 1$; as an independent parameter, we take, instead of ε, the first component of the angular velocity p. Omitting the index of the sole nonzero component λ_3, from (1.22) we obtain the parametric equations of the three-dimensional manifold, which will be denoted by $\mathcal{M}_1$:

$$\mathcal{M}_1 : \begin{cases} \omega_1 = p, \quad \omega_2 = 0, \quad \omega_3 = r, \\ \alpha_1 = \dfrac{1}{2}r^2 + p^2 - h, \quad \alpha_2 = \sqrt{R(r)}, \quad \alpha_3 = -p(r-\lambda). \end{cases} \tag{1.25}$$

Here

$$R = -\frac{1}{4}r^4 - (2p^2 - h)r^2 + 2\lambda p^2 r + 1 - (p^2 - h)^2 - p^2\lambda^2. \tag{1.26}$$

The dynamics on $\mathcal{M}_1$ is governed by Eq. (1.24), which determines periodic solutions and their possible bifurcations if immovable points appear. The exact solution (1.24), (1.25), (1.26) generalizes the family of remarkable motions of the fourth Appelrot class of the classical Kovalevskaya top to the case of a gyrostat. Note that generalizations of the fourth Appelrot class to the cases of a top and a gyrostat in double potential fields (including fields with gyroscopic terms, see [33]) were obtained in [41, 61, 62].

1.2.2. Solution of P. V. Kharlamov and E. I. Kharlamova. Another exact solution for a gyrostat in the gravitational field was constructed in [37, 51]. The initial assumptions are as follows: first, the center of mass and the gyrostatic moment belong to one of the principal planes of the tensor of inertia and second, there exist particular algebraic integrals that guarantee the possibility of expression of all phase variables through one additional variable. Under the conditions (1.8), the most general form of the corresponding solutions was presented in [37], where they was united into a single family. We write it in an appropriate notation, as was proposed in [48]. We fix the constant ℓ of the area integral; let s be a nonzero constant. We set

$$\varkappa^2 = \ell^2 + \lambda^2 s^2, \quad \rho^2 = 1 - \frac{2\varkappa^2}{s}, \quad \mathcal{G}^2 = \frac{1}{2}\left[\left(X + \frac{\lambda}{\varkappa}\right)^2 + \left(\rho Y + \frac{\ell}{s\varkappa}\right)^2 - 1\right],$$
$$(X, Y) = \begin{cases} (\cos\sigma, \sin\sigma), & \rho^2 \geq 0, \\ (\cosh\sigma, \mathrm{i}\sinh\sigma), & \rho^2 < 0. \end{cases} \tag{1.27}$$

Here i is the imaginary unit and σ is an auxiliary variable. The invariant manifolds $\mathcal{M}_2$ and $\mathcal{M}_3$ are defined, respectively, for $s < 0$ and $s > 0$ by the following system of parametric equations:

$$\mathcal{M}_{2,3} : \begin{cases} \omega_1 = -\dfrac{\ell}{s} - \varkappa\rho Y, & \omega_2 = -\rho\sqrt{s}\,\mathcal{G}, & \omega_3 = \lambda + 2\varkappa X, \\ \alpha_1 = \dfrac{\lambda s X + \ell\rho Y}{\varkappa} - 2\varkappa^2 Y^2, & \alpha_2 = -2\varkappa Y\sqrt{s}\,\mathcal{G}, & \alpha_3 = \dfrac{\ell X - \lambda s\rho Y}{\varkappa}. \end{cases} \tag{1.28}$$

The dynamics induced by the system (1.9) is governed by the equation

$$\dot\sigma^2 = \operatorname{sgn}(\rho^2)\, s\, \mathcal{G}^2. \tag{1.29}$$

Since ℓ and s are free parameters, for given physical parameters of the problem we have a three-dimensional invariant submanifold in the phase space stratified into periodic trajectories (as in the first solutions, bifurcations of periodic trajectories can occur on this manifold).

We can immediately verify that for $\lambda = 0$, on the family of trajectories (1.28), (1.29), there exists the following relation between the integral constants:

$$(h - 2\ell^2)^2 - k = 0,$$

which corresponds to remarkable motions of the 2nd ($s < 0$) and 3rd ($s > 0$) Appelrot classes and the constant s is a multiple root of the polynomial in the Kovalevskaya differential equations. There exist corresponding generalizations for double fields (see [41, 61, 62]), but in the case $\lambda \neq 0$ they are not reduced to quadratures.

1.2.3. Solution of I. N. Gashenenko. Attempts at an explicit separation of variables in the reduced system on P^4_ℓ for the Kovalevskaya–Yehia gyrostat were unsuccessful even in the case $\ell = 0$. In [9, 52, 65], changes of variables on P^4_0 that lead to equations of Abel–Jacobi type with complex variables were proposed. Attempts at the reification of these equations falied, so they are not suitable for the study of the system (in particular, for the search for conditions of the existence of real solutions; C. Jacobi supposed that this is the main goal of the transition to equations with radicals; see [53]).

I. N. Gashenenko [11, 12] proposed the reduction to quadratures of solutions of the system (1.9) on a four-dimensional submanifold in P^5 distinct from the level of the area integral. The family of solutions obtained is completely classified by the type of motions (periodic, asymptotic to periodic, or two-periodic). We recall the main results of the papers [11, 12]. Consider the relations between the constants h, ℓ, and k of the first integrals (1.10) generated by the family of solutions (1.25):

$$\ell = -\frac{1}{2}p(2h - \lambda^2) + p^3, \quad k = 1 - p^2(2h - \lambda^2) + 3p^4. \tag{1.30}$$

The complete preimage of the set of such values (p and h are arbitrary) in P^5 is the stratified manifold $G^4 = N^4 \cup \mathcal{M}_1$, where $\dim N^4 = 4$ and $\partial N^4 = \mathcal{M}_1$. We pass on N^4 from $(\boldsymbol{\omega}, \boldsymbol{\alpha})$ to the new coordinates $(x, y, z, \alpha, \beta, \gamma)$ by setting (see [11])

$$\begin{aligned}
&\omega_1 = p - xM^{-1}, && \omega_2 = -yM^{-1},\\
&\omega_3 = 2z + \lambda + 4x\gamma M^{-1}, && M = x^2 + y^2 \neq 0,\\
&\alpha_1 = -2\alpha + 4(x^2 - y^2)\gamma^2 M^{-2} + 2px(1 - 2px)M^{-1} + 4\lambda x\gamma M^{-1},\\
&\alpha_2 = -2\beta + 8xy\gamma^2 M^{-2} + 2py(1 - 2px)M^{-1} + 4\lambda y\gamma M^{-1},\\
&\alpha_3 = 2(1 - 2px)\gamma M^{-1} - 2pz.
\end{aligned} \tag{1.31}$$

By (1.30), from the set of equations of motion and first integrals, one can extract the following closed subsystem:

$$\begin{gathered}
\dot z = \sqrt{f(z)}, \quad \dot\alpha = \left(z - \frac{1}{2}\lambda\right)^2 + \frac{1}{2}(p^2 - h), \quad \beta = \sqrt{f(z)},\\
f(z) = \frac{1}{4} - p^2 z^2 - \left[\left(z - \frac{1}{2}\lambda\right)^2 + \frac{1}{2}(p^2 - h)\right]^2;
\end{gathered} \tag{1.32}$$

its solution $z(t)$, $\alpha(t)$, $\beta(t)$ can be expressed through elliptic functions of time. Introducing the notation

$$L_1 = \frac{1}{16}(2h - 2p^2 - \lambda^2), \quad L_2 = \frac{1}{4}(2h - 6p^2 - \lambda^2), \quad L_3 = 4(p^2 + \lambda^2)L_1 - \frac{1}{4} \tag{1.33}$$

for independent parameters, the function Φ, and the auxiliary variable η by the formulas

$$\Phi(z) = (z-\lambda)^2 - L_2, \quad \eta = y\,\Phi^{-1/2}(z), \tag{1.34}$$

we obtain an elliptic quadrature for η and finite expressions for other variables:

$$\begin{gathered}\int \frac{d\eta}{\sqrt{L_1 - L_2 L_3 \eta^2}} + \int \frac{dz}{\Phi(z)\sqrt{f(z)}} = \text{const},\\ y = \eta\Phi^{1/2}(z), \quad x = -\left(\frac{1}{2}pL_2^{-1} + \eta\beta\Phi^{-1/2}(z) + \dot\eta\Phi^{1/2}(z)(z-\lambda)L_2^{-1}\right),\\ \gamma = \frac{1}{2}pzL_2^{-1} + \lambda\eta\beta\Phi^{-12}(z) + \dot\eta\Phi^{1/2}(z)(\alpha+p^2)L_2^{-1}.\end{gathered} \tag{1.35}$$

The classification of motions in the solution obtained is performed with respect to the parameters (1.33). One can indicate the following cases (see [11]):

$$\begin{aligned}&\text{(I)} && L_1>0,\ L_2>0,\ L_3>0;\\ &\text{(II)} && L_1>0,\ L_2<0,\ L_3<0;\\ &\text{(III)} && L_1>0,\ L_2<0,\ L_3>0;\\ &\text{(IV)} && L_1>0,\ L_2>0,\ L_3<0;\\ &\text{(V)} && L_1<0;\\ &\text{(VI)} && L_1=0;\\ &\text{(VII)} && L_2=0;\\ &\text{(VIII)} && L_3=0.\end{aligned} \tag{1.36}$$

As was noted in [11], in the cases I and II, two-periodic motion are possible; in the cases III, IV, VII, and VIII, motions distinct from (1.25) asymptotically tend to trajectories on $\mathcal{M}_1$; in the cases V and VI, motions distinct from (1.25) are impossible. Below, we discuss these classes and find the relationship between them and types of singular points of the moment mapping.

2. Critical Set of Moment Mapping

2.1. Lax representation. Although in [69] the Kovalevskaya integral was generalized to the case of a double field, this problem was not treated as an integrable problem since double fields prevents the existence of the area integral. However, later in [24], Reiman and Semenov-Tyan-Shansky obtained a Lax representation with a spectral parameter for a gyrostat of the Kovalevskaya type in a double field, which implied the existence of another first integral, which turns into the square of the area integral if the second field disappears. We present the corresponding Lax representation and resulting consequences under the Kovalevskay–Yehia conditions.

Following S. V. Kovalevskaya, we introduce the complex variables ($\mathrm{i}^2 = -1$):

$$\begin{aligned} x_1 &= \alpha_1 + \mathrm{i}\,\alpha_2, & x_2 &= \alpha_1 - \mathrm{i}\,\alpha_2,\\ w_1 &= \omega_1 + \mathrm{i}\,\omega_2, & w_2 &= \omega_1 - \mathrm{i}\,\omega_2,\\ z &= \alpha_3, & w_3 &= \omega_3\end{aligned} \tag{2.1}$$

(the last row is accepted for convenience and uniformity). We denote the differentiation $d/d(\mathrm{i}\,t)$ by the prime and write the system (1.9) as follows:

$$\begin{aligned} 2w_1' &= -(w_1w_3 + z), & 2w_2' &= w_2w_3 + z, & 2w_3' &= x_1 - x_2,\\ x_1' &= -x_1w_3 + zw_1, & x_2' &= x_2w_3 - zw_2, & 2z' &= x_1w_2 - x_2w_1.\end{aligned} \tag{2.2}$$

The Lax representation for this system, as a particular case of results obtained in [24], has the form

$$B' = BA - AB, \tag{2.3}$$

where

$$B=\begin{Vmatrix} 2\lambda & \frac{x_2}{\kappa} & -2w_1 & \frac{z}{\kappa} \\ -\frac{x_1}{\kappa} & -2\lambda & -\frac{z}{\kappa} & 2w_1 \\ -2w_1 & \frac{z}{\kappa} & -2w_3 & -\frac{x_1}{\kappa}-4\kappa \\ -\frac{z}{\kappa} & 2w_2 & \frac{x_2}{\kappa}+4\kappa & 2w_3 \end{Vmatrix}, \quad A=\begin{Vmatrix} -\frac{w_3}{2} & 0 & \frac{w_2}{2} & 0 \\ 0 & \frac{w_3}{2} & 0 & -\frac{w_1}{2} \\ \frac{w_1}{2} & 0 & \frac{w_2}{2} & \kappa \\ 0 & -\frac{w_2}{2} & -\kappa & -\frac{w_3}{2} \end{Vmatrix}, \tag{2.4}$$

κ is the spectral parameter, and the derivative in (2.3) is taken with respect to (2.2). The equation for eigenvalues μ of the matrix B defines an algebraic curve associated with this representation [55]. We set $s=2\kappa^2$. The equation of the algebraic curve becomes

$$\mu^4-4\left[\frac{1}{s}-(2h+\lambda^2)+2s\right]\mu^2+4\left[\frac{1}{s^2}+\frac{2}{s}(4\ell^2-2h-\lambda^2)+(4k+8\lambda^2h)-8\lambda^2s\right]=0. \tag{2.5}$$

We introduce the integral mapping (the moment mapping) generated by the integrals (1.10):

$$J=L\times H\times K: P^5\to\mathbb{R}^3. \tag{2.6}$$

The set Σ of its critical values is called the bifurcation diagram; it is a classifying set in the study of the phase topology of the system. Research shows, in the presence of a Lax representation, the bifurcation diagram of the mapping J is contained in the set of values (ℓ,h,k) for which the curve (2.5) ceases to be nonsingular, i.e., either becomes reducible (the left-hand side of Eq. (2.5) splits into the product of rational expression) or has a singular point in the standard sense. Thus, we can predict the result of the following assertion. However, for a rigorous proof, one needs to perform direct calculations on the set of critical points of J. This set will be stated below.

Theorem 2. *The bifurcation diagram of the integral mapping $L\times H\times K$ is contained in the union of the following (intersecting) surfaces in $\mathbb{R}^3(\ell,h,k)$:*

$$\Pi_1:\quad \begin{cases} k=1+\left(h-\dfrac{\lambda^2}{2}\right)^2-4\left(h-\dfrac{\lambda^2}{2}\right)s+3s^2, \\ \ell^2=\left(h-\dfrac{\lambda^2}{2}-s\right)s^2, \quad s\in\mathbb{R}; \end{cases} \tag{2.7}$$

$$\Pi_{2,3}:\quad \begin{cases} k=-2\lambda^2\left(h-\dfrac{\lambda^2}{2}-2s\right)-\lambda^4+\dfrac{1}{4s^2}, \\ \ell^2=\dfrac{1}{2}\left(h+\dfrac{\lambda^2}{2}\right)-\lambda^2s^2-\dfrac{1}{4s}, \quad s\in\mathbb{R}\backslash\{0\}. \end{cases} \tag{2.8}$$

Here $s<0$ for Π_2 and $s>0$ for Π_3.

Remark 1. In the form presented above, the equations of bifurcation diagram have been obtained from (2.5). As independent parameters on the surfaces, the parameters h and s were chosen. Since in this case h and ℓ^2 are linearly dependent, we can express k and h through s and ℓ. There is no problems on the surfaces Π_2 and Π_3. On Π_1, due to the relation $s=0$, an artificial singularity appears. From the geometric point of view, this corresponds to the self-intersection line of the surface Π_1, which is not a singularity in the parametric representation (2.7). However, for the study of bifurcation diagrams of reduced systems on P^4_ℓ, we need their expressions through s and ℓ, which can be written in the form

$$\Pi_1=\left\{h=\frac{\ell^2}{s^2}+\frac{\lambda^2}{2}+s,\ k=\frac{\ell^4}{s^4}-\frac{2\ell^2}{s}+1,\ \ell s\neq 0\right\} \cup\left\{k=1,\ \ell=0\right\}\cup\left\{k=1+\left(h-\frac{\lambda^2}{2}\right)^2,\ \ell=0\right\}. \tag{2.9}$$

2.2. Description of the critical set. In [25], the set of critical points of the moment mapping was first described and parametric equations of singular surfaces Π_j were also obtained. A more detailed presentation is contained in [26]. In [13], similar results were independently obtained; it was also proved that the surfaces Π_j naturally appear as discriminant sets of some polynomials. The equations of the surface Π_1 follow from the results of [11], but in this paper, the corresponding conditions for the constants of integrals were not related to the notion of critical points.

The set $\mathcal{C}$ of critical points of the moment mapping is stratified by the rank of this mapping. Since the integral L is regular everywhere and stratifies P^5 into smooth symplectic leaves (1.7), we naturally use the following terms.

Definition 1. The rank of a point $x \in P^4_\ell \subset P^5$ is the rank at this point of the restriction mapping

$$\mathcal{J}_\ell = H \times K|_{P^4_\ell} : P^4_\ell \to \mathbb{R}^2. \tag{2.10}$$

Hence, the rank of a point is one less than the rank at this point of the mapping (2.6). Therefore, we have

$$\mathcal{C} = \mathcal{C}^0 \cup \mathcal{C}^1, \quad \mathcal{C}^i = \{x \in P^4_\ell \mid \operatorname{rank} \mathcal{J}_\ell(x) = i\}. \tag{2.11}$$

The bifurcation diagram defined above is the J-image of the set $\mathcal{C}$.

The presence of two singular surface (2.7) and (2.8) generates another partition of the critical set.

Theorem 3 ([13, 25, 26])**.** *The set of critical points of the moment mapping has the form*

$$\mathcal{C} = \mathcal{M}_1 \cup \mathcal{M}_2 \cup \mathcal{M}_3, \tag{2.12}$$

where $\mathcal{M}_1$, $\mathcal{M}_2$, and $\mathcal{M}_3$ are defined by Eqs. (1.25) *and* (1.28)*. In this case, each set $\mathcal{M}_j$ is the closure of the corresponding set $J^{-1}(\Pi_j) \cap \mathcal{C}^1$ $(j = 1, 2, 3)$.*

Equality (2.12) follows from the analytic description of the set $\mathcal{C}$ obtained in [25, 26] by examining the minors of the Jacobi matrix

$$\frac{\partial(L, H, K, \Gamma)}{\partial(\boldsymbol{\omega}, \boldsymbol{\alpha})}.$$

An elegant proof based on the reduction of integral equations to a symmetric system of six complex coordinates on $\mathbb{R}^6(\boldsymbol{\omega}, \boldsymbol{\alpha})$ can be found in [13]. The fact that the image of each of the manifolds $\mathcal{M}_j$ is contained in the corresponding surface Π_j can be immediately verified. For $\mathcal{M}_1$, we must take

$$s = h - \frac{\lambda^2}{2} - p^2 \tag{2.13}$$

in the formulas (1.30).

Definition 2. The manifolds $\mathcal{M}_1$, $\mathcal{M}_2$, and $\mathcal{M}_3$ with induced dynamics are called the first, second, and third critical subsystems in the Kovalevskaya–Yehia case, respectively.

Remark 2. We use the term "manifold" for the set $\mathcal{M}_j$ meaning their invariant properties ("invariant manifolds"). In fact, it may occur that they are smooth manifolds only almost everywhere.

The representation of $\mathcal{C}$ in the form of the set of solutions of the system of invariant relations can be obtained as a particular case of the corresponding result from [41].

Theorem 4. *The set of critical points of the integral mapping J consists of the following subsets in P^5:*

(1) *the set determined by the system*

$$R_1 = 0, \quad R_2 = 0, \tag{2.14}$$

where

$$R_1 = \omega_2, \quad R_2 = (\omega_3 - \lambda)\omega_1 + \alpha_3;$$

(2) *the set determined by the system*

$$F_1 = 0, \quad F_2 = 0, \tag{2.15}$$

where

$$\begin{aligned}
F_1 &= \Big[\alpha_2\omega_2 + \omega_1\big(\omega_1^2+\omega_2^2+\alpha_1\big)\Big]\Big[\big(\alpha_1^2+\alpha_2^2\big)\omega_3 - 2\alpha_3\big(\alpha_1\omega_1+\alpha_2\omega_2\big)\Big] \\
&+ \Big\{ -2\alpha_3^2\omega_1\big(\omega_1^2+\omega_2^2\big) - \alpha_2\alpha_3\omega_2\big(3\alpha_3+2\omega_1\omega_3\big) \\
&+ \alpha_1\Big[-3\alpha_3^2\omega_1 + 2\alpha_2\omega_2\big(\omega_1^2+\omega_2^2\big) + \alpha_3\big(-\omega_1^2+\omega_2^2\big)\omega_3\Big] \\
&+ \alpha_2^2\Big[\alpha_3\omega_3 - \omega_1\big(\omega_1^2+\omega_2^2-\omega_3^2\big)\Big]\alpha_1^2\Big[\omega_1^3+\alpha_3\omega_3+\omega_1\big(\omega_2^2+\omega_3^2\big)\Big]\Big\}\lambda \\
&+ \Big\{ -\alpha_3^3 - 2\alpha_3^2\omega_1\omega_3 + \Big[\big(\alpha_1^2-\alpha_2^2\big)\omega_1 + 2\alpha_1\alpha_2\omega_2\Big]\omega_3 + \alpha_1\alpha_3\big(\omega_1^2+\omega_2^2+\omega_3^2\big)\Big\}\lambda^2 \\
&+ \alpha_1\alpha_3\omega_3\lambda^3, \\
F_2 &= \Big[\alpha_2\omega_1 + \omega_2\big(\omega_1^2+\omega_2^2-\alpha_1\big)\Big]\Big[\big(\alpha_1^2+\alpha_2^2\big)\omega_3 - 2\alpha_3\big(\alpha_1\omega_1+\alpha_2\omega_2\big)\Big] \\
&+ \Big\{\alpha_2\Big[\omega_1\big(-\alpha_3^2+2\alpha_1\big(\omega_1^2+\omega_2^2\big)\big) + \alpha_3\big(\omega_1^2-\omega_2^2\big)\omega_3\Big] + \alpha_2^2\omega_2\big(\omega_1^2+\omega_2^2+\omega_3^2\big) \\
&- \omega_2\Big[2\alpha_3^2\big(\omega_1^2+\omega_2^2\big) - \alpha_1\alpha_3\big(\alpha_3-2\omega_1\omega_3\big) + \alpha_1^2\big(\omega_1^2+\omega_2^2-\omega_3^2\big)\Big]\Big\}\lambda \\
&+ \Big\{\alpha_2^2\omega_2\omega_3 - \big(\alpha_1^2+2\alpha_3^2\big)\omega_2\omega_3 + \alpha_2\Big[2\alpha_1\omega_1\omega_3 + \alpha_3\big(\omega_1^2+\omega_2^2+\omega_3^2\big)\Big]\Big\}\lambda^2 \\
&+ \alpha_2\alpha_3\omega_3\lambda^3.
\end{aligned}$$

We can prove that the systems (2.14) and (2.15) are invariant by differentiation with respect to the system (1.9). We immediately verify that the points (1.25) satisfy the system (2.14) and the points (1.28) satisfy the system (2.15); taking into account the dimensions of the corresponding subsets, we obtain the relation (2.12).

From the results of [41] we obtain, as a particular case, that the systems (2.14) and (2.15) describe the set of critical points of the restriction to P^5 of the function with undefined Lagrange multipliers

$$2L^2 + (\tau-1)H + sK. \tag{2.16}$$

The differential of this function is preserved by phase flows; therefore, s and τ expressed through the phase variables become particular integrals of the critical subsystems $\mathcal{M}_j$:

$$\mathcal{M}_1: \quad s = -\frac{\ell}{\omega_1}, \qquad \tau = 1 + 2\ell\omega_1, \tag{2.17}$$

$$\mathcal{M}_{2,3}: \quad s = \frac{\omega_3 - 2\ell\alpha_3}{2(\omega_1^2+\omega_2^2+\lambda\omega_3)\lambda}, \quad \tau = 2\lambda^2 s. \tag{2.18}$$

These values of s determine the corresponding points of singular surfaces Π_j in (2.7) and (2.8). We note that, as (2.17) shows, on the set $\mathcal{M}_1$ the function (2.16) can be "cancelled" by L without loss of critical points. On the set $\mathcal{M}_{2,3}$ this cannot be done since there exists a set of points of global dependence of the functions K and H on P^5: on this set L vanishes and hence the undefined multiplier of dL in the nontrivial zero combination of differentials is proportional to L.

We also note that the results of [41] imply that the Poisson brackets of pairs of functions from (2.14) and (2.15) have the form

$$\{R_1, R_2\} = \frac{3}{2}s - \left(h - \frac{\lambda^2}{2}\right), \tag{2.19}$$

$$\{F_1, F_2\} = \frac{\lambda F_0}{s\sqrt{2}}\left(1 - 8\lambda^2 s^3\right)\sqrt{2s^2 - 2\left(h + \frac{\lambda^2}{2}\right)s + 1}, \tag{2.20}$$

where

$$F_0^2 = \left(\omega_1^2 + \omega_2^2 + \lambda\omega_3\right)^3\Big[\left(\alpha_1\omega_1 + \alpha_2\omega_2 + \lambda\alpha_3\right)^2 + \left(\alpha_2\omega_1 - \alpha_1\omega_2\right)^2\Big]. \tag{2.21}$$

Vanishing of the brackets (2.19) and (2.20) corresponds to the cases of degeneration of the symplectic structure induced on the two-dimensional manifolds $\mathcal{M}_j \cap P^4_\ell$, which are the phase spaces of Hamiltonian systems with one degree of freedom. Below, we clarify the relation of this phenomenon with types of critical points. Looking ahead, without rigorous proofs, we say that, since nondegenerate critical points are organized into symplectic submanifolds (see the corresponding assertion in [8]), points on the critical set at which the induced symplectic structure is degenerate must be degenerate as critical points of the moment mapping.

3. Relative Equilibria Are Critical Points of Rank 0

3.1. Dependence of the energy and area integrals. Immovable points of the Euler–Poisson equations are the projections on P^5 of motions of the body in which the trajectory in $SO(3)$ coincides with an orbit of the symmetry group, i.e., rotations about the vertical with a constant angular velocity. In Routh's theory of reduction of order such immovable points are called *relative equilibria*. In Smale's theory (see [68]), these points are critical points of the *energy-moment* mapping. In the dynamics of a rigid body, this means that the energy integral and the are integral are dependent. Bifurcation diagrams of the mapping

$$L{\times}H : P^5 \to \mathbb{R}^2 \tag{3.1}$$

are called Smale diagrams.

In its turn, on a symplectic leaf (1.7), critical points of the mapping (3.1) are critical points of the "reduced" Hamiltonian

$$H_\ell = H|_{P^4_\ell} : P^4_\ell \to \mathbb{R}. \tag{3.2}$$

If we want to emphasize the dependence on λ, we write $P^4_\ell(\lambda)$ and $H_{\ell,\lambda}$. The results of [30] imply that almost all such points are nondegenerate in the sense of Morse (below we consider a classification of these points in more detail). However, a nondegenerate critical point of the Hamiltonian is critical for all other first integrals. Therefore, the set considered coincides with $\mathcal{C}^0$. Thus, the problem of the study of critical points of the mapping (3.1) coincides with the problem of the study of the set of rank-0 critical points of the mapping (2.6) in the sense of Definition 1.

In the sequel, we will use the following assertion for the search for critical points of functions on P^5 without introducing an additional undefined multiplier corresponding to the constraint (1.3).

Lemma 1. *Let f be a smooth function on $\mathbb{R}^6(\boldsymbol{\omega}, \boldsymbol{\alpha})$. The set of critical points of the restriction of f on the submanifold P^5 is determined by the system of equations*

$$\frac{\partial f}{\partial \boldsymbol{\omega}} = 0, \quad \boldsymbol{\alpha} \times \frac{\partial f}{\partial \boldsymbol{\alpha}} = 0. \tag{3.3}$$

In the complex variables (2.1) *this system has the form*

$$\begin{gathered} \frac{\partial f}{\partial w_1} = \frac{\partial f}{\partial w_2} = \frac{\partial f}{\partial w_3} = 0, \\ 2z\frac{\partial f}{\partial x_1} - x_1\frac{\partial f}{\partial z} = 0, \quad 2z\frac{\partial f}{\partial x_2} - x_2\frac{\partial f}{\partial z} = 0, \quad x_1\frac{\partial f}{\partial x_2} - x_2\frac{\partial f}{\partial x_1} = 0. \end{gathered} \tag{3.4}$$

The proof is obvious. Note that the last three equations in both systems (3.3) and (3.4) are linearly dependent. The choice of an independent pair in the case of general position is determined by reasons of convenience.

We write Eq. (3.3) for the function $f_H = H - 2\sigma L$. We have

$$\begin{gathered}\omega_1 = \sigma\alpha_1, \quad \omega_2 = \sigma\alpha_2, \quad \omega_3 = \sigma\alpha_3,\\ \alpha_3 - [\alpha_1(\omega_3+\lambda) - 2\alpha_3\omega_1]\sigma = 0, \quad \alpha_2 - 2(\alpha_1\omega_2 - \alpha_2\omega_1)\sigma = 0,\\ [2\alpha_3\omega_2 - \alpha_2(\omega_3+\lambda)]\sigma = 0.\end{gathered} \tag{3.5}$$

This rank-5 system together with Eq. (1.3) allows one to express the phase variables and the undefined multiplier σ through one variable chosen as an independent parameter. In [29], the parametrization of the set $\mathcal{C}^0$ by the variable α_1 was used.

Proposition 1 (P. E. Ryabov [29]). *The set of rank-*0 *critical points is described by the following system of equations*:

$$\begin{aligned}&\omega_1 = \frac{x}{2d_1}(\lambda - d_2), && \omega_2 = 0, && \omega_3 = \frac{1}{2}(\lambda - d_2),\\ &\alpha_1 = x, && \alpha_2 = 0, && \alpha_3 = d_1,\end{aligned} \tag{3.6}$$

where

$$d_1 = \pm\sqrt{1-x^2}, \quad d_2 = \pm\sqrt{\lambda^2 - \frac{4}{x}(1-x^2)},$$

the signs of d_1 *and* d_2 *are arbitrary, and the parameter* x *satisfies the conditions*

$$x \in \begin{cases}[-1,0)\cup[c_\lambda,1], & d_2 > 0,\\ (-1,0)\cup[c_\lambda,1), & d_2 < 0,\end{cases} \qquad c_\lambda = \frac{1}{8}\left(\sqrt{\lambda^4+64} - \lambda^2\right).$$

In this case, the values of the first integrals and the undefined multiplier σ *are as follows*:

$$\ell = \frac{1}{d_1}\Big[(3-x^2)\lambda - (1+x^2)d_2\Big], \quad h = \frac{\lambda(1-x^2) - d_2(1+3x^2)}{2x(\lambda+d_2)}, \sigma = \frac{1}{2d_1}(\lambda - d_2). \tag{3.7}$$

Note that the system (3.5) has no solutions in P^5 with $\alpha_1 = 0$ and hence the singularity $x = 0$ is nonremovable.

Equation (3.7) is a parametric equation of the Smale diagram. In the study of bifurcation diagrams of the mapping (2.10), the first equation in (3.7) allows one to find all rank-0 critical points containing in a given level P^4_ℓ.

Another parametrization of the set $\mathcal{C}^0$ was proposed by Gashenenko (see [13]); he noted that such points belong to the intersection of $\mathcal{M}_1$ with the union of the set $\mathcal{M}_2$ and $\mathcal{M}_3$. Therefore, it is convenient to take $\omega_3 = r$ as an independent parameter in the relations (1.25). In this case, the polynomial (1.26) must have a multiple root, which allows one to express all unknowns through r. Surely, the same expressions follow from the system (3.5). Taking into account the results of [13, 16], we arrive at the following assertion.

Proposition 2 (I. N. Gashenenko [13]). *The set of rank-*0 *critical points is described by the following system of equations*:

$$\begin{aligned}&\omega_1 = \pm\sqrt{\frac{r}{2}\left[-r + \frac{1}{r-\lambda}d\right]}, && \omega_2 = 0, && \omega_3 = r,\\ &\alpha_1 = -\frac{r-\lambda}{2}\left[-r + \frac{1}{r-\lambda}d\right], && \alpha_2 = 0, && \alpha_3 = \mp(r-\lambda)\sqrt{\frac{r}{2}\left[-r + \frac{1}{r-\lambda}d\right]},\end{aligned} \tag{3.8}$$

where

$$d = \pm\sqrt{r^2(r-\lambda)^2 + 4}, \tag{3.9}$$

the parameter r *runs over the set*

$$r \in (-\infty, 0] \cup [0, \lambda) \cup (\lambda, +\infty), \tag{3.10}$$

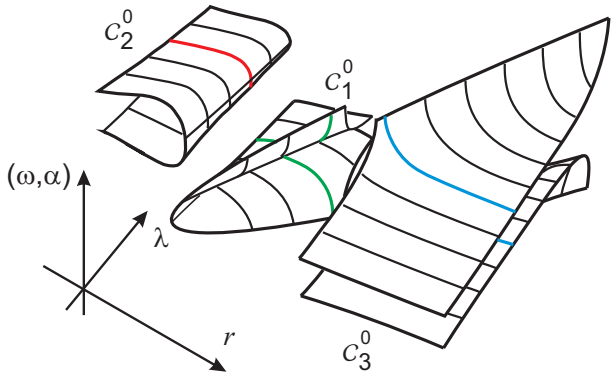

Fig. 1. Surfaces of relative equilibria

and the sign of d coincides with the sign of $r(r-\lambda)$ for $r \neq 0$ and is arbitrary for $r = 0$. The values of the first integrals are as follows:

$$\ell = \mp\frac{1}{2}[\lambda(r-\lambda)+d]\sqrt{\frac{r}{2}\left[-r+\frac{1}{r-\lambda}d\right]}, \quad h = -\frac{1}{2}r(r-\lambda)+\frac{2r-\lambda}{2(r-\lambda)}d, \tag{3.11}$$

and the undefined multiplier is equal to

$$\sigma = \mp\frac{1}{\sqrt{2}\sqrt{\frac{r}{r-\lambda}\left[r(r-\lambda)+d\right]}}.$$

The signs of ω_1, α_3, ℓ, and σ are matched (all upper or all lower).

Comparing with Eqs. (1.25), we see that rank-0 points appear in the subsystem $\mathcal{M}_1$ if we set

$$p^2 = \frac{r}{2}\left[-r+\frac{1}{r-\lambda}d\right]. \tag{3.12}$$

Remark 3. We verify that at all point found above the differential $d(K|_{P_\ell^4})$ also vanishes. For this, we write Eq. (3.3) for the function

$$f_K = K - 4\gamma L, \quad \gamma = \mp\frac{\lambda}{r-\lambda}\sqrt{\frac{r}{2}\left[-r+\frac{1}{r-\lambda}d\right]}.$$

For Smale diagrams, the value of the integral K is irrelevant, but we need this value at the points (3.8) below. By [13], we can represent it in the form

$$k = \frac{\lambda}{4(r-\lambda)^2}\Big[r(r-\lambda)-d\Big]\Big[r(r-\lambda)(4r-3\lambda)-\lambda d\Big]. \tag{3.13}$$

We also calculate the values of the particular integrals s in the systems $\mathcal{M}_j$ at the points (3.8), i.e., the values of the parameter s on the surfaces Π_j at rank-0 point. Using (2.17) and (2.18), we find

$$\mathcal{M}_1: \quad s = \frac{1}{2}[\lambda(r-\lambda)+d], \tag{3.14}$$

$$\mathcal{M}_{2,3}: \quad s = \frac{r-\lambda}{4\lambda}[r(r-\lambda)-d]. \tag{3.15}$$

From (3.8) and (3.10) we immediately obtain that the set $\mathcal{C}^0$ has exactly four connected components that are homeomorphic to $\mathbb{R}$. In correspondence with the domain of r, we introduce the following

notation for subsets in $\mathcal{C}^0$ determined by the formulas (3.8):

$$\begin{aligned}
&\mathcal{C}^0_1: \quad r \in [0,\lambda), && d<0, \quad \lim_{r\to+0} d = -2,\\
&\mathcal{C}^0_2: \quad r \in (-\infty,0], && d>0, \quad \lim_{r\to-0} d = 2,\\
&\mathcal{C}^0_3: \quad r \in (\lambda,+\infty), && d>0.
\end{aligned} \tag{3.16}$$

The first two sets are connected, whereas the last set consists of two components that differ by the sign of ω_1. In $\mathcal{C}^0_1$ and $\mathcal{C}^0_2$, each value of $r \neq 0$ corresponds to exactly two points, and in $\mathcal{C}^0_1$ the value $r=0$ corresponds to the point $\boldsymbol{\omega}=0$, $\boldsymbol{\alpha}=\{1,0,0\}$ of the lower equilibrium position of the body (for further convenience, we denote it, in correspondence with the fact that $r\to+0$, by c_+). In the set $\mathcal{C}^0_2$, the zero value of r leas us to the point $\boldsymbol{\omega}=0$, $\boldsymbol{\alpha}=\{-1,0,0\}$ of the upper equilibrium position (we denote it by c_-). On the sets (3.16), there exists an obvious symmetry

$$\operatorname{symm}: (\omega_1,\alpha_3) \mapsto (-\omega_1,-\alpha_3), \tag{3.17}$$

which changes the sign of the area constant ℓ, preseves the connected sets $\mathcal{C}^0_1$ and $\mathcal{C}^0_2$, and in the set $\mathcal{C}^0_3$ swaps the connected components. The structure of the family of sets $\mathcal{C}^0(\lambda)$ is shown in Fig. 1.

3.2. Classification of rank 0 critical points. Here we present results related to an analytic classification of types of rank-0 critical points in correspondence with [44].

We recall some facts and definitions related to the notion of the type of a critical point of an integrable system (see [8]).

Let M be a symplectic manifold. To each smooth function $F: M\to\mathbb{R}$, we put in correspondence a Hamiltonian vector field $\operatorname{sgrad} F$ on M. We denote the Poisson bracket generated by the symplectic structure by $\{\cdot,\cdot\}$; then the differential equations of the system $\operatorname{sgrad} F$ have the form

$$\dot{x} = \{F, x\}.$$

We note that usually the arguments of the bracket in the right-hand side are written in the reverse order. It can be easily verified that just the expression $\{F,x\}$ allows one to obtain Eqs. (1.1) from the definitions (1.6) and (1.4). There also exist other approaches to this inconsistency; for example, in [10], opposite signs in the definition of the bracket (1.6) are used, whereas in [23] the components of the kinetic moment with opposite sign are taken as momenta.

Let $\dim M = 2n$ and let a Hamiltonian system $\operatorname{sgrad} H$ have n functionally independent, involutive first integrals $F_1,\dots,F_n$, i.e., $\{F_i,F_j\}\equiv 0$. A point $\xi\in M$ is called a critical point of rank $k<n$ if the rank of the system of vectors $\operatorname{sgrad} F_i$ at the point ξ is equal to k. We introduce the notion of the type of a critical point following [8].

Consider a critical point ξ of rank $n-m$ $(m>0)$. We assume that below in this section the subscript i runs over the set $1,\dots,m$. By a linear change of variables with constant coefficients in the system of functions $F_1,\dots,F_n$, we can achieve that the point ξ be critical for each of the functions F_i and regular for all other points. Then $\operatorname{sgrad} F_i(\xi)=0$ and the linearization of this field at the point ξ is a symplectic operator $\mathfrak{a}_i: T_\xi M\to T_\xi M$. The linear span $\mathfrak{A}(\xi)$ of such operators is a subalgebra in the algebra of all symplectic operators on $T_\xi M$.

Definition 3 (see [8])**.** A point ξ is called a nondegenerate critical point of rank $n-m$ if $\mathfrak{A}(\xi)$ is a Cartan subalgebra; this is equivalent to the following conditions:

(i) symplectic operators $\mathfrak{a}_i$ are linearly independent $(\dim\mathfrak{A}(\xi)=m)$;
(ii) there exists an operator $\mathfrak{a}\in\mathfrak{A}(\xi)$ whose eigenvalues are distinct.

We recall that eigenvalues of an symplectic operator can be split into groups: pairs of purely imaginary $\pm\mathrm{i}\,a$, pairs of real $\pm b$, and quadruples of complex $\pm b\pm\mathrm{i}\,a$ $(ab\neq 0)$. For an operator $\mathfrak{a}_i$, the projections of the field $\operatorname{sgrad} F_i$ on root subspaces of such groups have respectively a center, a saddle, or a focus. An operator $\mathfrak{a}\in\mathfrak{A}(\xi)$ with distinct eigenvalues is called a regular element. Choosing a

regular element at a nondegenerate point, we denote by m_1, m_2, and m_3, the numbers of centers, saddles, and focuses, respectively ($m = m_1 + m_2 + 2m_3$). These nonnegative numbers are independent of the choice of the regular element.

Definition 4 (see [8])**.** A quadruple $(n - m, m_1, m_2, m_3)$ i called the type of a nondegenerate critical point ξ.

For systems with two degrees of freedom, the following more illustrative terms are usually used. For rank-0 points, the type $(0, 2, 0, 0)$ is called "center-center," the type $(0, 1, 1, 0)$ is called "center-saddle," and the type $(0, 0, 2, 0)$ is called "saddle-saddle." For rank-1 points, the type $(1, 1, 0, 0)$ is called "center" and the type $(1, 0, 1, 0)$ is called "saddle." In the problem considered, other types (in particular, focuses) do not occur.

The type of a nondegenerate critical point largerly (but not completely) determines the Liouville fibration (i.e., the fibration of common levels of n involutive first integrals) in a neighborhood of this point. To construct a rough topological description of the Liouville fibration (for example, as a loop molecules without marks in a system with two degrees of freedom), it suffices additionally to know the number of connected components of regular and critical integral surfaces. For critical levels of low complexity (i.e., when each connected component contains few critical orbits), for example, for rank-0 critical points with one point on a fiber, these data are sufficient for the search for a fine topological invariant (a marked loop molecule) since one has descriptions of all possibilities (see [8]). Below, we present such a description for the problem considered.

Definition 5. A critical point ξ is said to be *strongly* degenerate if the condition (i) of Definition 3 is violated and *weakly* degenerate in the opposite case.

We note that these terms are not conventional; we use them here for convenience.

For the Euler–Poisson equations, the 2-form induced on P^5 by the symplectic structure of the manifold $TSO(3)$ is degenerate. The notions introduced above can be considered from the point of view of systems on P^4_ℓ. The explicit transition to these systems makes calculations boundless. However, these calculations are not necessary. To the function F, the degenerate Poisson bracket (1.6) assings the field $\operatorname{sgrad} F$ determined by the equations

$$\dot{\mathbf{M}} = \mathbf{M} \times \frac{\partial F}{\partial \mathbf{M}} + \boldsymbol{\alpha} \times \frac{\partial F}{\partial \boldsymbol{\alpha}}, \quad \dot{\boldsymbol{\alpha}} = \boldsymbol{\alpha} \times \frac{\partial F}{\partial \mathbf{M}}. \tag{3.18}$$

Remark 4. If F is a Casimir function, i.e., it is identically dependent with L and $\Gamma = \boldsymbol{\alpha}^2$, then the right-hand sides of Eqs. (3.18) identically vanish. In this connection, in the calculation of linearizations of the fields $\operatorname{sgrad} F$ of arbitrary functions F and eigenvalues of the corresponding operators in $\mathbb{R}^6$, there is no need to consider undefined Lagrange multipliers for the functions L and Γ; we must only take into account Definition 1 and discard two zero eigenvalues, which necessarily exist.

The physical model of a gyrostat is a system with four degrees of freedom (a body and a rotor) for which λ is the constant of a cyclic integral. The Euler–Poisson equations are obtained by reduction of order in this system. Therefore, all reasonings on the constance of any properties in the space of integral or other parameters must be naturally considered in the extended space of these parameters including the axis $\mathbb{R} = \mathbb{R}(\lambda)$. In this connection, we will use the following notation. Let A be a set and $B(\lambda)$ be a family of its subsets depending on a parameter λ. We introduce the notation

$$\Lambda(A) = A \times \mathbb{R}, \quad \Lambda(B) = \bigcup_\lambda B(\lambda) \times \{\lambda\} \subset \Lambda(A). \tag{3.19}$$

Hence we consider the extended set $\Lambda(\mathcal{C}^0) \subset \Lambda(P^5) = P^5 \times \mathbb{R}$. Recall that by (1.8) we assume that $\lambda > 0$; the case $\lambda = 0$ is considered only as a limit possibility where explicitly stated. By Proposition 2, the set $\Lambda(\mathcal{C}^0)$ continuously twice covers the domain

$$\mathcal{D}^0 = \big\{(r, \lambda) \in \mathbb{R}^2 : \lambda > 0,\ r \neq \lambda\big\}.$$

Remark 5. In the sequel, we denote the images of the sets $\Lambda(\mathcal{C}_i^0)$ in various spaces of parameters (constant general integrals and particular integrals, physical parameter λ) by δ_i, $i = 1, 2, 3$. In particular, as subsets in $\mathcal{D}^0$, they have the form

$$\begin{aligned} \delta_1 :&\quad \big\{(r,\lambda) : 0 \le r < \lambda,\ \lambda > 0\big\},\\ \delta_2 :&\quad \big\{(r,\lambda) : r \le 0,\ \lambda > 0\big\},\\ \delta_3 :&\quad \big\{(r,\lambda) : r > \lambda,\ \lambda > 0\big\}. \end{aligned} \tag{3.20}$$

Subsets of these sets obtained as results of further detailed elaboration are marked by double indices.

We recall the existence of a symmetry (3.17) on $\mathcal{C}^0$.

Definition 6. We say that points $\xi_1, \xi_2 \in \Lambda(\mathcal{C}^0)$ belong to the same class if there exists a continuous path in $\Lambda(\mathcal{C}^0)$ connecting these points (or connecting the point ξ_1 with the point $\operatorname{symm}(\xi_2)$) along which the type of critical points is preserved.

Let $(r,\lambda) \in \mathcal{D}^0$. We denote by $\xi_\pm(r,\lambda)$ the point (3.8) for $r \ne 0$ and, due to Proposition 2, for the chosen sign of (3.9), $\operatorname{sgn} d = \operatorname{sgn}[r(r-\lambda)]$. By the notation adopted,

$$\lim_{r\to+0} \xi_\pm(r,\lambda) = c_+ \in \mathcal{C}_1^0, \quad \lim_{r\to-0} \xi_\pm(r,\lambda) = c_- \in \mathcal{C}_2^0.$$

Definition 7. A point $(r,\lambda) \in \mathcal{D}^0$ is said to be separating if any its neighborhood contains images of points from $\Lambda(\mathcal{C}^0)$ belonging to different classes.

The ray of prohibited points $r = \lambda$, $\lambda > 0$ is a separating ray; we denote in by $\overline{\pi}$. Since $\xi_1 \in \mathcal{C}_1^0$ and $\xi_2 \in \mathcal{C}_2^0$ cannot belong to the same class, points of the form $(0,\lambda)$ are always separating. We denote the semiaxis $r = 0$, $\lambda > 0$ by π_0. For $r \ne 0$, the types of critical points $\xi_\pm(r,\lambda)$ always coincide, hence the point (r,λ) is separating if and only if both critical points $\xi_\pm(r,\lambda)$ are degenerate.

Let $\mathfrak{a}_H$ and $\mathfrak{a}_K$ be symplectic operators of the linearizations of the fields $\operatorname{sgrad} H$ and $\operatorname{sgrad} K$ at the point (3.8).

Proposition 3. *The set of strongly degenerate critical points $\xi_\pm(r,\lambda)$ corresponds to the curve*

$$\pi_{21} :\quad r = \lambda - \frac{1}{\lambda^{1/3}}, \quad 0 < \lambda \le 1, \tag{3.21}$$

in the domain δ_2.

Proof. At strongly degenerate points, we consider the combination

$$\mathfrak{b} = \nu_1 \mathfrak{a}_H + \nu_2 \mathfrak{a}_K = 0. \tag{3.22}$$

Arranging the variables and, respectively, the elements of matrices in the order ω_1, ω_2, ω_3, α_1, α_2, α_3, we have

$$\mathfrak{b}_{12} = \frac{1}{2}(r-\lambda)\Big[\nu_1 - 2\nu_2\lambda(Q^2 + \lambda + r)\Big], \tag{3.23}$$

where we have introduced the notation

$$Q = \sqrt{\frac{1}{2}\left[-r + \frac{1}{r-\lambda}d\right]}.$$

Obviously, $Q \ne 0$. From (3.22) and (3.23) we obtain

$$\nu_1 = 2\nu_2\lambda(Q^2 + \lambda + r), \quad \nu_2 \ne 0.$$

Substituting this in (3.22), we have

$$\mathfrak{b} = 2\nu_2(\lambda - r)Q(Q^2 + \lambda)\mathfrak{C} = 0,$$

where

$$\mathfrak{C} = \begin{pmatrix} 0 & 0 & 0 & 0 & 0 & 0 \\ 0 & 0 & 0 & 0 & 0 & 0 \\ 0 & -2\sqrt{r} & 0 & 0 & \dfrac{\lambda + r}{Q(\lambda - r)} & 0 \\ 0 & -2r\sqrt{r} & 0 & 0 & \dfrac{r(\lambda + r)}{Q(\lambda - r)} & 0 \\ 2r\sqrt{r} & 0 & -\lambda Q & -\dfrac{r(\lambda + r)}{Q(\lambda - r)} & 0 & \dfrac{2\lambda\sqrt{r}}{\lambda - r} \\ 0 & 2rQ & 0 & 0 & -\dfrac{\sqrt{r}(\lambda + r)}{\lambda - r} & 0 \end{pmatrix}$$

is a nonzero matrix. Therefore, $Q^2 + \lambda = 0$, which is equivalent to the equation

$$1 + \lambda(r - \lambda)^3 = 0 \tag{3.24}$$

with the condition $Q^2 < 0$. But $\operatorname{sgn} Q^2 = \operatorname{sgn}[(r - \lambda)d]$ coincides with $\operatorname{sgn} r$ (see Proposition 2). Therefore, from the solutions (3.24) we must take only points lying in δ_2, which yields the curve (3.21). □

Lemma 2. *Under the condition*

$$(2r - \lambda)(r - \lambda) + d = 0 \tag{3.25}$$

all critical points are nondegenerate.

Proof. Let the condition (3.25) hold. If we assume that $d > 0$, then $r \in (-\infty, 0] \cup (\lambda, +\infty)$. But on this interval $(2r - \lambda)(r - \lambda) > 0$, which contradicts (3.25). Therefore, $d < 0$, $r \in [0, \lambda)$, and

$$\frac{1}{2}|d| = \left(r - \frac{\lambda}{2}\right)(r - \lambda)$$

and finally $r \in [0, \lambda/2]$. By squaring, we obtain the equation

$$(r - \lambda)^3(3r - \lambda) - 4 = 0. \tag{3.26}$$

We represent its solutions on the required interval in the parametric form; for this, we introduce the variable x by the formula

$$x = \lambda - r \tag{3.27}$$

(see [48]). From (3.26) and (3.27) we find

$$d = -\frac{x^4 + 4}{2x^2}$$

and

$$r = \frac{x^4 - 4}{2x^3}, \quad \lambda = \frac{3x^4 - 4}{2x^3}. \tag{3.28}$$

The condition $r \in [0, \lambda)$ is fulfilled if

$$x \geq \sqrt{2}. \tag{3.29}$$

The characteristic polynomial of the operator $\mathfrak{a}_H$ takes the form

$$\chi_H(\mu) = \left(\mu^2 + \frac{\sqrt{x^4 + 4}}{2x}\right)^2$$

(see (3.28)); we see that it is useless in the problem on nondegeneracy. However, we calculate the characteristic polynomial of the operator $\mathfrak{a}_K$:

$$\chi_K(\mu) = \left[\mu^2 + \frac{(x^4 - 4)^2(4 + x^4)}{x^{14}}\right]\left[\mu^2 + \frac{(x^4 + 4)(3x^8 - 7x^4 + 4)^2}{x^{14}}\right].$$

Under the condition (3.29), all its roots are distinct; therefore, it is a required regular element of the algebra. □

Proposition 4. *Assume that a point* $(r,\lambda)\in\mathcal{D}^0$ *does not lie on the curve* (3.21) *and does not satisfy any of the equations*

$$r+\lambda=0, \tag{3.30}$$

$$(2r-\lambda)(r-\lambda)-d=0, \tag{3.31}$$

$$(2r-\lambda)(r-\lambda)r+\lambda d=0. \tag{3.32}$$

Then the critical points $\xi_\pm(r,\lambda)$ *are nondegenerate.*

Proof. The characteristic polynomial of the operator $\mathfrak{a}_H$ at the point $\xi_\pm(r,\lambda)$ cancelled by μ^2 in correspondence with Remark 4 has the form

$$\chi_H(\mu)=\mu^4-2a\mu^2+b, \tag{3.33}$$

where

$$a=\frac{1}{8(r-\lambda)}\Big[-(3r-\lambda)(2r-\lambda)(r-\lambda)+(r-3\lambda)d\Big],$$

$$b=\frac{1}{8(r-\lambda)}\Big[(r-\lambda)^3(4r-\lambda)r-4\lambda-(2r-\lambda)(r-\lambda)^2d\Big].$$

The discriminant of the polynomial (3.33)

$$a^2-b=\frac{(r+\lambda)^2}{64(r-\lambda)^2}\Big[(2r-\lambda)(r-\lambda)+d\Big]^2$$

by Lemma 2 vanishes only if the condition (3.30) holds. The roots of χ_H with respect to μ^2 can be explicitly expressed:

$$\mu_1^2=-\frac{1}{4}\Big[(2r-\lambda)(r-\lambda)-d\Big], \tag{3.34}$$

$$\mu_2^2=-\frac{1}{2(r-\lambda)}\Big[(2r-\lambda)(r-\lambda)r+\lambda d\Big]. \tag{3.35}$$

These values that determine the types of rank-0 points were first calculated in [30]. Thus, outside the set determined by the equations (3.30)–(3.32), all roots of χ_H are distinct and outside the curve (3.21) the algebra generated by the operators $\mathfrak{a}_H$ and $\mathfrak{a}_K$ is two-dimensional. The proposition is proved. □

Proposition 5. *On the curve*

$$\pi_{22}:\quad r=-\lambda,\quad \lambda>0, \tag{3.36}$$

i.e., under the condition (3.30)*, all critical points are degenerate.*

Proof. We calculate the characteristic polynomial of the combination $\mathfrak{b}=\nu_1\mathfrak{a}_H+\nu_2\mathfrak{a}_K$ at the points (3.8) under the condition (3.30). We have

$$\chi(\mu)=\left[\mu^2+\frac{(Z^2-2)(\nu_1Z+\nu_2)}{2Z^3}\right]^2,\quad Z=\lambda^2+\sqrt{\lambda^4+1}.$$

Therefore, the linear span of the operators $\mathfrak{a}_H$ and $\mathfrak{a}_K$ does not contain regular elements. □

Note that if $\nu_1Z+\nu_2=0$, then all eigenvalues of the operator $\mathfrak{b}$ are equal to zero, but the operator itself is nonzero, except for the value $\lambda=1/2^{3/4}$, which corresponds to the intersection point π_{22} with the curve (3.21) of strong degeneration.

Proposition 6. *The condition* (3.31) *is realized in the domain* $\mathcal{D}^0$ *on the following curves*:

$$\pi_{23}: \quad r=\frac{x^4-4}{2x^3}, \qquad \lambda=\frac{3x^4-4}{2x^3}, \qquad x\in\left(\sqrt[4]{4/3},\sqrt{2}\right], \tag{3.37}$$

$$\pi_{31}: \quad r=\frac{x^4-4}{2x^3}, \qquad \lambda=\frac{3x^4-4}{2x^3}, \qquad x\in\left(-\sqrt[4]{4/3},0\right). \tag{3.38}$$

All corresponding critical point are degenerate.

Proof. From Eq. (3.31) we obtain Eq. (3.26), whose solutions can be represented in the form (3.28). If we assume that $d<0$, then $r\in[0,\lambda)$, and hence $r\in[0,\lambda/3)$ and $(2r-\lambda)(r-\lambda)>0$, i.e., Eq. (3.31) does not have such solutions. If $d>0$, then in the domains δ_2 and δ_3 we must substitute the corresponding range for x in (3.37) and (3.38). At such points, the characteristic polynomial of the combination $\nu_1\mathfrak{a}_H+\nu_2\mathfrak{a}_K$ has the form

$$\chi(\mu)=\mu^4-\frac{\left(x^8+2x^4-8\right)\left[-2\nu_1x^2+\nu_2(x^4-4)\right]^2}{8x^{10}}\mu^2 \tag{3.39}$$

and always has two zero roots. Therefore, the algebra of operators does not contain regular elements. □

Proposition 7. *The condition* (3.32) *is satisfied in the domain* $\mathcal{D}^0$ *on the curve*

$$\pi_{24}: \quad r=\frac{1}{2}\left(\lambda-\sqrt{\lambda^2+4\lambda^{2/3}}\right), \quad \lambda>0. \tag{3.40}$$

All corresponding critical points are degenerate.

Proof. The equation

$$r(r-\lambda)=\lambda^{2/3} \tag{3.41}$$

is a consequence of Eq. (3.32) Obviously, it has exactly two solutions, one in each of the domains δ_3 ($r>\lambda$) and δ_2 ($r<0$), where we must choose $d>0$. But in the domain δ_3 we have $(2r-\lambda)(r-\lambda)r>0$, so Eq. (3.32) does not hold. Therefore, only one root of Eq. (3.41) is a solution, namely, the lower root; this leads to the points of the curve (3.40). Setting $Z=\lambda^{2/3}+\sqrt{4+\lambda^{4/3}}$, we write the characteristic polynomial of the combination $\nu_1\mathfrak{a}_H+\nu_2\mathfrak{a}_K$ at these points in the form

$$\chi(\mu)=\mu^4+\frac{(Z^2-8)(4+Z^2)\left\{\nu_2\left[Z^2(Z^2-8)^2-64\right]-4\nu_1Z^3\right\}^2}{512Z^7}\mu^2. \tag{3.42}$$

It always has two zero roots. Therefore, the algebra of operators does not contain regular elements. □

The domain $\mathcal{D}^0$ with separating curves is shown in Fig. 2 (see also the notation for classes of nondegenerate rank-0 points. We see that the set $\Lambda(\mathcal{C}_1^0)$ contains a single class, which is denoted, as a subdomain in $\mathcal{D}^0$, by δ_1. It also includes the subset with the value $r=0$; through this subset one can pass to symmetric points, so that this class consists of a single connected component. The set $\Lambda(\mathcal{C}_3^0)$ contains two classes, which are denoted by δ_{31} and δ_{32}; they do not contain points with $r=0$ and hence each such class consists of two connected components. The set $\Lambda(\mathcal{C}_2^0)$ contains eight classes $\delta_{21},\dots,\delta_{28}$. Three of them, namely, δ_{21}, δ_{26}, and δ_{27}, contain points with $r=0$ and hence have one connected component; the other classes consist of two connected components. Figure 2 also contains the curve ℓ_0, which is generated by the possibility specific for gyrostats, namely, by the presence of uniform rotations about the vertical axis ($r\neq0$), for which the area constant vanishes. This means that a pair of symmetric points lies on the same level of all first integrals (but not in the same connected component). If we cross the curve ℓ_0, then the type of critical points does not change, but we show below that it causes a surgery of the Smale diagram and changes the topology of the common level of first integrals and topological invariants. We see from (3.11) that the relation

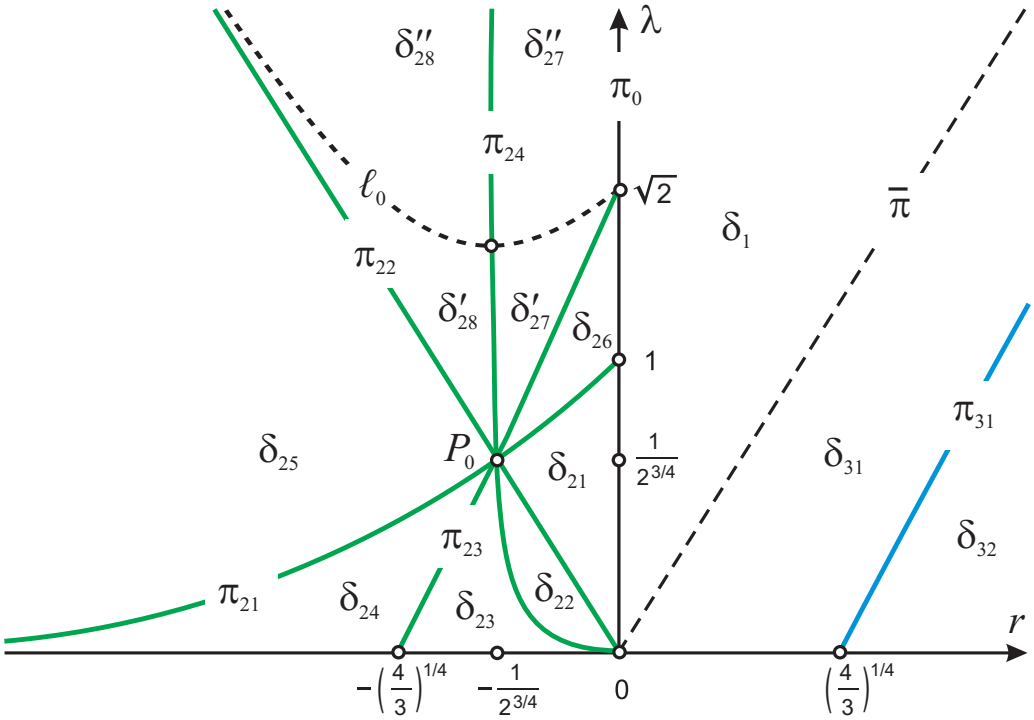

Fig. 2. Separating set and the classes of rank-0 critical points

$\ell = 0$ for $r \neq 0$ implies $\lambda(r-\lambda)+d=0$. In correspondence with the definition of the sign of d, this is possible only on δ_2; therefore, the curve ℓ_0 is determined by the conditions

$$\ell_0: \quad (r-\lambda)^3(r+\lambda)+4=0, \quad r \leq 0. \tag{3.43}$$

We recall once more that, according to the agreement, $\lambda \geq 0$. The curve ℓ_0 divides the classes δ_{27} and δ_{28} into subdomains, which we will mark with primes (see the figure).

Since we have analyzed all cases where the values (3.34) and (3.35) vanish, the analysis of their signs in the generated subdomains of the (r,λ)-plane leads to the following classification of rank-0 points.

Theorem 5. *In the extended phase plane $\Lambda(P^5)$, the rank-0 critical points of the Kovalevskaya–Yehia case form four manifolds diffeomorphic to $\mathbb{R}^2$. Degenerate critical points correspond to the following five separating curves on the parameter plane: the curves π_{21}–π_{24} and π_{31}.*

According to the equivalence relation introduced above (the presence of a continuous path with a constant type of critical points that contains the first point with the second point or with the point symmetric to the second point with respect to the given inversion mapping), nondegenerate critical points can be divided into 11 classes. The four classes that contain one of equilibria are connected. The other classes that contain only the images of uniform rotations (relative equilibria) consists of two connected components that are mutually symmetric with respect to the inversion mapping. According to the notation of classes in Fig. 2, critical points have the following type (we list them in the order corresponding to the order of pairs of roots μ_1^2 and μ_2^2):

(i) *δ_{21}, δ_{22}, and δ_{26} are "saddle-saddle";*
(ii) *δ_{23} and δ_{31} are "saddle-center";*
(iii) *δ_{27} is "center-saddle";*
(iv) *δ_{24}, δ_{25}, δ_{28}, δ_1, and δ_{32} are "center-center."*

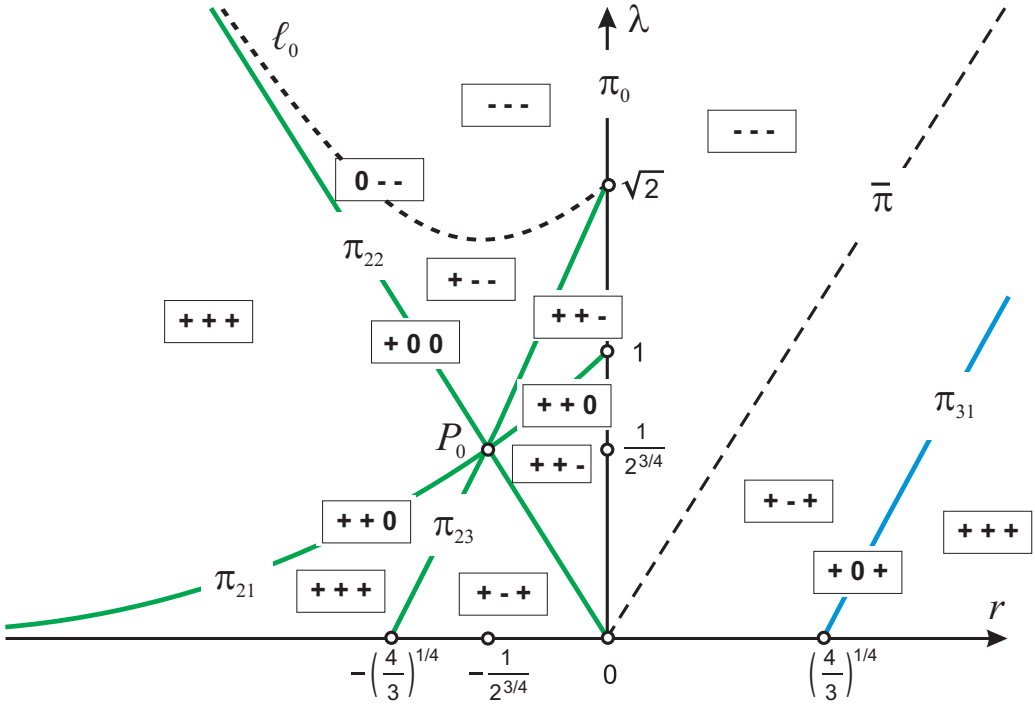

Fig. 3. Signs of triples (L_1, L_2, L_3)

Now we compare the classification of relative equilibria with respect to their types types and the classification of of relative equilibria in Gashenenko's solution (1.31), (1.32), (1.35) with respect to the parameters (1.33). In Fig. 3, we show the signs of triples (L_1, L_2, L_3) and zero values of parameters on separating curves. It turns that the curve π_{24} does not affect the signs of triples, L_3 vanishes on the curve π_{21}, but in the adjacent domains the signs of triples are the same. The parameters L_2 and L_3 vanish on the curve π_{22}. Finally, we obtain the following correspondence between domains and classes (1.36):

$$\begin{array}{llll} \text{(I)} & \delta_{24}, \delta_{25}, \delta_{32}; & \text{(V)} & \delta_1, \delta''_{27}, \delta''_{28}; \\ \text{(II)} & \delta'_{27}, \delta'_{28}; & \text{(VI)} & \ell_0; \\ \text{(III)} & \delta_{22}, \delta_{23}, \delta_{31}; & \text{(VII)} & \pi_{22}, \pi_{23}, \pi_{31}; \\ \text{(IV)} & \delta_{21}, \delta_{26}; & \text{(VIII)} & \pi_{21}, \pi_{22}. \end{array} \tag{3.44}$$

We formulate as separate assertions an important property that was implicitly used by Ryabov and Gashenenko for classification of bifurcation diagrams and rough Fomenko invariants (we discuss these problems in more detail below). Proposition 8 shows that all rank-0 singularities have complexity 1 (the notion of the complexity was introduced in [8]). Proposition 9 shows that, moreover, two such points cannot lie on the same level of first integrals if the area constant is nonzero. The possibility of coincidence of values of all first integrals at distinct rank-0 points is important in the study of bifurcation diagrams of various moment mappings that appear in this problem. Note that in the literature there is no explicit and clear proofs of these two assertions.

Proposition 8. *For all values of first integrals, the connected component of the integral manifold cannot contain more than one rank-0 critical point.*

Proposition 9. *One of common levels of first integrals (different components of this level) contains two rank-0 points corresponding to the curve ℓ_0 on the plane (r, λ). All other common levels of first integrals contain a rank-0 point, and such a point is unique.*

Proof. All rank-0 point belong to the subsystem $\mathcal{M}_1$. We fix $\lambda \neq 0$. By (1.25), a rank-0 point is uniquely determined by the values h, p, and r, where r is a multiple root of the polynomial (1.26). If we assume that there exist two multiple roots, i.e., that $4R(r) = -(r-r_1)^2(r-r_2)^2$, where $r_1 \neq r_2$, then we obtain the system

$$r_2 = -r_1, \quad p = 0, \quad r_2^2 = 2h, \quad r_2^4 - 4h^2 + 4 = 0.$$

Thus, for given λ, h, and p a rank-0 critical point is unique (if exists). Now we fix λ and h and assume that a (ℓ, k) is determined by two different $p_1 \neq p_2$. From (1.30) we obtain two possibilities. The first possibility is $p_1 = -p_2$, and from the relation $h - \lambda^2/2 = p_1^2$ we obtain $\ell = 0$; this is the curve ℓ_0 whose preimage contains two points with the same r but with opposite p. If $p_1 + p_2 \neq 0$, then we obtain the system

$$p_1^2 + p_1p_2 + p_2^2 = h - \frac{\lambda^2}{2}, \quad p_1^2 + p_2^2 = \frac{1}{6}(h - \frac{\lambda^2}{2}),$$

which is obviously inconsistent. Thus, if $R(r)$ has a multiple root, then this root is determined by h and p uniquely and, moreover, these values are uniquely determined by ℓ and k. Proposition 9 is proved. □

Note that for $\ell \neq 0$ this also implies Proposition 8. For $\ell = 0$, the proof of Proposition 8 easily follows from Gashenenko's solution presented above.

Thus, in the Kovalevskaya–Yehia case, *all* rank-0 points have complexity 1.

In [18], a weaker assertion was stated (without proof) in which cases that separate various types of bifurcation diagrams of the mapping (2.10) in the plane (ℓ, λ) are not considered. This separating set Θ_L was found by Ryabov [27–29]. In [18], nonseparating values of the pair (ℓ, λ) were called *nonbifurcation*. As the proof of Proposition 9 shows, the bifurcation character of the pair (ℓ, λ) is irrelevant to the complexity of a rank-0 point.

The equations of the curves of the Ryabov separating set Θ_L can be found, e.g., in [46]. This set classifies bifurcation diagrams of the mappings $\mathcal{J}_\ell(\lambda)$. We calculate the set $\widehat{\Theta}$, i.e., the image in the octant $\{(\ell, \lambda) : \ell \geq 0,\ \lambda \geq 0\}$ of the curves π_{ij}, which are separating curves in the classification of rank-0 points, together with their limit points for $\lambda = 0$. Keeping the notation of the images of curves we obtain

$$\pi_{21}: \quad \ell = \frac{1}{2\lambda^{1/3}}\sqrt{1-\lambda^{4/3}}, \qquad 0 \leq \lambda \leq 1;$$

$$\pi_{22}: \quad \ell = \frac{1}{\sqrt{2}}\left(\sqrt{1+\lambda^4} - \lambda^2\right)^{3/2}, \qquad \lambda \geq 0;$$

$$\pi_{23}: \quad \begin{cases} \ell = \dfrac{(4-x^4)^{3/2}}{4x^3}, \\ \lambda = \dfrac{3x^4-4}{2x^3}, \end{cases} \qquad x \in \left[\sqrt[4]{4/3}, \sqrt{2}\right]; \tag{3.45}$$

$$\pi_{24}: \quad \ell = \frac{|\sqrt{4+\lambda^{4/3}} - 2\lambda^{2/3}|}{\sqrt{2}\left(\sqrt{4+\lambda^{4/3}} - \lambda^{2/3}\right)^{1/2}}, \qquad \lambda \geq 0;$$

$$\pi_{31}: \quad \begin{cases} \ell = \dfrac{(4-x^4)^{3/2}}{4x^3}, \\ \lambda = \dfrac{3x^4-4}{2x^3}, \end{cases} \qquad x \in \left[-\sqrt[4]{4/3}, 0\right).$$

Recall that the curve $\pi_0 = \{r = 0, \lambda \geq 0\}$ is not a separating curve in the class δ_2 in the sense of the equivalence relation introduced above. Therefore, its whole image $\{\ell = 0, \lambda \geq 0\}$ is not contained

in the separating set: Θ_L contains only endpoints of the curves π_{2j}: $\lambda = 0, 1, \sqrt{2}$. Thus, we see that $\Theta_L \setminus \widehat{\Theta}$ consists of one curve $\ell = (4\lambda)^{-1}$ whose sense will be clarified below. It was proved in [50] that this curve corresponds to the extremal value of the integral L in the family of rank-1 degenerate critical points. Therefore, the majority of surgeries of bifurcation diagrams of the mappings $\mathcal{J}_\ell(\lambda)$ occur in the cases where the reduced system possesses a *degenerate* rank-0 critical point, whereas the set Θ_L of bifurcation pairs (ℓ, λ) is, except for a single curve, the image of degenerate rank-0 points. The set Θ_L is irrelevant to the possibility of the situation where several rank-0 critical points are contained in the same integral level.

Note that Theorem 9 in [18] (and the same Theorem 8 in [32]), in some sense, plays a key role for the nondegeneracy of rank-0 points corresponding to *nonbifurcation* values (ℓ, λ). This fact is the basis of their further classification and description of marked loop molecules and, as a consequence, we can find some marks on Fomenko graphs. However, this part of the assertion, which is obvious in the analysis of Eqs. (3.45), has not been proved in [18, 32]. It was indicated that for all nonbifurcation values (ℓ, λ), the verification of nondegeneracy conditions can be performed by a computer. However, the characteristic polynomials of the corresponding symplectic operators cannot be expressed through ℓ and λ. The same holds true for the verification of the condition that the subalgebra generated by the operators $\mathfrak{a}_H$ and $\mathfrak{a}_K$ is two-dimensional. It seems that this subalgebra is always two-dimensional, but this hypothesis is invalid. Above we have presented a set of values of parameter for which the subalgebra is one-dimensional.

We also note that the paper [32] contains a reference to [3], concerning, in particular, information on the number of families of tori in chambers, which allows one to construct loop molecules for rank-0 points (in [18], the number of families is invalid). The paper [3] also does not contain a proof since it is based on numerical simulations with a hypothetical algorithm that allows one to choose one initial point on each of the corresponding regular tori (and, in particular, to find the number of these points) for an arbitrary set of constant first integrals. However, such an algorithm has not been constructed in [3]. The following Ryabov hypothesis was also used (this is known from reports in conferences; see, e.g., [2]): each regular torus in P^5 is related to the subset $\{\omega_2 = 0,\ \alpha_2 = 0\}$; this hypothesis has not been proved.

The papers [30, 44] appeared before [32].

In [30, 44], explicit exact analytic expressions for eigenvalues of symplectic operators were obtained; these expressions allow one to find the type of critical points. The paper [44] contains an exact analytic classification of rank-0 points with respect to the degenerateness, with respect to their types in the nondegenerate case, and with respect to the complete common level of first integrals, and the first (and unique at the present moment) rigorous proof of the nondegenerateness of rank-0 points outside Ryabov's separating set.

3.3. Smale diagrams and isoenergetic surfaces. For the Kovalevskaya problem ($\lambda = 0$), the bifurcation diagram for energy and area integrals was constructed by Jacob [60]. Using the Smale construction (the reduced bundle of unit spheres over the domain where the motion is possible), he also found the topological type of isoenergetic manifolds that are three-dimensional levels of the "reduced Hamiltonian" (3.2)

$$Q^3_{\ell,h} = \big\{\zeta \in P^4_\ell : H_\ell(\zeta) = h\big\}. \tag{3.46}$$

In this case, the diagram $\mathcal{S}_{LH}$ of the mapping

$$L{\times}H : P^5 \to \mathbb{R}^2$$

consists of the two parabolas

$$\delta^0_1 :\ h = -1 + \ell^2, \quad \delta^0_2 :\ h = 1 + \ell^2$$

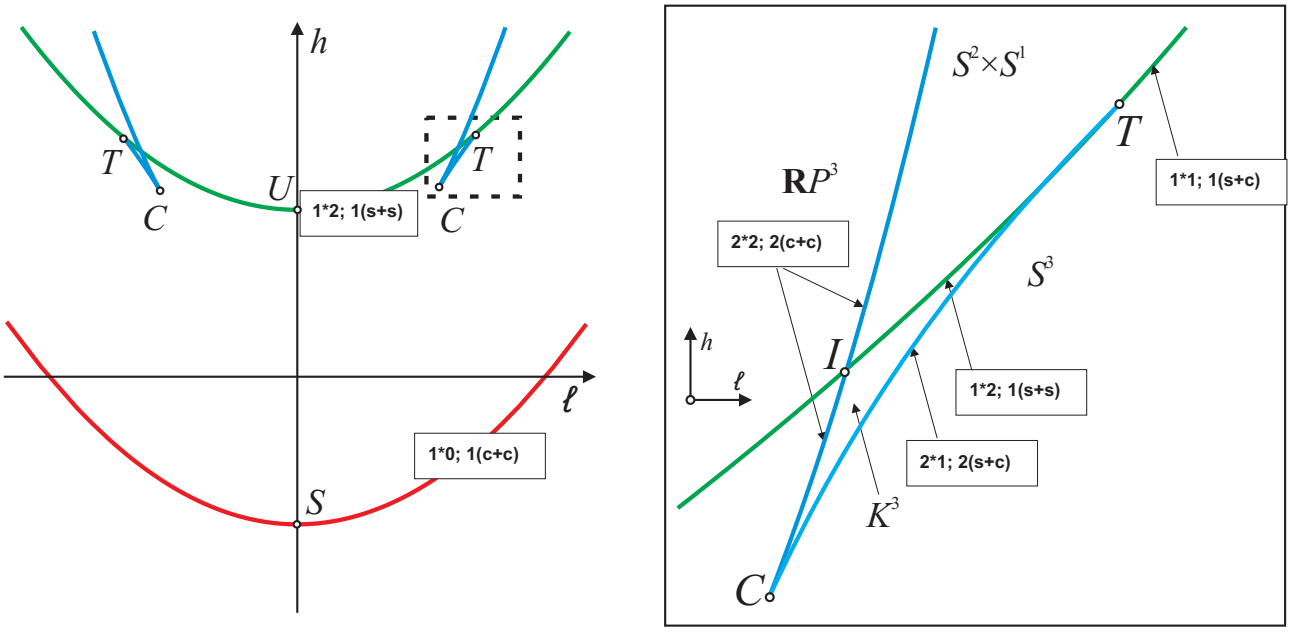

Fig. 4. Smale diagram of the classical problem

and the pair of curves whose equations can be written in the parametric form:

$$\delta_3^0:\ \ell=\frac{x^2+4}{4\sqrt{2x}},\quad h=\frac{3x}{4}+\frac{1}{x},\quad x\in(0,2]; \tag{3.47}$$

these curves are symmetric with respect to the axis Oh. These values are attained at relative equilibria whose phase coordinates are

$$\omega_1=-\sqrt{\frac{x}{2}},\qquad \omega_2=0,\qquad \omega_3=\frac{\sqrt{4-x^2}}{2\sqrt{x}},$$
$$\alpha_1=-\frac{x}{2},\qquad \alpha_2=0,\qquad \alpha_3=\frac{\sqrt{4-x^2}}{2},$$

where $\sqrt{x}$ and $\sqrt{4-x^2}$ are algebraic radicals. The curves (3.47) touch the upper parabola at the points $(\pm1,2)$ and pass it transversally at the points

$$\left(\pm\sqrt{2(\sqrt{2}-1)},2\sqrt{2}-1\right).$$

The cusps have the coordinates $\left(\pm2/3^{3/4},\sqrt{3}\right)$; they correspond to $x^2=4/3$ (note that $\omega_3^4=4/3$).

The isoenergetic surfaces are empty in the domain $h<-1+\ell^2$. For other domains they are diffeomorphic to the following manifolds (see Fig. 4):

$$S^3,\quad K^3=(S^2\times S^1)\#(S^2\times S^1),\quad S^2\times S^1,\quad \mathbb{R}P^3. \tag{3.48}$$

The smoothness type $Q^3_{\ell,h}$ at each point (ℓ,h) can be found by the index of the Morse function H_ℓ at its critical points lying in the preimages of bifurcation curves that arrive at the point (ℓ,h) along a vertical line from a point that lies sufficiently low and has a nonadmissible value of h (i.e., from a point $Q^3_{\ell,h}=\varnothing$).

Now we recall the results for the classical problems (see, e.g., [8, 38, 39, 57]; note that explicit calculations have never been published). The characteristic polynomials of the operator $\mathfrak{a}_H$ are obrained

from (3.33) by passage to the limit:

$$\begin{aligned}
&\delta_1^0: \quad \chi_H(\mu) = \left(\mu^2 + \frac{1}{2}\right)\left[\mu^2 + (1+\ell^2)\right],\\
&\delta_2^0: \quad \chi_H(\mu) = \left(\mu^2 - \frac{1}{2}\right)\left[\mu^2 - (1-\ell^2)\right],\\
&\delta_3^0: \quad \chi_H(\mu) = (\mu^2 + r^2)\left[\mu^2 - \frac{1}{4}\Big(\sqrt{4+r^4} - 2r^2\Big)\right].
\end{aligned} \tag{3.49}$$

Therefore, on the lower parabola, all rank-0 critical points in the preimage have type "center-center," whereas on the upper parabola they have type "saddle-saddle" on a bounded segment between two points of tangency with the third curve T; these points are symmetric with respect to the axis Oh (in particular, rotations where the center of mass occupies the highest position for $|\ell| < 1$ are unstable with respect to all variables). Further, these critical points have type "saddle-center" on unbounded segments outside the points of tangency (rotations where the center of mass occupies the highest position for $|\ell| > 1$ are stable with respect to some variables). The preimage of each point of the parabola contains one critical point of such type. On the curves (3.47), the preimage contains two points of type "saddle-center" for $r^4 < 4/3$ (on bounded segments between the cusps C and the points of tangency T) and two points of type "center-center" for $r^4 > 4/3$ (on unbounded segments from the cusps to infinity). The type is independent of the passing through a transversal point I along a smooth branch.

Due to the mechanical nature of the Hamiltonian H_ℓ, its Morse index is equal to the Morse index of the "effective potential," i.e., the function defined on the Poisson sphere whose sublevels are domains where the motion is possible (domains of possible motion). The effective potential for the Kovalevskaya—Yehia case calculated by the Smale scheme has the form

$$U_{\ell,\lambda} = -\alpha_1 + \frac{(2\ell - \lambda\alpha_3)^2}{2[2(\alpha_1^2 + \alpha_2^2) + \alpha_3^2]}.$$

For the coordinate-free calculation of the Morse index of the restriction of the function of three variables $f(\alpha_1, \alpha_2, \alpha_3)$ to the Poisson sphere (1.3), we use the following assertion.

Lemma 3. *Consider the differential operator*

$$\Xi = \boldsymbol{\alpha} \times \frac{\partial}{\partial \boldsymbol{\alpha}} \tag{3.50}$$

that generates the second group of equations (3.3). *Let* $\boldsymbol{\alpha}_0 \in S^2 = \{\boldsymbol{\alpha} : |\boldsymbol{\alpha}| = 1\}$ *be a critical point of the restriction of the function* $f(\boldsymbol{\alpha})$ *to* S^2, *which is nondegenerate in the sense of Morse. The Morse index of the function* f *at the point* $\boldsymbol{\alpha}_0$ *is equal to the number of negative roots of the polynomial*

$$\xi_f(\mu) = \frac{1}{\mu}\det\Big[(\Xi^2 f)(\boldsymbol{\alpha}_0) - \mu E\Big].$$

Applying this lemma to the function $U_{\ell,0}$, we obtain

$$\begin{aligned}
&\delta_1^0: \quad \xi_H(\mu) = (\mu - 1)\big[\mu - (\ell^2 + 1)\big],\\
&\delta_2^0: \quad \xi_H(\mu) = (\mu + 1)\big[\mu - (\ell^2 - 1)\big],\\
&\delta_3^0: \quad \xi_H(\mu) = \left[\mu + \frac{1}{2}\Big(\sqrt{4+r^4} + r^2\Big)\right]\left[\mu - \frac{r}{\sqrt{4+r^4}}\Big(\sqrt{4+r^4} - 2r^2\Big)\right].
\end{aligned}$$

We obtain the arrangement of Morse indexes and types along bifurcation curves shown in Fig. 4. The notation $n * m$ means that the preimage contains n points of index m, and the symbols $c + c$, $s + c$, and $s + s$ show the type of the point ("center-center," "saddle-center," or "saddle-saddle").

It is known that if the value h passes through a critical value, then the following surgeries of the domain of possible motion (projections of the energy level to the configuration space) occur:

supplement of the disk D^2 for index 0, pasting a handle for index 1 (a single disk becomes a disk with a hole, i.e., a ring, or produces a single disk from two disks), and sealing a hole with a disk for index 2.

We draw a vertical line $\ell = \text{const}$ on the plane $\mathbb{R}^2(\ell, h)$ between the points I and T. Along this line, the Hamiltonian and the effective effective potential have the critical values

$$h_1 = -1 + \ell^2 < h_2 < h_3 = 1 + \ell^2 < h_4;$$

the numbers of critical points in the preimage are 1, 2, 1, and 2, respectively, and their indexes are 0, 1, 2, and 2. The corresponding domains of possible motion on the sphere are as as follows: a disk, a disk with two holes (a sphere with three holes), a ring (a sphere with two holds), and a sphere. Reduced bundles of unit circles over these domains yield the manifolds (3.48), respectively.

In the general case, calculations for $\lambda > 0$ yield the following Morse indexes.

Theorem 6. *The roots of the characteristic polynomial $\xi_H(\mu)$ at the critical points* (3.8) (*in the notation of Proposition* 2) *are as follows*:

$$\mu_1 = -\frac{1}{2}\Big[r(r-\lambda) + d\Big],$$
$$\mu_2 = -\frac{1}{2(r-\lambda)d}\Big[(2r-\lambda)(r-\lambda) - d\Big]\Big[(2r-\lambda)(r-\lambda)r + \lambda d\Big].$$

In particular, the sign of μ_1 is always opposite to the sign of d; therefore, μ_1 is positive in the domain δ_1 and is negative in the domains δ_2 and δ_3. The sign of μ_2 is determined by the position of the point (r, λ) relative to the separating curves $\overline{\pi}$, π_0, π_{23}, π_{24}, and π_{31}. Finally, the Morse index of the effective potential $U_{\ell,\lambda}$ and the Hamiltonian $H_{\ell,\lambda}$ is equal to

(i) 0 *in the domain δ_1*;
(ii) 1 *in the domains δ_{23}, δ_{27}, and δ_{31}*;
(iii) 2 *in the domains δ_{21}, δ_{22}, δ_{24}, δ_{25}, δ_{26}, δ_{28}, and δ_{32}.*

In Fig. 5, we present the pairs of Morse indexes and information necessary for for analysis of modifications of the Smale diagram for nonzero λ (see below).

Remark 6. In Fig. 5, we use the following notation for two key values of the parameter λ:

$$\lambda_* = 1/2^{3/4}, \quad \lambda^* = (4/3)^{3/4}. \tag{3.51}$$

The first of them is the ordinate of the node point P_0, where several separating curves meet. The second value is the minimum of λ on the curve ℓ_0 determined by Eq. (3.43). These important values will be useful in the sequel.

The evolution of Smale diagrams is as follows. When λ becomes nonzero, the curve δ_1^0 is transformed to δ_1; it ceases to be a parabola, but no singular points appear on it. Each connected part of the curve δ_3^0 followed by two critical points splits, and one of the segments obtained from the bounded segment joins with the branch of the curve δ_2^0 lying above the point T. The curve δ_3 appears: each of its components is symmetric with respect to Oh and consists of twi infinite branches that meet at the cusp (the perturbation of C). The second part of δ_3^0 and the curve δ_2^0 generate the curve δ_2; the triangle CTI on it generates a swallowtail on it. Taking into account the Morse indexes known, we obtain the situation shown in Fig. 6. This type of diagram is valid for all $\lambda \in (0, \lambda_1)$, where λ_1 is the value of the parameter such that the rightmost cusp on the curve δ_2 (corresponding to the separating curve π_{24}) lies on the curve δ_3. The existence of such a value was predicted earlier on the basis of numerical simulation [27–29], but nobody can calculate it analytically. Modern system of analytical calculations allows one to perform this. We write the system of equations starting from (3.11) and (3.40) (we must choose the sign $d > 0$):

$$\ell(r, \lambda) = \ell(r_0, \lambda), \quad h(r, \lambda) = h(r_0, \lambda), \quad r_0 = \frac{1}{2}\left(\lambda - \lambda^{1/3}\sqrt{4 + \lambda^{4/3}}\right). \tag{3.52}$$

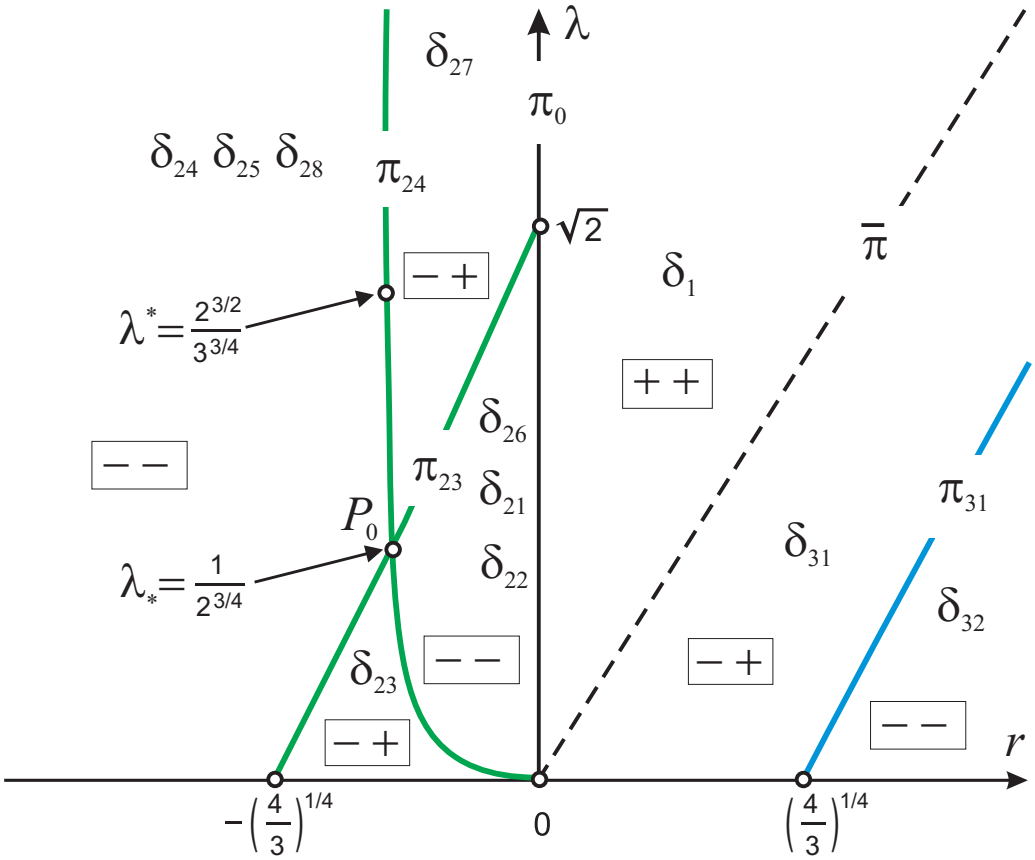

Fig. 5. Morse indexes of the effective potential

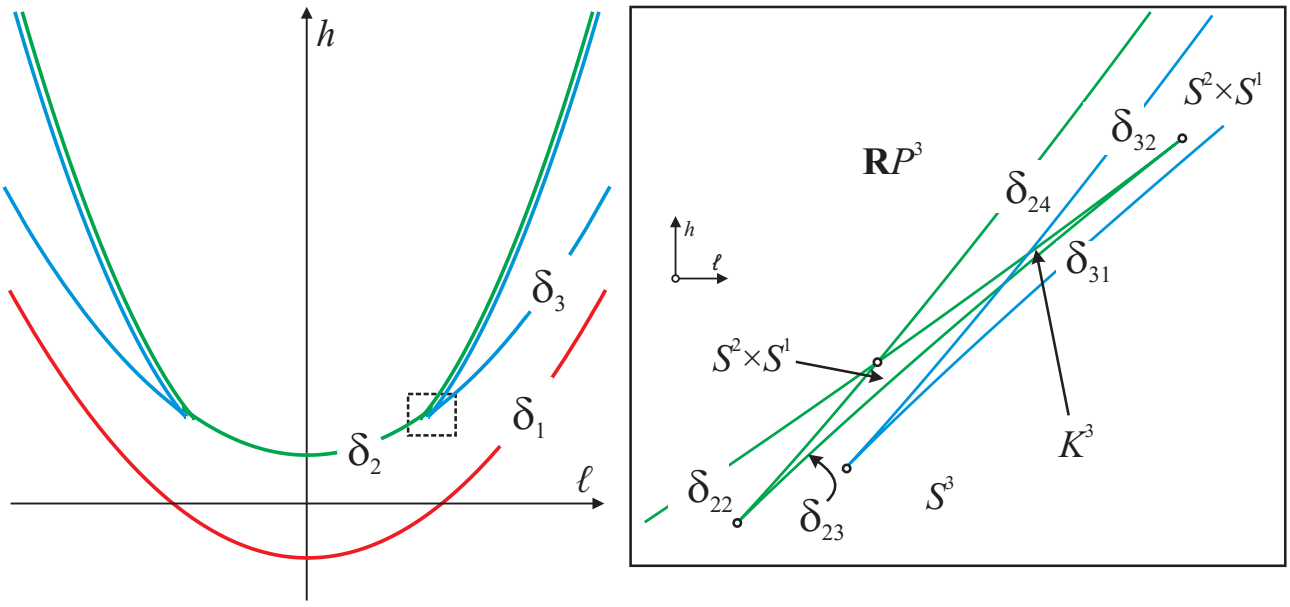

Fig. 6. Diagram $\mathcal{S}_{LH}$ for small λ

Note that it describes not only all possible cases where the point π_{24} lies on the curve δ_3, but also the hypothetic possibility of the case where this point lies on the other branch of the curve δ_2. We eliminate r_0 and r from this system assuming that $r_0 \neq r$. We proceed as follows. First, we eliminate the radical of d in the first two equation, substitute r_0, and perform the change of variables $U = \lambda^{1/3}$. The two equations obtained can be cancelled by $(2r - U^3 + U\sqrt{4+U^4})^2$ (this corresponds to the case $r = r_0$). We arrive at the system

$$\begin{aligned} p_{13}(U,r) + (U^3 - r)p_8(U,r)\sqrt{4+U^4} = 0, \\ p_{25}(U,r) + (U^3 - r)p_{20}(U,r)\sqrt{4+U^4} = 0, \end{aligned} \tag{3.53}$$

where $p_i(U,r)$ is a polynomial of degree i with respect to U. We calculate the resultant of the left-hand sides with respect to r in the substitution $X = (U^2 + \sqrt{4+U^4})^2$; this corresponds to the change of variables

$$X = (\lambda^{2/3} + \sqrt{4+\lambda^{4/3}})^2. \tag{3.54}$$

We obtain the equation

$$(X-8)^2(X^2-16)^4(X+4)^2P_1(X)P_2(X) = 0,$$

where

$$\begin{aligned} P_1 &= X^4 - 24X^3 + 720X^2 - 2048X - 3072, \\ P_2 &= 4X^{15} - 293X^{14} + 7864X^{13} - 70320X^{12} - 831232X^{11} + 26316032X^{10} - 263235584X^9 \\ &\quad + 1223192576X^8 - 2241200128X^7 + 323747840X^6 + 1465909248X^5 - 16521363456X^4 \\ &\quad - 25736249344X^3 - 74155294720X^2 - 75161927680X - 17179869184. \end{aligned}$$

Under the obvious condition $X \geq 4$, which is implied by (3.54), the equation $P_2(X) = 0$ has a unique real root $X \approx 11.2707$, for which $\lambda \approx 1.1268$ and the unique common real root of Eqs. (3.53) is $r \approx 0.002089 \in (0, \lambda)$, i.e., we do not obtain points from $\delta_{2,3}$. If we assume that we have obtained a point on δ_1, then we must choose the sign $d < 0$ in Eqs. (3.52), but then the values (r, λ) obtained above do not satisfy these equations. Thus, all roots of the polynomial $P_2(X)$ are extraneous. The condition $X = 8$ leads to the separating value $\lambda_* = 1/2^{3/4}$, which corresponds to the meeting of both cusps and the self-intersection point of the curve δ_2. The equation $P_1(X) = 0$ has a unique admissible root $X \approx 4.3418$ for which $\lambda \approx 0.02349$ and a unique common real root $r \approx 1.47328 \in (\lambda, +\infty)$ of Eqs. (3.53). Therefore, this value of λ corresponds to the required case $\pi_{24} \in \delta_3$. In addition, we have proved that the cusp π_{24} cannot lie on the other branch δ_3. We denote the separating value λ by $\lambda_1 \approx 0.0235$. The exact result is as follows:

$$\begin{aligned} \lambda_1 &= \left(-\frac{7}{6} - \frac{1}{12}p_2 + \frac{1}{2}\sqrt{-\frac{205}{9} + \frac{3823}{4}p_1^{-1/3} - \frac{1}{4}p_1^{1/3} + \frac{16393}{9p_2}} \right)^{3/4}, \\ p_1 &= 1045767 + 183872\sqrt{34}, \quad p_2 = \sqrt{-410 - 34407p_1^{-1/3} + 9p_1^{1/3}}. \end{aligned} \tag{3.55}$$

For $\lambda > \lambda_1$, the curves δ_2 and δ_3 do not have other common points (see Fig. 7). In particular, the domain in which $Q^3_{\ell,h} = K^3$ (the superposition of the "angle" δ_3 and the "tail" of the curve δ_2) disappears.

Further surgeries of the Smale diagram are related only to evolution of the curve δ_2. In this case, degenerate rank-0 critical points generating the separating curves π_{21} and π_{22} do not affect the diagram itself since they lie on its smooth segments. On passing through λ_*, the "ends of the tail" are swapped (see Fig. 8); this can be easily seen if one draw a horizontal line ($\lambda = \text{const}$) in Fig. 5 and move it upward.

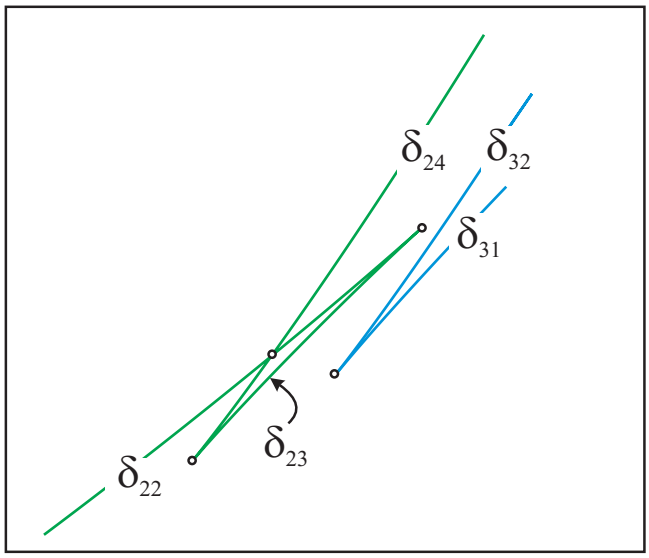

Fig. 7. A fragment of the diagram $\mathcal{S}_{LH}$ for $\lambda > \lambda_1$

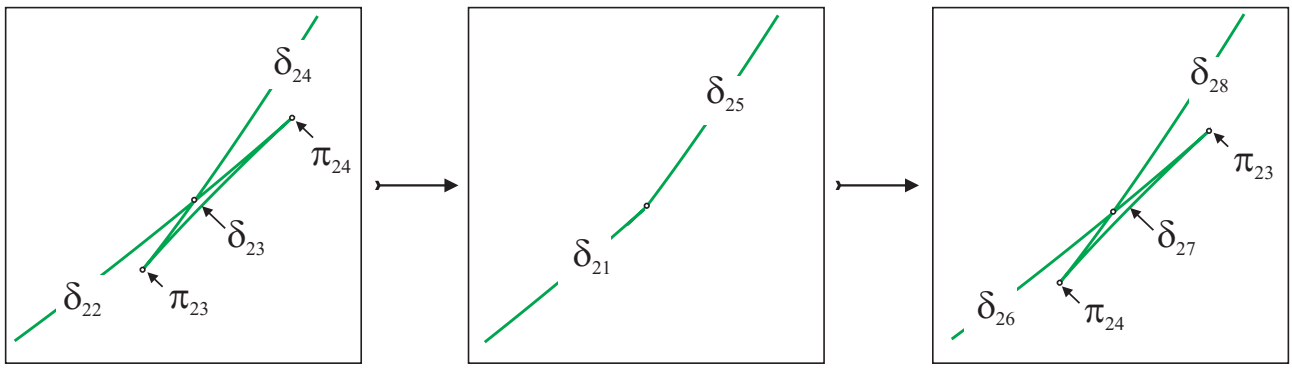

Fig. 8. Passing through λ_*

Now we examine the possibility of the case where the cusp of the curve π_{23} lies on the other branch of the curve δ_2. For this case, based on (3.37), we write the system

$$\ell(r,\lambda) = \ell(r_0,\lambda), \quad h(r,\lambda) = h(r_0,\lambda),$$
$$r_0 = \frac{x^4-4}{2x^3}, \quad \lambda = \frac{3x^4-4}{2x^3}, \quad x^4 - 2rx^3 - 4 \neq 0, \quad x \in \left(\sqrt[4]{4/3}, \sqrt{2}\right].$$

Eliminating r_0, r, and λ from this system, we arrive at the equation for $X = x^4$:

$$(X-2)^2 Q_1(X) Q_2(X) = 0,$$

where

$$\begin{aligned} Q_1 &= 3X^4 + 32X^3 - 180X^2 + 96X - 64, \\ Q_2 &= 6903X^{11} - 153216X^{10} + 1489200X^9 - 9324352X^8 + 44169408X^7 \\ &\quad - 160186880X^6 + 425104384X^5 - 806682624X^4 + 1108361216X^3 \\ &\quad - 1120534528X^2 + 784072704X - 285212672. \end{aligned}$$

The equation $Q_2(X)=0$ does not have roots in the interval $X\in(4/3,4]$ and the equation $Q_1(X)=0$ has exactly one root in this interval:

$$X=\frac{1}{3}\left(\sqrt{308+\frac{435}{q_1}+3q_1+\frac{3400}{q_2}}-q_2-8\right),$$
$$q_1=\left(2951-408\sqrt{34}\right)^{1/3},\quad q_2=\left(154-\frac{435}{q_1}-3q_1\right)^{1/2}.$$

Respectively, in terms of λ, we have the equation

$$64\lambda^{16}+2784\lambda^{12}-274803\lambda^8+15476896\lambda^4-45349632=0$$

with a unique real solution $\lambda_2\approx 1.3263$. Its exact value is

$$\begin{aligned}
\lambda_2&=\left(-\frac{87}{8}-\frac{1}{16}p_2+\frac{1}{2}p_3\right)^{1/4},\\
p_1&=10467417865895+1809781698048\sqrt{34},\\
p_2&=\sqrt{213478-1093516839p_1^{-1/3}+9p_1^{1/3}},\\
p_3&=\sqrt{\frac{106739}{16}+\frac{1093516839}{64}p_1^{-1/3}-\frac{9}{64}p_1^{1/3}+\frac{88449457}{16p_2}}.
\end{aligned}\tag{3.56}$$

Other changes are related to the axis Oh (see [29]). The constant ℓ vanishes not only at equilibrium positions of the body ($r=0$), but also under the condition (3.43) that follows from (3.11). The corresponding curve (above it was denoted by ℓ_0) is shown in Fig. 2. The minimum of λ on this curve is equal to $\lambda^*=(4/3)^{3/4}$. Therefore, except for the points $h=\pm1$ and $\ell=0$, which always exist, the diagram has two additional points of intersection with the axis Oh for $\lambda^*<\lambda<\sqrt{2}$ and one point for $\lambda>\sqrt{2}$. This collection of points on the axis Oh is reconstructed at the moment when two of these points coincide. One can easily calculate that this occurs when $\lambda=2\sqrt{\sqrt{2}-1}\approx 1.2872\in(\lambda^*,\sqrt{2})$. Thus, we have the types of diagrams whose significant fragments are shown in Fig. 9:

(a) $\lambda_*<\lambda<\lambda^*$;
(b) $\lambda^*<\lambda<2\sqrt{\sqrt{2}-1}$;
(c) $2\sqrt{\sqrt{2}-1}<\lambda<\lambda_2$;
(d) $\lambda_2<\lambda<\sqrt{2}$;
(e) $\lambda>\sqrt{2}$.

Taking into account the Morse indexes calculated above, we obtain the arrangement of isoenergetic manifold shown in the same figure.

We prolong the symmetry (3.17) to the whole phase space:

$$\mathrm{symm}:(\omega_1,\omega_2,\alpha_3)\mapsto(-\omega_1,-\omega_2,-\alpha_3).\tag{3.57}$$

It states an isomorphism of phase flows on $Q^3_{\ell,h}$ and $Q^3_{-\ell,h}$. Recall that in correspondence with (3.19), the extended Smale diagram

$$\Lambda(\mathcal{S}_{LH})=\bigcup_{\lambda}\mathcal{S}_{LH}(\lambda)\times\{\lambda\}$$

appears in the space $\Lambda(\mathbb{R}^2(\ell,h))=\mathbb{R}^3(\ell,h,\lambda)$. It divides the space $\mathbb{R}^3(\ell,h,\lambda)$ into open connected components called *chambers*. Due to the symmetry symm, we also accept the agreement that the union of two components symmetric with respect to the plane $\ell=0$ forms a single chamber. We obtain the following assertion.

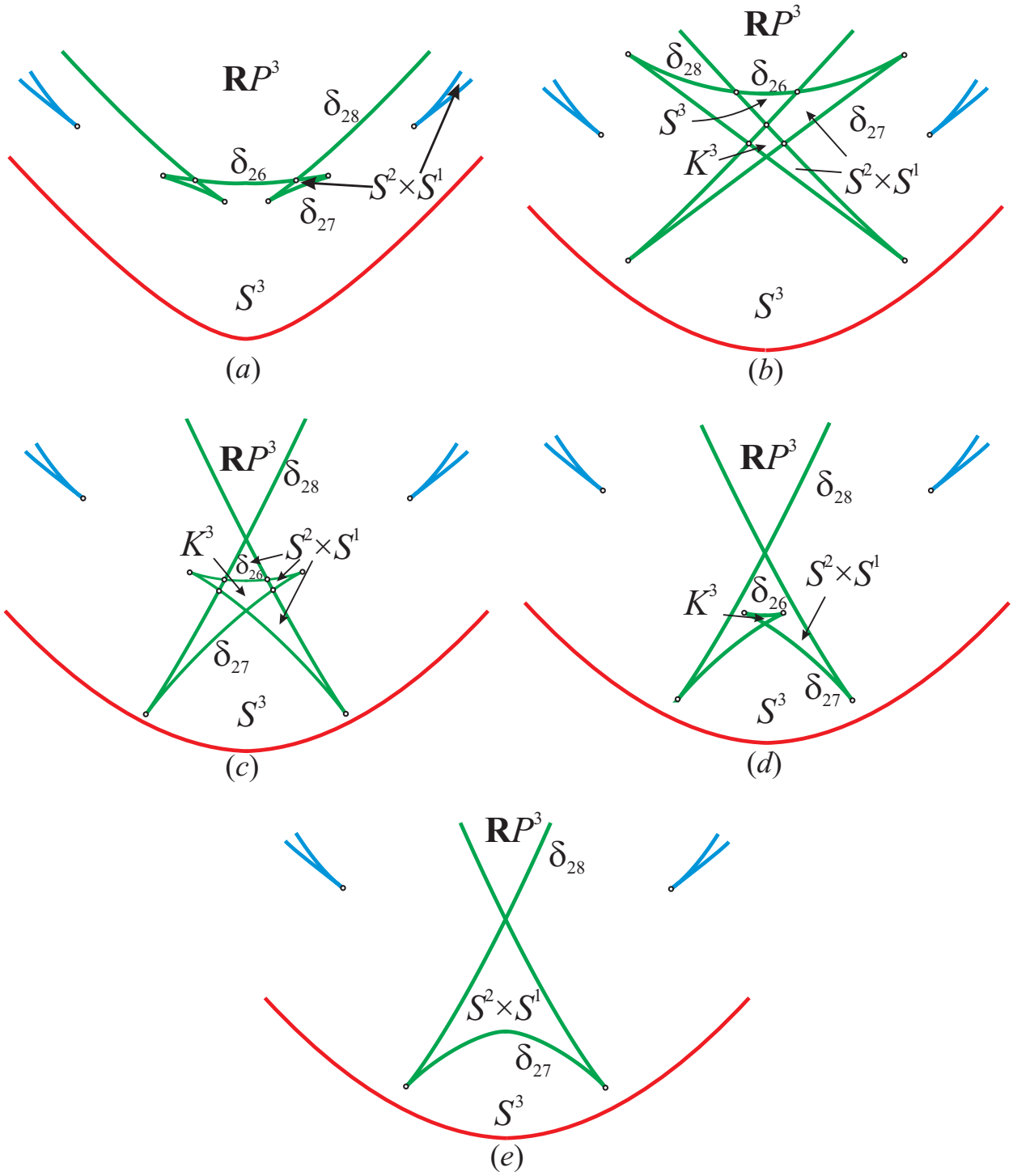

Fig. 9. Surgeries of $\mathcal{S}_{LH}$ on the axis Oh

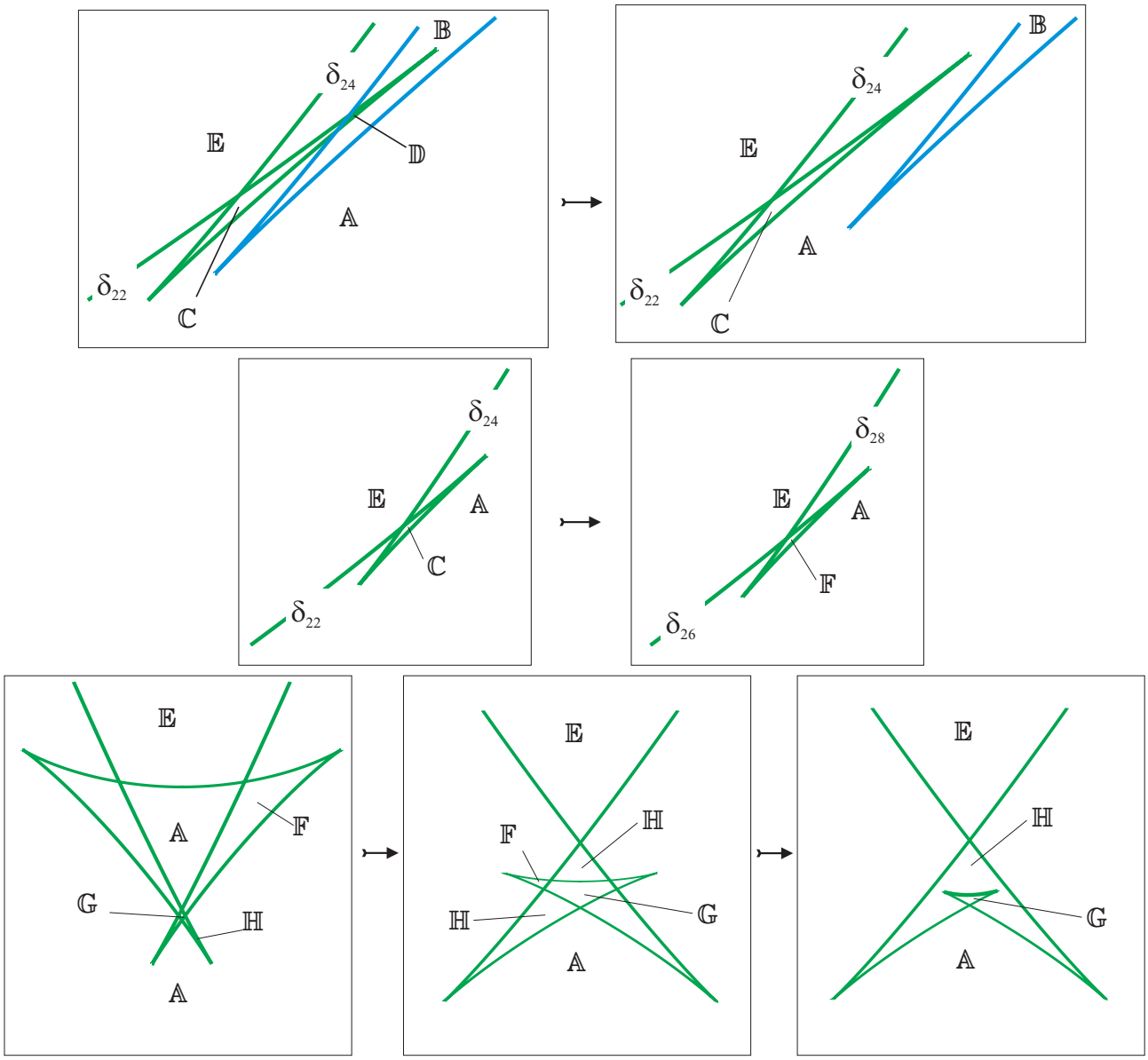

Fig. 10. Chambers of the Smale diagram

Theorem 7. *In the Kovalevskaya–Yehia case, there exist seven Smale diagrams* $\mathcal{S}_{LH}(\lambda)$ *that are structurally stable with respect to the parameter* λ *. The separating values of the parameter* λ *are*

$$0, \quad \lambda_1, \quad \lambda_* = 1/2^{3/4}, \quad \lambda^* = (4/3)^{3/4}, \quad 2\sqrt{\sqrt{2}-1}, \quad \lambda_2, \quad \sqrt{2},$$

where λ_1 *and* λ_2 *are defined by the relations* (3.55) *and* (3.56)*. The extended diagram* $\Lambda(\mathcal{S}_{LH})$ *divides the space* $\mathbb{R}^3(\ell, h, \lambda)$ *into eight chambers* $\mathbb{A}, \ldots, \mathbb{H}$ *with nonempty manifolds* $Q^3_{\ell,h}(\lambda)$*. Corresponding information is represented in Fig.* 10 *and in Table* 3.1*.*

Now we examine generic critical points that appear in rank-1 systems with two degrees of freedom.

Table 3.1

Code of chamber	Lifetime w.r.t. λ	Numbers of components in chamber	$Q^3_{\ell,h}$
$\mathbb{A}$	$\lambda \in [0, +\infty)$	1	S^3
$\mathbb{B}$	$\lambda \in [0, +\infty)$	2	$S^2 \times S^1$
$\mathbb{C}$	$\lambda \in (0, \lambda_*)$	2	$S^2 \times S^1$
$\mathbb{D}$	$\lambda \in [0, \lambda_1)$	2	K^3
$\mathbb{E}$	$\lambda \in [0, +\infty)$	1	$\mathbb{R}P^3$
$\mathbb{F}$	$\lambda \in (\lambda_*, \lambda_2)$	2	$S^2 \times S^1$
$\mathbb{G}$	$\lambda \in (\lambda^*, \sqrt{2})$	1	K^3
$\mathbb{H}$	$\lambda \in (\lambda^*, +\infty)$	2	$S^2 \times S^1$

4. Classification of Rank-1 Critical Points

4.1. Formulas for calculation the type. We study the type of rank-1 critical points in the first critical subsystem, i.e., points of the set'$\mathcal{M}_1 \backslash \mathcal{C}^0$.

Proposition 10 (P. E. Ryabov [30])**.** *The type of rank-*1 *critical points in the first critical subsystem is completely defined by the eigenvalues of the symplectic operator* $\mathfrak{a}_{F_1}$*, where*

$$F_1 = K - 2\nu H, \tag{4.1}$$

and the undefined multiplier at the corresponding point is equal to $\nu = p^2$*. The characteristic polynomial of the operator* $\mathfrak{a}_F$ *has the form*

$$\chi_{F_1}(\mu) = \mu^2 - 4C_1, \quad C_1 = \left[\frac{3}{2}s - \left(h - \frac{\lambda^2}{2}\right)\right]\left[2s^2 - 2\left(h + \frac{\lambda^2}{2}\right)s + 1\right].$$

*Rank-*1 *points are degenerate if and only if*

$$\left[\frac{3}{2}s - \left(h - \frac{\lambda^2}{2}\right)\right]\left[2s^2 - 2\left(h + \frac{\lambda^2}{2}\right)s + 1\right] = 0 \tag{4.2}$$

and have type "center" for $C_1 < 0$ *and type "saddle" for* $C_1 > 0$*.*

Proof. In the coordinates $(\boldsymbol{\omega}, \boldsymbol{\alpha})$, the Hamiltonian field generated by the function F_1 at the points (1.25) has the form

$$\operatorname{sgrad} F_1 = 2(p^2 - \nu)\left\{0,\ 0,\ \sqrt{R(r)},\ r\sqrt{R(r)},\ -\frac{1}{2}R'(r), -p\right\};$$

it vanishes for $\nu = p^2$. We note that for other values ν, the condition $\operatorname{sgrad} F_1 = 0$ implies that $R(r)$ and $R'(r)$ simultaneously vanish, which leads to immovable points, i.e., rank-0 critical points.

Recall that due to (2.13)

$$s = h - \frac{\lambda^2}{2} - p^2.$$

Owing to Eqs. (1.25), the calculation of the polynomial $\chi_{F_1}(\mu)$ for the manifold $\mathcal{M}_1$ is easy. Thus, if $C_1 \neq 0$, then rank-1 critical points are nondegenerate. Let $C_1 = 0$. Assume that at such a point, there exists another combination $G = \nu_1 K - 2\nu_2 H$ satisfying the relation $\operatorname{sgrad} G = 0$. By the assumption $\operatorname{rank}\{K, H\}|_{P^4_\ell} = 1$ we obtain that the undefined multipliers are proportional:

$$dF = dK - 2\nu dH|_{P^4_\ell} = 0, \quad dG = \nu_1 dK - 2\nu_2 dH|_{P^4_\ell} = 0 \quad \Rightarrow \quad \nu_2 = \nu_1 \nu.$$

This implies that $\nu_1 \neq 0$, i.e., the characteristic numbers of the operator $\mathfrak{a}_G$ are proportional to (zero) characteristic numbers of the operator $\mathfrak{a}_{F_1}$ and hence they are also equal to zero. Therefore, the integral generating a regular element in the algebra of symplectic operators does not exist at the points (4.2). □

We have presented this proof since the results of [41] (where the function (2.16) was used for the construction of the system $\mathcal{M}_1$) cannot be applied immediately. The roots of the characteristic polynomial also vanish on the set $s = 0$, which implies the relation $\ell = 0$. The appearance of this extraneous singularity is explained by the degeneration of the Reiman–Semenov-Tyan-Shansky integral (see [41]) in L^2.

Proposition 11 (P. E. Ryabov [30])**.** *The type of rank-*1 *critical points in the second and third critical subsystems is completely defined by the eigenvalues of the symplectic operator* $\mathfrak{a}_{F_2}$*, where*

$$F_2 = K + \left(2\lambda^2 - \frac{1}{s}\right) H \tag{4.3}$$

and s *is the value that determine the point* (1.28)*. The characteristic polynomial of the operator* $\mathfrak{a}_{F_2}$ *has the form*

$$\chi_{F_2}(\mu) = \mu^2 - C_2,$$
$$C_2 = -\frac{1}{s^3}\left(8\lambda^2 s^3 - 1\right)\left[2s^2 - 2\left(h + \frac{\lambda^2}{2}\right)s + 1\right] = \frac{2}{s^2}\left(8\lambda^2 s^3 - 1\right)\left(2\lambda^2 s^2 - s + 2\ell^2\right).$$

*All rank-*1 *points in* $\mathcal{M}_2$ *are nondegenerate and have type "center." Rank-*1 *points in* $\mathcal{M}_3$ *are degenerate if and only if*

$$\left(8\lambda^2 s^3 - 1\right)\left[2s^2 - 2\left(h + \frac{\lambda^2}{2}\right)s + 1\right] = 0,$$

and have type "center" for $C_2 < 0$ *and type "saddle" for* $C_2 > 0$*.*

Proof. Setting $F_2 = K + \nu H$, we obtain from (1.27) and (1.28)

$$\operatorname{sgrad} F_2 = (2\lambda^2 s - 1 - \nu s)\left\{\frac{\mathcal{G}\varkappa\rho X}{\sqrt{s}},\ -\frac{\rho\, n_1}{2\varkappa s},\ \frac{2\mathcal{G}\varkappa Y}{\sqrt{s}},\ \frac{\mathcal{G}(n_1 + 2\varkappa^3 XY)}{\varkappa\sqrt{s}},\ \frac{n_2}{s^2},\ \frac{\mathcal{G}(\lambda\rho s X + \ell Y)}{\sqrt{s}\varkappa}\right\},$$

where

$$n_1 = -\ell\rho X + \lambda s Y + 2\varkappa^3 XY, \quad n_2 = \varkappa X + sXY(3\ell\rho - 4\varkappa^3 Y) + \lambda s^2(2 - 3Y^2).$$

If $2\lambda^2 s - 1 - \nu s \neq 0$, then this vector vanishes only under the condition

$$64\ell^6\lambda^2 s^4 + 4\ell^4 s^2\Big(-1 + 20\lambda^2 s - 4\lambda^4 s^2 + 48\lambda^4 s^4\Big)$$
$$- 4\ell^2 s\Big(1 - 8\lambda^2 s + 4\lambda^4 s^2 + 20\lambda^2 s^3 - 4\lambda^4 s^4 + 8\lambda^6 s^5 - 48\lambda^6 s^7\Big)$$
$$- (1 - 4s^2)\Big(1 - 2\lambda^2 s + 4\lambda^4 s^4\Big)^2 = 0.$$

This condition can be obtained as follows. Note that in the case where $X = 0$ and $Y = \pm 1$ the vector $\operatorname{sgrad} F_2$ does not vanish even if $\rho = 0$. Therefore, $\mathcal{G} = 0$. Expressing X from this relation, we substitute in relations for n_1 and n_2, calculate the resultants with respect to Y, and find the required relation for ℓ and s. Since the condition found does not become an identity on the surfaces $\Pi_{2,3}$, it determines a one-dimensional subset. On the other hand, it becomes an identity for the corresponding expressions of ℓ and s through r and λ from (3.11) and (3.15); therefore, it corresponds to the curves δ_i, $i = 1, 2, 3$, i.e., it is valid at rank-0 critical points. Thus, at rank-1 critical points, the relation

$$2\lambda^2 s - 1 - \nu s = 0$$

holds, and the function (4.3) is a required integral that determines the type of these points.

The direct calculation of the characteristic polynomial leads to the required expression for $\chi_{F_2}(\mu)$. Obviously, for $s < 0$ the value C_2 is always negative, whereas for $s > 0$ it can have various signs, which determine the corresponding type of singular points. The fact that critical points are degenerate for $C_2 = 0$ (i.e., there is no another element in the algebra of symplectic operators that has nonzero eigenvalues) is proved similarly to Proposition 10 (actually, this follows from the fact that the coefficient of K can be chosen equal to 1). □

We see that for all critical points (rank-0 and rank-1), the characteristic polynomial of the defining symplectic operator depends only on constant first integrals. Therefore, the following important property is valid.

Theorem 8. *All critical points of the same rank lying on the same common level of the first integrals L, H, and$K$ have the same type.*

In particular, this implies that the molecule denoted by W_7 in [14, 16] is impossible in the problem considered. Below we show that this molecule cannot be realized by a significant cause.

We introduce some terms related to the study of critical subsystems.

It is known (see [8]) that geometric singularities of bifurcation diagrams of integrable systems with n degrees of freedom correspond to rank-m ($m < n-1$) critical points and rank $(n-1)$ degenerate critical points. It has not yet been proved in the general case that this correspondence is bijective. Additional singularities appear in families of Hamiltonian systems obtained by the factorization procedure of a system with symmetry. The problem considered here is an example of such situation. The surface Π_1 has a singularity of the type "self-intersection," which appears in all planar sections of it except for the sections $\ell = \text{const}$ (the curve $s = 0$ in the representation (2.7) and the singular parabola in the representation (2.10)). Among sections by a fixed constant of area, the section $\ell = 0$ is singular due to the presence of a singular "multiple" parabola.

Definition 8. A nondegenerate rank-1 critical point is said to be *multiple* if the bifurcation diagram Σ of the moment mapping $J = L \times H \times K$ is not a smooth two-dimensional surface in a neighborhood of its image.

Recall that the rank of a critical point is its rank in the reduced system with two degrees of freedom; this number is one less than its rank with respect to the mapping J.

Since the structure of a neighborhood of a nondegenerate rank-1 critical point in $Q^3_{\ell,h}$ is similar to the structure of one of standard atoms and can preserve its structure under small variations of h, we conclude that such a multiple point cannot be detected by a local analysis of singularity in the reduced system with two degrees of freedom on P^4_ℓ. We can only conclude that to some points on arcs of the bifurcation diagram of the system on P^4_ℓ, several critical circles correspond. In this case, the decay of a multiple point can occur under a perturbation of ℓ, i.e., under the passing to another system with two degrees of freedom. In the general integrable cases of problems of the dynamics of a rigid body, the zero level of the cyclic integral L is always singular in this sense. There are other causes for a point to become a multiple point. For example, as in the problem considered, rank-0 points can lie on the same level with rank-1 points. Then this "multiplicity" is irrelevant since rank-0 points also affect the surgery diagram. Finally, the system can also contain "decaying" topologically instable atoms. This effect was described in [8]; it also cannot be detected by local analysis. Note that topologically instable atoms appeared in specific mechanical systems of the classical dynamics of rigid bodies (see [40]), but the decay itself did not occur. The decay of a topologically instable atom was analyzed by numerical simulation in [22] for a system on the sphere (the so-called Dullin–Matveev case, [58]), which is a particular case of an integrable system constructed by Yehia [70]). Various versions of similar surgeries of fibrations on three-dimensional isoenergetic levels were described in [66]. Recently, decaying atoms were detected in subsystems of an irreducible problem on the motion of a rigid body in a double field; however, this effect is closely related to degeneration of the induced symplectic structure (see [63]).

Definition 9. A *key set* in P^5 is the union of all rank-0 critical points and degenerate and multiple rank-1 critical points. We denote the key set by $\mathcal{K}$. The intersection $\mathcal{K}_j = \mathcal{K} \cap \mathcal{M}_j$ is called the *key set* of the critical subsystem $\mathcal{M}_j$.

Definition 10. Let Φ and Ψ be first integrals (possibly, particular) of the critical subsystem $\mathcal{M}_j$ that are independent almost everywhere. The image of the key set $\mathcal{K}_j$ under the mapping $\Phi \times \Psi : \mathcal{M}_j \to \mathbb{R}^2$ is called the (Φ, Ψ)-diagram of the subsystem $\mathcal{M}_j$

Definition 11. If an integral mapping $\mathcal{M}_j \to \mathbb{R}^k$ exists, then its image is called an *admissible domain*; notation $\mathcal{D}_j$. Points of the admissible set is said to be admissible.

In other words, values of integrals are admissible if they correspond to some motions (the integral manifold is nonempty). It will be clear from the context which mapping is considered and to which space admissible points belong.

In [48, 50], (S, H)- and (S, L)-diagrams of critical subsystems were studied. Here S is a particular integral that appears from the Lax representation, whose constant is a parameter on surfaces in Eqs. (2.7) and (2.8). If we introduce the function with undefined Lagrange multipliers to describe critical subsystems by the formulas (2.16), (2.17), and (2.18), then this integral naturally appears as the coefficient of the integral K. For the classification of bifurcations that appear when the point (ℓ, h, k) crosses the surfaces Π_j in $\mathbb{R}^3(\ell, h, k)$, it is convenient to choose a plane of constants of functionally independent integrals of critical subsystems whose admissible points are in a bijective correspondence with points of the corresponding bifurcation surfaces (then, for example, information on the number of rank-0 points or rank-1 circles in the preimage becomes definite).

We also consider the problem of classification of bifurcation diagrams $\Sigma_{HK}(\ell, \lambda)$ of the mappings $H \times K$ of reduced systems on P^4_ℓ (see [46, 50]) and bifurcation diagrams $\Sigma_{LK}(h, \lambda)$ of the mappings $L \times K$ restricted to four-dimensional isoenergetic levels $Q^4_h = H^{-1}(h)$ in P^5 (see [48]). These diagrams are the sections of the bifurcation diagram $\Sigma(\lambda)$ of the general integral mapping $J = L \times H \times K$ by the planes $\ell = \text{const}$ and $h = \text{const}$, respectively. Due to the free physical parameter λ, one can consider the problem on the search for the so-called *separating set* in the corresponding plane (λ, ℓ) or (λ, h). We state a general assertion that allows one to state an algorithm of construction of separating sets.

Let $F : P^5 \to \mathbb{R}$ be a general integral of the system. We fix $f \in \mathbb{R}$ and consider the mapping

$$J_{(F,f)} = J|_{F^{-1}(f)} : F^{-1}(f) \to \mathbb{R}^2,$$

where $\mathbb{R}^2$ is the plane of values of a pair of integrals that supplement F to a complete involutive triple of integrals that are independent almost everywhere. Let $\sigma_{(F,f)}(\lambda)$ be the bifurcation diagram of the mapping $J_{(F,f)}$. Clearly, if the pair of integrals U, V supplements F to an involutive triple of functionally independent integrals, we can naturally identify $\sigma_{(F,f)}(\lambda)$ with the bifurcation diagram $\Sigma_{UV}(f, \lambda)$ of the restriction of the mapping $U \times V$ to the submanifold $F^{-1}(f)$. In particular, below we consider the case where $F = L$ (in this case, $\sigma_{(L,\ell)}(\lambda) = \Sigma_{HK}(\ell, \lambda)$), and where $F = H$ (in this case, $\sigma_{(H,h)}(\lambda) = \Sigma_{LK}(h, \lambda)$).

Proposition 12 (M. P. Kharlamov [43, 45])**.** *Consider the set Θ_F in the plane (λ, f) such that the type of the diagram $\sigma_{(F,f)}(\lambda)$ changes after passing through it. The set Θ_F consists of pairs (λ, f), where f is the critical value of the restriction of the function F to the key set $\mathcal{K}$ for a given λ.*

If necessary, one can state this statement rigorously, clarifying the notions of diagrams of the same type and critical values of functions on a stratified manifold. In particular, we assume that the integral F is "rationally" selected and has no critical points on regular levels of the moment mapping. One of possible approaches using the concept of equipped admissible intervals was proposed in [50]. In practice, it means the following. For each critical subsystem $\mathcal{M}_j$, we consider its (G, F)-diagram, where G is an integral on $\mathcal{M}_j$, which is functionally independent of F. Critical values of F on $\mathcal{K}$ correspond to nodal points of this diagram (the images of degenerate rank-0 critical points), extreme

values of the coordinates f on smooth domains that are the images of the set of degenerate or multiple rank-1 critical points, and various self-intersections of smooth domains of the diagram.

The set Θ_F is called the separating set in the classification of bifurcation diagrams $\sigma_{(F,f)}(\lambda)$. For brevity, we call it the *F-atlas*.

4.2. Specification. The first critical subsystem. For the first critical subsystem, none xof the pairs of functionally independent integrals (S, H) or (S, L) solves the problem of providing a bijection of the selected plane and the surface Π_1. Indeed, on the (s, h)-plane, *each admissible point* satisfying the condition

$$h - \frac{\lambda^2}{2} - s > 0$$

has two preimages on the surface Π_1, whereas in the (s, ℓ)-representation, the *whole admissible segment of the parabola*

$$k = 1 + \left(h - \frac{\lambda^2}{2}\right)^2, \quad \ell = 0, \quad h \geq \frac{\lambda^2}{2}, \tag{4.4}$$

corresponding to the value $s = 0$ on the surface Π_1, is mapped to the same point. Thus, this correspondence is either two-valued on a set of full measure, or there is a "bad singularity," i.e., a point possessing an infinite number of preimages lying on the surface. Note that since the surface Π_1 contains a self-intersection line, a bijective parametrization does not exist. However, one can provide a parametrization in which each point of the self-intersection line naturally corresponds to a pair of points on the parameter plane. For this, we choose a particular integral $P = \omega_1$ on $\mathcal{M}_1$ instead of S. Then Eqs. (1.30) yield a bijective correspondence of admissible domains on the (p, h)-plane and the surface Π_1, with the following obvious sole exception: any interior point of the segment of the parabola (4.4), i.e., for $h > \lambda^2/2$, corresponds to two points with opposite signs of p. Next, we consider the diagrams and key sets of the subsystem $\mathcal{M}_1$ in terms of (p, h); taking into account the problem on the classification of bifurcation diagrams $\Sigma_{HK}(\ell, \lambda)$ and $\Sigma_{LK}(h, \lambda)$, we also present the description of the (S, H)- and (S, L)-diagrams for $\mathcal{M}_1$.

To find topological invariants, such as Fomenko graphs, one needs to know another indicator, namely, the Morse–Bott index of K integral at nondegenerate rank-1 critical points (i.e., the Morse index of the restriction of K to a small domain transversal to the trajectory consisting of rank-1 points). It gives information on the behavior of critical circles on the isoenergetic surface $Q^3_{\ell,h}(\lambda)$ if the value of the additional integral increases. In the space of these three integrals, we can trace events that occur when a line parallel to the axis Ok intersects the corresponding bifurcation surface Π_i. The form of the functions (4.1) and (4.3)(1.3) allows one to perform the corresponding calculations explicitly.

At points of the manifold, we find a couple of vectors that define a domain transversal to the critical circle (at the rank-1 critical point). We choose this domain so that it is orthogonal to the vectors $\operatorname{grad}\Gamma$, $\operatorname{grad} L$, $\operatorname{grad} H$, and $\operatorname{sgrad} H$. Note that on any trajectory (1.24), (1.25), the variable r oscillates between the roots of the polynomial (1.25); hence we can choose a point x_0 on the trajectory at which $R(r) = 0$. Then the tangent plane to the transversal domain is spanned by the vectors

$$v_1 = \big(0,\ 1,\ 0,\ 0,\ 0,\ 0\big), \quad v_2 = \left(\lambda + r,\ 0,\ -4p,\ 2p(\lambda - r),\ 0,\ 2\left(h - p^2 - \frac{r^2}{2}\right)\right).$$

These vectors are obtained from the equations for $u = (u_1, \ldots, u_6)$:

$$u \cdot \operatorname{grad}\Gamma = 0, \quad u \cdot \operatorname{grad} L = 0, \quad u \cdot \operatorname{grad} H = 0, \quad u \cdot \operatorname{sgrad} H = 0$$

under the conditions $(u_2, u_3) = (1, 0)$ and $(u_1, u_2) = (0, \lambda + r)$.

At the point x_0, the function K achieves the conditional extremum on the common level $Q^3_{\ell,h}$ of the functions Γ, L, and H in P^6 . In particular, x_0 is a critical point of the function with undefined Lagrange multipliers

$$K_1 = K - 2\nu H - \varkappa_1 L - \varkappa_2 \Gamma.$$

Obviously, the part of this function that does not contain the Casimir functions L and Γ coincides with (4.1), i.e., $\nu = p^2$. We directly calculate that $\varkappa_1 = 4p$ and $\varkappa_2 = 1$.

The type of a conditional extremum is determined by the restriction of the second differential of the function with Lagrange multipliers to the tangent space of the restriction manifold (see [1]). This fact was used in the study of the phase topology of Hamiltonian systems by A. A. Oshemkov (see [23]).

The restriction of d^2K_1 to the linear span of the vectors v_1 and v_2, under the condition $R = 0$, is a diagonal matrix with elements (eigenvalues)

$$\begin{aligned}
\mu_1 &= 4\left[h - \left(\lambda^2 + p^2\right) + \lambda r - \frac{1}{2}r^2\right] = 2\left[2s - \left(\lambda - r\right)^2\right],\\
\mu_2 &= -8\left(h - \frac{\lambda^2}{2} - 3p^2\right)\left[h - \frac{\lambda^2}{2} - 3p^2 - \frac{1}{2}\left(\lambda + r\right)^2\right]\\
&= -32\left(h - \frac{\lambda^2}{2} - \frac{3}{2}s\right)\left[h - \frac{\lambda^2}{2} - \frac{3}{2}s - \left(\lambda + r\right)^2\right].
\end{aligned}$$

In particular the product

$$\begin{aligned}
\mu_1\mu_2 &= 16\left(-2h + \lambda^2 + 6p^2\right)\left[1 - \left(2h - \lambda^2 - 2p^2\right)\left(\lambda^2 + p^2\right)\right]\\
&= -32\left(2h - \lambda^2 - 3s\right)\left[\left(2h + \lambda^2 - 2s\right)s - 1\right]\\
&= -64\left[\frac{3}{2}s - \left(h - \frac{\lambda^2}{2}\right)\right]\left[2s^2 - 2\left(h + \frac{\lambda^2}{2}\right)s + 1\right]
\end{aligned}$$

is independent of r and is determined by the location of the point (s, h) relative to the degeneracy curves of rank-1 critical points given by Eq. (4.2). Therefore, on nondegenerate trajectories, the values of μ_1 and μ_2 (they are called the Morse–Bott indexes) do not vanish and hence therefore do not change their signs.

Proposition 13. *If the integral K increases on the isoenergetic level $Q^3_{\ell,h}$, we have the following bifurcations at points of the critical subsystem $\mathcal{M}_1$ on nondegenerate critical circles*:

(1) *for elliptic trajectory (type "center"): the appearance of a torus if $\mu_1 > 0$ and $\mu_2 > 0$ (the atom A with the edge up); the disappearance of a torus if $\mu_1 < 0$ and $\mu_2 < 0$ (the atom A with the edge down);*

(2) *for a hyperbolic trajectory at a critical level of K for $\mu_1 > 0$ and $\mu_2 < 0$: the atom B with the "outer" edge ("head") up and a pair of "inner" edges ("feet") down; if $\mu_1 < 0$ and $\mu_2 > 0$, then we have the atom B with an "outer" edge ("head") down and a pair of "inner" edges ("feet") up;*

(3) *for the two hyperbolic trajectories at a critical level of K if two pairs (μ_1, μ_2) coincide: two atoms B whose directions of the "outer" edges is determined by the same rule (both "heads" up for $\mu_1 > 0$ and $\mu_2 < 0$ or both "heads" down for $\mu_2 > 0$);*

(4) *for the two hyperbolic trajectories at a critical level of K with different combinations of signs in the pairs (μ_1, μ_2): two A^* atoms.*

Proof. The proposition is obvious for elliptic trajectories (the function K has a local minimum or maximum on the transversal domain).

It can be shown that for hyperbolic trajectories the vector v_1 is directed into the exterior domain of the "figure-eight": the direction of the axis $O\omega_2$ is responsible for the transition from a critical surface to its enveloping torus. This can be easily obtained by analyzing, for example, projections of the integral manifolds on the plane $O\omega_1\omega_2$ (this analysis was partially performed in [16]). Clearly, similarly to the classical problem (see, e.g., [4, 17]) projections never have discontinuities in the direction of the axis $O\omega_2$. Now, if $\mu_1 > 0$, then this means that the function K on the transversal domain increases in the direction toward the "outer" circle and decreases in the direction toward the pair of "inner" circles.

If the sets of signs in the pairs (μ_1, μ_2) are different on two hyperbolic circles, then, suggesting the existence of two B-atoms with opposite directions of "heads," we obtain a bifurcation of three tori into three. As was noted in [14, 15], the number of tori at a regular level may be equal only to 1, 2, or 4 (for all chambers in $\mathbb{R}^3(\ell, h, k) \setminus \Sigma$, the number of regular tori can be strictly calculated below by using only obvious A-type atoms). Therefore, in this case, we would have a bifurcation of four tori into four tori. However, as we will see below, there is no such chambers in this problem. If we assume that at the point considered, there is a C_2-atom, then the analytic solution of problem (1.34)–(1.35) would contain a heteroclinic trajectory, but such a trajectory does not exist. Hence, there are two A^* atoms at this point. □

The criterion of the existence of motions in the system $\mathcal{M}_1$ is obvious (see [50, Proposition 1]). Since there is no "double" points on the (p, h)-plane, we can easily calculate the number of critical circles on the appropriate level of integrals.

Proposition 14. *For given p and h, real solutions of (1.25) exist if and only if $R(r) \geq 0$ for some $r \in \mathbb{R}$. If all roots of $R(r)$ are simple (i.e., there are no rank-0 critical points on the integral level considered), the number of periodic solutions is equal to the number of intervals on which $R(r)$ is nonnegative.*

Remark 7. Recall again that, due to the formulas (1.30), after the transition to the space $\mathbb{R}^3(\ell, h, k)$, any pair of points with opposite p from the preimage of the parabola (4.4) is mapped into the same point. In [14], this fact was noted as a special case.

Remark 8. Proposition 14 allows the following obvious generalization. If $R(r)$ has a multiple root (as was shown above, in this case it is a unique root), the number of periodic solutions is the same as the number of intervals *between simple roots* in which $R(r)$ is nonnegative. Now, taking into account Proposition 9, we obtain complete information on critical motions on the general level of common integrals that contain a rank-0 critical point of the corresponding class, since the number and location of roots of the polynomial $R(r)$ can be easily examined for all classes, based on the dependences $h(r, \lambda)$ and $p(r, \lambda)$ defined by the formulas (3.11) and (3.12). We present this information in the third column of Table 6.1; it will be used in the further study of the topology of full levels of integrals for rank-0 points.

Introduce the following notation:

$$\varphi_\pm(r) = \frac{1}{2}\left[r(\lambda - r) \pm \frac{2r - \lambda}{r - \lambda} D\right], \quad \psi_\pm(r) = \frac{r}{2}\left[-r \pm \frac{1}{r - \lambda} D\right], \qquad D = |d| = \sqrt{4 + r^2(r - \lambda)^2} > 0. \tag{4.5}$$

We denote by $h_C(\lambda)$ the value of the energy at the degenerate critical point π_{31} defined by (3.38). The index C is introduced since in the sequel we will mark the image of this degenerate point in the diagrams of critical subsystems by C. For a given $\lambda > 0$, the value of h_C is determined in accordance with (3.38) and (3.11) as follows:

$$\begin{cases} 3x^4 - 2x^3\lambda - 4 = 0, \\ x \in (-\sqrt[4]{4/3}, 0) \end{cases} \quad \Rightarrow \quad h_C = \frac{3}{8}x^2 + \frac{2}{x^6}. \tag{4.6}$$

Theorem 9. *The (P,H)-diagram of the critical subsystem $\mathcal{M}_1$ consists of the following sets*:

$$\begin{aligned}
&\delta_1: && p^2=\psi_-(r), \quad h=\varphi_-(r), && r\in[0,\lambda);\\
&\delta_2: && p^2=\psi_+(r), \quad h=\varphi_+(r), && r\in(-\infty,0];\\
&\delta_3: && p^2=\psi_+(r), \quad h=\varphi_+(r), && r\in(\lambda,+\infty);\\
&\Delta_1: && h-\left(3p^2+\frac{\lambda^2}{2}\right)=0, && \frac{\lambda^2}{2}\le h\le h_C(\lambda);\\
&\Delta_0: && h-\left(p^2+\frac{\lambda^2}{2}\right)-\frac{1}{2(\lambda^2+p^2)}=0, && p\in\mathbb{R};\\
&\ell_0: && h-\left(p^2+\frac{\lambda^2}{2}\right)=0, && p\in\mathbb{R}.
\end{aligned} \tag{4.7}$$

The boundary of the admissible $\mathcal{D}_1$ domain consists of the connected curve δ_1 and two connected components of the curve δ_3. The curve δ_2 is connected and breaks the admissible domain into two subdomains. The points of the domain below the curve δ_2 correspond to one critical circle, whereas the points of the domain above the curve δ_2 correspond to two critical circles.

Proof. Since all rank-1 critical points belong to $\mathcal{M}_1$ and the values of the functions P and H at these points are given by the formulas (3.8) and (3.11), we conclude, taking into account the notation (3.20), that the images of these points are the curves δ_i, $i=1,2,3$. The curves Δ_1 and Δ_0 are obtained from Proposition 10 and (2.13). The curve ℓ_0 corresponds to the singular parabola (4.4), which, as was noted above, is the image of the set of multiple points. It remains to clarify the conditions of the existence of motions in the system $\mathcal{M}_1$. These motions exist if and only if there exist intervals on which the polynomial $R(r)$ defined by the formula (1.26) is nonnegative. Since its discriminant set consists exactly of the curves δ_i, we see that such intervals exist between the curves δ_1 and δ_3, whereas below δ_1 (in the direction of the axis Oh) and above δ_3 such motions do not exist. Below the curve δ_2, the polynomial R has two real roots and hence there is only one interval (and one critical circle), whereas above this curve there are four roots and hence two intervals (and two critical circles). The part of the curve Δ_1 on which rank-1 critical points are degenerate and which is contained in the admissible domain is bounded from below by the natural boundary $h=\lambda^2/2$ and from above by the point of intersection with the curve δ_3 whose ordinate is the value $h_C(\lambda)$ described above. □

Theorem 10. *For nonnegative λ, surgeries of the (P,H)-diagrams of the critical subsystem $\mathcal{M}_1$ occur for the following values of the parameters*:

$$0,\ \lambda_*=\frac{1}{2^{3/4}},\ 1,\ \lambda^*=\left(\frac{4}{3}\right)^{3/4},\ \sqrt{2}.$$

Proof. Due to the choice of particular integrals that provide a bijective correspondence between the set key and its image (except for the cases noted above), if λ changes, surgeries of the diagrams occur simultaneously with surgeries of the set of rank-0 degenerate points and multiple points. Since all curves of degenerate and multiple points are known (see Fig. 2), these surgeries are as follows: if $\lambda=0$, then the point π_{21} disappears (the corresponding curve goes to infinity) and the points π_{22} and π_{24} merge; if $\lambda=\lambda_*$, then all curves of degenerate points of the class δ_2 merge at the double point P_0; if $\lambda=1$, then the point π_{21} disappears (the corresponding curve terminates); if $\lambda=\lambda^*$ (the minimum of λ on ℓ_0, see Remark 6), then multiple points appear; if $\lambda=\sqrt{2}$, then the point π_{23} disappears (the corresponding curve terminates). There are no other surgeries. □

In Fig. 11(a)–(e) the (P,H)-diagrams of the subsystem $\mathcal{M}_1$ stable with respect to the parameter λ are shown:

(1) $0<\lambda<\lambda_*$;

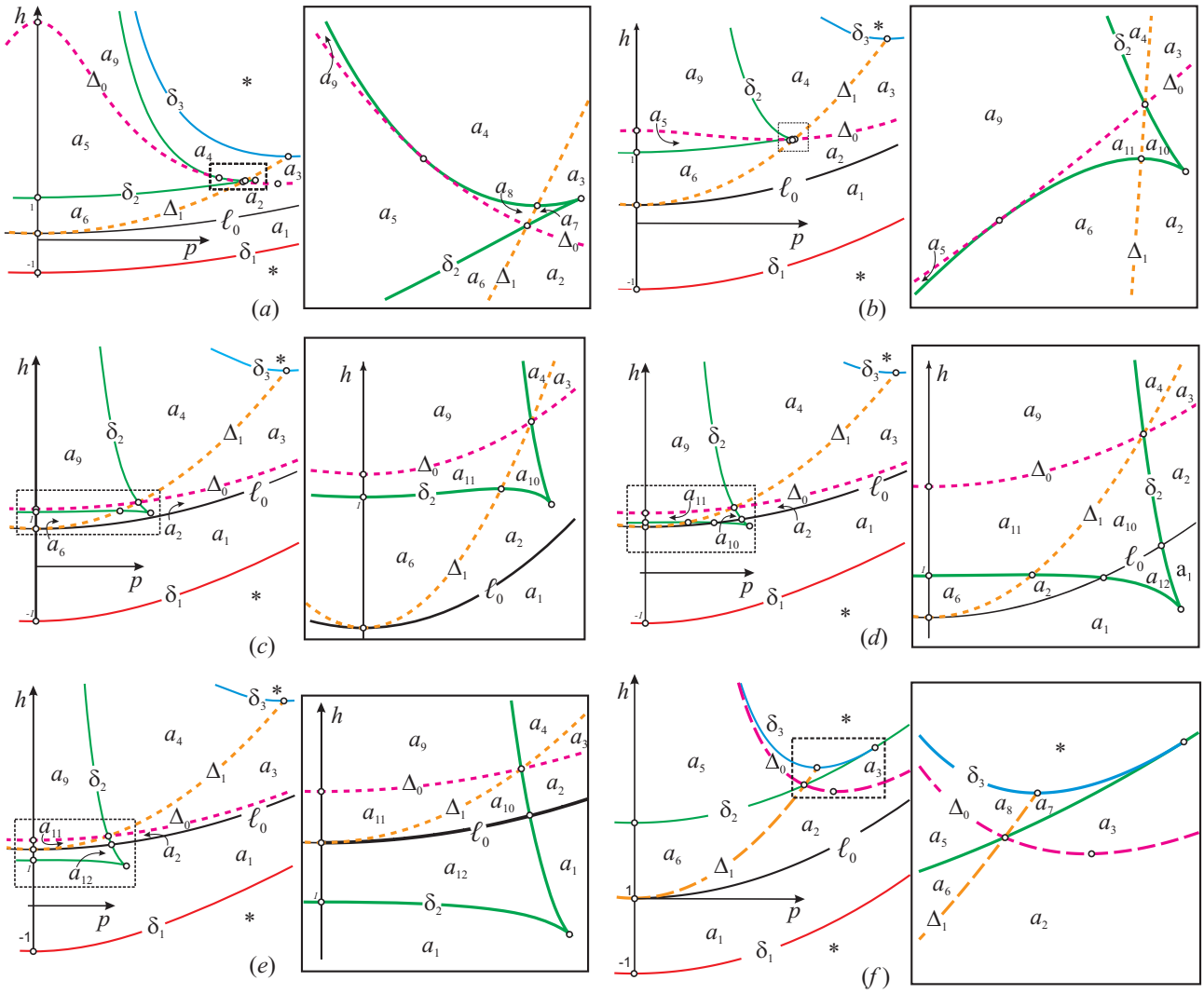

Fig. 11. (P,H)-Diagrams of the system $\mathcal{M}_1$ and its enlarged fragments

(2) $\lambda_* < \lambda < 1$;
(3) $1 < \lambda < \lambda^*$;
(4) $\lambda^* < \lambda < \sqrt{2}$;
(5) $\lambda > \sqrt{2}$.

The connected components of the admissible domain in the space $\{(p,h,\lambda)\}$ formed by the extended (P,H)-diagram are denoted by a_1–a_{12}. We recall the existence of the symmetry (3.57). Domains that pass one into the other under this mapping are denoted by the same symbols.

In terms of the types of critical points, the transition through the value $\lambda = \lambda^*$ does not imply any qualitative changes; the points of the domains a_{10} and a_{12} and their common boundary ℓ_0 are the same. For $\lambda = \lambda^*$, the curves δ_2 and ℓ_0 intersect; this demonstrates the exit point of the domain $a_{10} \cup a_{12}$ to the manifold $L = 0$ and allows one to compare bifurcations and atoms with the case $L = 0$, which was examined in detail by P. E. Ryabov and P. V. Morozov. Moreover, from the local point of view, critical points of the domains a_1 and a_2 and and their common boundary ℓ_0 are also the same. However, points of the bifurcation diagram Σ in $\mathbb{R}^3(\ell,h,k)$ generated by these domains differs by a nonlocal feature found in [11], which, in terms of the parameters (1.33), consists of the presence or

absence of regular tori on the complete joint levels of common integrals (two-frequency motions). This will be discussed below.

On flat sections $h = \text{const}$ or $\ell = \text{const}$ (i.e., isoenergetic bifurcation diagrams or bifurcation diagrams of reduced systems with two degrees of freedom on P^4_ℓ) of the surfaces Π_i, smooth arcs correspond to the domains a_j, where the type and number of singular points and the character of bifurcation are fully preserved, i.e., the atom that appears along a segment of small length that transversely crosses Π_i at the corresponding point.

For additional information, see Fig. 11(f), which shows the diagram of the first critical subsystem in the classical problem ($\lambda = 0$) corresponding to particularly remarkable motions of the fourth Appelrot class. It consists of two parabolas $h = \pm 1 + p^2$, the curve obtained from δ_3 and the part of δ_2

$$p = \pm\sqrt{\frac{1}{2}\left(\sqrt{4+r^4} - r^2\right)}, \quad h = \frac{1}{2}\left(2\sqrt{4+r^4} + r^2\right),$$

and the limit curves

$$\Delta_0 : h = \frac{1}{2}\left(2p^2 + \frac{1}{p^2}\right),\ p \in \mathbb{R}\backslash\{0\}, \quad \Delta_1 : h = 3p^2,\ p \in \left[0, \frac{1}{\sqrt[4]{3}}\right].$$

Analyzing all characteristics calculated for the domains a_j, we collect information in Table 4.1. Here we introduce the following notation for the atoms A and B: the index "+" means that the number of tori increases when K increases, whereas the index "−" respectively indicates decreasing. In other words, A_- means that the edge terminates at the top and A_+ means that the edge terminates at the bottom; B_- is the "outer" circle of the "figure-eight" ("head") at the top, B_+ is the "outer" circle of the "figure-eight" ("head") at the bottom. We see that all domains except for a_4 are related with the classical Kovalevskaya problem ($\ell = 0$) and to the problem with gyrostatic moment at zero area constant ($\ell = 0$). For these cases, bifurcations are found in the papers [38, 46] (for a detailed presentation for the Kovalevskaya case, see [39, 40]), and marks on the corresponding molecules are calculated in [7, 20]. Thus, in the column "Analogs" we provide references to the notation of parts [7, 20, 40] or paths crossing the corresponding parts [38, 46]. If an analog exists, all atoms were described in [38, 39, 46]. In these papers, a language for the description of atoms was proposed, including the orientation of asymmetric atoms (the concept of atoms did not exist at that time). Comparing them with analogs considered in [7, 20], one can specify many marked molecules.

Now it is possible to clarify the relationship between the parameters (1.33), conditions (1.36), and the classification of points of the first critical subsystem given here. For brevity, we denote by ℓ_0, Δ_1, and Δ_0 the values of the left-hand sides of the equations (4.7) of the corresponding curves (this will not lead to confusion). Then, in the notation (1.33), we have

$$L_1 = \frac{\ell_0}{8}, \quad L_2 = \frac{\Delta_1}{2}, \quad L_3 = \frac{\Delta_0}{2}. \tag{4.8}$$

From (4.5) and (4.7) we see that on the curve δ_1, there is a unique relationship

$$h = H_1(p), \quad p \in \mathbb{R},$$

and on the curve δ_3, for nonzero p, there is a unique relationship

$$h = H_3(p), \quad p \in \mathbb{R}\backslash\{0\}.$$

Moreover, for all $p \neq 0$, we have $H_3(p) > H_1(p)$. The curves δ_i form the discriminant set of the polynomial (1.26). If

$$h \in (-\infty, H_1(p)) \cup (H_3(p), +\infty), \tag{4.9}$$

this polynomial does not have real roots and, therefore, motions on $\mathcal{M}_1$ are impossible. We show that under the condition (1.30), motions in the domains (4.9) are also impossible on the whole manifold G^4 (we recall that G^4 is the complete preimage of the surface Π_1 in P^5 under the moment mapping J). For this, it suffices to note that at the point where the restrictions of the functions H and $P = \omega_1$ to the manifold G^4 are dependent, the rank of J does not exceed 2, so this point is critical of rank 0 or 1

Table 4.1

Domain (life time)	Number of circles	Morse–Bott indexes	Exit on $\lambda = 0/\ell = 0$	Atom	Analogs
a_1 $(0 \le \lambda < +\infty)$	1	$(-\,-)$	Yes/Yes	A_-	$2, 3$ [40, Fig. 6.3] a_1, a_2 [46, Fig. 2] γ_1, γ_4 [7, Fig. 11] α_2, α_3 [20, Fig. 1]
a_2 $(0 \le \lambda < +\infty)$	1	$(-\,-)$	Yes/Yes	A_-	$3, 3'$ [40, Fig. 6.3] a_2 [46, Fig. 2] γ_1, γ_4 [7, Fig. 11] α_2, α_3 [20, Fig. 1]
a_3 $(0 \le \lambda < +\infty)$	1	$(+\,-)$	Yes/No	B_-	9 [40, Fig. 6.3] γ_5 [7, Fig. 11]
a_4 $(0 < \lambda < +\infty)$	1	$(+\,+)$	No/No	A_+	Absent.
a_5 $(0 \le \lambda < 1)$	2	$(+\,-)$, $(-\,+)$	Yes/Yes	$2A^*$	6 [40, Fig. 6.3] a_4 [46, Fig. 2] γ_2 [7, Fig. 11] δ_1, δ_2 [20, Fig. 1]
a_6 $(0 \le \lambda < \sqrt{2})$	1	$(-\,+)$	Yes/Yes	B_+	5 [40, Fig. 6.3] b_2 [46, Fig. 3] γ_3 [7, Fig. 11] β_1 [20, Fig. 1]
a_7 $(0 \le \lambda < \lambda_*)$	2	$(+\,-)$, $(+\,-)$	Yes/No	$2B_-$	D [38, Fig. 2] γ_6 [7, Fig. 11]
a_8 $(0 \le \lambda < \lambda_*)$	2	$(+\,+)$, $(+\,+)$	Yes/No	$2A_+$	E [38, Fig. 2] γ_7 [7, Fig. 11]
a_9 $(0 < \lambda < +\infty)$	2	$(+\,+)$, $(-\,-)$	No/Yes	A_+, A_-	a_5 [46, Fig. 2] α_5, α_6 [20, Fig. 1]
a_{10} $(\lambda_* < \lambda < +\infty)$	2	$(-\,-)$, $(-\,-)$	No/Yes	$2A_-$	c_3, c_4 [46, Fig. 4] α_3, α_8 [20, Fig. 1]
a_{11} $(\lambda_* < \lambda < +\infty)$	2	$(-\,+)$, $(-\,+)$	No/Yes	$2B_+$	b_4 [46, Fig. 3] β_5, β_6 [20, Fig. 1]
a_{12} $(\lambda^* < \lambda < +\infty)$	2	$(-\,-)$, $(-\,-)$	No/Yes	$2A_-$	d_2, d_3 [46, Fig. 5] $\alpha_3, \alpha_8, \alpha_9, \alpha_{10}$ [20, Fig. 1]

and belongs to $\mathcal{M}_1$. Therefore, the maximal and minimal values of H for fixed P on G^4 coincide with these values on $\mathcal{M}_1$:

$$\max_{G^4\cap\{P=p\}} H = \max_{\mathcal{M}_1\cap\{P=p\}} H = H_3(p), \quad \min_{G^4\cap\{P=p\}} H = \min_{\mathcal{M}_1\cap\{P=p\}} H = H_1(p).$$

In this regard, we introduce the additional parameters

$$L_4 = h - H_1(p), \quad L_5 = h - H_3(p)$$

and the following notation for domains on the (p,h)-plane:

$$\overline{a_1} = \{(p,h) : L_4 < 0\}, \quad \overline{a_2} = \{(p,h) : L_5 > 0\}.$$

In particular, the facts proved above imply the following assertion on the existence of degenerate rank-1 critical motions in the first subsystem.

Proposition 15. *The admissible domain of the bifurcation diagram Σ of the moment mapping J consists of the following segments of singular points on the surface Π_1—the images of degenerate rank-1 critical motions*:

(1) *the whole curve along which the surfaces Π_1 and Π_3 touch*:

$$\Delta_0: \quad \begin{cases} \ell = \pm\sqrt{\dfrac{s}{2}\big(1-2\lambda^2 s\big)}, \\ h = \dfrac{1-\lambda^2 s+2s^2}{2s}, \end{cases} \qquad 0 < s \le \frac{1}{2\lambda^2};$$

(2) *the cusp of the surface Π_1 between its intersections with the curve δ_3*:

$$\Delta_1: \quad \ell = \pm\frac{2}{3\sqrt{3}}\left(h-\frac{\lambda^2}{2}\right)^{3/2}, \quad \begin{cases} \dfrac{\lambda^2}{2} \le h \le h_C(\lambda), \\ |\ell| \le \ell_C(\lambda), \end{cases}$$

or, in terms of the parameter s,

$$\Delta_1: \quad \begin{cases} \ell = \pm\sqrt{\dfrac{s^3}{2}}, \\ h = \dfrac{3}{2}s + \dfrac{\lambda^2}{2}, \end{cases} \qquad s \in [0, s_C(\lambda)], \tag{4.10}$$

where the functions $h_C(\lambda)$ and $\ell_C(\lambda)$ that determine the extrema of the corresponding coordinates on δ_3 for $\lambda \ge 0$ and the value of the s-coordinate $s_C(\lambda)$ at the extremum point are obtained from Eqs. (3.11) *and* (4.6) *by using the auxiliary parameter*:

$$\begin{cases} 3x^4 - 2\lambda x^3 - 4 = 0, \\ x \in \Big[-\sqrt[4]{4/3}, 0\Big) \end{cases} \quad \Rightarrow \quad \begin{cases} h_C = \dfrac{3}{8}x^2 + \dfrac{2}{x^6}, \\ \ell_C = \left|\dfrac{(4-x^4)^{3/2}}{4x^3}\right|, \\ s_C = \dfrac{4-x^4}{2x^2}. \end{cases}$$

The information in Table 4.2 supplements the results obtained in [14, 16] concerning the classification of motions on G^4.

The existence of of asymptotic motions or regular tori was proved in [14] by the analysis of explicit quadratures (1.34)–(1.35). Thus, we see that regular tori may be located on a critical level of the first integrals only in the neighborhood of type-A atoms, whereas asymptotic motions are, of course, form a part of hyperbolic atoms. The nonlocal distinction between pairs of points in the domains separated by the curve ℓ_0, i.e., points of the domains a_{10} and a_{12}, consists of the fact that at the level of common

Table 4.2

Domain (see [14])	Conditions	Domain of $\mathcal{M}_1$	Periodic motions	Asymptotic motions	Regular tori
I	$L_1 > 0$, $L_2 > 0$, $L_3 > 0$, $L_5 > 0$	$\overline{a_2}$	No	No	No
I	$L_1 > 0$, $L_2 > 0$, $L_3 > 0$, $L_5 < 0$	a_8 $(0 \le \lambda < \lambda_*)$, a_4, a_9 $(0 < \lambda < +\infty)$	"center"	No	Yes
II, VI	$L_1 \ge 0$, $L_2 < 0$, $L_3 < 0$	a_2 $(0 \le \lambda < +\infty)$, a_{10} $(\lambda > \lambda_*)$	"center"	No	Yes
III	$L_1 > 0$, $L_2 < 0$, $L_3 > 0$, $L_5 > 0$	$\overline{a_2}$	No	No	No
III	$L_1 > 0$, $L_2 < 0$, $L_3 > 0$, $L_5 < 0$	a_3	"saddle"	Yes	No
IV	$L_1 > 0$, $L_2 > 0$, $L_3 < 0$	a_5 $(0 \le \lambda < 1)$, a_6 $(0 \le \lambda < \sqrt{2})$, a_{11} $(\lambda_* < \lambda < +\infty)$	"saddle"	Yes	No
V	$L_1 < 0$, $L_2 < 0$, $L_3 < 0$, $L_4 > 0$	a_1 $(0 \le \lambda < +\infty)$, a_{12} $(\lambda > \lambda^*)$	"center"	No	No
V	$L_1 < 0$, $L_2 < 0$, $L_3 < 0$, $L_4 < 0$	$\overline{a_1}$	No	No	No
VII	$L_2 = 0$	Δ_1	degener.	Yes	No
VIII	$L_3 = 0$	Δ_0	degener.	Yes	No

first integrals for the domains a_2 and a_{11}, regular tori exist, whereas for the domains a_1 and a_{12}, there are no such tori. This difference in terms of parameters of analytical solutions is found in [11].

Due to (2.13) and (1.30),

$$\ell = -p\left(h - \frac{\lambda^2}{2} - p^2\right), \quad s = h - \frac{\lambda^2}{2} - p^2,$$

it is easy to classify (S, H)-diagrams and (S, L)-diagrams of the first critical subsystem. The separating values λ remain the same (they are defined by surgeries of sections of the key set). In Fig. 12, we present the (S, H)-diagrams for the folloiwng cases:

(a) $0 < \lambda < \lambda_*$;
(b) $\lambda_* < \lambda < 1$;
(c) $1 < \lambda < \lambda^*$;
(d) $\lambda^* < \lambda < \sqrt{2}$;
(e) $\lambda > \sqrt{2}$;
(f) $\lambda = 0$.

We indicate all points on the planes (p, h) and (s, h) that are important for the construction of the H-atlases of bifurcation diagrams of systems on Q^4_h (points of the extreme values of h-coordinates on the key sets). The corresponding notation is given in Figs. 13 and 14. Points associated with the curves δ_1, δ_2, and δ_3 are denoted by the letters A, B, and C, respectively (with indexes if necessary).

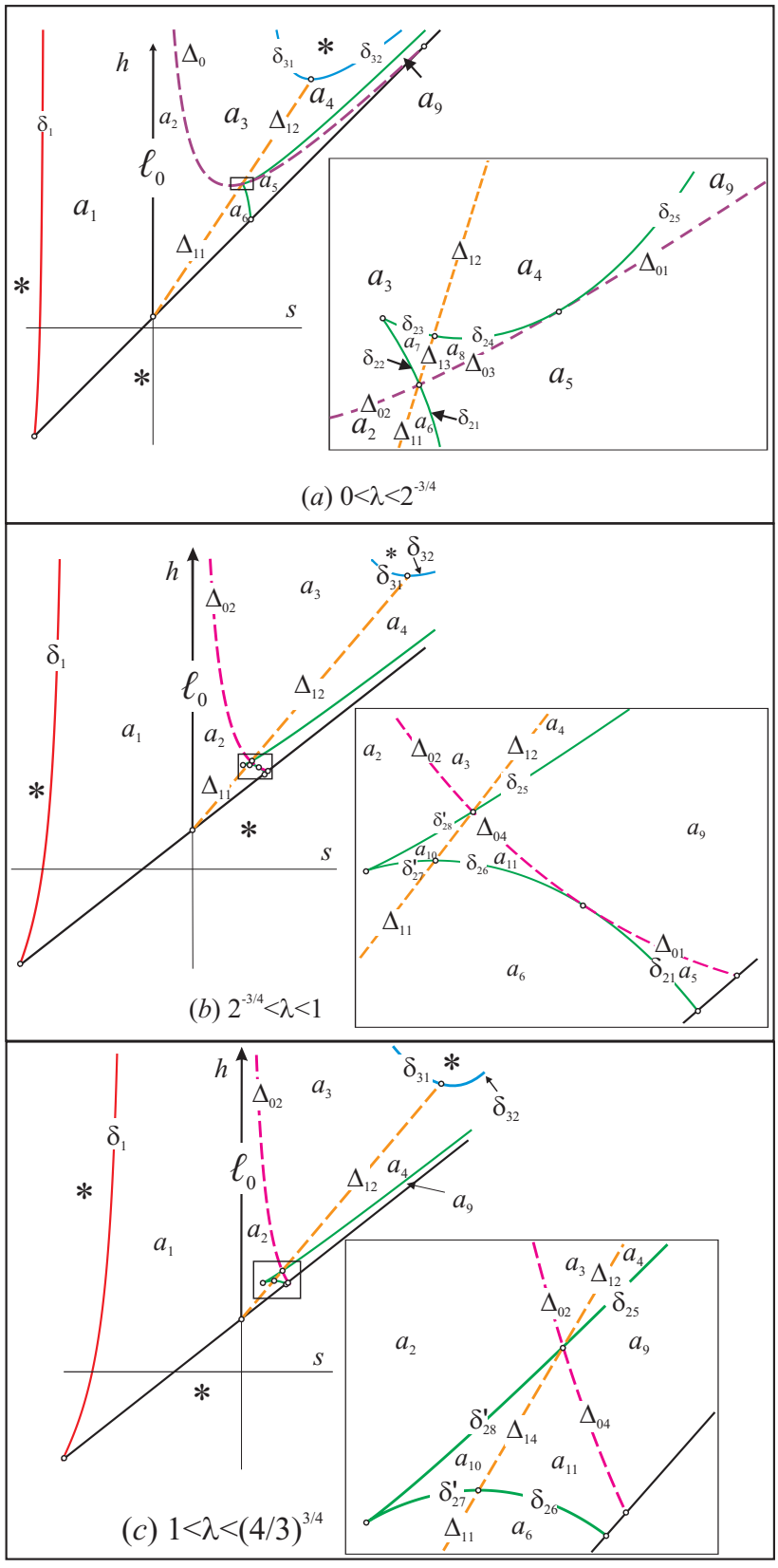

Fig. 12. (S, H)-diagrams of the systems $\mathcal{M}_1$ and their enlarged fragments

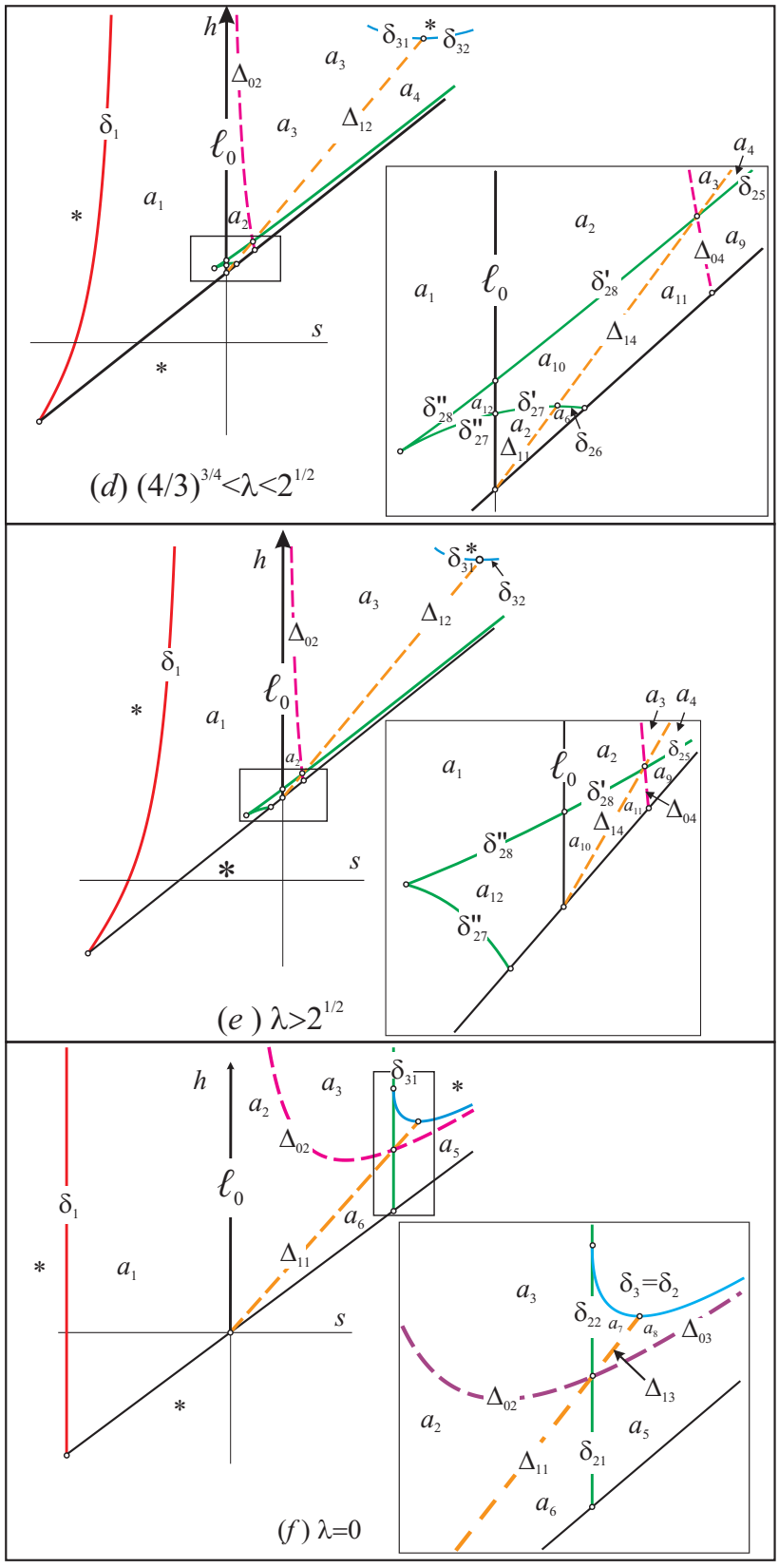

Fig. 12 (continued). (S, H)-diagrams of $\mathcal{M}_1$ systems and their enlarged fragments

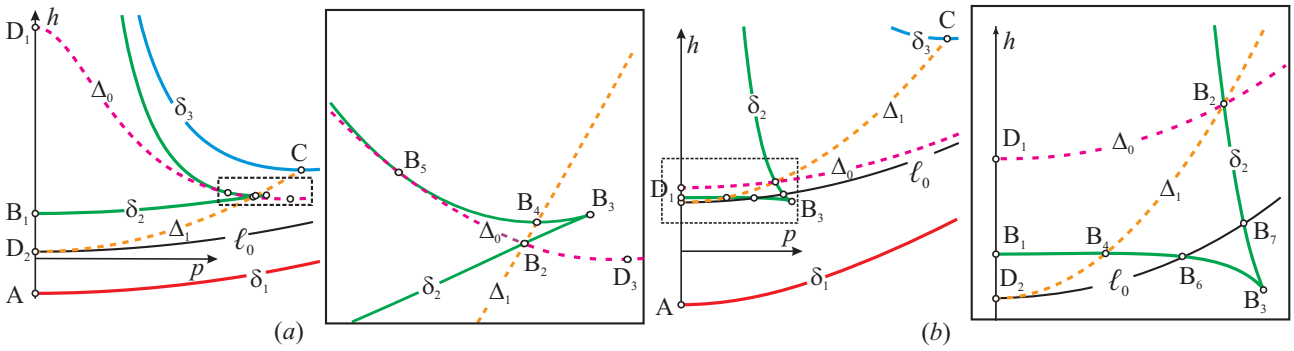

Fig. 13. Singular points of the (P, H)-diagram of the system $\mathcal{M}_1$

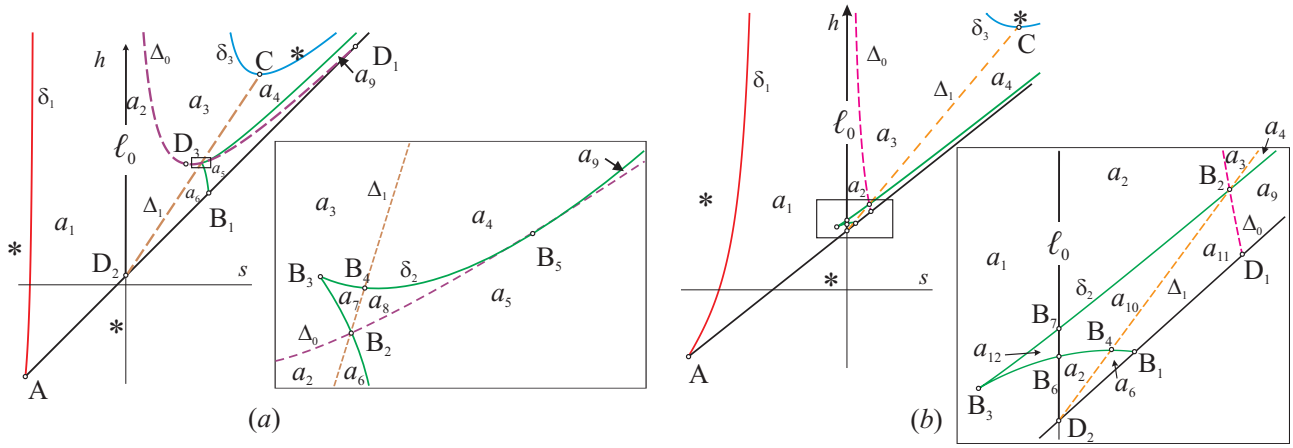

Fig. 14. Singular points of the (S, H)-diagram of the system $\mathcal{M}_1$

The letter D is used for points on Δ_j (here $j = 0, 1$; in the third system, Δ_3 appears). To see all singular points, it suffices to consider the cases (a) $0 < \lambda < \lambda_*$ and (b) $\lambda^* < \lambda < \sqrt{2}$ in these figures.

In Fig. 15 we present the (S, L)-diagrams of the subsystem $\mathcal{M}_1$ for nonseparating cases:

(1) $0 < \lambda < \lambda_*$;
(2) $\lambda_* < \lambda < 1$;
(3) $1 < \lambda < \lambda^*$;
(4) $\lambda^* < \lambda < \sqrt{2}$;
(5) $\lambda > \sqrt{2}$;
(6) $\lambda = 0$.

Critical points that are relevant to the construction of an L-atlas of bifurcation diagrams for systems on P^4_ℓ are marked here. Note that, in comparison with the diagrams containing H, the additional point D_4 appears: it is an extremum of the ℓ-coordinate on the image of degenerate points Δ_0.

We clearly list all values of the parameters and integrals (general and particular) at marked critical points. We obtain the image of degenerate rank-0 critical points cutting the separating set in Fig. 2 at the set level λ. The points on the axis $r = 0$ are considered only on the curve δ_2. The curve δ_1 does not contain degenerate points but contains an extremum of h, namely, the global smallest value of energy reached at the point

$$A: \quad r = 0, \quad p = 0, \quad s = -1 - \frac{\lambda^2}{2}, \quad h = -1, \quad \ell = 0. \tag{4.11}$$

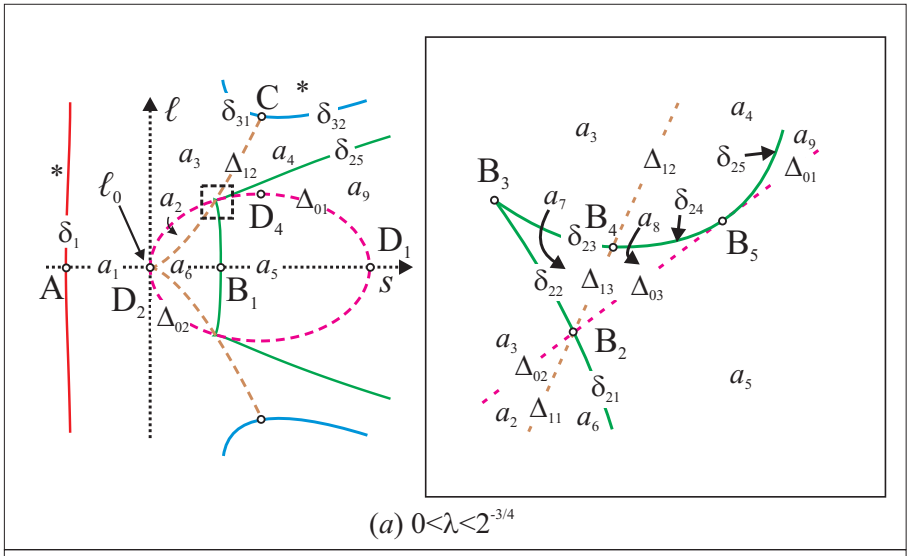

(*a*) $0<\lambda<2^{-3/4}$

(*b*) $2^{-3/4}<\lambda<1$

(*c*) $1<\lambda<(4/3)^{3/4}$

Fig. 15. (S, L)-diagrams of $\mathcal{M}_1$ subsystem (detailed elaboration)

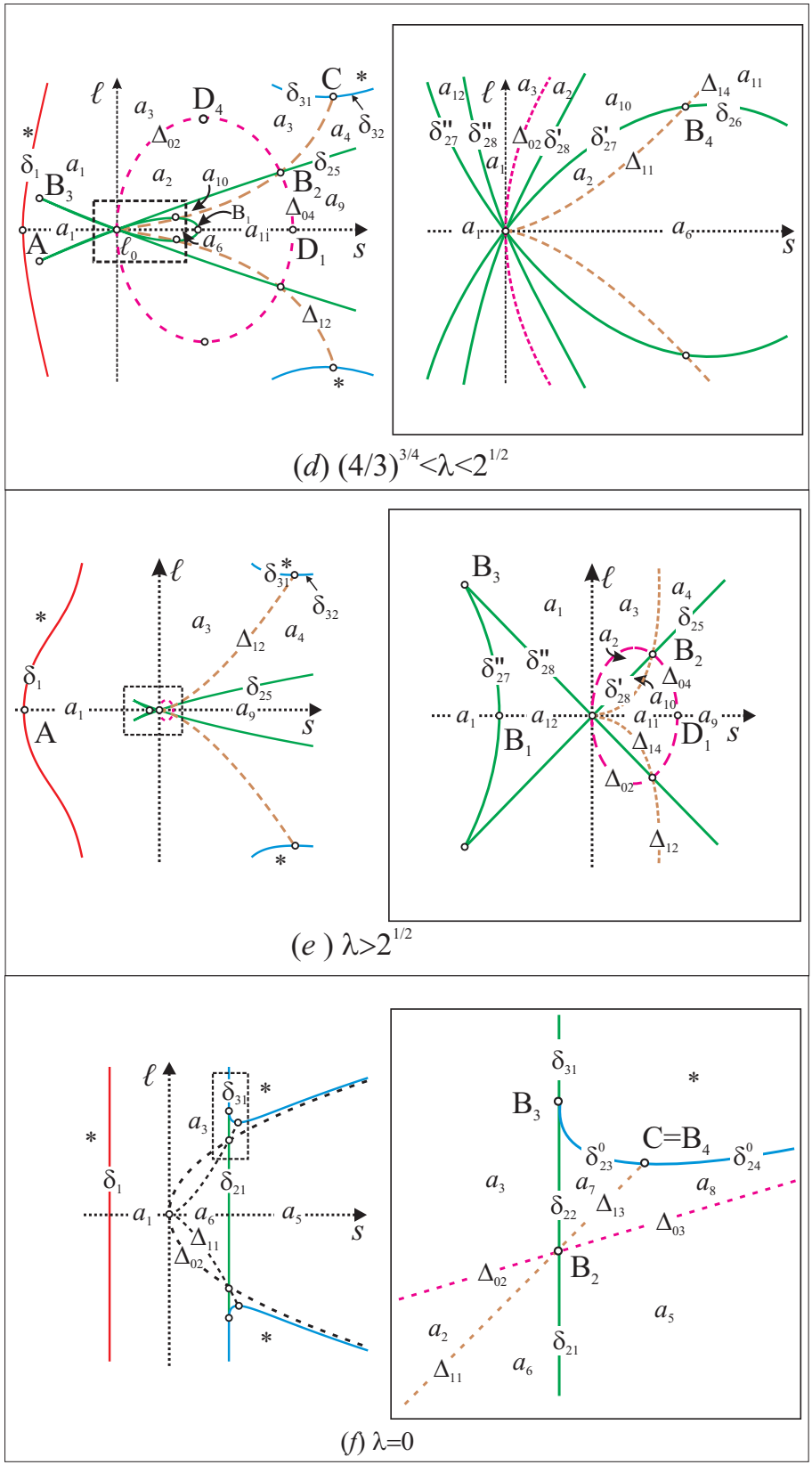

Fig. 15 (continued). (S, L)-diagrams of $\mathcal{M}_1$ subsystem (detailed elaboration)

Introduce the notation

$$Q_0 = \lambda(r-\lambda) + D, \qquad Q_1 = (r-\lambda)(2r-\lambda) - D,$$
$$Q_2 = r(r-\lambda)(2r-\lambda) + \lambda D, \qquad Q_3 = r(\lambda - r) + D.$$

On the curve δ_2 ($r < 0$) we find

$$\frac{dh}{dr} = \frac{1}{2(\lambda-r)^2 D} Q_1 Q_2, \qquad \frac{ds}{dr} = \frac{1}{2D} Q_3,$$
$$\frac{dp^2}{dr} = -\frac{1}{2(r-\lambda)^2 D} Q_2 Q_3, \qquad \frac{d\ell^2}{dr} = \frac{1}{8(r-\lambda)^2 D} Q_0 Q_1 Q_2 Q_3.$$

In particular, this implies

$$\frac{dh}{dp} = -\sqrt{\frac{2r}{r-\lambda}} \frac{Q_1}{\sqrt{Q_3}}, \quad \frac{d\ell}{ds} = -\frac{1}{2\sqrt{2r}(r-\lambda)^{3/2}} Q_1 \sqrt{Q_3}. \tag{4.12}$$

Thus, the extrema of $h(r)$ on δ_2 are as follows: the point B_1 (at $r = 0$), the degenerate point B_4 (the curve π_{23})

$$(\lambda - r)(\lambda - 2r) - D = 0, \tag{4.13}$$

and the cusp B_3 (the curve π_{24})

$$r(\lambda - r)(\lambda - 2r) + \lambda D = 0. \tag{4.14}$$

The touching of the curves δ_2 and Δ_0 generates the point B_5 (the curve of degenerate points π_{21}, Eq. (3.21)), and the intersection of the three curves δ_2, Δ_0, and Δ_1 occurs at the point B_4 (the curve of degenerate points π_{22}, $r = -\lambda$). In accordance with (3.11), the intersection of δ_2 with the curve of multiple points ℓ_0 is determined by the equation

$$\lambda(r-\lambda) + D = 0. \tag{4.15}$$

Solutions of Eq. (4.13) are written in the parametric form (3.37) by using the substitution (3.27); solutions of (4.14) can be found explicitly. Equation (4.15) can be reduced to the equation

$$(r-\lambda)^3(r+\lambda) + 4 = 0$$

under the condition $r < 0$. Using the same substitution (3.27), we obtain the necessary parametric representation of the coordinates of the points B_6 and B_7 for $\lambda \geq \lambda^*$. In addition, according to (4.12), critical points of the curve δ_2 on the plane (s, ℓ) are generated by the condition $Q_3 = 0$, which implies that $p = 0$ and $\ell = 0$, i.e., this is again the point A. Recall that, due to the identity $\ell = -sp$, the whole curve ℓ_0 corresponding to the value $s = 0$ "collapses" on the plane (s, ℓ) to the origin; in particular, the axis $O\ell$ consists of inadmissible points except for $(0, 0)$. Therefore, in Fig. 15, it is shown by the dot line. Thus, the curve δ_2 generates the following set of points and values of the first integrals:

$$B_1: \quad r = 0, \quad p = 0, \quad s_1 = 1 - \frac{\lambda^2}{2}, \quad s_2 = \frac{1}{2}, \quad h = 1, \quad \ell = 0; \tag{4.16}$$

$$B_2 = \pi_{22}: \begin{cases} r = -\lambda, & p = \pm\sqrt{\dfrac{\sqrt{1+\lambda^4} - \lambda^2}{2}}, \\ s_1 = \sqrt{1+\lambda^4} - \lambda^2, & s_2 = s_1, \\ h = \dfrac{3}{2}\sqrt{1+\lambda^4} - \lambda^2, & \ell = \mp\dfrac{1}{\sqrt{2}}\left(\sqrt{1+\lambda^4} - \lambda^2\right)^{3/2}; \end{cases} \tag{4.17}$$

$$B_3=\pi_{24}:\ \begin{cases} r=-\dfrac{1}{2}\sqrt{U}\left(\sqrt{4+U^2}-U\right), & p=\pm\dfrac{1}{2\sqrt{2}}\left(\sqrt{4+U^2}-U\right)^{3/2},\\ s_1=2\dfrac{\sqrt{4+U^2}-2U}{\left(\sqrt{4+U^2}-U\right)^2}, & s_2=\dfrac{1}{2U}\quad (U=\lambda^{2/3}),\\ h=\dfrac{1}{4}\left[(4+U^2)^{3/2}-U(6+U^2)\right], & \ell=\mp\dfrac{\sqrt{4+U^2}-2U}{\sqrt{2}\left(\sqrt{4+U^2}-U\right)^{1/2}}; \end{cases} \tag{4.18}$$

$$B_4=\pi_{23}:\ \begin{cases} r=\dfrac{x^4-4}{2x^3}, & \lambda=\dfrac{3x^4-4}{2x^3},\\ p=\pm\dfrac{\sqrt{4-x^4}}{2x}, & s_1=\dfrac{4-x^4}{2x^2}, \quad s_2=\dfrac{x^6}{2(3x^4-4)},\\ h=\dfrac{3}{8}x^2+\dfrac{2}{x^6}, & \ell=\mp\dfrac{(4-x^4)^{3/2}}{4x^3}, \quad x\in\left(\sqrt[4]{4/3},\sqrt{2}\right]; \end{cases} \tag{4.19}$$

$$B_5=\pi_{21}:\ \begin{cases} r=\lambda-\lambda^{-1/3}, & p=\pm\lambda^{1/3}\sqrt{1-\lambda^{4/3}},\\ s_1=\dfrac{1}{2\lambda^{2/3}}, & s_2=s_1, \qquad \lambda\in(0,1],\\ h=-\dfrac{\lambda^2}{2}+\lambda^{2/3}+\dfrac{1}{2\lambda^{2/3}}, & \ell=\mp\dfrac{\sqrt{1-\lambda^{4/3}}}{2\lambda^{1/3}}; \end{cases} \tag{4.20}$$

$$B_{6,7}:\ \begin{cases} r=-\dfrac{1}{2}x+\dfrac{2}{x^3}, & \lambda=\dfrac{1}{2}x+\dfrac{2}{x^3}\ge\lambda^*,\\ p=\pm\dfrac{\sqrt{x^4-4}}{x^3}, & s_1=0, \quad s_2=\dfrac{2x^2}{4+x^4},\\ h=\dfrac{1}{8}x^2+\dfrac{2}{x^2}-\dfrac{2}{x^6}, & \ell=0,\\ B_6:\ x\in\left[\sqrt{2},\sqrt{2\sqrt{3}}\right], & B_7:\ x\in\left[\sqrt{2\sqrt{3}},+\infty\right). \end{cases} \tag{4.21}$$

Here s_1 and s_2 are the values of the parameter s on the surfaces Π_1 and $\Pi_{2,3}$, respectively. Formulas (4.18) at the cusp B_3 can be simplified by introducing the parameter z:

$$B_3=\pi_{24}:\ \begin{cases} \lambda=\left(\dfrac{1}{z}-z\right)^{3/2}, & 0<z<1,\\ r=-\sqrt{z(1-z^2)}, & p=\pm z^{3/2},\\ s_1=\dfrac{3z^2-1}{2z^3}, & s_2=\dfrac{z}{2(1-z^2)},\\ h=\dfrac{1}{2}z(3+z^2), & \ell=\mp\dfrac{3z^2-1}{2z^{3/2}}. \end{cases} \tag{4.22}$$

On the curve δ_3, the minimum point of h corresponding to the degeneration curve π_{31} is determined by the same equation (4.13), and the parametrization of this point is given by Eqs. (3.38). We have

$$C=\pi_{31}:\ \begin{cases} r=\dfrac{x^4-4}{2x^3}, & \lambda=\dfrac{3x^4-4}{2x^3},\\ p=\mp\dfrac{\sqrt{4-x^4}}{2x}, & s_1=\dfrac{4-x^4}{2x^2}, & s_2=\dfrac{x^6}{2(3x^4-4)},\\ h=\dfrac{3}{8}x^2+\dfrac{2}{x^6}, & \ell=\pm\dfrac{(4-x^4)^{3/2}}{4x^3}, & x\in\left[-\sqrt[4]{4/3},0\right). \end{cases} \tag{4.23}$$

Finally, the extremum values of h on the curves Δ_0 and Δ_1 are reached at the points

$$D_1:\ \begin{cases} p=0, \quad s_1=\dfrac{1}{2\lambda^2}, & s_2=s_1,\\ h=\dfrac{1+\lambda^4}{2\lambda^2}, & \ell=0, \end{cases} \qquad \lambda>0; \tag{4.24}$$

$$D_2:\ \begin{cases} p=0, & s_1=0,\\ h=\dfrac{\lambda^2}{2}, & \ell=0, \end{cases} \qquad \lambda\ge 0; \tag{4.25}$$

$$D_3:\ \begin{cases} p=\pm\sqrt{\dfrac{1-\sqrt{2}\lambda^2}{\sqrt{2}}}, & s_1=\dfrac{1}{\sqrt{2}},\\ h=\sqrt{2}-\dfrac{\lambda^2}{2}, & \ell=\mp\sqrt{\dfrac{1-\sqrt{2}\lambda^2}{2\sqrt{2}}}, \end{cases} \qquad \lambda^2\le\frac{1}{\sqrt{2}}. \tag{4.26}$$

In addition, we see from (4.10) that, as was mentioned above, there is an extremal value of ℓ on Δ_0 at the point (see Fig. 15)

$$D_4:\ \begin{cases} h=\dfrac{1+6\lambda^4}{4\lambda^2}, & \ell=\pm\dfrac{1}{4\lambda}, & s_1=\dfrac{1}{4\lambda^2},\\ s_2=s_1, & p=\mp\lambda, \end{cases} \qquad \lambda>0. \tag{4.27}$$

4.3. Specification. Second and third critical subsystems. For the second and third critical subsystems, we rewrite the equations of the surfaces (2.8) in the form

$$\Pi_2\cup\Pi_3=\left\{h=2\ell^2+\frac{1}{2s}-\frac{\lambda^2}{2}(1-4s^2),\ k=-4\ell^2\lambda^2+\frac{1}{4s^2}-\frac{\lambda^2}{s}(1-\lambda^2 s)(1-4s^2)\right\}.$$

As above, $s<0$ for Π_2 and $s>0$ for Π_3. This implies that the pair (s,ℓ) determines a unique point on the corresponding surface and this correspondence is bijective. So, we can consider the (S,L)-diagrams for the subsystems $\mathcal{M}_2$ and $\mathcal{M}_3$.

To obtain a simple criterion for the existence of solutions to systems (1.27)–(1.29), we represent them in algebraic form. We perform the substitution

$$X=\frac{1-\zeta^2}{1+\zeta^2}, \quad Y=\frac{2\zeta}{1+\zeta^2}.$$

We have single-valued dependences

$$\omega_1=-\frac{\ell}{s}-\frac{2\varkappa\rho\zeta}{1+\zeta^2}, \qquad \omega_3=\lambda+2\varkappa\frac{1-\zeta^2}{1+\zeta^2},$$

$$\alpha_1=\frac{\lambda s(1-\zeta^4)+2\ell\rho\zeta(1+\zeta^2)-8\varkappa^3\zeta^2}{\varkappa(1+\zeta^2)^2}, \qquad \alpha_3=\frac{\ell(1-\zeta^2)-2\lambda\rho s\zeta}{\varkappa(1+\zeta^2)}$$

and the formulas with radicals

$$\omega_2 = -\frac{1}{\sqrt{2}(1+\zeta^2)}\sqrt{\frac{\rho^2}{\varkappa s}Z(\zeta)}, \quad \alpha_2 = -\frac{2\sqrt{2}\varkappa\zeta}{(1+\zeta^2)^2}\sqrt{\frac{1}{\varkappa s}Z(\zeta)},$$

where

$$Z(\zeta) = (\varkappa - 2\lambda s^2)\zeta^4 + 4\ell\rho s\zeta(1+\zeta^2) + 2\varkappa(1-4\varkappa^2 s)\zeta^2 + (\varkappa + 2\lambda s^2).$$

The dynamics is governed by the equation

$$\frac{d\zeta}{dt} = \frac{1}{2\sqrt{2}}\sqrt{\frac{1}{\varkappa s}Z(\zeta)}.$$

Further, due to (1.27), we set

$$\begin{aligned} &\zeta = z \qquad (z\in\mathbb{R}), \qquad \rho = \rho_+, \qquad \rho^2 \geq 0;\\ &\zeta = \mathrm{i}\, z \qquad (z\in\mathbb{R}), \qquad \rho = \mathrm{i}\,\rho_-, \qquad \rho^2 < 0 \end{aligned}$$

(we assume that ρ_+ and ρ_- are nonnegative). We obtain the solutions in the following form. For $\rho^2 \geq 0$, we have single-valued dependences

$$\begin{aligned} &\omega_1 = -\frac{\ell}{s} - \frac{2\varkappa\rho_+ z}{1+z^2}, && \omega_3 = \lambda + 2\varkappa\frac{1-z^2}{1+z^2},\\ &\alpha_1 = \frac{\lambda s(1-z^4) + 2\ell\rho_+ z(1+z^2) - 8\varkappa^3 z^2}{\varkappa(1+z^2)^2}, && \alpha_3 = \frac{\ell(1-z^2) - 2\lambda\rho_+ sz}{\varkappa(1+z^2)} \end{aligned}$$

and the formulas with radicals

$$\omega_2 = -\frac{\rho_+}{\sqrt{2}(1+z^2)}\sqrt{\frac{1}{\varkappa s}Z_+(z)}, \quad \alpha_2 = -\frac{2\sqrt{2}\varkappa z}{(1+z^2)^2}\sqrt{\frac{1}{\varkappa s}Z_+(z)}.$$

Similarly, for $\rho^2 < 0$ we obtain

$$\begin{aligned} &\omega_1 = -\frac{\ell}{s} + \frac{2\varkappa\rho_- z}{1-z^2}, && \omega_3 = \lambda + 2\varkappa\frac{1+z^2}{1-z^2},\\ &\alpha_1 = \frac{\lambda s(1-z^4) - 2\ell\rho_- z(1-z^2) + 8\varkappa^3 z^2}{\varkappa(1-z^2)^2}, && \alpha_3 = \frac{\ell(1+z^2) + 2\lambda\rho_- sz}{\varkappa(1-z^2)} \end{aligned}$$

and the formulas with radicals

$$\omega_2 = -\frac{\rho_-}{\sqrt{2}(1-z^2)}\sqrt{\frac{1}{\varkappa s}Z_-(z)}, \quad \alpha_2 = -\frac{2\sqrt{2}\varkappa z}{(1-z^2)^2}\sqrt{\frac{1}{\varkappa s}Z_-(z)}.$$

Here

$$\begin{aligned} Z_+(z) = &\quad (\varkappa - 2\lambda s^2)z^4 + 4\ell\rho_+ sz(1+z^2) + 2\varkappa(1-4\varkappa^2 s)z^2 + (\varkappa + 2\lambda s^2),\\ Z_-(z) = &-(\varkappa - 2\lambda s^2)z^4 + 4\ell\rho_- sz(1+z^2) + 2\varkappa(1-4\varkappa^2 s)z^2 - (\varkappa + 2\lambda s^2). \end{aligned}$$

The dynamics is governed by the corresponding equation (the upper sign is for $\rho^2 \geq 0$ and the lower sign is for $\rho^2 < 0$):

$$\frac{dz}{dt} = \frac{1}{2\sqrt{2}}\sqrt{\frac{1}{\varkappa s}Z_\pm(z)}. \tag{4.28}$$

From these expressions we obtain the following criterion.

Proposition 16. *For given values s and ℓ corresponding to a level in $\mathcal{M}_{2,3}$ that does not contain rank-0 critical points, the number of critical circles in the systems $\mathcal{M}_{2,3}$ is equal to the number of trajectories in the phase space $\overline{\mathbb{R}}\times\mathbb{R}$ of the corresponding equation* (4.28)*, where $Z_\pm$ is a straight line supplemented by the point $Z_\pm$. Thus, if the corresponding polynomial $Z_\pm$ has $2m$ of real roots $(m = 0, 1, 2)$, then the critical levels s, ℓ contains m critical circles, except for the case where $m = 0$*

and the leading coefficient of the polynomial is positive. In this case, there are two critical circles (z runs over all $\overline{\mathbb{R}}$), and the variable ω_2 preserves its sign on each of them.

The last case ($m = 0$) is considered as a *special* case:

$$\rho^2 > 0, \quad \varkappa - 2\lambda s^2 > 0, \quad Z_+(z) > 0 \quad \forall z \in \mathbb{R}. \tag{4.29}$$

It is impossible to write out both Morse–Bott indexes explicitly for $\mathcal{M}_{2,3}$ systems. However, it is possible to obtain simple formulas for their calculation and, which is more important, to distinguish clearly a vector on the transversal area to the trajectory at hyperbolic points on which a gap of the "figure-eight" cannot occur (except for the special case (4.29)). This allows one to determine the direction of type-B atoms when the integral K increases.

As above, we select the orthogonal complement to the vectors $\operatorname{grad}\Gamma$, $\operatorname{grad} L$, $\operatorname{grad} H$, and $\operatorname{sgrad} H$ as a transversal area for the critical circle (at a rank-1 critical point).

We consider the case that does not satisfy (4.29). On any trajectory, the variable z oscillates between the roots of the corresponding polynomial $Z(z)$, including infinity. Consider a point x_0 on the trajectory such that $Z(z) = 0$. Then the vectors $\operatorname{grad}\Gamma$, $\operatorname{grad} L$, and $\operatorname{grad} H$ are orthogonal to the plane $O\omega_2\alpha_2$ and the vector $\operatorname{sgrad} H$ lies in this plane and has the form

$$\operatorname{sgrad} H = \bigl(0,\ b_2,\ 0,\ 0,\ b_5,\ 0\bigr).$$

The constrained extremum of the function K at the common level of the functions Γ, L, and H in P^6 is a critical point with undefined Lagrange multipliers

$$K_2 = K + \left(2\lambda^2 - \frac{1}{s}\right) H + 2sL^2 - \frac{2\varkappa^2}{s}\Gamma.$$

Obviously, the part of this function that does not contain the Casimir functions L and Γ coincides with (4.3). Let $\mathcal{L} = d^2K_2(x_0)$ be the matrix with elements $\mathcal{L}_{ij}$. Since the vector $\operatorname{sgrad} H$ belongs to the kernel of $\mathcal{L}$ core, we have

$$\mathcal{L}_{22}b_2 + \mathcal{L}_{25}b_5 = 0, \quad \mathcal{L}_{25}b_2 + \mathcal{L}_{55}b_5 = 0.$$

In particular, since $b_2b_5 \neq 0$ and the coefficients $\mathcal{L}_{25}$ and $\mathcal{L}_{55}$ have the form

$$\mathcal{L}_{25} = -\frac{8\varkappa\rho\zeta}{1+\zeta^2}, \quad \mathcal{L}_{55} = 2\rho^2,$$

we can perform some simplifying:

$$\mathcal{L}_{22} = \frac{\mathcal{L}_{25}^2}{\mathcal{L}_{55}} = \frac{32\varkappa^2\zeta^2}{(1+\zeta^2)^2}, \quad b_5 = -\frac{\mathcal{L}_{25}\,b_2}{\mathcal{L}_{55}} = \frac{4\varkappa\,\zeta b_2}{\rho(1+\zeta^2)}.$$

As the first vector of the transversal area, we choose the vector lying in the same plane $O\omega_2\alpha_2$ and orthogonal to $\operatorname{sgrad} H$:

$$v_1 = \bigl(0,\ -b_5,\ 0,\ 0,\ b_2,\ 0\bigr).$$

Then for computer calculations, the vector v_2 can be easily found as the null space of the matrix consisting of the five vectors: $\operatorname{grad}\Gamma$, $\operatorname{grad} L$, $\operatorname{grad} H$, $\operatorname{sgrad} H$, and v_1. Although its analytic expression is quite complicated, all necessary calculations can be easily performed in the dynamic mode. In addition, the matrix of the restriction of the quadratic form $\mathcal{L}$ to the transversal area is diagonal in the basis (v_1, v_2), so the Morse–Botta indexes have the following form:

$$\mu_1 = \mathcal{L}v_1 \cdot v_1, \quad \mu_2 = \mathcal{L}v_2 \cdot v_2.$$

The analysis of projections of integral manifolds to the plane $O\omega_1\omega_2$ shows that the critical surface of the hyperbolic circle never has discontinuities in the direction of the axis $O\omega_2$ in a neighborhood of the systems $\mathcal{M}_{2,3}$.

In particular, this means that for type-B atoms, the vector v_1 is always directed to the exterior domain of the "figure-eighth." Therefore, if $\mu_1 > 0$, then the function K increases in the direction of

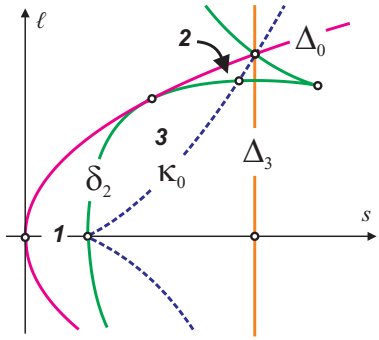

Fig. 16. Special case

the "head" of the atom ("head" up), whereas if $\mu_1 < 0$, then the K function decreases in the direction of the "head of the atom ("head" down). From the expressions obtained we have

$$\mu_1 = \mathcal{L}_{22}b_5^2 - 2\mathcal{L}_{25}b_2b_5 + \mathcal{L}_{55}b_2^2 = 2\frac{\left[16\varkappa^2\zeta^2 + \rho^2(1+\zeta^2)^2\right]^2}{\rho^2(1+\zeta^2)^4}b_2^2.$$

Thus, the direction of edges of asymmetric atoms is determined by the sign of ρ^2. Since in $\mathcal{M}_2$ all rank-1 points have elliptic type and $\rho^2 > 0$, we obtain the following statement.

Proposition 17. *If the integral K increases on an isoenergetic level $Q^3_{\ell,h}$, then at points of the critical subsystem $\mathcal{M}_2$ for each nondegenerate critical circle, the bifurcation A_+ of the torus birth occurs.*

In the system $\mathcal{M}_3$ the situation is more complicated since we know from the classical problem that in this case C_2-type atoms can appear (see [39]). For the nonsingular case, it was proved above that for two trajectories at the same integral level, the distribution of signs of the Morse–Botta indexes is the same. Let us consider the special case (4.29). On the plane (s,ℓ) plane, the domain

$$\lambda^2 s^2(2s^2-1) < \ell^2 < \frac{s}{2}(1-2\lambda^2 s)$$

corresponds to the positivity condition of these constants. In Fig. 16, these conditions are fulfilled in the domains 1–3. The curve κ_0 corresponds to the boundary case where the leading coefficient of the polynomial Z_+ vanishes. According to the agreement adopted above, in all spaces of integral constant, the curve δ_2 is the image of the corresponding set of rank-0 critical points; certainly, it is the discriminant set of the polynomial Z_+. The notation Δ_0 and Δ_3 has the same sense as above. In the domains 2 and 3, the polynomial Z_+ has respectively two and four real roots. In the domain 1, there are no real roots, so the case (4.29) is realized. Obviously, the domain 1 has an intersection with the axis $\ell = 0$ at

$$s \in (0, \min\{1/2, 1/2\lambda^2\}); \tag{4.30}$$

since $Z_+ > 0$ on the whole axis, it is convenient to take $z = 0$. Then one can easily find vectors determining the transversal area to the periodic solution:

$$v_1 = \left(-(1+2\lambda^2 s),\ 0,\ 0,\ 0,\ \frac{\sqrt{2s(1-2\lambda^2 s)}}{\sqrt{1+2s}}\left[(1+s)\lambda^2 s - 1\right],\ \lambda s(3-2\lambda^2 s)\right),$$

$$v_2 = \left(0,\ \frac{\lambda\sqrt{s(1+2s)}}{\sqrt{2(1-2\lambda^2 s)}},\ 1,\ 0,\ 0,\ 0\right).$$

The matrix $\mathcal{K}$ of the quadratic form on this pair of vectors is a diagonal matrix whose eigenvalues are as follows:

$$\mu_1 = \frac{4s}{1+2s}\left[1+\lambda^2 s^2(5-2\lambda^2 s)\right]^2, \quad \mu_2 = \frac{1}{s}(8\lambda^2 s^3 - 1).$$

It is clear that $\mu_1 > 0$. The vanishing of μ_2 corresponds to the set Δ_3 where rank-1 points become degenerate (the vertical straight line in Fig. 16). On the interval (4.30), we always have $\mu_2 < 0$. Thus, in the special case, the Morse–Bott indexes have opposite signs (this fact is obvious since trajectories are hyperbolic) and, by the above, the distribution of signs is the same on both trajectories of this level, namely, $(+,-)$ for chosen basis. We note that the calculation of the Morse–Bott indexes does not allow one to distinguish the atoms $2B$ and C_2 by local analysis.

We obtain the following proposition.

Proposition 18. *If the integral K increases on the isoenergetic level $Q^3_{\ell,h}$, at points of the critical subsystem $\mathcal{M}_3$ on the nondegenerate critical circles we have the following bifurcations*:

(1) *for elliptic trajectories (type "center") we have the appearance of a torus for $\rho^2 > 0$ (the atom A_+) and the disappearance of a torus for $\rho^2 < 0$ (the atom A_-)*;
(2) *for a hyperbolic trajectory at a critical level of K: the atom B_- for $\rho^2 > 0$ (an "outer" edge up and a couple of "inner" edges down) and the atom B_+ for $\rho^2 < 0$ (an "outer" edge down and a pair of "inner" edges up)*;
(3) *for two hyperbolic trajectories at a critical level of K: two atoms B the direction of whose "outer" edges is defined by the same rule (both "heads" up for $\rho^2 > 0$ or both "heads" down for $\rho^2 < 0$)or the atom C_2.*

Item 4 of Proposition 13 (i.e., for two hyperbolic trajectories at a critical level of K, we have different combinations of signs in the pairs (μ_1, μ_2)) is impossible for the subsystem $\mathcal{M}_3$ namely due to the fact that the sign of μ_1 coincides with the sign of ρ^2, i.e., is the same for all critical circles on the same level of integrals.

Conditions of the existence of motion in the subsystems $\mathcal{M}_{2,3}$ were obtained in [48, 50] in terms of the integral constants (s,h) and (s,ℓ), respectively. From Eqs. (1.28) and (1.29) it follows that

$$\operatorname{sgn}(\rho^2) = \operatorname{sgn}(Y^2), \quad \operatorname{sgn}(\rho^2) = \operatorname{sgn}(s\,\mathcal{G}^2).$$

Let $Y_* = Y$ for real ρ and $Y_* = \mathrm{i}\,Y$ for purely imaginary ρ. Then the curve 0 in the plane (X, Y_*) defined by the equation $X^2 + Y^2 = 1$ (the necessity of this equation is implied by (1.27)) is a circle or a hyperbola, whereas the curve Γ_1 defined by the equation $\mathcal{G}^2(X,Y) = 0$ is an ellipse for all $\rho^2 \neq 0$. We obtain the following result (see [48]).

Proposition 19. *Real solutions of the system* (1.27) *for given s, h, and ℓ related by the equations of the surfaces $\Pi_{2,3}$ exist if and only if the following conditions hold*:

(1) *if $s < 0$, then the circle Γ_0 and the ellipse Γ_1 have a common point*;
(2) *if $s > 0$ and $\rho^2 \geq 0$, then the circle Γ_0 does not lie entirely in the interior of the domain bounded by the ellipse Γ_1*;
(3) *if $s > 0$ and $\rho^2 < 0$, then the hyperbola Γ_0 and the ellipse Γ_1 have a common point.*

Indeed, one can immediately verify that for $s < 0$, the point $X = 1$, $Y = 0$ lies outside the ellipse. The motion on Γ_0 is performed along a segment where $\mathcal{G}^2 < 0$, i.e., inside the ellipse. Therefore, segments of the circle inside the ellipse exist if and only if the intersection $\Gamma_0 \cap \Gamma_1$ is nonempty. If $s > 0$ and $\rho^2 < 0$, for an actual motion we have $\mathcal{G}^2 < 0$, i.e., at least one point of the hyperbola lies inside the ellipse, which again means that $\Gamma_0 \cap \Gamma_1 \neq \varnothing$. Finally, if $s > 0$ and $\rho^2 > 0$, then there exists a point on the circle at which $\mathcal{G}^2 > 0$, i.e., a point outside the ellipse. This does not hold only if the circle Γ_0 lies entirely inside the ellipse Γ_1.

Obviously, this assertion and Proposition 16 are consistent.

Moreover, the number of critical circles at a fixed level of first integrals is equal to the number of segments of the circle Γ_0 lying inside the ellipse Γ_1 for $s < 0$ and to the number of segments of the hyperbola Γ_0 for $s > 0$ and $\rho^2 < 0$. For $s > 0$ and $\rho^2 > 0$, the number of critical circles is equal to the number of segments of the circle inside the ellipse, except for the special case (4.29). In this case, the

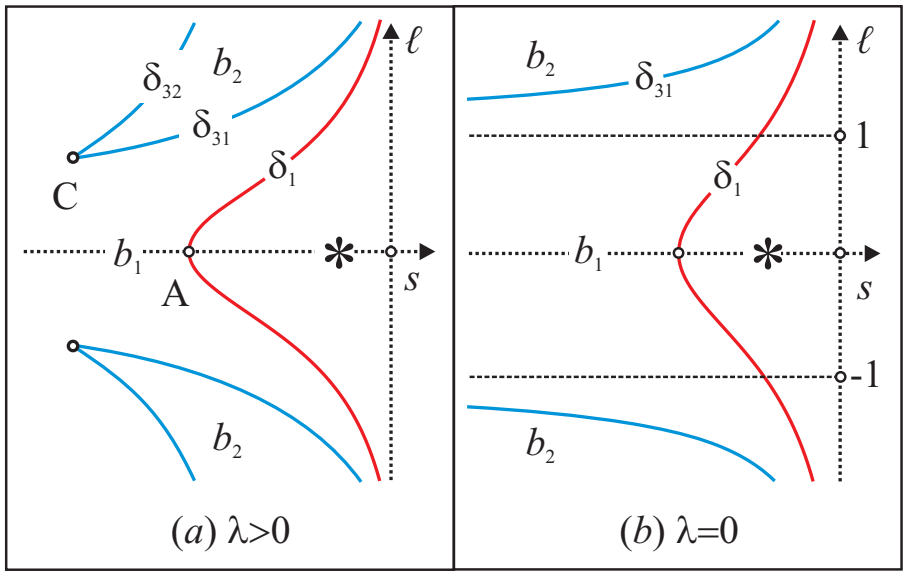

Fig. 17. The (S, L)-diagram of the system $\mathcal{M}_2$ with the full detailing

whole circle lies outside the ellipse, i.e., there is no intersection points; there exists one segment but two trajectories due to the possibility of choosing the sign of the nonzero radical $\mathcal{G}$.

Recall that $D = \sqrt{4 + r^2(r-\lambda)^2} > 0$. In addition to (4.5), we set

$$\theta_\pm(r) = \frac{r-\lambda}{4\lambda}\big[r(r-\lambda) \mp D\big],$$
$$\eta_\pm(r) = \frac{1}{2}\big[\lambda(r-\lambda) \pm D\big]\sqrt{\psi_\pm(r)}.$$

As follows from (3.11) and (3.15), the functions $\varphi_\pm(r)$, $\theta_\pm(r)$, and $\eta_\pm(r)$ are expressions of the integrals H, S, and L at rank-0 critical points that belong to the subsystems $\mathcal{M}_2$ and $\mathcal{M}_3$.

The following theorem corresponds to [50, Proposition 4].

Theorem 11. *The (S, L)-diagram of the critical system $\mathcal{M}_2$ consists of the following sets*:

$$\delta_1: \quad s = \theta_-(r), \quad \ell = \pm\eta_-(r), \quad r \in [0, \lambda);$$
$$\delta_3: \quad s = \theta_+(r), \quad \ell = \pm\eta_+(r), \quad r \in (\lambda, +\infty).$$

The outer boundary of the admissible domain $\mathcal{D}_2$ is the connected curve δ_1. The curve δ_3 consists of two components and divides $\mathcal{D}_2$ into three subdomains. Points of the subdomain containing the values $\ell = 0$ correspond to a critical circle; points of the other two subdomains bounded by the curve δ_3 correspond to two critical circles. There are no surgeries of the diagrams with respect to the parameter λ, except for the limit case $\lambda = 0$.

In Fig. 17, together with the (S, L)-diagram of the second critical subsystem (for the general case (a) $\lambda > 0$ and for the limit case (b) $\lambda = 0$), the domain b_1 with one critical circle and two domains b_2 symmetric with respect to $\ell = 0$ with two critical circles are shown. In the domain marked with an asterisk, $\Gamma_0 \cap \Gamma_1 \neq \varnothing$; this means that there is no motions here. According to Proposition 11, all rank-1 points have the "center" type. The key set here contains only rank-0 critical points. As usual, we denote by the same symbols the images of singular points generated by the extremal values of first integrals on the key set for the same points of the preimages in $\mathcal{M}_1$ and $\mathcal{M}_2$ (in our case, these are the points A and C). The properties of the corresponding atoms are collected in Table 4.3.

Table 4.3

Domain (life time)	Number of circles	Morse–Bott indexes	Exit to $\lambda = 0$/ $\ell = 0$	Atom	Analogs
b_1 $(0 \le \lambda < +\infty)$	1	$(+\,+)$	Yes/Yes	A_+	1 [40, Fig. 6.3] a_1 [46, Fig. 2] α_1 [7, Fig. 11] α_1 [20, Fig. 1]
b_2 $(0 \le \lambda < +\infty)$	2	$(+\,+)$, $(+\,+)$	Yes/No	$2A_+$	Transition III→VI [40, Fig. 6.1e] α_2 [7, Fig. 11]

The results obtained for critical subsystems $\mathcal{M}_1$ and $\mathcal{M}_2$ imply the following simple description of the admissible domain $\mathcal{D}$ in the space $\mathbb{R}^3(\ell, h, k)$ of constants of general integrals, which is the image of the phase space P^5 under the moment mapping (2.6). We assume that λ is given.

Theorem 12. *The admissible domain $\mathcal{D} = J(P^5)$ is a simply connected set whose exterior boundary consists of the images of the domains a_1 and a_{12} of the first critical subsystem and the domains b_1 and b_2 of the second critical subsystem.*

Proof. We fix a point (ℓ, h) for which $Q^3_{\ell,h} \neq \varnothing$. The set of such points is a simply connected domain on the plane $O\ell h$ bounded by the curve δ_1 below (see Fig. 6) and homeomorphic to the closed half-plane. All $Q^3_{\ell,h}$ are compact and connected; therefore, $K(Q^3_{\ell,h})$ is a segment retracting over δ_1 to a point. In particular, $\mathcal{D}$ is a reduced bundle of segments over the closed half-plane homeomorphic (but not diffeomorphic) to the closed half-space.

We fix h and consider the compact invariant subset $Q^4_h = H^{-1}(h)$ in P^5 and the bifurcation diagram $\Sigma_{LK}(h)$ of the mapping

$$L{\times}K|_{Q^4_h} : Q^4_h \to \mathbb{R}^2.$$

Obviously, $\Sigma_{LK}(h)$ is the image under the moment mapping of the intersections of Q^4_h with the critical subsystems $\mathcal{M}_i$. We consider the closed domain on the surface Π_1 bounded by the image of the band of the plane (p, h) between δ_1 and ℓ_0 (i.e., the image of the domains a_1 and a_{12}) and the image of the whole subsystem $\mathcal{M}_2$ on Π_2 (i.e., the image of the domains b_1 and b_2). The image of the subsystem $\mathcal{M}_3$ contains points inside this domain (for example, for $\ell = 0$). In the space $\mathbb{R}^3(\ell, h, k)$, the image of $\mathcal{M}_3$ is connected; therefore, if there exists a point in $J(\mathcal{M}_3)$ outside this domain, then the transversal intersection of the image $J(\mathcal{M}_3 \cap Q^4_h)$ and the closure of the union of the curves $a_1 \cup a_{12}$ is nonempty (it is easy to understand from the geometry of Π_1 and Π_3 that the common part, which is the tangent curve, does not go beyond the surface Π_3). This intersection contains a part of the curve δ_2 on the boundary between a_1 and a_{12}; however, by the above, on a small domain transversal to $\mathcal{M}_1$ in the preimage of the corresponding points of the diagram of the system $\mathcal{M}_1$, all rank-0 and rank-1 critical points have elliptic type and hence going beyond the boundary of this domain is impossible. □

Different types of envelopes of intersections of the set $\Sigma \subset \mathbb{R}^3(\ell, h, k)$ with planes on which the coordinate h is constant are shown in Fig. 18:

(a) $-1 < h < \lambda^2/2$;
(b) $\lambda^2/2 < h < h_C(\lambda)$;

(c) $h > h_C(\lambda)$

(without sections of the surface Π_3 lying entirely inside). For $h = -1$, the section of the admissible domain contracts to a point. In the case (c), the image of the domain $\overline{a_2}$ is shown by the dotted line; as was shown above, for points of this domain, there is no real motion. Thus, the admissible domain has the shape of the "bow" of a boat whose "deck" is smooth at its beginning and then an "edge" appears in the middle.

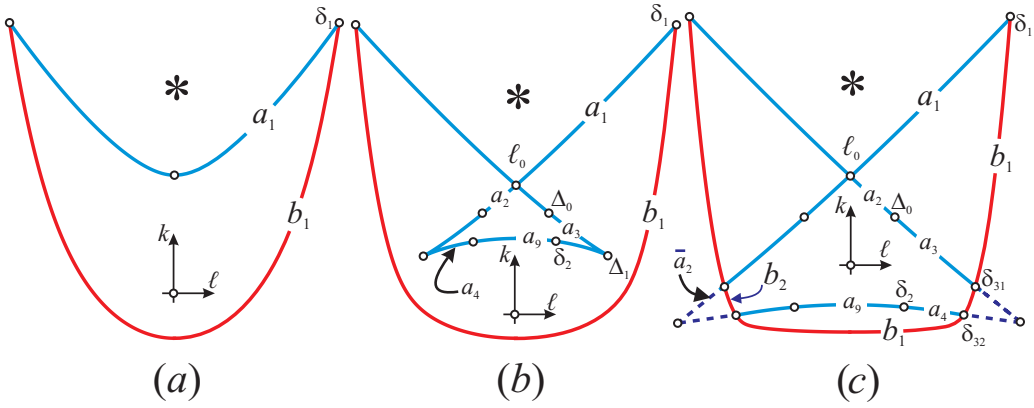

Fig. 18. Intersection of the admissible domain with the planes $h = \text{const}$

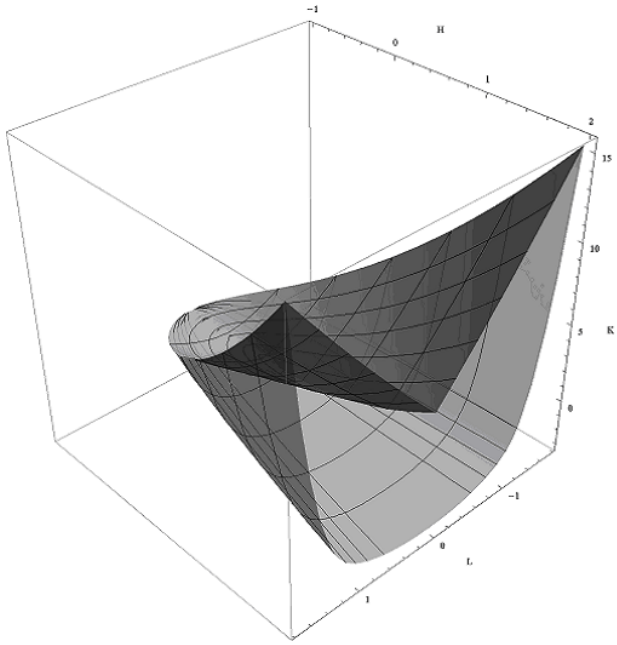

Fig. 19. The "bow" of the admissible domain

Now we turn to the classification of domain in the image of the subsystem $\mathcal{M}_3$. A complete description of the admissible domain on the planes of constants of the integrals (S, H) and (S, L) is given in [48, 50]. The following theorem corresponds to [50, Proposition 5].

Theorem 13. *The (S,L)-diagram of the critical system $\mathcal{M}_3$ consists of the following sets*:

$$\delta_2 : s=\theta_+(r),\quad \ell=\pm\eta_+(r),\quad r\in(-\infty,0];$$

$$\Delta_0 : \ell=\pm\sqrt{\frac{s}{2}(1-2\lambda^2 s)},\quad 0<s\le\frac{1}{2\lambda^2};$$

$$\Delta_3 : s=\frac{1}{2\lambda^{2/3}},\quad \begin{cases}\ell\in\mathbb{R}, & \lambda\le\lambda^*,\\ |\ell|\ge\dfrac{2\lambda^{2/3}-\sqrt{4+\lambda^{4/3}}}{\sqrt{2}(\sqrt{4+\lambda^{4/3}}-\lambda^{2/3})^{1/2}}, & \lambda>\lambda^*.\end{cases}$$

The admissible domain $\mathcal{D}_3$ does not contain the following components of the completion to the diagram in which critical motions do not exist: *the domain adjacent to the axis $s=0$ and bounded the branches of the curves Δ_0 and δ_2 for all λ; the domain bounded by the curve δ_2 between two points of intersection with the axis $\ell=0$ $(r\ne 0)$ for $\lambda>\lambda^*$.*

Surgeries of diagram types in the domain $\lambda\ge 0$ occur for the following values of the parameter: 0, λ_*, 1, λ^*, *and* $\sqrt{2}$.

Inequalities for r, s, and ℓ that determine the admissible domain for points of the key set are immediately implied by the criterion stated in Proposition 16.

For critical points of the subsystems $\mathcal{M}_{2,3}$, we separately formulate an assertion on the existence of degenerate periodic solutions, which is similar Proposition 15.

Proposition 20. *The admissible domain of the bifurcation diagram Σ of the moment mapping J contains the segment of the cusp of the surface Π_3, which is the image of degenerate rank-1 critical motion*:

$$\Delta_3 :\quad \ell=\pm\sqrt{\frac{h-h^*}{2}},\quad h\in\begin{cases}[h^*,+\infty) & \text{for } \lambda\le\lambda^*,\\ [h^{**},+\infty) & \text{for } \lambda>\lambda^*,\end{cases}$$

where

$$h^*=\frac{\lambda^{2/3}}{2}(3-\lambda^{4/3}),$$

$$h^{**}=\frac{1}{4}\left[(4+\lambda^{4/3})^{3/2}-\lambda^{2/3}(6+\lambda^{4/3})\right]=\frac{1}{8}\left(\sqrt{4+\lambda^{4/3}}-\lambda^{2/3}\right)^2\left(2\sqrt{4+\lambda^{4/3}}+\lambda^{2/3}\right),$$

or, in terms of the constants s and ℓ,

$$\Delta_3 :\quad s=\frac{1}{2\lambda^{1/3}},\qquad \begin{cases}\ell\in\mathbb{R}, & \lambda\le\lambda^*,\\ |\ell|\ge\dfrac{2\lambda^{2/3}-\sqrt{4+\lambda^{4/3}}}{\sqrt{2}\left(\sqrt{4+\lambda^{4/3}}-\lambda^{2/3}\right)^{1/2}}, & \lambda>\lambda^*.\end{cases}\tag{4.31}$$

The assertion in the coordinates (s,ℓ) is a part of Theorem 13. The transition to the plane (ℓ,h) is performed by the formulas (2.8), which imply that on the surface Π_3

$$h=2\ell^2+h_0(s),\quad h_0(s)=\frac{1}{2s}-\frac{\lambda^2}{2}+2\lambda^2 s^2.\tag{4.32}$$

It is easy to see that the minimal value of $h_0(s)$ is attained at $s=1/(2\lambda^{1/3})$, i.e., at the intersection point of the minimum curve h on $\mathcal{M}_3$ with the image of the cusp Δ_3; this value is

$$\min_{s>0} h_0(s)=h^*.$$

Then for $\lambda\le\lambda^*$ and $\ell\in\mathbb{R}$, we have $h\in[h^*,+\infty)$. The boundary point is a new singular point on the key sets, which is important when considering H-atlases, since it is an extremum point of the h-coordinate on the image Δ_3 of the family of rank-1 degenerate points:

$$D_5 :\ \ell=0,\quad s_2=\frac{1}{2\lambda^{1/3}},\quad h=\frac{\lambda^{2/3}}{2}(3-\lambda^{4/3}),\quad \lambda\in[0,\lambda^*].\tag{4.33}$$

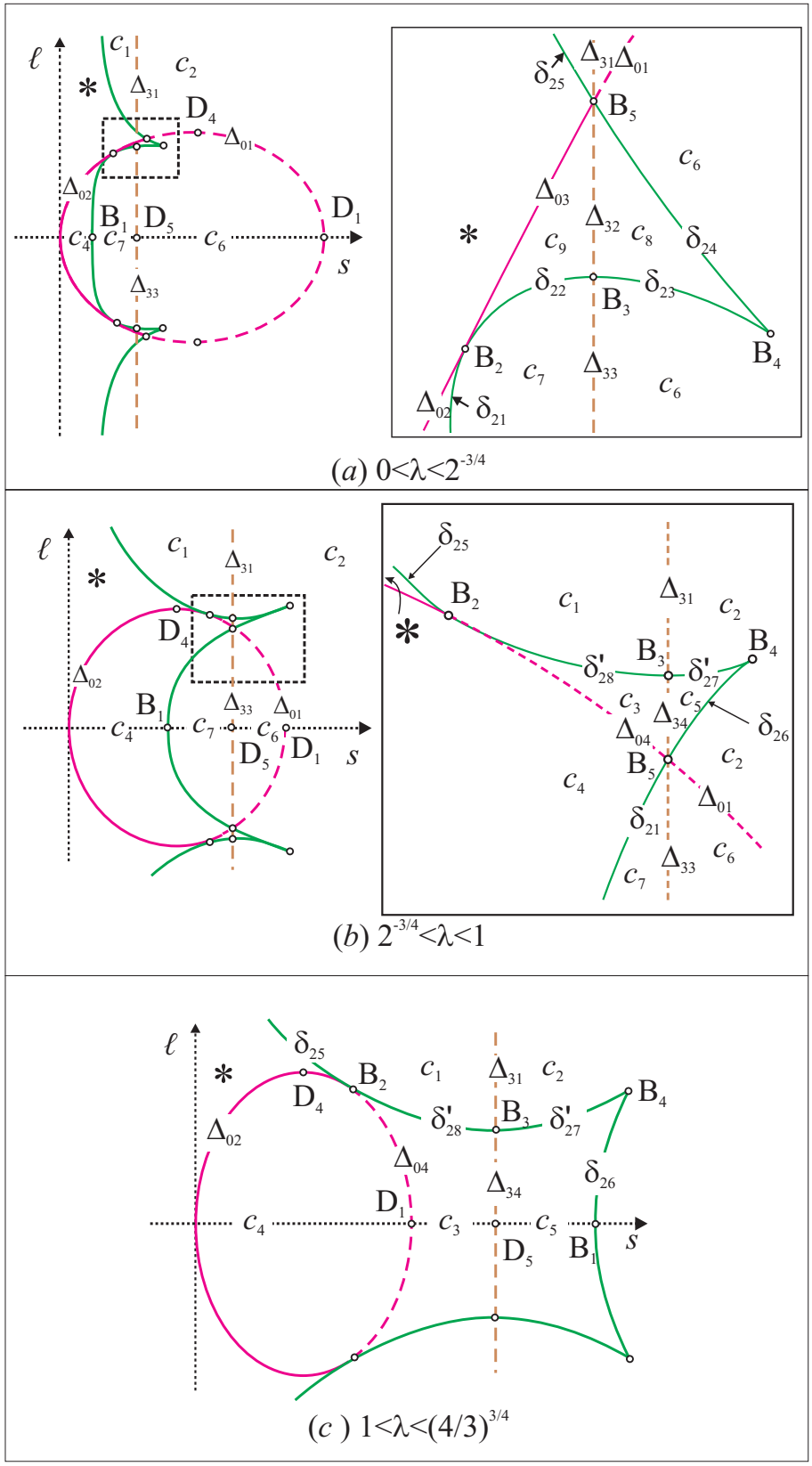

Fig. 20. The (S, L)-diagrams of the subsystem $\mathcal{M}_3$: detailing

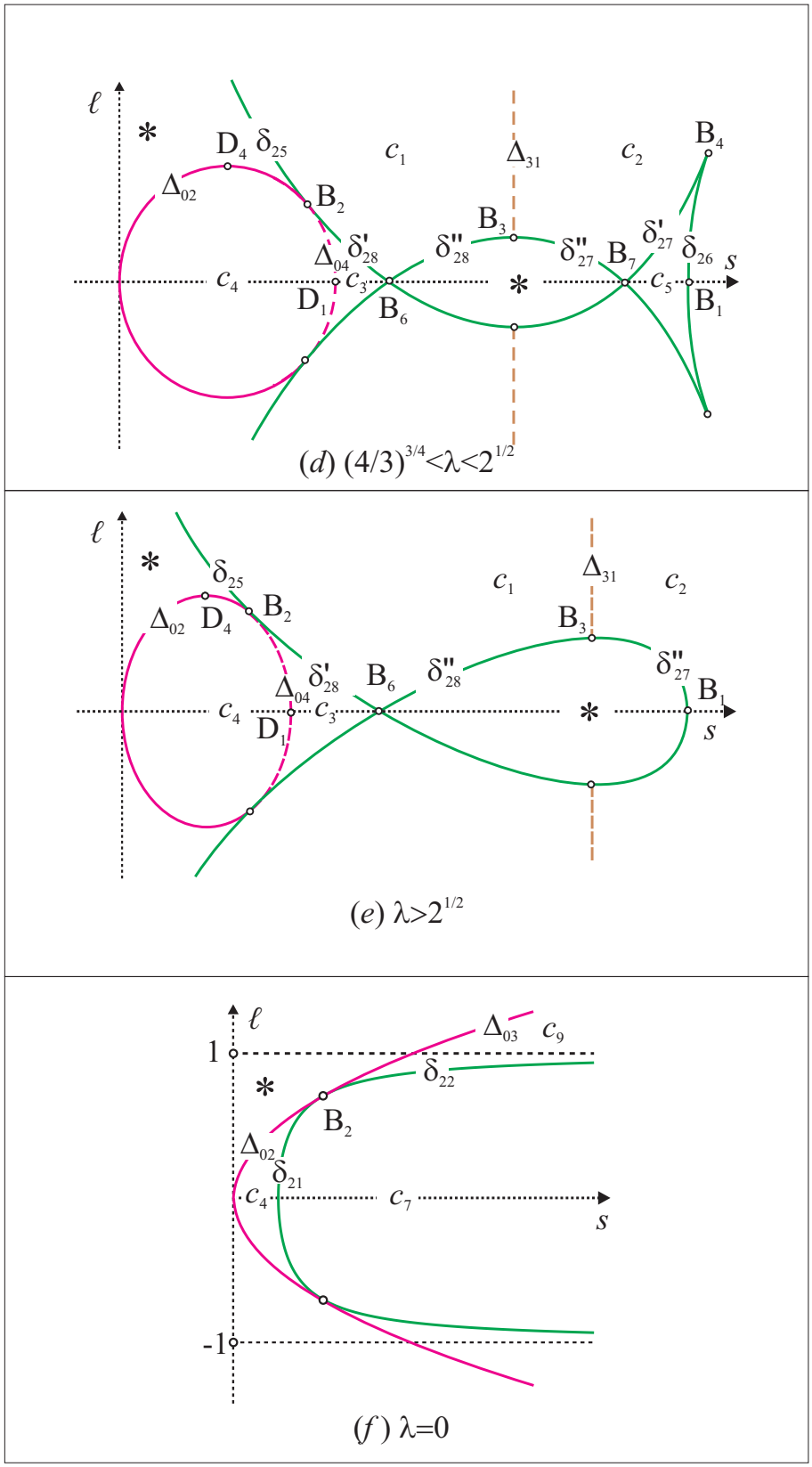

Fig. 20 (continued). The (S, L)-diagrams of the subsystem $\mathcal{M}_3$: detailing

In the case where $\lambda > \lambda^*$, calculating the value (4.32) on Δ_3 for the minimal admissible value of $|\ell|$ from (4.31), we arrive at the value h^{**}. These values correspond to the singular point B_3 of the key sets obtained earlier.

In Fig. 20, the (S, L)-diagrams of the critical subsystem $\mathcal{M}_{2,3}$ are shown:

(a) $0 < \lambda < \lambda_*$;
(b) $\lambda_* < \lambda < 1$;
(c) $1 < \lambda < \lambda^*$;
(d) $\lambda^* < \lambda < \sqrt{2}$;
(e) $\lambda > \sqrt{2}$;
(f) the limit case $\lambda = 0$.

Here we should recall the notation (3.51). The dotted lines represent the degeneracy curves Δ_0 and Δ_3, except for a part of the curve Δ_0, which is the exterior boundary of the admissible domain $\mathcal{D}_3$ (the solid line). As above, in domains marked with an asterisk (here $\overline{c_1}$ and $\overline{c_2}$), critical motions are impossible. The diagrams also contain the detailing of key sets in accordance with the classification of rank 0 critical points given above and also with a clear decomposition of the smooth curves Δ_0 and Δ_3 into smooth sections (for Δ_0, the decomposition has already been obtained earlier in the subsystem $\mathcal{M}_1$). Recall that this decomposition is generated by common points of these curves with the image of rank-0 points and intersection points. A relevant analysis will be performed in the next section.

The assertions of Theorem 13 that regard curves involved in the diagram are consequences of the definition of the diagram. Surgeries of the diagram with respect to λ are calculated directly (for detail, see [50]) or by the general property: they correspond to separating values of λ for sections $\lambda = \text{const}$ of the family of separating curves for rank-0 points in the plane (r, λ) and the set of extrema ℓ on the images of rank-1 degenerate points. To prove the part of the theorem regarding the existence of motions, it suffices to analyze the distribution of roots and signs of leading coefficients of the corresponding polynomials $Z_\pm$ and apply Proposition 16. A computer visualization of the curves Γ_0 and Γ_1 yields a visual proof in accordance with Proposition 19. The fact that in the domain $\overline{c_1}$ adjacent to the axis $O\ell$ (see Fig. 20(a)) motions are impossible is almost obvious since $s \neq 0$. The absence of critical motions in the domain $\overline{c_2}$ (see Fig. **??**(d), (e)) was proved in [29] by the analysis of points lying on the axis $\ell = 0$.

In Fig. 20, we also show singular points appearing on the (S, L)-diagrams of the subsystem $\mathcal{M}_3$. We can immediately verify that all of them have already been seen in the subsystem $\mathcal{M}_1$, except for the point D_5 defined by Eqs. (4.33) for the use in the H-atlas.

We reformulate Theorem 13 in terms of the integrals S and H (see [48]).

Theorem 14. *The (S, H)-diagram of the critical system $\mathcal{M}_3$ consists of the following curves*:

$$
\begin{aligned}
\Delta_0 &: \quad h = h_{\tan}(s), \qquad 0 < s \le \frac{1}{2\lambda^2};\\
\delta_2 &: \quad h = \varphi_+(r), \qquad s = \theta_+(r), \quad r \in (-\infty, 0];\\
\Delta_3 &: \quad s = \frac{1}{2\lambda^{2/3}}, \qquad \begin{cases} h \ge h^*, & \lambda \le \lambda^*,\\ h \ge h^{**}, & \lambda > \lambda^*; \end{cases}\\
h_{\min} &: \quad h = h_0(s), \qquad s \in I(\lambda),
\end{aligned}
$$

where

$$
h_{\tan}(s) = \frac{1 - \lambda^2 s + 2s^2}{2s},
$$

and the range of s on the curve $h_{\min}$ is defined as follows:

$$I(\lambda) = \begin{cases} (0, +\infty), & \lambda \le \lambda^*, \\ (0, s_0] \cup [s^0, +\infty), & \lambda^* \le \lambda \le \sqrt{2}, \\ (0, s_0] \cup [1/2, +\infty), & \lambda \ge \sqrt{2}. \end{cases}$$

Here $s_0(\lambda)$ and $s^0(\lambda)$ are abscissas of the tangency points of the curves δ_2 and $h_{\min}$ that exist if $\lambda \ge \lambda^*$. They satisfy the inequalities $s_0(\lambda) < s^0(\lambda)$ for $\lambda > \lambda^*$ and $s^0(\lambda) < 1/2$ for $\lambda^* \le \lambda < \sqrt{2}$.

The exterior boundaries of the admissible domains are as follows:

(1) *the curve $h_{\min}$ within the limits $s \in I(\lambda)$;*
(2) *the curve Δ_0 within the limits*

$$s \in \begin{cases} (0, 1/(2\lambda^{2/3})], & \lambda \le \lambda_*, \\ (0, \sqrt{1+\lambda^4} - \lambda^2], & \lambda \ge \lambda_*; \end{cases}$$

(3) *the curve δ_2 within the limits*

$$s \in \begin{cases} [s_0, s^0], & \lambda^* \le \lambda \le \sqrt{2}, \\ [s_0, 1/2], & \lambda \ge \sqrt{2}. \end{cases}$$

Surgeries of diagram types in the domain $\lambda \ge 0$ occur at the following values of the parameter: 0, λ_*, 1, λ^*, *and* $\sqrt{2}$.

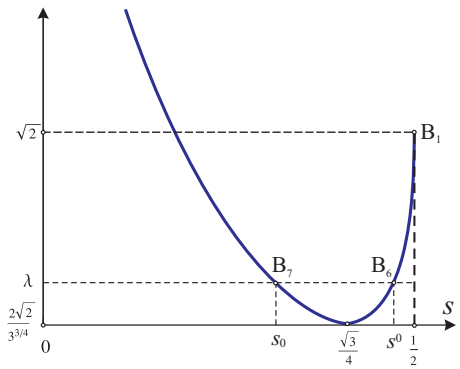

Fig. 21. The connection of s and λ at the points $B_{6,7}$

The curve $h_{\min}$ corresponds to the value $\ell = 0$, and its occurrence is naturally associated with the fold that appears on the covering of the plane (s, h) by the surface Π_3, since h is expressed through ℓ^2. A complete analysis of (S, H)-diagrams of the subsystem $\mathcal{M}_3$ and its computer visualization was performed in [31, 48]. The values s_0 and s^0 correspond to singular points B_6 and B_7 marked on the (S, L)-diagrams in Figs. 20(d) and (e). These points exist for $\lambda \ge \lambda^*$ (note that they coincide when $\lambda = \lambda^*$) and at the moment $\lambda = \sqrt{2}$, the points B_7 and B_1 merge and then pass into the inadmissible domain (the corresponding value of r would be positive on δ_2, which is not so). For proofs and explanations, see [48]; they easily follow from the constraint equation for s and λ at these points. The constraint equation can be obtained by eliminating the auxiliary parameter x from the corresponding parametric representation (4.21) of the values s_2 and λ at these points (see Fig. 21):

$$\lambda = \frac{\sqrt{1+2s} - \sqrt{1-2s}}{(2s)^{3/2}}, \quad s \in (0, \frac{1}{2}].$$

Table 4.4

Domain (life time)	Number of circles	Morse–Bott indexes	Exit on $\lambda = 0/\ell = 0$	Atom	Analogs
c_1 $(0 < \lambda < +\infty)$	1	$(- -)$	No/No	A_-	Absent
c_2 $(0 < \lambda < +\infty)$	1	$(- +)$	No/Yes	B_+	a_5 [46, Fig. 2] β_3 [20, Fig. 1]
c_3 $(\lambda_* < \lambda < +\infty)$	2	$(- -)$, $(- -)$	No/Yes	$2A_-$	b_4 [46, Fig. 3] α_7 [20, Fig. 1]
c_4 $(0 \le \lambda < +\infty)$	2	$(+ -)$, $(+ -)$	Yes/Yes	C_2	8 [40, Fig. 6.3] a_4, b_5 [46, Fig. 2, 3] β_2 [7, Fig. 11] γ [20, Fig. 1]
c_5 $(\lambda_* < \lambda < \sqrt{2})$	2	$(- +)$, $(- +)$	No/Yes	$2B_+$	b_3 [46, Fig. 3] β_4 [20, Fig. 1]
c_6 $(0 < \lambda < 1)$	1	$(+ +)$	No/Yes	A_+	a_3, a_4 [46, Fig. 2] α_4 [20, Fig. 1]
c_7 $(0 \le \lambda < 1)$	1	$(+ -)$	Yes/Yes	B_-	7 [40, Fig. 6.3] a_3 [46, Fig. 2] β_1 [7, Fig. 11] β_2 [20, Fig. 1]
c_8 $(0 < \lambda < \lambda_*)$	2	$(+ +)$, $(+ +)$	No/No	$2A_+$	Absent
c_9 $(0 \le \lambda < \lambda_*)$	2	$(+ -)$, $(+ -)$	Yes/No	$2B_-$	E [38, Fig. 2] β_3 [7, Fig. 11]

Application of the results obtained to points of the domains c_1–c_9 in the (s, ℓ)-image of the subsystem $\mathcal{M}_3$ leads to the description of characteristics and atoms collected in Table 4.4. As we can see, all domains except for c_1 and c_8, when considering the expanded diagram in the space (s, ℓ, λ), are related with the corresponding domains of problems studied earlier ($\lambda = 0$ or $\ell = 0$), so only the atom direction is added here. In particular, the presence of the atom C_2 in the domain c_4 and the two atoms B in the domain c_9 is explained in [38–40](in another notation). The presense of the two atoms B in the domain c_5 follows from the results of [46]. In the new domain c_1 and c_8, according to what was proved above, critical circles have elliptical type, their number is calculated according to the criteria proposed, and the direction is defined by the Morse–Bott indexes.

4.4. Classes of rank-1 degenerate points.

4.4.1. The set Δ_0. The first class of rank-1 degenerate points consists of points in the preimage of the tangent line of bifurcation surfaces. The image of this set in the space of integral constants is denoted by Δ_0; this is the tangent line of the surfaces Π_1 and Π_3. The equation of this line is

$$2s^2 - 2\left(h + \frac{\lambda^2}{2}\right)s + 1 = 0 \tag{4.34}$$

in the parameters s and h and

$$2\lambda^2 s^2 - s + 2\ell^2 = 0 \tag{4.35}$$

in the parameters s and ℓ. Together with the realness condition, we obtain the following representation for Δ_0:

$$\ell = \pm\sqrt{\frac{s}{2}\big(1 - 2\lambda^2 s\big)}, \quad h = s + \frac{1}{2s} - \frac{\lambda^2}{2}, \quad s \in \left(0, \frac{1}{2\lambda^2}\right].$$

The intersection of this set with the image of the set of rank-0 critical points (i.e., with the subsets δ_i, $i = 1, 2, 3$, of the space of integral constants) divides it into several parts with completely different behavior. Indeed, outside this intersection, a neighborhood of a point of the set Δ_0 is mapped by a diffeomorphism as a stratified manifold and the topology of the corresponding preimage is preserved.

Let us recall the equations of the sets δ_i:

$$\begin{gathered}\ell = \mp\frac{1}{2}\Big[\lambda\big(r - \lambda\big) + d\Big]\sqrt{\frac{r}{2}\left[-r + \frac{1}{r - \lambda}d\right]}, \quad h = -\frac{1}{2}r(r - \lambda) + \frac{2r - \lambda}{2(r - \lambda)}d, \\ d^2 = 4 + r^2(r - \lambda)^2, \quad r \in (-\infty, 0] \cup [0, \lambda) \cup (\lambda, +\infty).\end{gathered} \tag{4.36}$$

The correspondence of the numbers of subsets, the intervals of values of the constant r that defines the relative equilibrium, and the signs of d are as follows:

$$\begin{aligned}&\delta_1: \quad r \in [0, \lambda), && d < 0;\\ &\delta_2: \quad r \in (-\infty, 0], && d > 0;\\ &\delta_3: \quad r \in (\lambda, +\infty), && d > 0.\end{aligned}$$

The parameter s of the surfaces Π_i, which is a particular integral for the critical subsystems $\mathcal{M}_i$, takes the following values at the points (4.36): in the subsystem $\mathcal{M}_1$ (for all three curves δ_i)

$$s = \frac{1}{2}\Big[\lambda\big(r - \lambda\big) + d\Big] \tag{4.37}$$

and in the subsystems $\mathcal{M}_2$ (the curves δ_1 and δ_3) and $\mathcal{M}_3$ (the curve δ_2)

$$s = \frac{r - \lambda}{4\lambda}\Big[r\big(r - \lambda\big) - d\Big]. \tag{4.38}$$

Now we use the expression on $\mathcal{M}_1$; then at surgery points of Δ_0, the equation (4.36) must be compatible, for example, with (4.34). We obtain

$$r^2 - 2\lambda^2 + \frac{2}{\lambda(r - \lambda) + d} - \frac{r}{r - \lambda}d = 0.$$

Hence either

$$r = -\lambda \tag{4.39}$$

or

$$2 + \big(r - \lambda\big)^2\big(r^2 - 2\lambda r + 2\lambda^2\big) - \big(r - \lambda\big)\big(r - 2\lambda\big)d = 0.$$

The last equation can be rewritten in the form

$$\frac{1}{2}\Big[(r - \lambda)(r - 2\lambda) - d\Big]^2 = 0. \tag{4.40}$$

In particular, this means that it described the tangency point of Δ_0 with one of the curves δ_i. We examine which curves δ_i correspond to the values (4.39) and (4.40). For (4.39), it is obvious that $r < 0$, so that it is an intersection point of Δ_0 with δ_2. A consequence of Eq. (4.40) is

$$\lambda(r - \lambda)^3 + 1 = 0,$$

which implies

$$r = \lambda - \frac{1}{\lambda^{1/3}}. \tag{4.41}$$

At the same time, according to (4.40), the equation

$$\operatorname{sgn} d = \operatorname{sgn}(r-\lambda)(r-2\lambda)$$

holds, which, under the obvious inequality $r < \lambda$, is possible only for $r \le 0$, i.e., on the curve $r \le 0$. Thus, the tangency point (4.41) of Δ_0 and δ_2 exists only when $\lambda \le 1$.

Thus, taking s and λ as independent parameters on Δ_0 (if we replace s by h or by ℓ, then the correspondence in the domain is not bijective), we obtain the following separating curves in the square $\{(\lambda, s) : \lambda \ge 0,\ s > 0\}$:

(1) the upper boundary of admissible values corresponding to the point D_1 in the key sets:

$$\varphi_0 : s = \frac{1}{2\lambda^2}, \quad \lambda > 0;$$

(2) the curve obtained from (4.36) and (4.39) and corresponding to the point B_5 in the key sets:

$$\varphi_1 : s = \sqrt{1+\lambda^4} - \lambda^2, \quad \lambda \ge 0;$$

(3) the curve obtained from (4.37) and (4.41) and corresponding to the point B_5 in the key sets:

$$\varphi_2 : s = \frac{1}{2\lambda^{2/3}}, \quad \lambda \in (0, 1].$$

The corresponding domain is shown in Fig. 22, where we denote the appearing subdomains in accordance with Fig. 15 and 20, where each such subdomain generates a segment of the key set. These subdomains play the role of nodal points in the bifurcation diagrams $\Sigma_{HK}(\ell, \lambda)$. Note that the separating curves for Δ_0 correspond to structurally unstable diagrams $\Sigma_{HK}(\ell, \lambda)$: on the plane (λ, ℓ) the calculation of $\ell(\lambda)$ by the formula (4.35) maps the curve φ_0 into the axis $\ell = 0$, the curve φ_1 into the curve π_{22} of the separating set Θ_L, and the curve φ_3 into the curve π_{21} in accordance with formulas (3.45).

As we see in Fig. 22, the points Δ_{02} and Δ_{03} are related with the classical Kovalevskaya problem ($\lambda = 0$), whereas the points Δ_{01} and Δ_{04} also exist in the Ryabov–Morozov case ($\ell = 0$). So, at first glance, it may seem that the description of the relevant loop molecules can be performed within the frameworks of [7, 20]. However, this is not quite true. The topology of all levels of first integrals in punctured neighborhoods of these points was examined in [39, 46], but this does not answer the following question: How must one join different families while traversing the test points? Depending on this, the manifold in the preimage of a small circle centered at the point can have various number of connected components. Let us denote by J_{0i} the union of connected components of the preimage of point Δ_{0i} that contain critical points of the moment mapping (i.e., critical circles consisting of rank-1 degenerate points).

Note that segments of Δ_{0i} *inside* the critical subsystem $\mathcal{M}_1$ are not bifurcation segments: they correspond to the degeneration of critical motions only relatively the complete system. In particular, the number of critical circles in the preimage Δ_{0i} is the same as in the preimage of the neighboring domains on both sides of a_j. According to the diagrams of the subsystem $\mathcal{M}_1$ and Table 4.1, we establish that Δ_{01} separates a_5 and a_9 (two critical circles in J_{01}), Δ_{02} separates a_9 and a_{11} (one critical circle), Δ_{03} separates a_5 and a_8 (two critical circles), and Δ_{04} separates a_9 and a_{11} (two critical circles). Thus, the surface J_{02} is connected. For the rest of the points on the level J_{0i}, there are two critical circles, so one cannot restore loop molecules by the available data. In [7, 20], the hypothesis was implicitly used that the loop molecules of these points have two connected components, but there are no motivation for this hypothesis, not to mention proofs. In fact, a "principle of maximum likelihood" was used, according to which molecules to be found are among the already known molecules. We prove that the answer obtained is correct.

Theorem 15. *The surfaces J_{01}, J_{03}, and J_{04} consist of two connected components.*

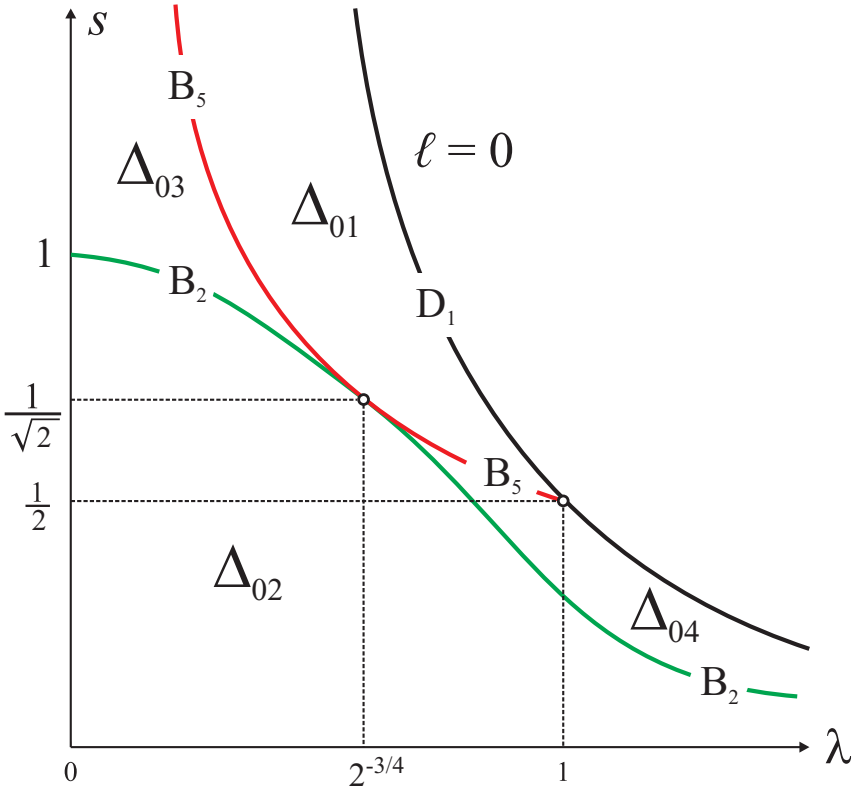

Fig. 22. Separating curves for points of Δ_0

Proof. For $\lambda \neq 0$, we use the quadratures obtained in [11]. The set Δ_0 corresponds to the following values of the parameters:

$$L_3 = 0, \quad L_1 = \frac{s}{8} > 0. \tag{4.42}$$

Therefore, the system is reduced to two equations

$$\dot{\eta}^2 = \frac{L_1}{F^2(z)}, \quad \dot{z} = \sqrt{f(z)}, \tag{4.43}$$

where

$$F(z) = z(z - 2\lambda) - \frac{1}{2}\left(s - \frac{1}{s}\right), \quad f(z) = \left(\frac{s}{2} - z^2\right) F(z),$$

the variable z is real, and the auxiliary variable η, which is not equal to infinity only on asymptotic motions, is introduced by the equality

$$\eta = \frac{y}{\sqrt{F(z)}},$$

where the variable y is also real. From (4.42) and (4.43) we conclude that $\dot{\eta}^2 > 0$, so the variable η is also real, and, in addition to the condition $f(z) \geq 0$ of the existence of a real interval where the variable z oscillates, we obtain the condition $F(z) \geq 0$ of the existence of asymptotic motions. Setting

$$\ell = 0, \quad s = \frac{1}{2\lambda^2},$$

we obtain

$$F(z) = \left[z - \left(\lambda + \frac{1}{2\lambda}\right)\right]\left[z - \left(\lambda - \frac{1}{2\lambda}\right)\right], \quad f(z) = \left(\frac{1}{4\lambda^2} - z^2\right) F(z).$$

The variable z oscillates on the intervals

$$\left[-\frac{1}{2\lambda},\ \lambda-\frac{1}{2\lambda}\right],\quad \left[\frac{1}{2\lambda},\ \lambda+\frac{1}{2\lambda}\right]$$

under the condition $\lambda<1$ and on the intervals

$$\left[-\frac{1}{2\lambda},\ \frac{1}{2\lambda}\right],\quad \left[\lambda-\frac{1}{2\lambda},\ \lambda+\frac{1}{2\lambda}\right]$$

under the condition $\lambda>1$. In both cases, $F(z)\geq 0$ in the first interval and $F(z)\leq 0$ in the second interval. Therefore, asymptotic motions exist for the first critical circle and do not exist for the second. Consequently, the second critical circle exhausts its connected component of the critical integral surface. Thus, for points Δ_{01} and Δ_{04}, the preimage contains two connected components with critical circles.

For the point Δ_{03} we can set $\lambda=0$. Then

$$F(z)=z^2-\frac{1}{2}\left(s-\frac{1}{s}\right),\quad f(z)=\left(\frac{s}{2}-z^2\right)F(z),\quad s>1.$$

Thus, z oscillates in the symmetric intervals

$$\left[-\sqrt{\frac{s}{2}},\ -\sqrt{\frac{1}{2}\left(s-\frac{1}{s}\right)}\right],\quad \left[\sqrt{\frac{1}{2}\left(s-\frac{1}{s}\right)},\ \sqrt{\frac{s}{2}}\right],$$

and for both critical circles, asymptotic motions exist. Clearly, different intervals of oscillation of z cannot have the same limit when they tend to distinct critical circles. However, this still must be strictly proved based on quadratures obtained in [11]; this requires certain technical calculations. As a result, we obtain that on a connected component of the integral surface, the variable z cannot change its interval of oscillation, so there are two such components (the same number as the number of critical circles). We also present another proof of the existence of two connected components. Note that, despite the strong degeneracy, the formulas derived from the equations of first integrals do not provide any foreseeable solution to this problem. We use equations obtained by Kovalevskaya and the results of [42]. Recall that in the Kovalevskaya separation variables s_1 and s_2 the equations of motion have the form

$$(s_2-s_1)\frac{ds_1}{dt}=\mathrm{i}\sqrt{2S(s_1)},\quad (s_2-s_1)\frac{ds_2}{dt}=-\mathrm{i}\sqrt{2S(s_2)},$$

where

$$S(x)=(x-h+\sqrt{k})(x-h-\sqrt{k})\varphi(x),\quad \varphi(x)=x(x-h)^2+(1-k)x-2\ell^2,$$

and $s_1\geq s_2$. S. Kovalevskaya also found expressions for all phase variables through separation variables in the form of single-valued functions of s_1 and s_2 and a set of algebraic radicals:

$$R_{i\gamma}=\sqrt{s_i-e_\gamma},\quad i=1,2,\ \gamma=1,\dots,5, \tag{4.44}$$

where e_γ are roots of the polynomial $S(x)$. We denote by e_1, e_2, and e_3 the roots of $\varphi(x)$ in the ascending order if they are real and set $e_{4,5}=h\mp\sqrt{k}$. It is known (see [4, 17]) that in the case where $\varphi(x)$ has three real roots, the separation variables vary in the domains

$$s_1\in\Big[\max\big\{e_1,\ e_2,\ e_3,\ e_4\big\},\ e_5\Big],\quad s_2\in\Big[-\infty,\min\big\{e_1,\ e_2,\ e_3,\ e_4,\ e_5\big\}\Big],$$

and, as was shown in [42] by the method of Boolean functions, the expressions for phase variables in the general case can be reduced to single-valued functions of the following products of algebraic

radicals in the real-valued form:

$$\begin{gathered}\sqrt{s_1-e_1}\,\sqrt{\frac{e_2-s_2}{e_5-s_2}}\,\sqrt{\frac{e_3-s_2}{e_5-s_2}}\,\sqrt{\frac{e_4-s_2}{e_5-s_2}},\\ \sqrt{s_1-e_2}\,\sqrt{\frac{e_1-s_2}{e_5-s_2}}\,\sqrt{\frac{e_3-s_2}{e_5-s_2}}\,\sqrt{\frac{e_4-s_2}{e_5-s_2}},\\ \sqrt{s_1-e_3}\,\sqrt{\frac{e_2-s_2}{e_5-s_2}}\,\sqrt{\frac{e_2-s_2}{e_5-s_2}}\,\sqrt{\frac{e_4-s_2}{e_5-s_2}}\end{gathered} \tag{4.45}$$

(the radicals containing quotients of differences do not change their sign for $s_2=-\infty$). In the case where the separation variable is reflected from the boundary of its oscillation domain, the corresponding radical should be considered to change its sign (the radical corresponding to the value $s_2=-\infty$ has already been excluded by the procedure of reduction to formulas (4.45)). If any of the boundary values is a multiple root, then the corresponding radical is also considered to change sign, since the asymptotic trajectory together with its boundary points is a connected set.

Now we consider the point Δ_{03} for $\lambda=0$. In this case,

$$e_1=\frac{1}{s}<e_2=e_3=e_4=s<e_5=s+\frac{1}{s}$$

(recall that $s>1$). Then, denoting the triple root by e_*, we obtain

$$s_1\in[e_*,e_5],\quad s_2\in[-\infty,e_1].$$

Among the expressions (4.45), the second and third ones coincide, amd the product of the pair of identical radicals becomes a single-valued function that does not influence the sign of algebraic expressions. The following algebraic expressions remain:

$$\sqrt{s_1-e_1}\,\sqrt{\frac{e_*-s_2}{e_5-s_2}},\quad \sqrt{s_1-e_*}\,\sqrt{\frac{e_1-s_2}{e_5-s_2}};$$

the second one changes its sign on the connected component of the integral surface and hence the number of connected components is independent of it. The first expression along the closure of any trajectory preserves its sign selected at the initial moment. Consequently, the surface J_{03} has two connected components. The theorem is proved. □

4.4.2. Δ_1 *set.* The following class of rank-1 degenerate points consists of points lying in the preimage of the cusp of the surface Π_1. For integral parameters on this set Δ_1, taking into account the conditions of existence of motions, we have

$$\ell=\pm\frac{1}{\sqrt{2}}s^{3/2},\quad h=\frac{3}{2}s+\frac{\lambda^2}{2},\quad s\in[0,s_*], \tag{4.46}$$

where $s_*=s_*(\lambda)$ is the largest real root of the equation

$$9s^4+2\lambda^2s^3-24s^2-24\lambda^2s+4(4-\lambda^4)=0, \tag{4.47}$$

which exist and is positive for all $\lambda\geq 0$. The intersection of the set Δ_1 with the image of the set of rank-0 critical points (i.e., with the subsets δ_i of the space of integral constants) and with the set Δ_0 examined above divides the set Δ_1 into several parts with completely different behavior. Obviously, the curve δ_1 is not involved in these intersections. We can immediately verify that all points of the intersection $\Delta_1\cap\Delta_0$ are contained in $\Delta_1\cap\delta_2$. The condition of intersection $\Delta_1\cap(\delta_2\cup\delta_3)$ can be represented either by Eq. (4.47) or by the equation

$$s^2+2\lambda^2s-1=0. \tag{4.48}$$

On the plane (λ, s) we obtain the separating curves

$$\psi_1: \quad \lambda = \left| \frac{\sqrt{s^2+4} - 2s}{\left(\sqrt{s^2+4} - s\right)^{1/2}} \right|, \quad s > 0; \tag{4.49}$$

$$\psi_2: \quad \lambda = \sqrt{\frac{1}{2}\left(\frac{1}{s} - s\right)}, \quad s \in (0,1] \quad \Leftrightarrow \quad s = \sqrt{1+\lambda^4} - \lambda^2, \quad \lambda \geq 0. \tag{4.50}$$

Taking into account (4.46), we see that the image of the curve ψ_1 on the plane (ℓ, λ) is the union of the curves π_{23} and π_{31}, which can be represented by the graph of the single-valued function

$$\lambda = \left| \frac{\sqrt{s^2+4} - 2s}{\left(\sqrt{s^2+4} - s\right)^{1/2}} \right|, \quad s = \left(\sqrt{2}\ell\right)^{2/3}, \quad \ell \geq 0.$$

The image of the curve ψ_2 is the curve π_{22} in the representation (3.45).

The upper boundary s_* of values of s is the branch of the curve (4.49) for $s \geq 2/\sqrt{3}$ obtained as the intersection of Δ_1 with δ_3 (the point C on the key sets). Another branch of the curve (4.49) for values $s \in (0, 2/\sqrt{3}]$ and the curve (4.50) is the intersections of Δ_1 with δ_2 (respectively, the points B_4 and B_2 on the key sets; note that B_4 and C merge for $\lambda = 0$). The separating set and the notation of the corresponding points on the diagrams of the subsystem $\mathcal{M}_1$ and on the bifurcation diagrams are presented in Fig. 23. The points Δ_{11} and Δ_{13} are related with the particular case $\lambda = 0$, the point Δ_{14} exists in the particular case $\ell = 0$, and the point Δ_{12} does not have such analogs.

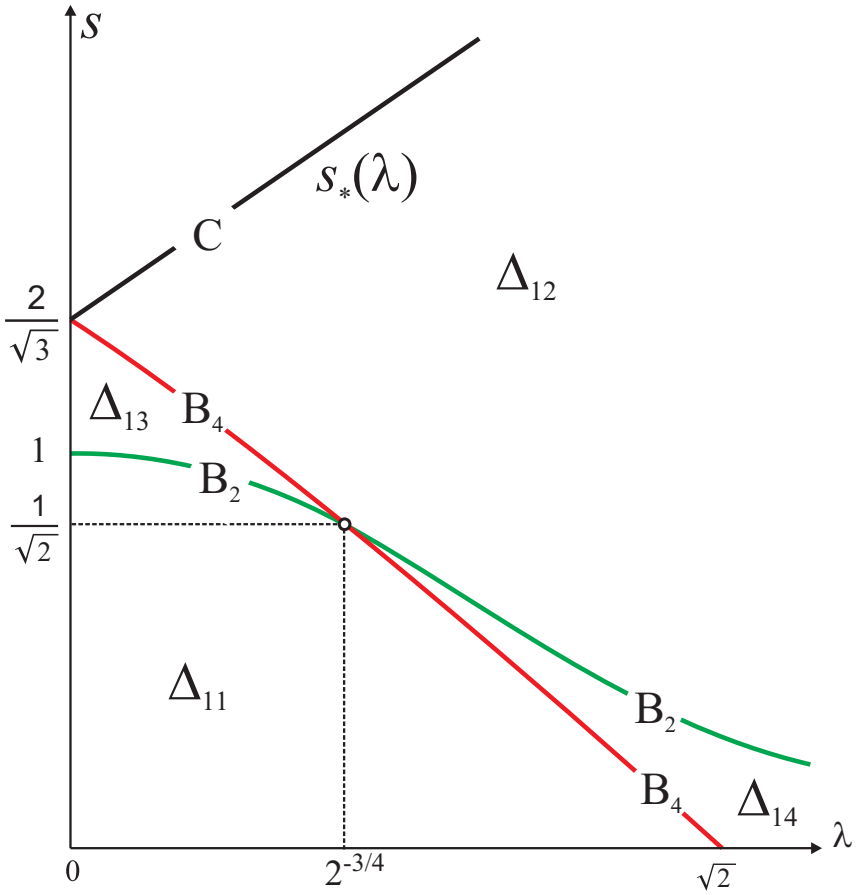

Fig. 23. Separating curves for points of Δ_1

As above, the number of critical circles in the preimage of Δ_{1i} can be found by the diagrams of the subsystem $\mathcal{M}_1$ and data for adjacent domains from Table 4.1. We see that Δ_{11} separates a_2 and a_6 (one critical circle in the preimage), Δ_{12} separates a_3 and a_4 (one critical circle), Δ_{13} separates a_7 and a_8 (two critical circles), and Δ_{14} separates a_{10} and a_{11} (two critical circles). In the case where the preimage of the point Δ_{1i} contains only one degenerate circle, i.e., the corresponding critical integral surface and the loop molecule are connected, we establish below the number of sets involved in bifurcations for accurate description of the topology of neighborhoods of these points. This easily follows from the results of adjacent chambers and numbers of families in these chambers. If there are two circles, then for justifying the structure of loop molecules, it is necessary to determine the number of connected components of the critical surface, which is the preimage of Δ_{1i}. By default, in [7] it was assumed that in the case where $\lambda = 0$, the loop molecule of the point Δ_{13} consists of two connected components, and also it was considered in [20] that the loop molecule of the point Δ_{14} also consists of two components for $\ell = 0$. We prove the following general assertion using quadratures found by Gashenenko. Similarly to the previous case, we denote by J_{1i} the union of connected components of the preimage of the point Δ_{1i} that contain critical points of the moment mapping.

Theorem 16. *The surfaces J_{13} and J_{14} consist of two connected components.*

Proof. By the definition of point classes, we assume that (λ, s) belongs to the corresponding open subdomain in Fig. 23. In terms of (λ, s), the polynomial $f(z)$ from (1.32) becomes

$$f(z) = -z^2(z-\lambda)^2 + \frac{1}{2}sz(z-2\lambda) - \frac{1}{4}(s^2-1).$$

Obviously, its discriminant is the product of the polynomials on the left-hand sides of (4.47) and (4.48). The polynomial $f(z)$ has four real roots in the domains Δ_{13} and Δ_{14} (it suffices to consider its traces on the coordinate axes when the corresponding equation is solved explicitly). As was noted above, the variable z cannot change its oscillation interval on the connected component of the integral manifold; therefore, there are exactly two such components. □

In general, according to (4.8), the points Δ_1 correspond to the case $L_2 = 0$ in the Gashenenko solution. Then from (1.33) and (1.34) we obtain

$$L_1 > 0, \quad F(z) = (z-\lambda)^2 \geq 0;$$

therefore, for both critical circles there exist asymptotic motions.

4.4.3. The set Δ_3. The last class Δ_3 of rank-1 degenerate points consists of points lying in the preimage of the cusp of the surface Π_3. For the integral parameters on this set, taking into account the conditions of existence of motions, we have

$$h = h^* + 2\ell^2, \quad \begin{cases} \ell \in \mathbb{R}, & \lambda \leq \lambda^*, \\ |\ell| \geq \ell^*, & \lambda > \lambda^*, \end{cases} \qquad s = \frac{1}{2\lambda^{2/3}}, \quad k = -4\lambda^2\ell^2 + k^*,$$

where

$$\lambda^* = \frac{2\sqrt{2}}{3^{3/4}}, \quad \ell^* = \frac{2\lambda^{2/3} - \sqrt{4+\lambda^{4/3}}}{\sqrt{2}\left(\sqrt{4+\lambda^{4/3}} - \lambda^{2/3}\right)^{1/2}} > 0 \qquad (\lambda > \lambda^*),$$

$$h^* = \frac{1}{2}\lambda^{2/3}\left(3 - \lambda^{4/3}\right), \quad k^* = (\lambda^{4/3}-1)^3 + 1.$$

The intersection of the set Δ_3 with the image of the set of rank-0 critical points (i.e., with the subsets δ_i of the space of integral constants) and with the sets Δ_0 and Δ_1 studied above divides this set into several parts with completely different behavior. Obviously, the curves δ_1 and δ_3 are not involved in these intersections since they have no common points with Π_3. We can directly verify that all points of intersections $\Delta_3 \cap \Delta_0$ and $\Delta_3 \cap \Delta_1$ are contained in $\Delta_3 \cap \delta_2$. Since s is constant on Δ_3 for fixed λ, as the parameters defining the point Δ_3 we can take λ and ℓ. Then the conditions of the

intersection $\Delta_3 \cap \delta_2$ (the point B_3 of the key sets for all λ and the point B_5 for $\lambda \in [0,1]$) are reduced to the equations of two separating curves θ_1 and θ_2 and allow one to classify the diagrams $\Sigma_{HK}(\ell, \lambda)$:

$$\theta_1: \quad \ell = \frac{1}{2\lambda^{1/3}}\sqrt{1-\lambda^{4/3}}, \qquad 0 < \lambda \le 1,$$

$$\theta_2: \quad \ell = \frac{|2\lambda^{2/3} - \sqrt{4+\lambda^{4/3}}|}{\sqrt{2}\left(\sqrt{4+\lambda^{4/3}} - \lambda^{2/3}\right)^{1/2}}, \qquad \lambda \ge 0.$$

Clearly, the equality $\ell(\lambda^*) = 0$ holds on θ_2 and

$$\ell(\lambda) = \frac{2\lambda^{2/3} - \sqrt{4+\lambda^{4/3}}}{\sqrt{2}\left(\sqrt{4+\lambda^{4/3}} - \lambda^{2/3}\right)^{1/2}} = \ell^*$$

for $\lambda > \lambda^*$. Therefore, the branch of the curve θ_2 for $\lambda \ge \lambda^*$ is the boundary of the domain Δ_3. Separating curves and the notation of points Δ_{3i} corresponding to Fig. 20 are shown in Fig. 24. Comparing it with (3.45), we see that the curve θ_1 is exactly π_{21} and the curve θ_2 is exactly π_{24}.

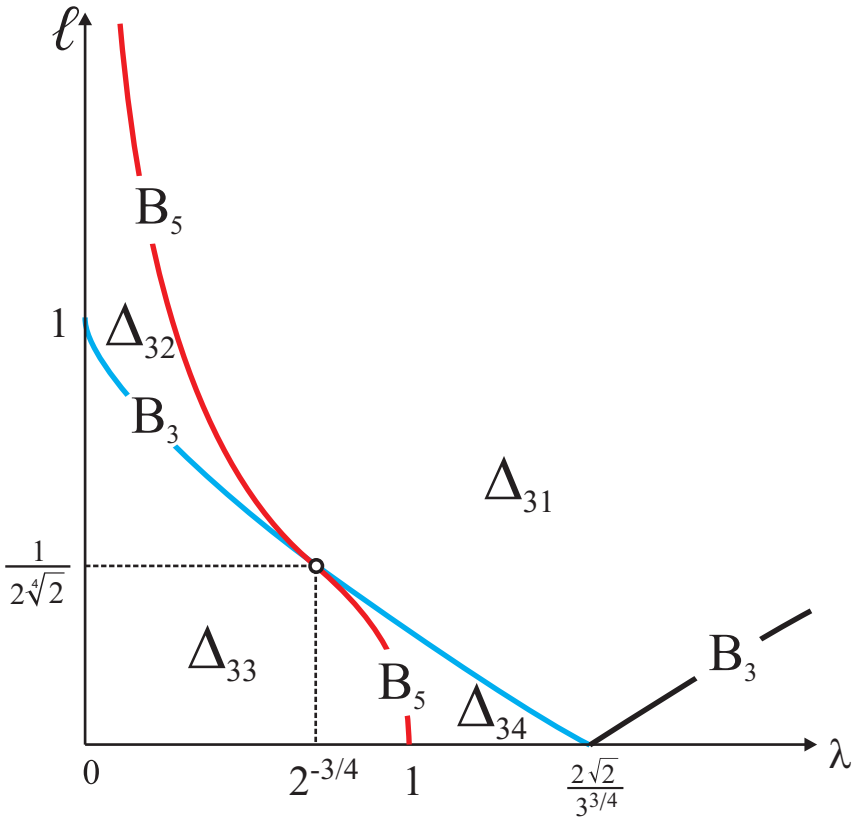

Fig. 24. Separating curves for points of Δ_3

The number of critical circles in the preimage of Δ_{3i} can be found by the diagrams of the subsystem $\mathcal{M}_3$ and the data for neighboring domains from Table 4.4. We see that Δ_{31} separates c_1 and c_2 (one critical circle in the preimage), Δ_{32} separates c_8 and c_9 (two critical circles), Δ_{33} separates c_6 and c_7 (one critical circle), and Δ_{34} separates c_3 and c_5 (two critical circles).

As for the sets Δ_0 and Δ_1, if the preimage of the point Δ_{3i} contains only one degenerate circle, then the corresponding critical integral surface J_{3i} is connected. We prove the following assertion, which will be useful in the sequel.

Theorem 17. *The critical manifold J_{32} consists of two connected components.*

Proof. As is seen from Fig. 24, the points of the class Δ_{32} are related to the classical Kovalevskaya problem $\lambda = 0$. We pass to the limit in the image in the parametric equations of Π_3, assuming $s = 1/(2\lambda^{2/3}) \to \infty$. As a result, $h = 2\ell^2$, $k = 0$, and the points Δ_{32} correspond to the values $\ell > 1$. The critical limit manifold is known (see [40]), namely, $J_{32}(0) = 2S^1$. Therefore, for small λ, this manifold is disconnected, and since there are two critical circles in the preimage, the number of connected component is also two. □

Note that points of the class Δ_{34} are related to the case $\ell = 0$. Loop molecules for this case were examined in [20, 21], but the existence of two connected components in molecules for these points was assumed without proof. Later, we will prove this hypothesis. This implies that the critical manifold J_{34} consists of two connected components.

5. Topology of Reduced Systems

5.1. Separating sets and bifurcation diagrams. In accordance with Proposition 12, the set Θ_L on the plane of the parameters (λ, ℓ) that classifies the bifurcation diagrams $\Sigma_{HK}(\ell, \lambda)$ of reduced systems on P^4_ℓ consists of pairs (λ, ℓ), where ℓ is the critical value of the restriction of the function L to one of the key sets $\mathcal{K}_i$ of the critical subsystems $\mathcal{M}_i$, $i = 1, 2, 3$, for fixed λ. Obviously, this is the value of ℓ at the points (4.11), (4.16)–(4.21), and (4.23)–(4.27). As was noted above, if $\lambda\ell \neq 0$, then only the point (4.27) does not correspond to degenerate rank-0 critical points. We recall that, due to existing obvious symmetries with respect to the parameters λ and ℓ, this set Θ_L is considered in the first quadrant:

$$\lambda \geq 0, \quad \ell \geq 0;$$

moreover, the semi-axes $\lambda = 0$ and $\ell = 0$ are included into the separating set by default. The points A, B_1, D_1, and D_2 give the values $\ell = 0$, $\lambda \in \mathbb{R}$, and for $\lambda = 0$ and any other ℓ there are multiple rank-1 critical points, corresponding, for example, to the merging of the subdomains c_2, c_6, c_8 with the domain b_1 (in the subsystem $\mathcal{M}_3$, we must also consider the possibility $s = \infty$). Obviously, multiple fragments also appear in the subsystem $\mathcal{M}_1$. A complete analysis of the corresponding diagrams for $\lambda = 0$ is performed in [40].

Theorem 18 (P. E. Ryabov)**.** *In the classification of bifurcation diagrams $\Sigma_{HK}(\ell, \lambda)$, the separating set Θ_L consists of the axes $\{\lambda = 0\} \cup \{\ell = 0\}$ and the following five curves determined by the explicit single-valued functions*:

$$\gamma_1 : \lambda = \lambda_1(\ell) = \frac{|\sqrt{s^2+4} - 2s|}{\left(\sqrt{s^2+4} - s\right)^{1/2}}, \qquad s = (2\ell^2)^{1/3}, \quad \ell \geq 0;$$

$$\gamma_2 : \ell = \ell_2(\lambda) = \frac{|2\lambda^{2/3} - \sqrt{4+\lambda^{4/3}}|}{\sqrt{2}\left(\sqrt{4+\lambda^{4/3}} - \lambda^{2/3}\right)^{1/2}}, \qquad \lambda \geq 0;$$

$$\gamma_3 : \ell = \ell_3(\lambda) = \frac{1}{\sqrt{2}\left(\sqrt{1+\lambda^4} - \lambda^2\right)^{3/2}}, \qquad \lambda \geq 0;$$

$$\gamma_4 : \ell = \ell_4(\lambda) = \frac{1}{2\lambda^{1/3}}\sqrt{1-\lambda^{4/3}}, \qquad 0 < \lambda \leq 1;$$

$$\gamma_5 : \ell = \ell_5(\lambda) = \frac{1}{4\lambda}, \qquad \lambda \geq 0.$$

We emphasize again that except for the new curve γ_5, all other curves correspond to (3.45):

$$\gamma_1 = \pi_{23} \cup \pi_{31}, \quad \gamma_2 = \pi_{24}, \quad \gamma_3 = \pi_{22}, \quad \gamma_4 = \pi_{21}.$$

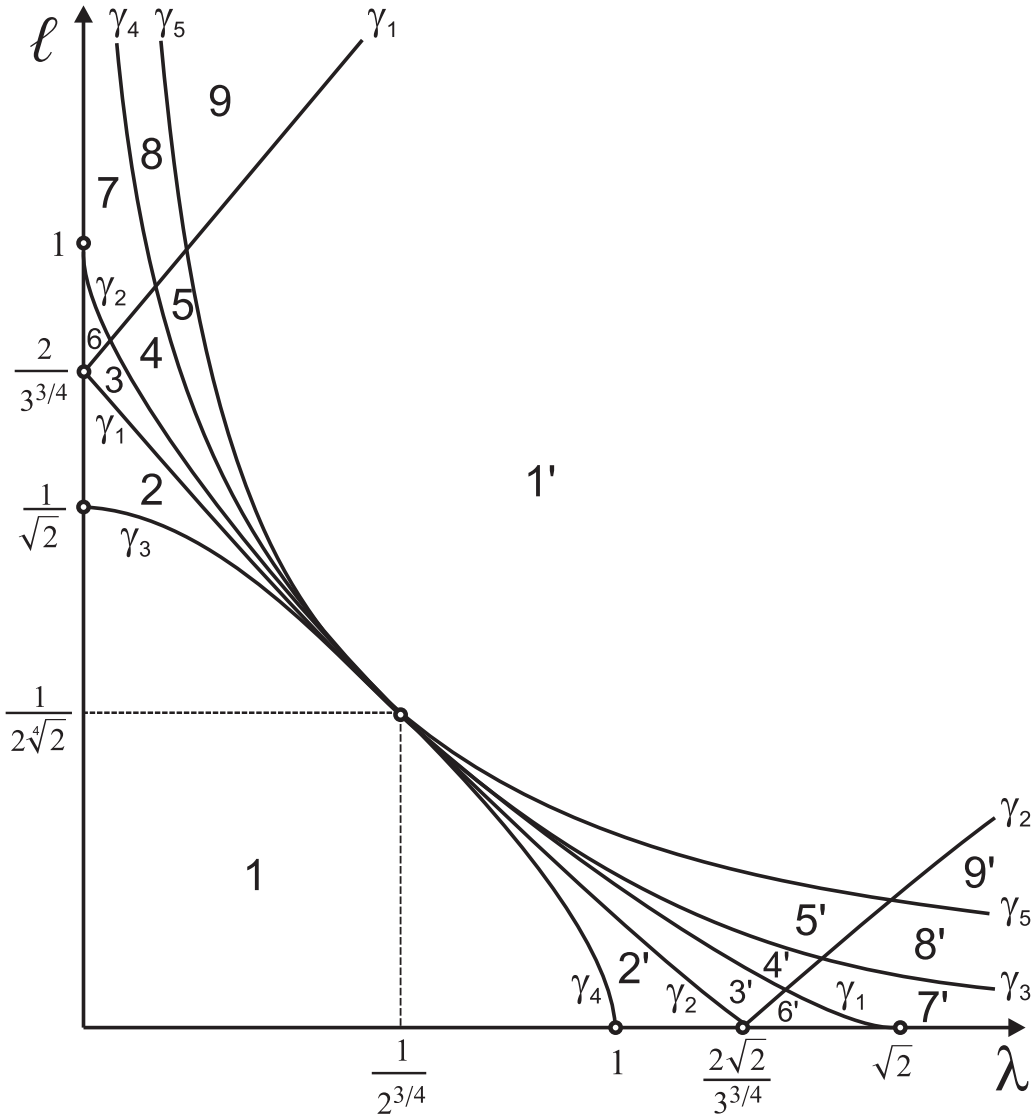

Fig. 25. Separating set and domains of parameters

The first quadrant is divided into 18 domains in which the diagrams $\Sigma_{HK}(\ell, \lambda)$ considered as one-dimensional stratified manifolds are identical. The separating set and the numeration of domains appeared are shown in Fig. 25. In what follows, the word "domain" means the connected component of the complement of a separating set on the parameter plane, whereas connected components of complements to diagrams are referred to as *chambers*.

In Figs. 26–31, the diagram $\Sigma_{HK}(\ell, \lambda)$ for each of the 18 domains of the plane (λ, ℓ) is constructed in two representations. The first representation contains notation of smooth segments and singular points in accordance with the diagrams of critical subsystems. In the second representation, atoms of bifurcations that occur in the system with two degrees of freedom on P^4_ℓ are indicated on smooth segments of the diagrams. Arrows on asymmetrical atoms indicate the direction of increasing the number of connected components of regular integral manifolds.

Combining the diagram $\Sigma_{HK}(\ell, \lambda)$ in the extended space

$$\Lambda(\mathbb{R}^3(\ell, h, k)) = \mathbb{R}^4(\lambda, \ell, k, h)$$

(see notation (3.19)), we trace the evolution of chambers, i.e., open domains that appear when $\Sigma_{HK}(\ell,\lambda)$ divides the plane (k,h). For this purpose, we introduce the expanded diagram

$$\Lambda(\Sigma)=\bigcup_{(\lambda,\ell)}\big\{(\lambda,\ell,k,h):(k,h)\in\Sigma_{HK}(\ell,\lambda)\big\}.$$

The open connected component of the complement of $\Lambda(\Sigma)$ in $\mathbb{R}^4$ is called an *extended chamber*. We do not distinguish between expanded chambers that differ only by signs of λ and ℓ. The integral manifolds corresponding to two points of the same expansion chamber are naturally diffeomorphic and can be obtained from one another by a smooth isotropy (possibly supplemented by a symmetry that changes the signs of λ and ℓ). In the sequel, we will not make notes about the signs of λ and ℓ. It follows that two chambers with given λ and ℓ should be considered the same if they are obtained as sections of the same extended chamber. Using the figures, it is easy to see that there are only eight different chambers; moreover, one of them (namely, the chamber containing arbitrarily large negative values of h) is inadmissible, i.e., the integral manifolds in the preimage of its points are empty. Thus, there are seven admissible chambers we are interested in. In the figures, they are marked by Roman numerals I–VII.

Summing up information presented above, we construct 18 bifurcation diagrams $\Sigma_{HK}(\ell,\lambda)$ of systems on P^4_ℓ that are stable with respect to parameters. These diagrams were initially presented in [29]. In the construction of these diagrams, the problem of visualization of small domains becomes important. Therefore, the diagrams $\Sigma_{HK}(\ell,\lambda)$ in our figures are severely distorted, and we do not intend to preserve the structure of levels $h=\text{const}$, which will allow one to see the rough isoenergetic Fomenko invariant in the sequel. Isoenergetic diagrams (see [31, 48]) are more convenient for this; we perform a classification of these diagrams below. It is important to see all arcs of diagrams that correspond to domains on the planes of the diagrams of critical subsystems and all nodal points. This will be used for classification of loop molecules.

5.2. Topological analysis. The first question of topological analysis is how many Liouville tori are contained in the preimage of a regular point in an integral manifold? If we do not know exactly the topological type of a critical integral manifold with hyperbolic singularities, we cannot answer this question for each specific system on P^4_ℓ. In a system with two degrees of freedom, the nature of a bifurcation that occurs at the intersection of rank-1 critical points is uniquely determined by the type of the point only in the case of elliptic singularities, i.e., atoms A. For this problem, only two particular cases $\lambda=0$ (see [38–40]) and $\ell=0$ (see [29, 46]) are examined. In the general case (see [14, 15]), the assertion on the number of tori contained in regular manifolds is based on the numerical simulation of their projections onto the plane of the first two components of the angular velocity (an analog of Zhukovsky domains). However, considering the entire picture in the four-dimensional space $\mathbb{R}^4(\lambda,\ell,k,h)$ of integral parameter (the extended space), we immediately obtain the answer without any additional studies. In fact, we reject all hyperbolic atoms whose exact form is unknown. For an extended chamber, an edge of the diagram $\Sigma_{HK}(\ell,\lambda)$ with a fixed notation generates a (three-dimensional) wall. For a selected chamber, an atom A on an edge or on a wall is called an *entrance* if its is directed inside the chamber (i.e., a Liouville torus is generated when entering the chamber) and an *exit* in the opposite case. In the extended space, we consider three sections corresponding to the domains 1, 2, and $2'$ (see Fig. 32). The bottom (with respect to the direction of the h-axis) point of the diagram corresponds to one nondegenerate rank-0 critical point of the type "center-center," which is the lowest relative equilibrium for given (λ,ℓ). Therefore, as was noted above, there is no motions in the unnumbered chamber below the diagram. Consequently, in the chamber I we have exactly one torus (each of the walls a_1 and b_1 contain one entrance). The diagram for the domain 1 shows that there exist one entrance from the chamber I to the chambers II and III (through the walls c_6 and c_4, respectively). Similarly, from the diagram for domain $1'$ we see that there is exactly one entrance from

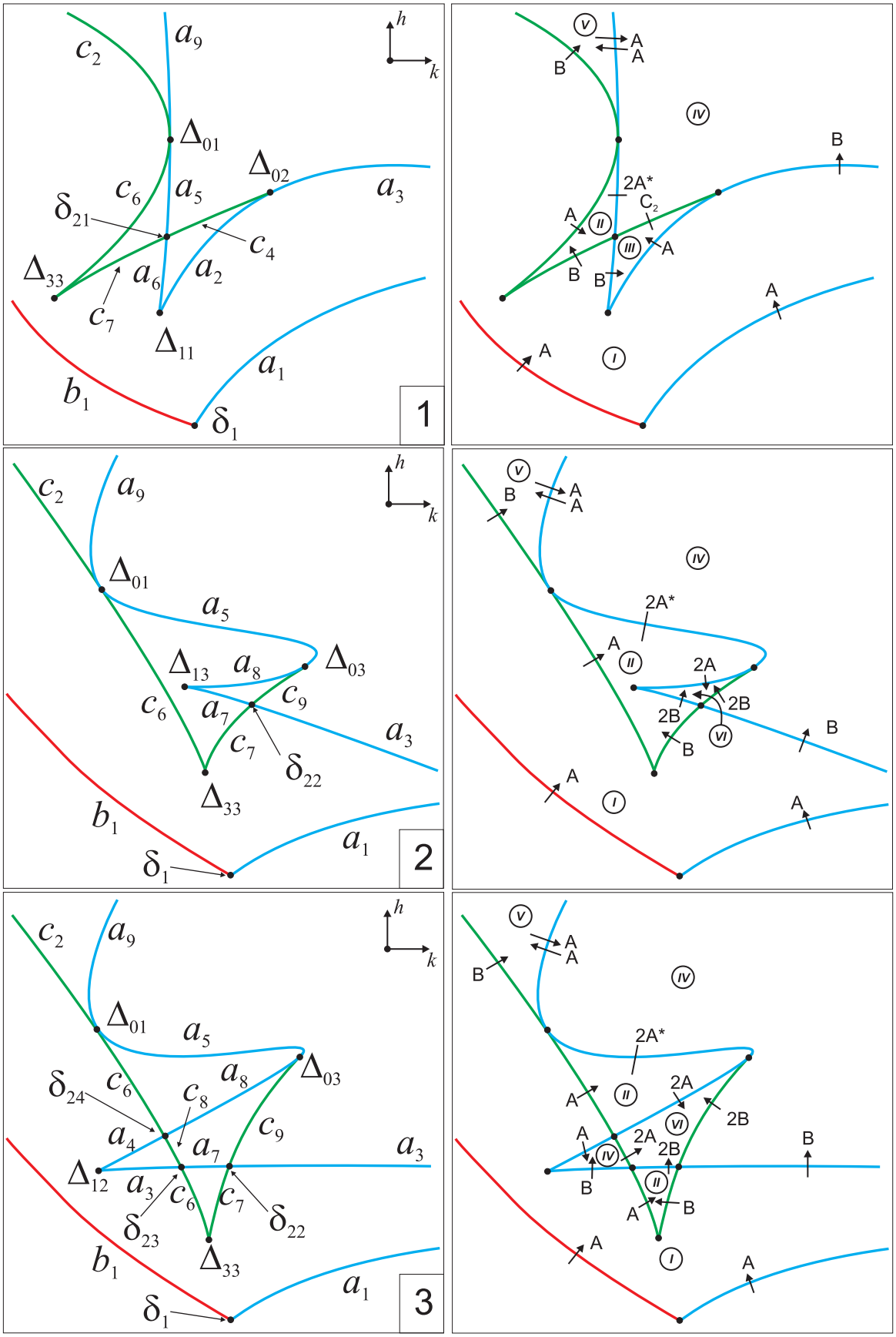

Fig. 26. Diagrams $\Sigma_{HK}(\ell, \lambda)$ for the domains 1–3

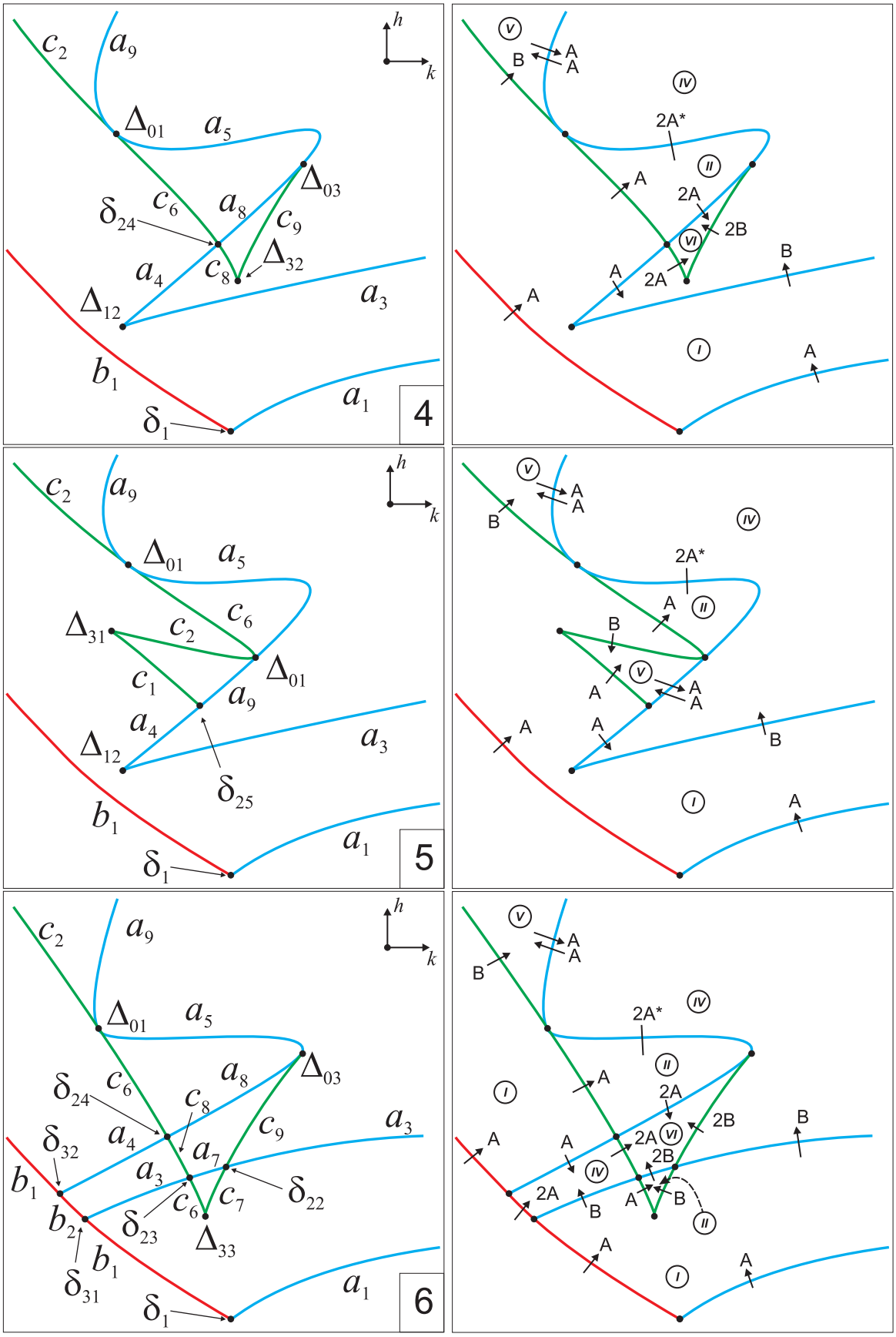

Fig. 27. Diagrams $\Sigma_{HK}(\ell, \lambda)$ for the domains 4–6

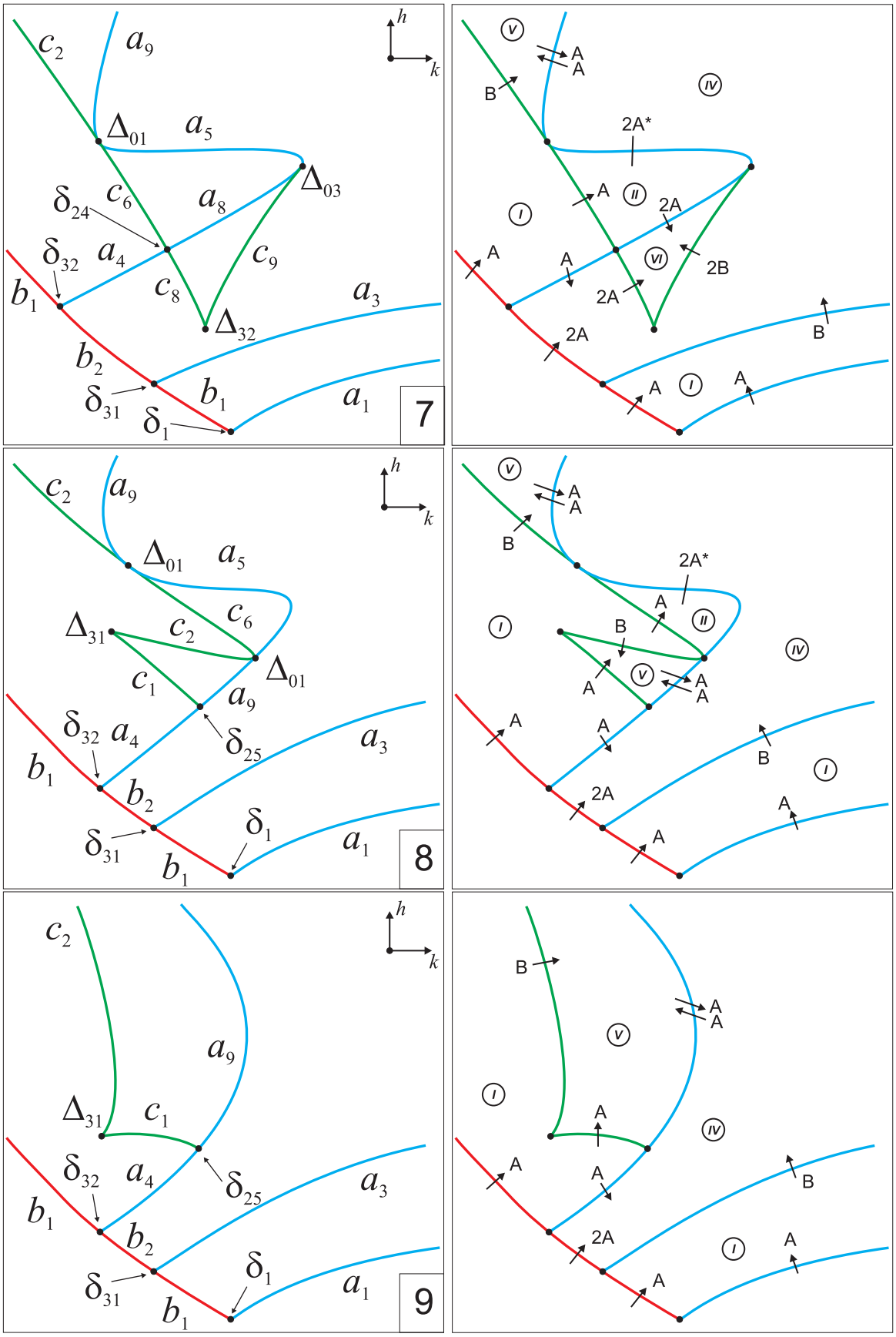

Fig. 28. Diagrams $\Sigma_{HK}(\ell, \lambda)$ for the domains 7–9

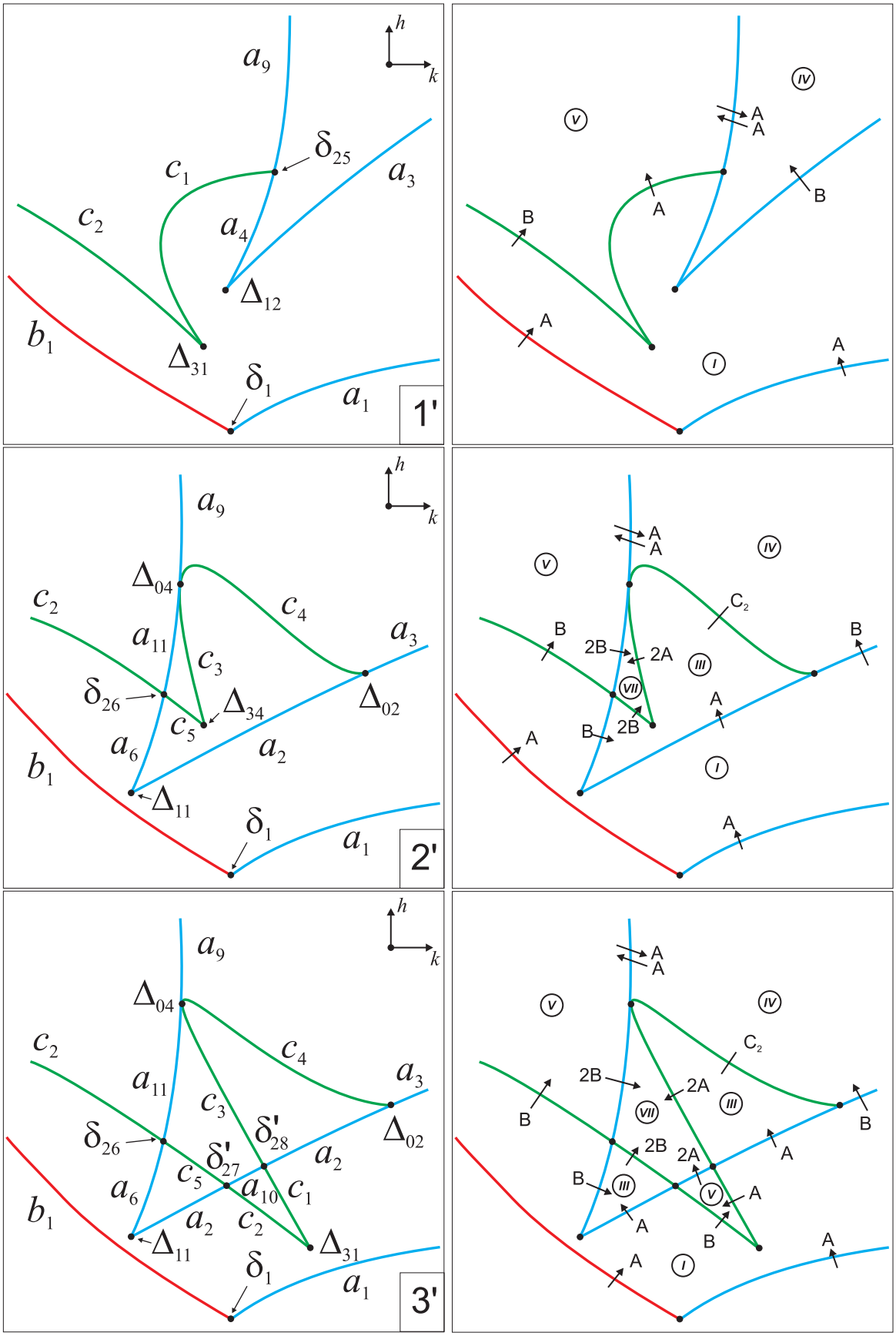

Fig. 29. Diagrams $\Sigma_{HK}(\ell, \lambda)$ for the domains $1'$–$3'$

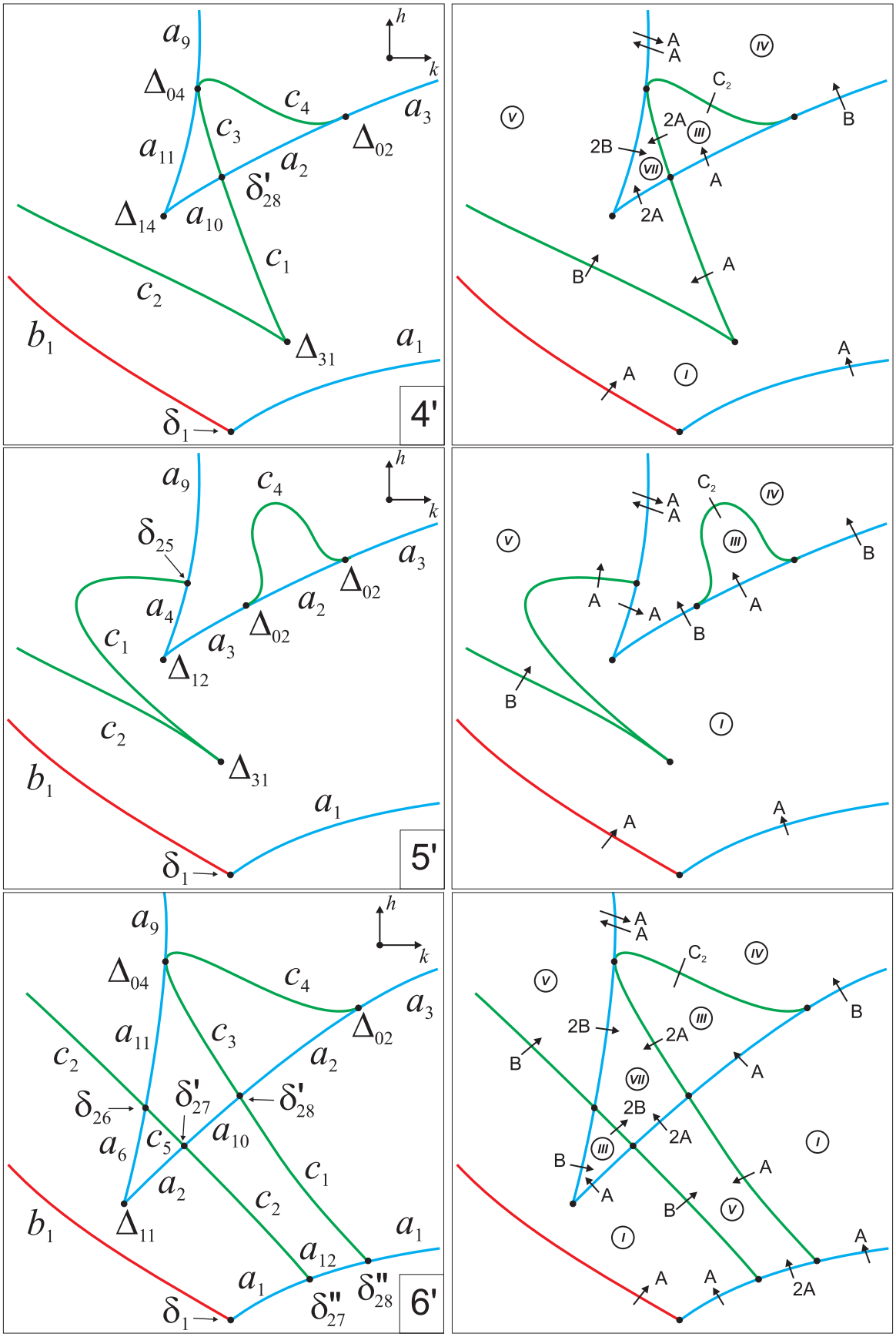

Fig. 30. Diagrams $\Sigma_{HK}(\ell, \lambda)$ for the domains 4′–6′

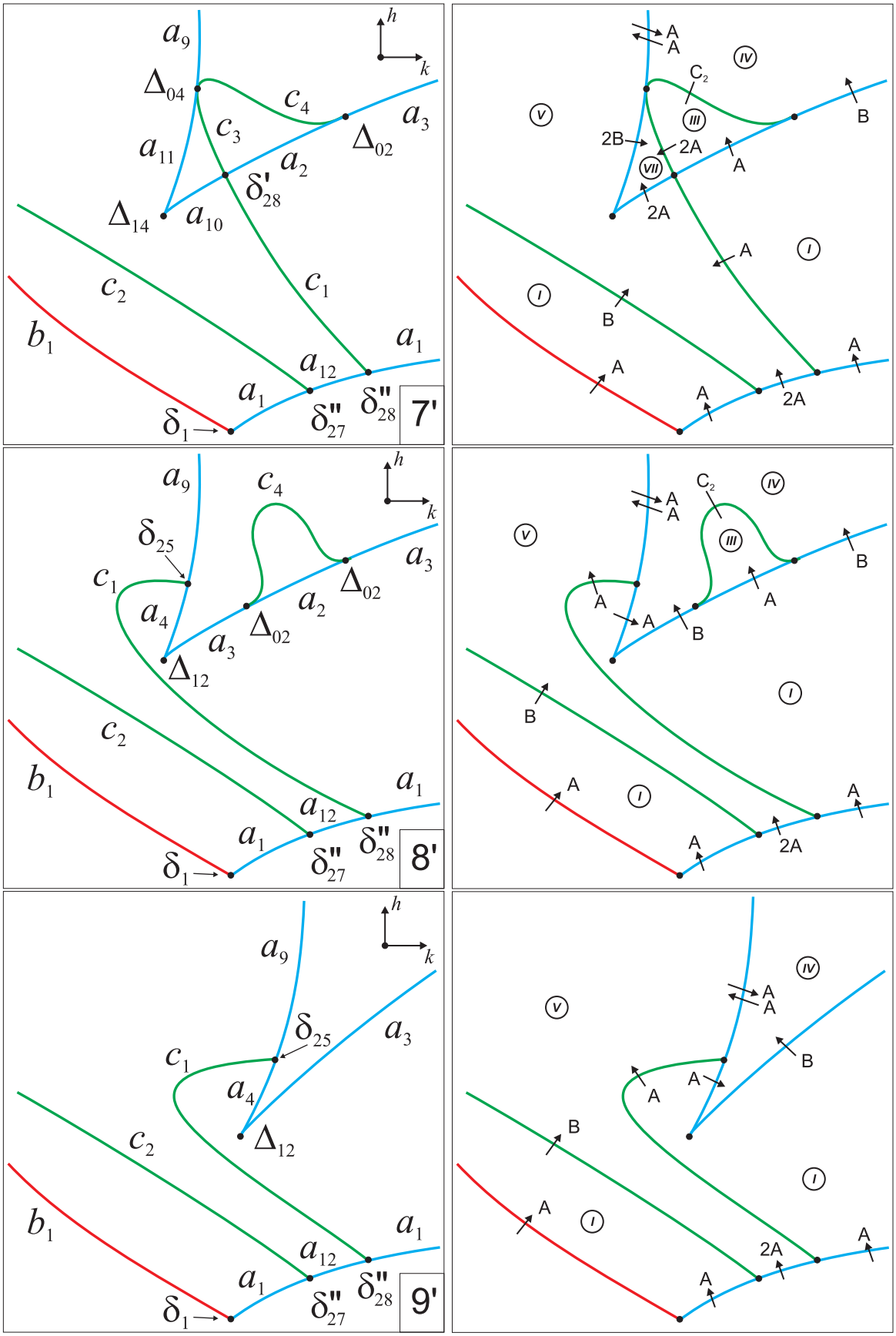

Fig. 31. Diagrams $\Sigma_{HK}(\ell, \lambda)$ for the domains 7′–9′

the chamber I to the chambers IV and V (through the walls a_4 and c_1, respectively). Therefore, in the chambers II–V, each point corresponds to two Liouville tori.

The diagram for the domain 2 shows exactly two entrances from the chamber II to the chamber VI (the wall a_8), and the diagram for the domain 2 yields exactly two entrances from the chamber III to the chamber VII (the wall a_8). Therefore, in the chambers VI–VII we have four Liouville tori. The following theorem clarifies the results of the papers [14–16], which contain the erroneous assertion on the existence of six rather than seven different chambers. In particular, for small nonzero values of λ, the existence of only five chambers is ascertained in [14–16], although, as one can see from the diagrams for the domains 1 and 2 in Fig. 26, for arbitrarily small λ, the chamber III of the domain 1 is transformed to the chamber VI of the domain 2. This means that in the space $\mathbb{R}^3(\ell, h, k)$ for arbitrarily small fixed λ, the diagram of the total moment mapping divides this space into six rather than five connected components with nonempty integral manifolds. If λ increases, then for $\lambda > 2^{-3/4}$ the sixth chamber disappears and the seventh chamber appears.

Theorem 19. *Integral manifolds in the preimages of points of chambers of the space of integral constants are as follows*:

(i) $\mathbf{T}^2$ *for the chamber* I;
(ii) $2\mathbf{T}^2$ *for the chambers* II–V;
(iii) $4\mathbf{T}^2$ *for the chambers* VI–VII.

In the study of fine topology of the system, one of the main objects, along with chambers and the number of tori in them, is the so-called families of Liouville tori. For brevity, we denote the extended phase space by $\widetilde{P}$:

$$\widetilde{P} = \Lambda(P^5) = \bigcup_{(\lambda,\ell)} P^4_\ell \times \{(\lambda, \ell)\} = \bigcup_{\lambda} S^2(\boldsymbol{\alpha}) \times \mathbb{R}^3(\boldsymbol{\omega}) \times \{\lambda\} = S^2(\boldsymbol{\alpha}) \times \mathbb{R}^3(\boldsymbol{\omega}) \times \mathbb{R}(\lambda).$$

All integral manifolds $J_{\ell,h,k}(\lambda)$ can be embedded in $\widetilde{P}$ as $J_{\ell,h,k}(\lambda) \times \{\lambda\}$. Naturally, the following definition arises.

Definition 12. We exclude from $\widetilde{P}$ all connected components of critical levels containing critical points of the moment mapping. The connected component of the remaining set is called the *family* of Liouville tori.

If the system has no minimum (maximum) regular tori (and there are no such tori in the problem considered: this can be easily seen from the classification of diagrams equipped by atoms), then the intersection of the preimage of any chamber with any family can consist of no more than one torus. In some problems, one can speak of several tori of the same family in the preimage of points of a chamber (see [7]) or, what is the same, of families consisting of several tori (see [20]). In this case, the definition of a family is as follows: each family consists of all tori that are affected by the same bifurcations on the boundaries of the chamber (see [20]). Such families exist in the classical Kovalevskaya case $\lambda = 0$ (see [7]) and in the particular case where $\lambda\ell \neq 0$ (see [20]). However, it is easy to see that in the general case where $\lambda\ell \neq 0$, there are no such families. Indeed, in the chambers II and III, there are two tori and a wall with one entrance; therefore, only one torus is affected by a bifurcation. Between the chambers IV and V, there is a wall with one entrance and and one exit; therefore, two tori of these chambers are affected by clearly different bifurcations. In the chambers VI and VII whose points correspond to four tori (not only in the extended space but also for any fixed λ and ℓ for which these chambers exist), there exist one or two walls with two entrances from neighboring chambers; moreover, if there are two walls, then distinct pairs of tori are affected by bifurcations on them. Hence, in this case, there are no four or even two tori that are affected by the same bifurcations. In particular, this implies that Theorem 6 from [18], which claims the presence of seven families, two of which consist of two tori, is invalid. Families in [18] are understood in the sense of the definition given in [20]. We

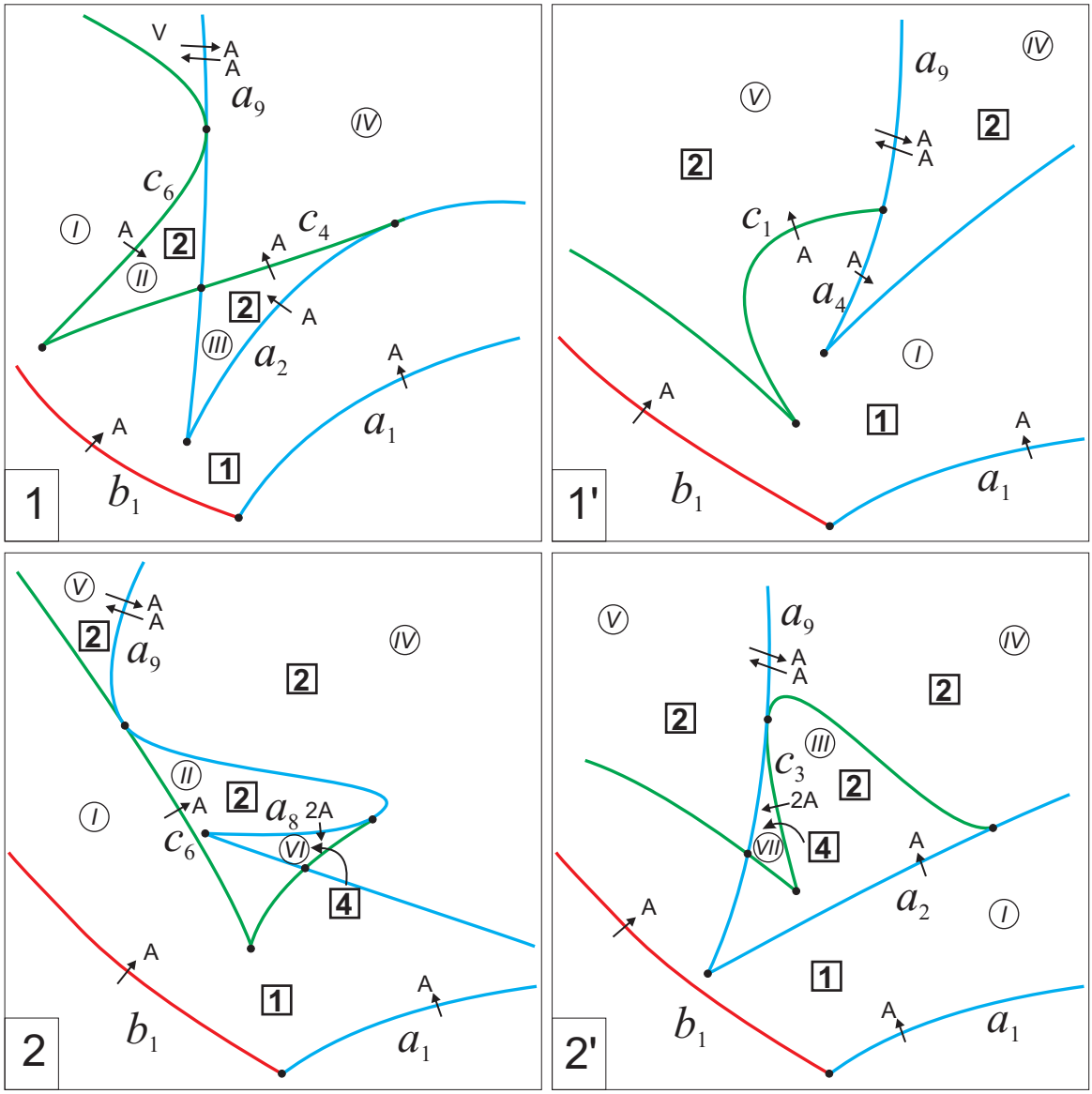

Fig. 32. Number of tori in chambers

emphasize once again that for any fixed λ and ℓ such that $\lambda\ell \neq 0$, there are no chambers such that all their tori are affected by the same bifurcations on the walls of these chambers.

Now we find the number of families and their distribution in chambers. We indicate the following property of the Kovalevskaya–Yehia case: in the preimage of a point of the bifurcation diagram, regular tori cannot coexist with hyperbolic atoms. In other words, if an edge of the diagram corresponds to hyperbolic atoms, then all tori of neighboring chambers are involved in bifurcations. Note that this property does not take place, for example, in the Goryachev–Chaplygin case. Therefore, in order to have the same family in two chambers, it is necessary (but certainly not sufficient) to have a path from one of them to another consisting of entrances or exits. If there is only one family in some chamber, then the existence of an exit into another chamber is a sufficient condition of the presence of this family in this second chamber.

Table 5.1

Chamber	Family
I	$\{1\}$
II	$\{1+2\}$
III	$\{1+3\}$
IV	$\{1+4\}$
V	$\{1+5\}$
VI	$\{1+2+4+6\}$
VII	$\{1+3+5+7\}$

Let us consider the diagrams for the domains 1, 1′, 3, and 3′' (see Fig. 33). Families are marked by Arabic numerals and, as is customary for sets, are denoted by braces (in contrast to the numbers of domains on the (λ, ℓ)-plane). We denote with $\{1\}$ the family starting in the chamber I. It can be seen from the diagram for the domain 1 that there is exactly one entrance into the chambers II and III from the chamber I. Therefore, the family $\{1\}$ also presents in these chambers. Can tori generated at the entrances into these chambers belong to the same family? On diagrams with type-A atoms indicated, we can see that there is no a path between the chambers II and III that passes through the chamber I and contains only type-A atoms (if a path passes through the chamber I, then new families disappear). Therefore, the second families in these chambers are distinct; we denote them by $\{2\}$ and $\{3\}$. From the diagram for the domain 1′ it follows that the family $\{1\}$ presents also in the chambers IV and V.

Can tori generated at entrances of these chambers belong to the same family? Obviously, they cannot, since the common wall has simultaneously an ebtrance and an exit, so the intersection of this wall preserves only the family $\{1\}$, and there is no other path between the chambers IV and V that does not pass through the chamber I and contains only type-A atoms. Similarly we can establish that families generated on a common wall of the chambers IV and V cannot coincide with any of families introduces earlier. Therefore, we denote these new families by $\{4\}$ and $\{5\}$. From the diagram for the domain 3 we can see that there are two entrances to the chamber VI with four tori from the chambers II and IV. Therefore, the families $\{1\}$, $\{2\}$, and $\{4\}$ are preserved in the chamber IV and one new family appears; we denote it by $\{6\}$. Similarly, from the diagram for the domain 3′ we can see that there are two entrances to the chamber VII with four tori from the chambers III and V. Therefore, the families $\{1\}$, $\{3\}$, and $\{5\}$ are preserved in the chamber VII and one new family appears; we denote it by $\{7\}$. We join the numbers of families that simultaneously present in the chamber by a plus sign.

Theorem 20. *In the Kovalevskaya–Yehia case, there exist exactly seven families of regular tori. Their distribution in the chambers is shown in Table* 5.1*.*

In the next section, we establish topological invariants of nodal points of bifurcation diagrams.

6. Fine Topology of Nodal Points

6.1. Definitions of rough and fine invariants (molecules). We briefly recall the notion of a topological invariant of a three-dimensional manifold equipped on which a Liouville foliation. A detailed description can be found in [7, 8, 35] and in many other subsequent works, where Fomenko–Zieschang invariants are described.

Let Q be a smooth, three-dimensional invariant manifold of an integrable Hamiltonian system sgrad H with two degrees of freedom that does not contain rank-0 critical points and degenerate rank-1 critical points of the integral mapping $\mathcal{F} = H \times K$. This manifold can be obtained by setting a closed path in the (h, k)-plane that does not pass through nodal points and transversely crosses all one-dimensional segments of the diagram (see [23]). Identifying each connected component of the integral manifold

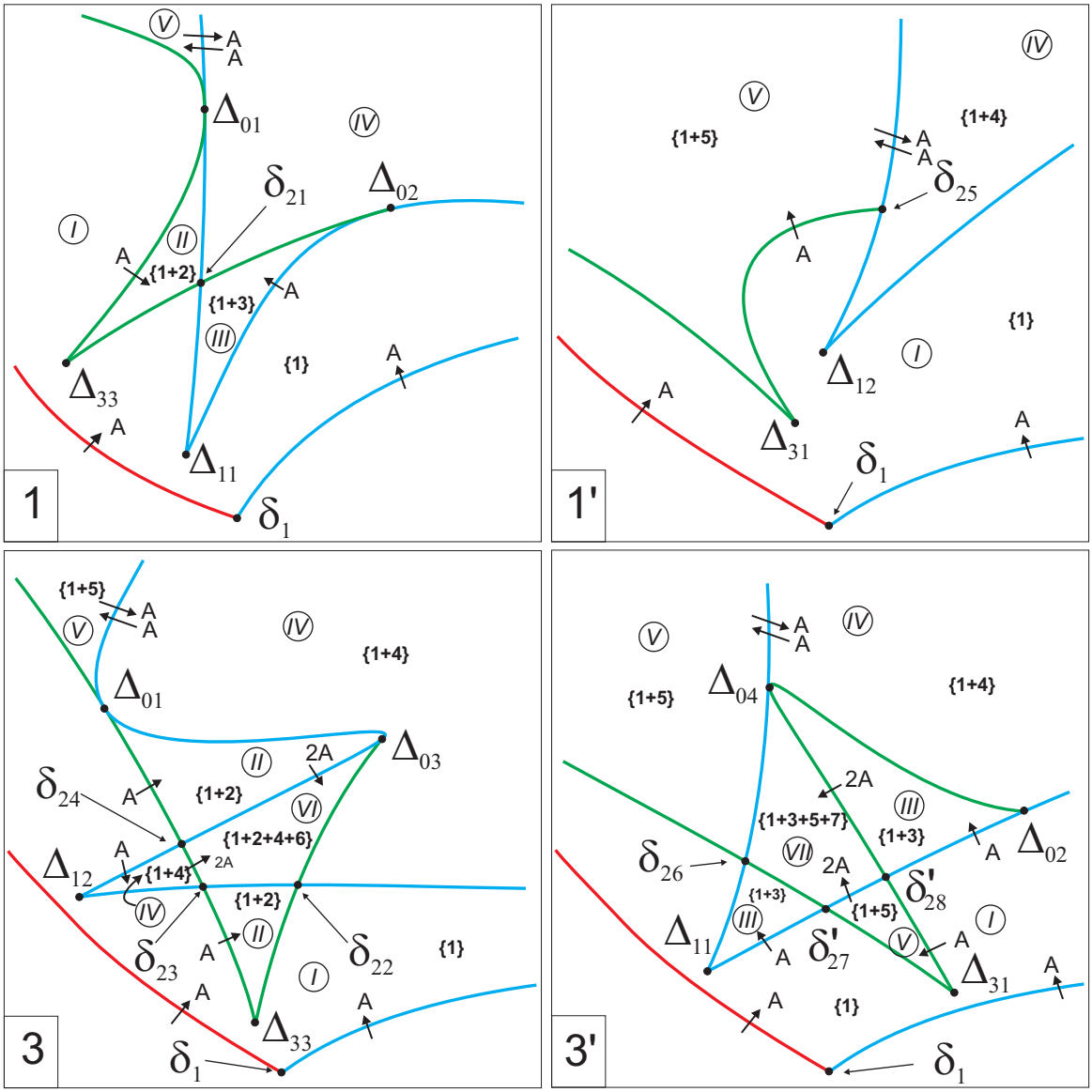

Fig. 33. Families of tori in chambers

or a critical integral surface with a point, we obtain a one-dimensional object, which can be turned into a graph whose edges are unions of points corresponding to components without critical points and vertices are points obtained from singular sheets (i.e., components that contain critical points of the moment mapping). Then we mark vertices by the bifurcation symbols and obtain a graph $W(Q)$ with equipped vertices (knots) called the *Fomenko graph* or a *rough molecule*. The pair $(Q, W(Q)))$ determines the topology of the foliation on Q up to a rough Liouville equivalence. Let us recall the definition.

For a Hamiltonian system $v = \operatorname{sgrad} H$ and a three-dimensional invariant manifold, we denote by $v(Q)$ the restriction of the field v to Q. Assume that two systems v' and v'' are given. The restrictions $v'(Q')$ and $v''(Q'')$ are said to be *roughly Liouville equivalent* (see [8]) if there exists a homeomorphism of bases of Liouville foliations (i.e., of simple graphs without additional marks), which can be lifted to a homeomorphism of Liouville foliations over a neighborhood of each point. It

is clear that in this case a homeomorphism of graphs preserves the marks of bifurcations at vertices. If there exists a global homeomorphism of $v'(Q')$ and $v''(Q'')$ preserving Liouville foliations, then these restrictions are said to be *Liouville equivalent*. To emphasize the distinction, the Liouville equivalence is sometimes called *complete*, or *fine*, or *exact* Liouville equivalence.

Thus, Fomenko graphs are rough topological invariants (i.e., invariants of the rough Liouville equivalence). It is easy to see that a Fomenko graph can be determined by a geometrical representation or as a sequence of bifurcations along a path. Having a sequence of bifurcations along some fairly informative set of paths in the (h, k)-plane, one can obtain a Fomenko graph for an arbitrary path. Such description of the rough phase topology of systems with two degrees of freedom for classical problems of rigid-body dynamics was proposed in [38] (a detailed description is presented in [40]).

As a rule, in problems obtained by reduction by a cyclic coordinate with the moment integral L, Fomenko graphs can be constructed for isoenergetic manifolds $Q^3_{\ell,h}$ of reduced systems. In such problems, the term "Fomenko graph" is used for graphs $W(Q^3_{\ell,h})$, i.e., rough isoenergetic topological invariants. However, for a more accurate description of the total topology of a system and isoenergetic invariants, the method of loop molecules proposed in [7] is very useful. Consider a nodal point of the bifurcation diagram of a system $\operatorname{sgrad} H$ and surround it by a sufficiently small closed path that does not contain other nodal points inside. Naturally, as in the general case, this path must intersect all one-dimensional segments of the diagram transversely. Consider the full preimage of this path. Each component Q_i of the preimage is a manifold satisfying the requirements stated above, and we can construct the corresponding graph $W(Q_i)$ for it. The resulting set of these graphs for the preimage of the chosen path is called the (rough) loop molecule of the nodal point considered. It defines the topology of the foliation on $Q = \cup_i Q_i$ up to the rough Liouville equivalence.

To obtain a complete (exact) topological invariant, the Fomenko graph must be equipped with information about gluing matrices on edges of the graph of tori that came to meet from the bifurcations of the atoms at the ends of edges. In [7, 8], a construction of admissible bases of cycles on boundary tori of atoms of all types is described. As a result, when meeting on the edge, such bases considered as elements of the one-dimensional homology group of the torus are connected by an integer-valued matrix with determinant of -1. Since this matrix is determined up to an admissible change of bases on the boundaries of the edge, one can introduce its invariants, which are called the r-mark (a rational number or ∞) and the ε-mark (taking values ± 1). Thus, each edge of the graph is equipped with a pair of numbers (r, ε). In addition, the global topology of the Liouville foliation on Q is determined by a set of n-marks that are assigned to families of hyperbolic atoms. A family is formally defined as follows. Cutting a Fomenko graph equipped with (r, ε)-marks on edges by all the edges with finite values of r, we obtain a set of connected graphs. A connected graph without elliptic atoms is called a *family* (*atom family*, in contrast to tori family). To each atom family, we assign an integer number called an n-mark, which is calculated by the set of gluing matrices; in fact, it describes an obstruction for spreading of sections of the S^1-foliation in the preimage of the family at the boundary tori to the whole preimage (by construction, the preimage of each family is a Seifert foliation). The Fomenko graph with all three types of marks is called a *marked molecule* or a *Fomenko–Zieschang invariant* and is denoted by $W^*(Q)$. It is shown in [8] that a marked molecule determines the class of fine Liouville equivalence of systems on three-dimensional manifolds. For this reason, marked molecules are also called fine topological invariants.

In the sequel, we examine rough and marked loop molecules of nodal points of bifurcation diagrams. A considerable amount of information is obtained from the classification of loop molecules of low complexity described in [6, 8, 56]. The main problem is the correct tracing of families meeting at bifurcation points. Knowledge of the rough topology, i.e., joint levels of first integrals, both regular and critical, cannot always uniquely assign marks of families. But, as one can see below, after this problem is solved, it becomes possible not only to construct a rough molecule but also to apply results of the general theory and studies of particular cases to the construction of all marked loop molecules.

6.2. Loop molecules of rank-0 points. We describe the topology of full integral levels of relative equilibria (rank-0 critical points). These results is presented in [44] and is based on [47], where Tables 4.1, 4.3, and 4.4 were initially obtained.

Let x be a point of nondegenerate relative equilibrium and $\ell = L(x)$. Consider the integral mapping (2.10) of the reduced system:

$$\mathcal{J}_\ell = H \times K : P^4_\ell \to \mathbb{R}^2.$$

We denote the complete preimage of the point $\mathcal{J}_\ell(x)$ (i.e., a critical integral surface) by $\mathfrak{J}(x)$ and a sufficiently small saturated neighborhood of the surface $\mathfrak{J}(x)$ that does not contain relative equilibria with other values of the mapping $\mathcal{J}_\ell$ by $U(x)$. The surface $\mathfrak{J}(x)$ can consist of several connected components. As was noted above, the component of the point x always contains exactly one relative equilibrium. At the same time, an analysis of critical subsystems shows that along with components of relative equilibria, components containing exactly one critical circle may also exist. The number and topology of these components can be found by the results for the critical subsystem $\mathcal{M}_1$ according to Remark 8. Next, we consider the point x in each of two critical subsystems containing it and analyze information on neighboring domains in the image of the critical subsystem. These domains produce arcs of the bifurcation diagram of the mapping $\mathcal{J}_\ell$ in a neighborhood of the point x. The structure of the critical set in the preimages of these arcs and surgeries in $U(x)$ at their intersections are presented in Tables 4.1, 4.3, and 4.4. After this, the type of loop molecules of relative equilibria themselves and marked critical periodic trajectories lying at the same level can be uniquely established by the exhaustive description of loop molecules of nondegenerate singularities of low complexity (see [8]). In addition to components containing critical point, the surface $\mathfrak{J}(x)$ can contain regular tori filled with doubly periodic trajectories. Their number can be uniquely found by the form of the bifurcation diagram of the mapping $\mathcal{J}_\ell$ supplemented with atoms on arcs.

The result of topological classification is given in Table 6.1. For loop molecules, we indicate only r-marks with the sole purpose to distinguish molecules of relative equilibria "center-center" (mark $r = 0$) from molecules lying on the same level of elliptic periodic trajectories (mark $r = \infty$). In fact, all marks (including ε- and n-marks) are set automatically in accordance with [8].

On fragments of the bifurcation diagram of the mapping $\mathcal{J}_\ell$ in a neighborhood of a relative equilibrium, we indicate atoms arising on critical circles at the intersection with arcs of the diagram; only atoms of the types A, B, A^*, and C_2 appear here. For nonsymmetric atoms, arrows indicate the direction of increasing the number of tori. This number itself in regular domains is set in the frame. When describing singular trajectories (singular components of the integral manifold), p_{CC} is a fixed point of the type "center-center," p_{CS} is a critical manifold of a fixed point of the type "center-saddle" (the figure-eight), p_{SS} is a critical manifold of a fixed point of the type "saddle-saddle" (two figure-eights with a common central point and four rectangles glued to them and filled with asymptotic trajectories of regular points; the rule of gluing is completely determined by the corresponding loop molecule). Further, S^1_E denotes a periodic trajectory of elliptic type that exhausts the corresponding connected component, and S^1_H is a surface of the periodic trajectory of hyperbolic type corresponding to an atom of the type B (the direct product of a figure-eight and a circle). This classification by the number of classes and the type of loop molecules of the complete preimages of the values of the moment mapping at relative equilibria differs from the results presented in [18]. Since the classification principle has not been clearly stated in [18], we do not compare the results. We only note that after the publication of the work [44], the description of classes of rank-0 points and their loop molecules (still without a precise definition of classification principles and necessary analytical studies) was particularly ordered in [32].

According to information from Table 6.1 and a remark about marks on loop molecules, to complete a fine classification of all loop molecules of nondegenerate rank-0 points it suffices to mark the edges of all molecules found by the numbers of families of regular tori. For molecules of points of the types "center-center" and "center-saddle" (with molecules lying on the same integral level of critical circles

Table 6.1

Class of points	Number of components in the preimage	Singular trajectories in the preimage	Fragment of the (H, K)-diagram	Molecules in the preimage	Regular tori
δ_1	1	p_{CC}	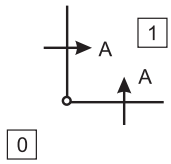	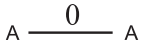	0
δ_{25}	3	$p_{CC} \cup S^1_E$	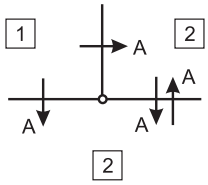	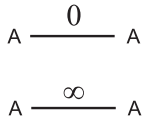	1
$\delta''_{28}, \delta_{32}$	2	$p_{CC} \cup S^1_E$	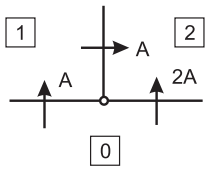	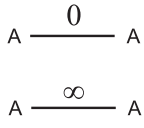	0
$\delta_{24}, \delta'_{28}$	4	$p_{CC} \cup 2S^1_E$	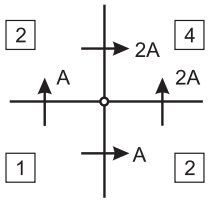	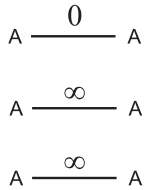	1
$\delta_{23}, \delta'_{27}$	2	$p_{CS} \cup S^1_H$	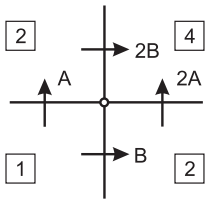	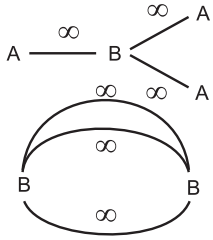	0
$\delta_{31}, \delta''_{27}$	1	p_{CS}	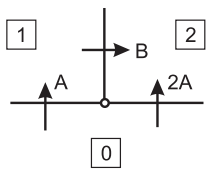	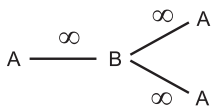	0

Table 6.1 (continued)

Class of points	Number of components in the preimage	Singular trajectories in the preimage	Fragment of the (H, K)-diagram	Molecules in the preimage	Regular tori
δ_{22}, δ_{26}	1	pss	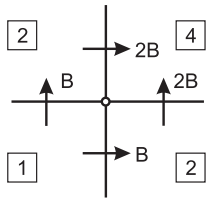	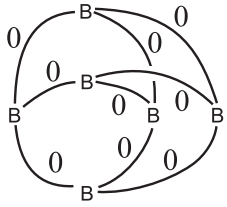	0
δ_{21}	1	pss	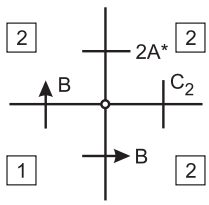	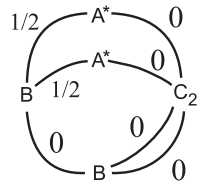	0

that consists of nondegenerate rank-1 points), this problem is solved directly based on the form of the adjacent fragment of the equipped bifurcation diagram $\Sigma_{HK}(\ell, \lambda)$.

For example, consider the point from the class δ_{23}, which can be found on the diagram for the domain 6. The atoms on the adjacent segments are as follows: $B_{[a_3]}$, $2B_{[a_7]}$ and $A_{[c_6]}$, $2A_{[c_8]}$. Here and in the sequel, we use the notation of atoms supplemented by the notation of the edge of the diagram (in brackets) at which the bifurcation considered occurs. Since the rank-0 point itself has the type "center-saddle," its loop molecule (i.e., a connected molecule corresponding to the connected component that contains the rank-0 critical point) describes the bifurcation

$$A_{[c_6]} \to B_{[a_7]} \to 2A_{[c_8]};$$

moreover, the family $\{2\}$ appears in the atom $A_{[c_6]}$ and the families $\{2\}$ and $\{6\}$ disappear in the atoms $2A_{[c_8]}$. Thus, in the atom $B_{[a_7]}$ that belongs to the connected molecule of the point δ_{23}, the family $\{2\}$ is transformed into the families $\{2\}$ and $\{6\}$. The smooth segment $B_{[a_3]} - B_{[a_7]}$ overlays the corresponding diagram; this segment corresponds to a nondegenerate critical saddle circle. As is seen from the fragment of the diagram, its left atom $B_{[a_3]}$ separates the chambers I and IV, so the family $\{1\}$ is transformed into the families $\{1\}$ and $\{4\}$ through a critical circle in the atom $B_{[a_3]}$, and hence in the atom $B_{[a_7]}$, which belongs to the second component of the preimage of the loop molecule (i.e., the component that does not contain the rank-0 point).

In the sequel (for the molecule of the points δ_{22} and Δ_{13}), we will need information on the surgery of families in the atoms $B_{[a_7]}$. For this reason, we state this as a separate proposition.

Proposition 21. *In the two atoms B on the edge a_7, the following bifurcations hold*: *on one atom, a torus of the family* $\{1\}$ *is transformed into two tori of the families* $\{1\}$ *and* $\{4\}$; *on the other atom, a torus of the family* $\{2\}$ *is transformed into two tori of the families* $\{2\}$ *and* $\{6\}$.

Information on loop molecules in preimages of nondegenerate points of the types "center-center" and "center-saddle" is collected in Table 6.2. For convenience, the first column, along with the notation of the class of points, contains the number of a domain on the plane (λ, ℓ) whose diagrams contain points of this class (certainly, such a point can be contained on the diagrams for other domains; for example, points of the class δ_1 exist on all diagrams).

Table 6.2

Class of points	Molecule	Class of points	Molecule
δ_1 (1)	$A[b_1] \xrightarrow[\{1\}]{r=0} A[a_1]$	δ_{25} (1′)	$A[c_1] \xrightarrow[\{5\}]{r=0} A[a_9]$ $A[a_4] \xrightarrow[\{4\}]{r=\infty} A[a_9]$
δ''_{28} (6′)	$A[a_{12}] \xrightarrow[\{5\}]{r=0} A[c_1]$ $A[a_{12}] \xrightarrow[\{1\}]{r=\infty} A[a_1]$	δ_{32} (6)	$A[b_2] \xrightarrow[\{4\}]{r=0} A[a_4]$ $A[b_2] \xrightarrow[\{1\}]{r=\infty} A[b_1]$
δ_{24} (3)	$A[a_8] \xrightarrow[\{6\}]{r=0} A[c_8]$ $A[c_6] \xrightarrow[\{2\}]{r=\infty} A[c_8]$ $A[a_8] \xrightarrow[\{4\}]{r=\infty} A[a_4]$	δ'_{28} (6′)	$A[c_3] \xrightarrow[\{7\}]{r=0} A[a_{10}]$ $A[a_2] \xrightarrow[\{3\}]{r=\infty} A[a_{10}]$ $A[c_3] \xrightarrow[\{5\}]{r=\infty} A[c_1]$
δ_{31} (9)	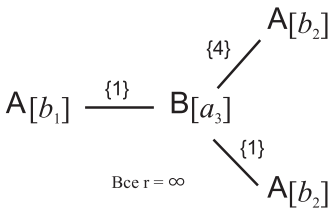	δ''_{27} (6′)	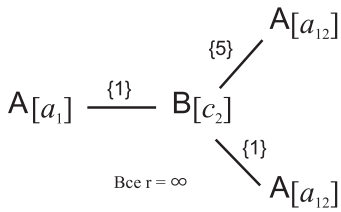
δ_{23} (6)	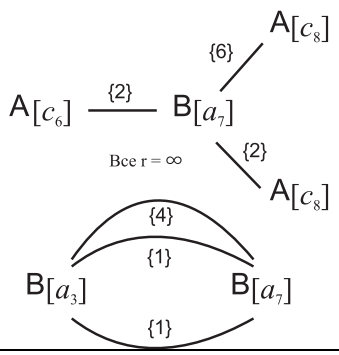	δ'_{27} (6′)	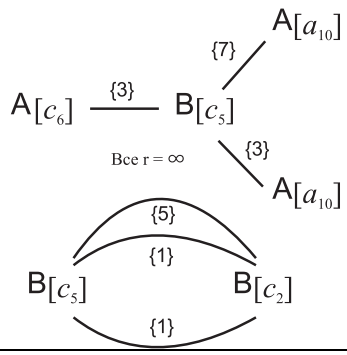

Consider loop molecules of the remaining three classes of nondegenerate rank-0 critical points of the type "saddle-saddle."

Let us take the point δ_{22}. It is contained, for example, in the diagrams for the domains 2 and 3. We already know that the surgeries of families on the adjacent edges of the bifurcation diagram are as follows:

$$\begin{aligned} B_{[c_7]}: &\quad \{1\} \mapsto \{1\} + \{2\};\\ B_{[a_3]}: &\quad \{1\} \mapsto \{1\} + \{4\};\\ 2B_{[a_7]}: &\quad \{1\} \mapsto \{1\} + \{4\}, \quad \{2\} \mapsto \{2\} + \{6\}. \end{aligned}$$

The remaining edge c_9 separates the chambers IV (with the families $\{1\} + \{4\}$) and VI (with the families $\{1\} + \{2\} + \{4\} + \{6\}$). Unfortunately, we cannot establish the rule of marking the four edges connecting $2B_{[a_7]}$ and $2B_{[c_9]}$ by families without considering degenerate rank-1 critical points. However, according to Theorem 17, we know that the loop molecule of the point Δ_{32} has two connected components; therefore, each of these components has a well-known form, namely, the family in the "head" again comes to one of the "feet." But the point Δ_{32} is a cusp at which the hyperbolic edge c_9 and the elliptic edge c_8 come in the diagram of the domain 7. Hence we immediately see that in the atoms $B_{[c_9]}$, the surgeries of families are as follows:

$$\{1\} \mapsto \{1\} + \{4\} \vee \{6\}, \quad \{4\} \mapsto \{2\} + \{4\} \vee \{6\}$$

(the notation $\{4\} \vee \{6\}$ means an uncertain alternative). Thus, the following logical problem appears. There are two males M_1 and M_2 (the families in the "heads" of the atoms $2B_{[a_7]}$) and two females F_1 and F_4 (the families in the "heads" of the atoms $2B_{[c_9]}$). It is known that each male has exactly one common child with every female; we denote these children by D_1, D_2, D_4, and D_6 (the families on the edges of the loop molecule of the point δ_{22} between a_7 and a_9). It is also known that D_1 and D_4 are children of M_1 and D_2 and D_6 are children of M_2. Further, we also know that F_1 is the mother of D_1 and F_4 is the mother of D_2. We must identify the pair of parents (namely, the mother) of each child. The answer is now obvious: the parents of D_2 are (M_1, F_1), the parents of D_2 are (M_2, F_4), the parents of D_4 are (M_1, F_2), and the parents of D_6 are (M_1, F_1). The bifurcation in the atoms $B_{[c_9]}$ is important for the sequel, so we describe it in the following assertion.

Proposition 22. *The surgeries of families in the two atoms $B_{[c_9]}$ are as follows*:

$$\{1\} \mapsto \{1\} + \{6\}, \quad \{4\} \mapsto \{2\} + \{4\}.$$

Finally, we obtain the first molecule in Table 6.3 for the point δ_{22}.

Consider the point δ_{26}. Here we do not know the rule of marking by families of the four edges that connect $2B_{[a_{11}]}$ and $2B_{[c_5]}$. The edge a_{11} separates the chambers V and VII, i.e., the families $\{1\} + \{5\}$ are transformed into the families $\{1\} + \{3\} + \{5\} + \{7\}$. Note that if the values of the parameters belong to the domain $4'$, then the edge a_{11} has an exit to the point Δ_{14}, at which, according to Theorem 16, the loop molecule has two connected components, so that the families in the "heads" of the atoms $B_{[a_{11}]}$ come to the "feet" of the same atoms. In particular, the bifurcation of the families in the atoms $B_{[a_{11}]}$ are as follows:

$$\{1\} \mapsto \{1\} + \{3\} \vee \{7\}, \quad \{5\} \mapsto \{5\} + \{3\} \vee \{7\}.$$

On the other hand, from the loop molecule of the point δ'_{27} (see Table 6.2) we know that the bifurcations in the atoms $B_{[c_5]}$ are as follows:

$$\{1\} \mapsto \{1\} + \{5\}, \quad \{3\} \mapsto \{3\} + \{7\}.$$

Since, according to the atoms set on the edges of the bifurcation diagram, the number of regular tori in the adjacent chambers, and the general classification (see [8]), the neighborhood of the point δ_{26} has the type $B \times B$, the alternative in the atoms $B_{[a_{11}]}$ is solved unambiguously.

Table 6.3

Class of points	Molecule	Class of points	Molecule
δ_{22} (2)	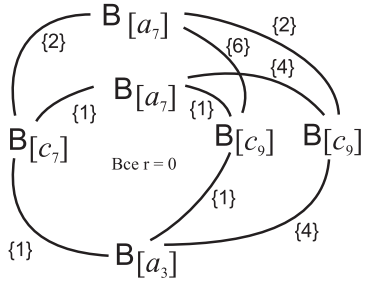	δ_{26} (2′)	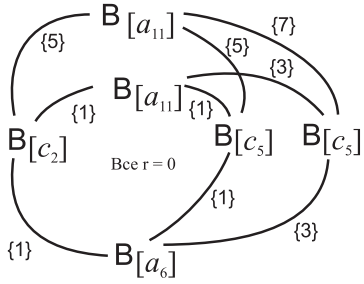
δ_{21} (1)	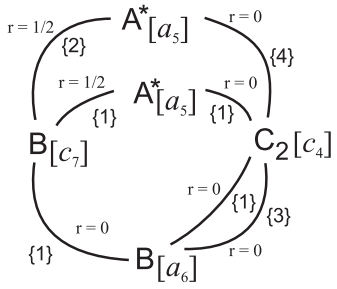		

Proposition 23. *In the two atoms $B_{[a_{11}]}$, the surgeries of families are as follows*:

$$\{1\} \mapsto \{1\} + \{3\}, \quad \{5\} \mapsto \{5\} + \{7\}.$$

As a result, for the point δ_{26}, we obtain the second molecule in Table 6.3.

For the last nondegenerate point δ_{21} (the diagram for the domain 1), the question is how one can join families in the bifurcation $2A^*_{[a_5]}$. The edge a_5 separates the chambers II and IV, i.e., the pair of the family $\{1\}+\{2\}$ is transformed into the pair $\{1\}+\{4\}$. The rule of the correspondence of families will be uniquely deduced below in the study of the loop molecules of the point Δ_{01}, which is always one of the endpoints of the edge a_5 (the diagrams for the domains 1–6). We state it now without proof (for the proof, see p. 337).

Proposition 24. *In the two atoms $A^*_{[a_5]}$, the surgeries of families are as follows*:

$$\{1\} \mapsto \{1\}, \quad \{2\} \mapsto \{4\}.$$

Again, we use the atoms on the edges of the bifurcation diagram, the number of regular tori in the adjacent chambers, and the general classification (see [8]) to determine the third molecule for a point δ_{21} in Table 6.3.

This concludes the study of loop molecules of nondegenerate rank-0 critical points and the structure of their full preimage under the moment mapping. We emphasize that Proposition 24 has not been proved.

6.3. Loop molecules of rank 1 degenerate points. The list of marked loop molecules of rank-1 singularities is given in [32]. Although the classification in [32] is purely visual (by the shape of bifurcation diagrams) without an analytical description of separating values of the parameter, this list

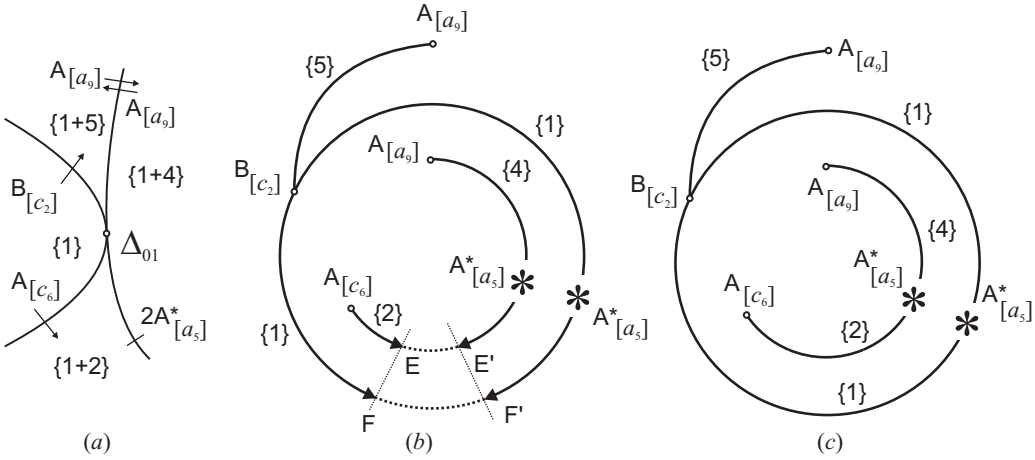

Fig. 34. Construction of a loop molecule for Δ_{01}

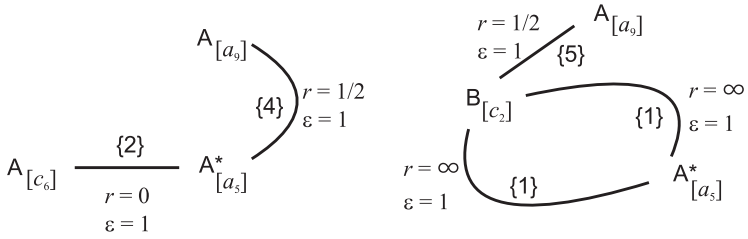

Fig. 35. Loop molecule for Δ_{01}

is exhaustive. The marks of molecules are mainly derived from already existing marks by the addition rules for marks (see [8]), but in some cases they are calculated by the Topalov formulas (see [34]), which requires knowledge of the topology of the loop manifold of a degenerate rank-1 critical trajectory (in particular, the number of connected components, which was not previously found proved in all cases). In this section, we present the classification of loop molecules with full argumentation.

6.3.1. Points Δ_0. We construct loop molecules for degenerate closed trajectories in the preimage of the set Δ_0.

Consider the point Δ_{01}, taking, for example, the diagram for the domain 1. The atoms on the edges of the diagram in a neighborhood of this point are indicated in Fig. 26 and families of tori in chambers in Fig. 33. All this information is collected in Fig. 34(a).

The graph of a molecule with vertices-atoms and edges-families can be restored by this information and gluing rules for families of two atoms A^*; this is shown in Fig. 34(b). However, we see that there are only two options of gluing, and if we glue the point E with F' and F with E', then we obtain a connected molecule, which is impossible, since, according to Theorem 15, the surface J_{01} consists of two components. Therefore, we must glue the point E with E' and F with F'. Then we obtain a molecule consisting of two components, as is shown in Fig. 34 (c). This, in particular, proves Proposition 24..

Since the assertion from [20] about the rough structure of the molecule has been rigorously proven, we can also use marks calculated in [20] (the point Δ_{01} corresponds to the point z_3 in [20]). The final result for the point z_3 is shown in Fig. 35 There is a difference with [20] in the gluing of families. Thus, in the second component of the atom A^*, tori of the same family converge. This cannot be established within the manifold $\ell = 0$, which was studied in [20]. In the present paper, families are treated in the

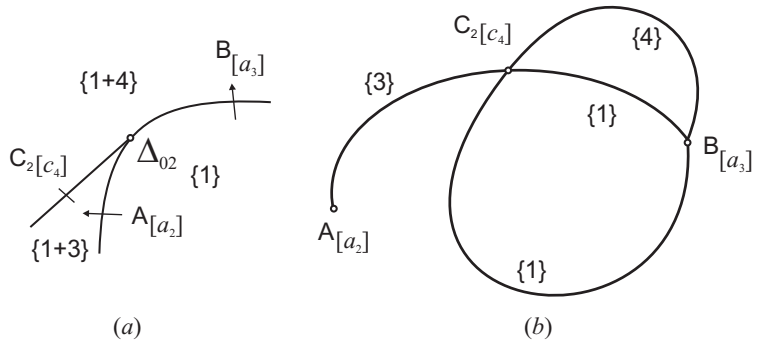

Fig. 36. Construction of a loop molecule for Δ_{02}

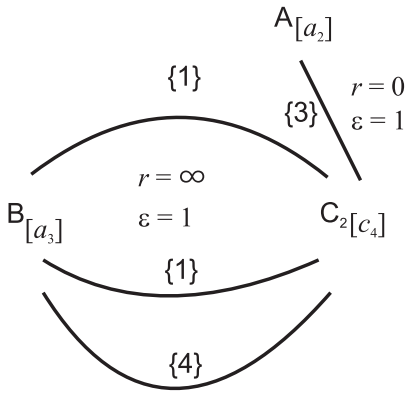

Fig. 37. Loop molecule for Δ_{02}

sense of the extended phase space. Therefore, two distinct families of tori in a one-parameter set of systems with two degrees of freedom $\ell = 0$, $\lambda \in \mathbb{R}$ turn out to be the same family in the two-parameter set of such systems.

Consider the point Δ_{02} on the diagram for the domain 1. As in the previous case, the atoms on the edges of the diagram in a neighborhood of this point are indicated in Fig. 26 and families of tori in the chambers in Fig. 33. All this information is collected in Fig. 36(a). Here rough molecules and families on the edges can be restored uniquely (see Fig. 36(b)). Marks on edges can be found in [7, 8], where only the r-marks are presented; however, all ε-marks are equal to $+1$, according to the corresponding result of [19]). The resulting molecule is shown in Fig. 37. The discrepancy between the numbers of families with [7] is due to the same reason as in the previous case: the impossibility of identifying some of the families in the framework of a particular case (here the particular case is $\lambda = 0$). We will make no further remarks about the number of families when comparing molecules.

Consider the point Δ_{03}. It can be found in the diagram for the domain 2. The atoms on the edges of the diagram in a neighborhood of this point are shown in Fig. 26, the chambers and the number of tori in them in Fig. 32, and the families are shown in Table 5.1. All this information is collected in Fig. 38(a). Gluing of families in the atoms A^* of the edge a_5 is described by Proposition 24, which was proved above (see the construction of the molecule for the point Δ_{01}). The families $\{4\}$ and $\{6\}$ arising on the atoms A of the edge a_8 come to the atom B of the edge c_9 in accordance with Proposition 22. The choice of alternative gluing of pairs of the points E, F and E', F' is determined uniquely: the point E cannot be connected with F' since a connected molecule appears, which is impossible due to Theorem 15: it must consists of two components. Thus, at this stage we have a rough molecule shown

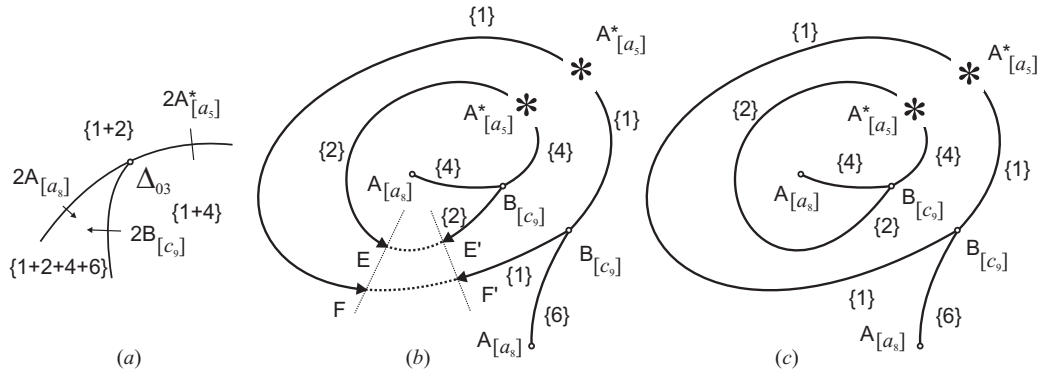

Fig. 38. Construction of a loop molecule for Δ_{03}

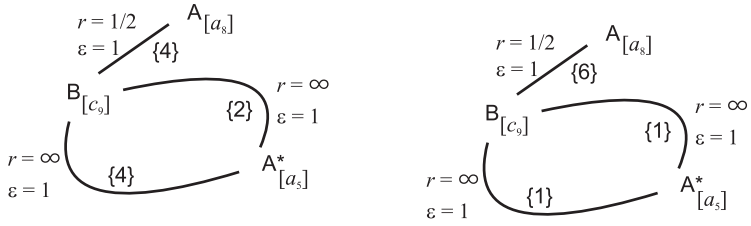

Fig. 39. Loop molecule for Δ_{03}

in Fig. 39(c). The marked molecule is shown in Fig. 39. Since the point Δ_{03} exists also for $\lambda = 0$, the marks on the edges of the molecule can be taken from [7], taking into account the results of [19] regarding the ε-marks.

Consider the last of the points on Δ_0, the point Δ_{04}; it can be found on the diagram for the domain $2'$. The atoms on the edges of the diagram in a neighborhood of this point are indicated in Fig. 29, the chambers and the number of tori in them in Fig. 32, and families corresponding to chambers are presented in Table 5.1. All this information is collected in Fig. 40(a). Here the only possible ambiguity is related to the surgery of families of the two atoms B of the edge a_{11}. Above, we have proved Proposition 23 on bifurcations of families on the edge a_{11}, using a forecast for a fairly simple molecule of the point Δ_{14}. We prove it once again for other reasons. Assuming that at least one of the families $\{5\}$ and $\{7\}$ generated on the edge c_3 comes to the "foot" of the atom $B_{[a_{11}]}$, which transforms two tori into one torus of the family $\{1\}$, then the molecule obtained is connected, which contradicts Theorem 15. Then none of the points G' and H' can be glued with the points E or F (Fig. 40(b)). Therefore, the unique possible result is shown in Fig. 40 (c). The molecule for this point also exists for $\ell = 0$; therefore, marks on its edges can be taken from [20] (the corresponding point was denoted by z_4 in [20]). As a result, for the point Δ_{04} we obtain a loop molecule shown in Fig. 41.

6.3.2. Points Δ_1. The following class of degenerate rank-1 points consists of point lying in the preimage of the cusp of the surface Π_1. Marks of the loop molecule of this type for cusps on the diagrams were described in [20], namely, r-marks are equal to ∞ on the edge $B - B$ and are finite on the edge $A - B$; all ε-marks are equal to $+1$. Therefore, for the point Δ_{11} (see, e.g., the diagram for the domain 1), we have the result shown in Fig. 42. Here the r-mark on the edge $A - B$ is equal to zero (see [8]). The vanishing of r-marks on the edge $A_{[a_4]} - B_{[a_3]}$ for the molecule of the point Δ_{12} shown in Fig. 43 and lying on the diagram for the domain 3 must be proved. We apply the method used in [20]. Recall the addition rule for marks (see [8]).

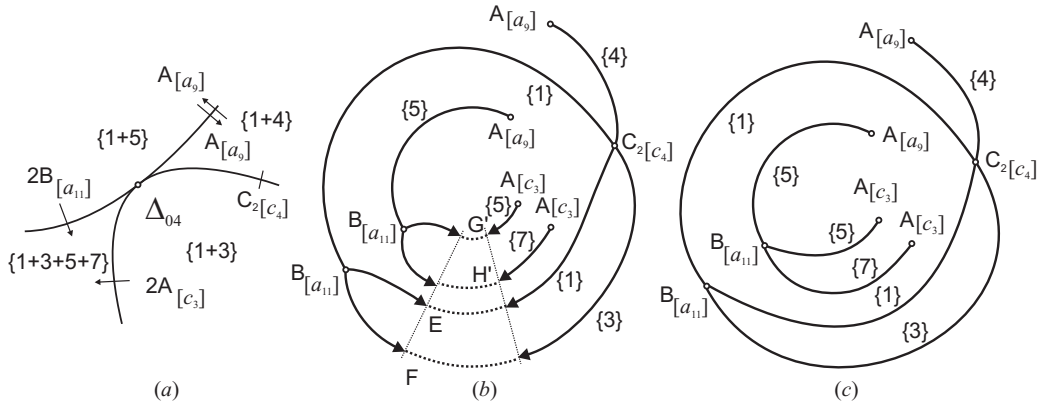

Fig. 40. Construction of a loop molecule for Δ_{04}

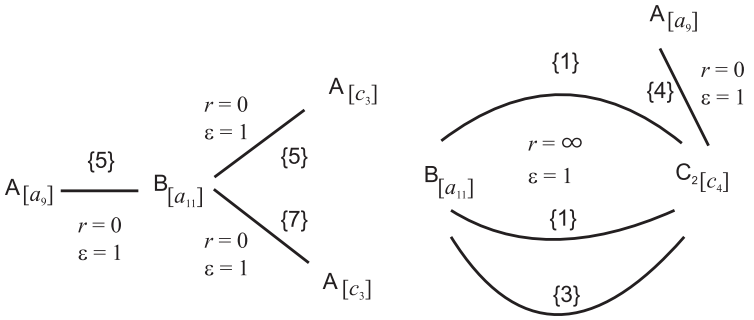

Fig. 41. Loop molecule for Δ_{04}

Lemma 4. *Let some family be involved in bifurcations of three walls u_1, u_2, and u_3 of the same chamber and for the transition $u_1 \to u_2$ we have $r = \infty$. Then the r-marks of the transitions $u_1 \to u_3$ and $u_2 \to u_3$ coincide.*

Proposition 25. *In the loop molecule of the point Δ_{12} on the edge joining the atom A with the saddle, the r-mark is equal to zero.*

Proof. We use Lemma 4. For the point Δ_{12}, we consider the transition in the family $\{4\}$ from $B_{[a_3]}$ to $A_{[a_4]}$. Using the bifurcation diagram, we see that these two walls can coexist with various other walls. For example, in the domain 3, we have the transitions

$$B_{[a_3]} \to 2A_{[c_8]} \to A_{[a_4]}.$$

However, the family $\{4\}$ is not involved in the bifurcation on the edge c_8. The point Δ_{12} is also present in the domain $1'$; however, we cannot indicate a decomposition of the desired transition into the sum of two transitions.

Consider the diagram for the domain 9. The point Δ_{12} itself does not lie on this diagram, but there are transitions in the family $\{4\}$ of the following form: the transition $B_{[a_3]} \to A_{[b_2]}$ belongs to the molecule of the nondegenerate point δ_{31} with mark $r = \infty$, and the transition $A_{[b_2]} \to B_{[a_4]}$ belongs to the molecule of the nondegenerate point δ_{32} with mark $r = 0$. Therefore, the missing r-mark is equal to 0. □

Consider the point Δ_{13}. At this point, the following edges of the diagram converge (the domain 2): the edge a_8 with two atoms A, in which tori of the families $\{4\}$ and $\{6\}$ appear, and the edge a_7 with two atoms B, in which each of tori of the families $\{1\}$ and $\{2\}$ is transformed into a pair of tori selected

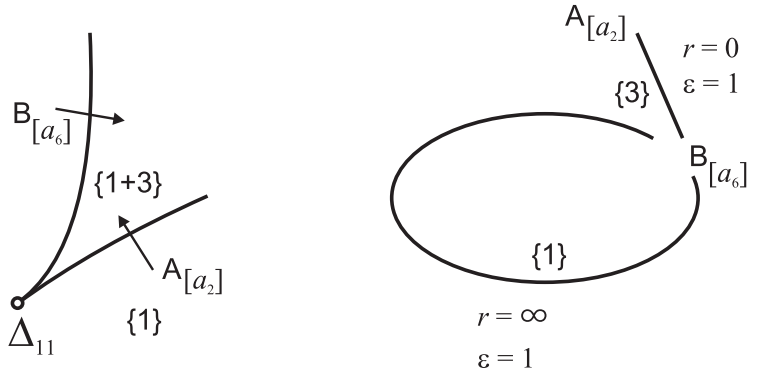

(a) (b)

Fig. 42. Diagram and loop molecule for Δ_{11}

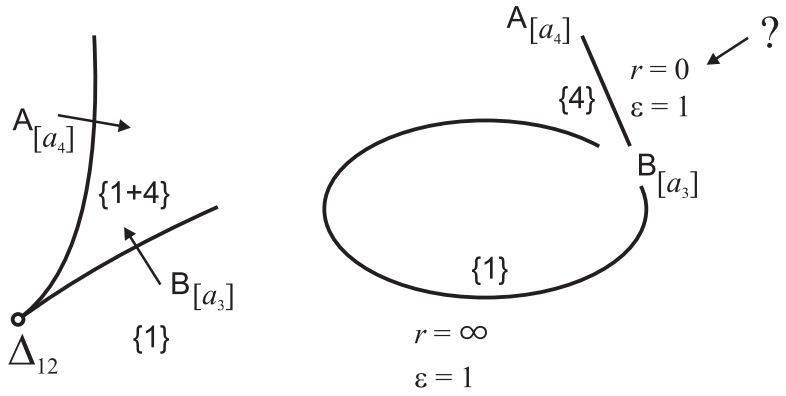

(a) (b)

Fig. 43. Diagram and loop molecule for Δ_{12}

from the families {1}, {2}, {4}, and {6}. The endpoint of this edge is the nondegenerate point δ_{23}; in the study of this point, we have proved Proposition 21 on surgeries of families in two atoms $B_{[a_7]}$. As a result, we obtain a loop molecule consisting of two components for Δ_{13}; it is shown along with a fragment of the diagram in Fig. 44.

Note that the fact that the loop molecule of a degenerate circular orbit consists of two components, even in the case where the diagram contains a return point, must be proved since there is no complete classification of such molecules. Earlier, we have proved this with the help of an analytical solutions in Theorem 16. But now it turns out that a molecule consisting of one component could arise only in the case where two tori of families that appear on the edge a_8 meet in the same atom B of the edge a_7, which contradicts Proposition 21. Thus, the presence of two components in J_{13} is also proved topologically. Therefore, marks can be taken from [8].

For the point Δ_{14}, the same question about the number of connected components in a loop molecule appears. The presence of two components was proved earlier with the help of analytical solutions in Theorem 16. On the other hand, in this case two atoms B are realized on the edge a_{11} (see the diagram for the domain $4'$). The endpoint of this edge is the point Δ_{04} examined above; thus, we know that

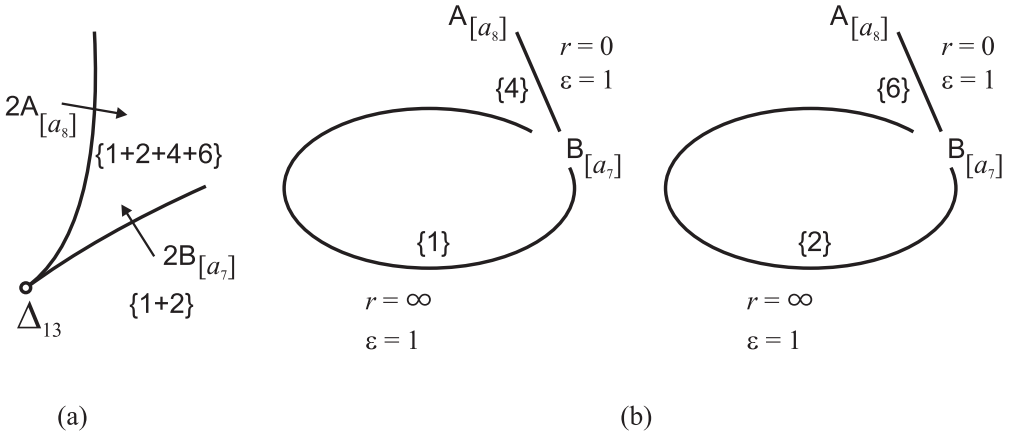

(a) (b)

Fig. 44. Diagram and loop molecule for Δ_{13}

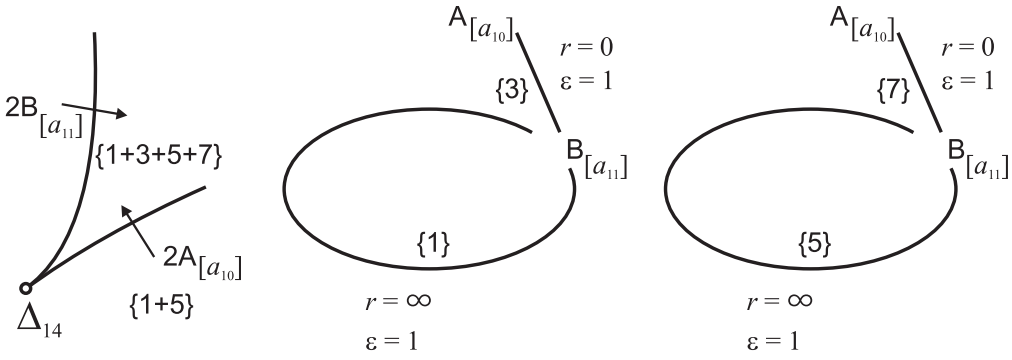

(a) (b)

Fig. 45. Diagram and loop molecule for Δ_{14}

on one atom B a torus from the family $\{1\}$ is transformed into two tori of the families $\{1\}$ and $\{3\}$, whereas on the other atom a torus from the family $\{5\}$ is transformed into two tori of the families $\{5\}$ and $\{7\}$, which is indicated in the components of the loop molecule in Fig. 41. For the point Δ_{14} we obtain the fragment of the diagram and two components of the loop molecule shown in Fig. 45; we obtained this result by using topological arguments. Marks are taken from [20].

6.3.3. Points Δ_3. The last class of rank-1 degenerate points consists of points lying in the preimage of the cusp edge of the surface Π_3.

As for the set Δ_1, if the preimage of the point Δ_{3i} contains only one degenerate circle, i.e., the corresponding critical integral surface and the loop molecule are connected, it suffices to find the numbers of families that are involved in bifurcations. Therefore, for the points Δ_{31} and Δ_{33} (see, e.g., the diagrams for the domain 1 and $1'$), we obtain the result shown in Figs. 46 and 47. Marks of the loop molecule of the point Δ_{33} are known from [7, 20]. For the point Δ_{31}, the infinite r-mark is a consequence of the general statement from [20] cited above; the fact that the r-mark equals zero on the edge $A_{[c_1]} - B_{[c_2]}$ requires further argumentation.

Proposition 26. *In the loop molecule of the point Δ_{31} on the edge connecting the atom A with the saddle, the r-mark is equal to zero.*

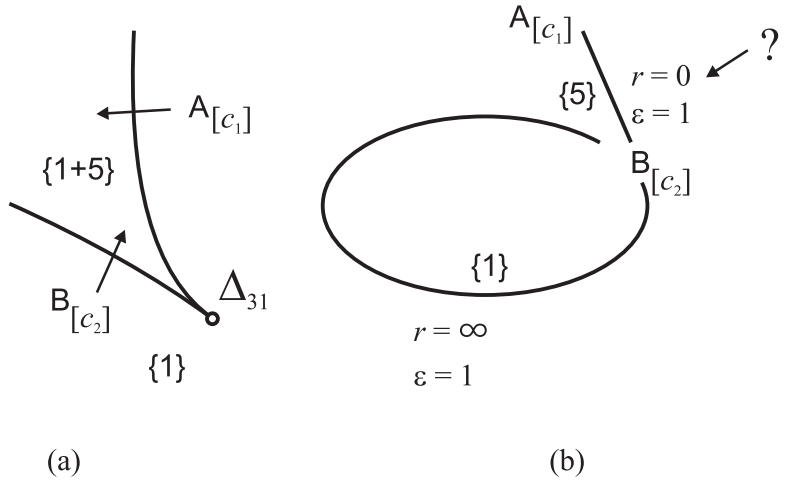

(a) (b)

Fig. 46. Diagram and loop molecule for Δ_{31}

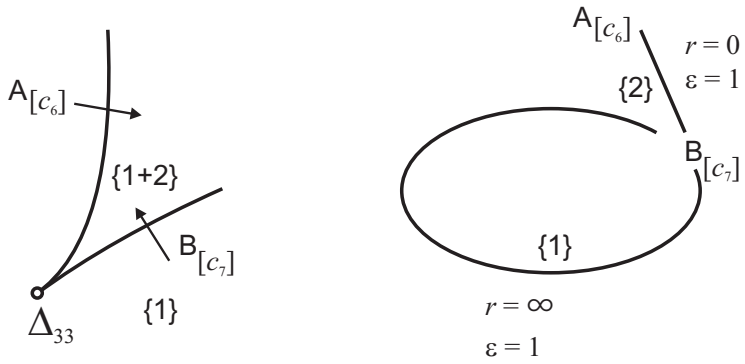

(a) (b)

Fig. 47. Diagram and loop molecule for Δ_{33}

Proof. Again, we apply the addition rule for marks in the case where one of the r-marks is infinite to the point Δ_{31} and transitions in the family $\{5\}$ from $B_{[c_2]}$ to $A_{[c_1]}$. We can also consider various diagrams. For example, in the domain 5, there are transitions $A_{[c_1]} \to A_{[a_9]} \to B_{[c_2]}$. However, both marks are finite: for the first transition, from the molecule of the point δ_{25} we have $r = 0$ and for the second transition, from the molecule of the point Δ_{03} we see that $r = 1/2$. Therefore, the "sum" of marks is defined nonuniquely. The point Δ_{31} also lies in the domain $1'$, but, as for the point Δ_{12}, we cannot indicate a required decomposition of the transformation in the sum of two transformations.

Consider the diagram for the domain $9'$. The point Δ_{31} itself does not belong to this diagram, but there are transitions in the family $\{5\}$ of the following form: the transition $B_{[c_2]} \to A_{[a_{12}]}$ belongs to the molecule of the nondegenerate point δ''_{27} with mark $r = \infty$; the transition $A_{[a_{12}]} \to A_{[c_1]}$ belongs to the molecule of the nondegenerate point δ''_{28} with mark $r = 0$. Therefore, the missing r-mark is 0. □

Consider the point Δ_{32}. We take a fragment of the diagram with marked edges and the corresponding atoms from the diagrams for the domain 4. For this point, we must find the number of connected components of the molecule (there is no analytical solution for the full integral surface). However, a molecule is connected only if the families $\{2\}$ and $\{6\}$ generated on the edge c_8 come to the same

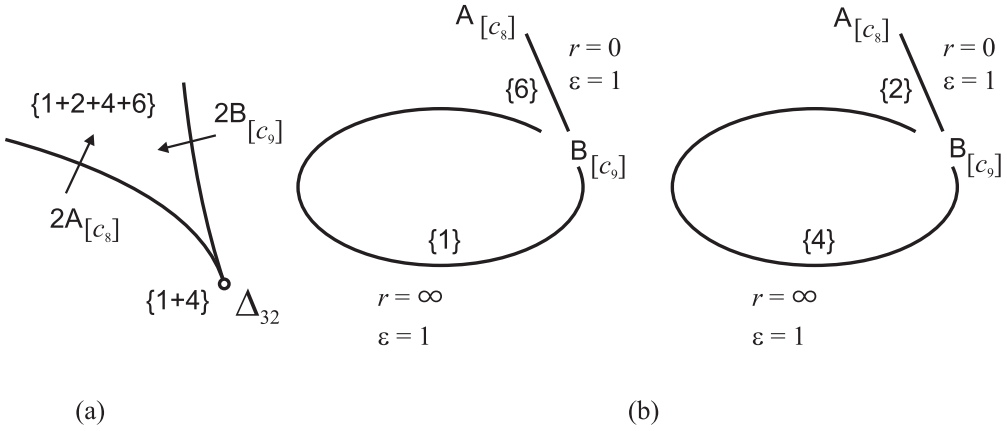

Fig. 48. Diagram and loop molecule for Δ_{32}

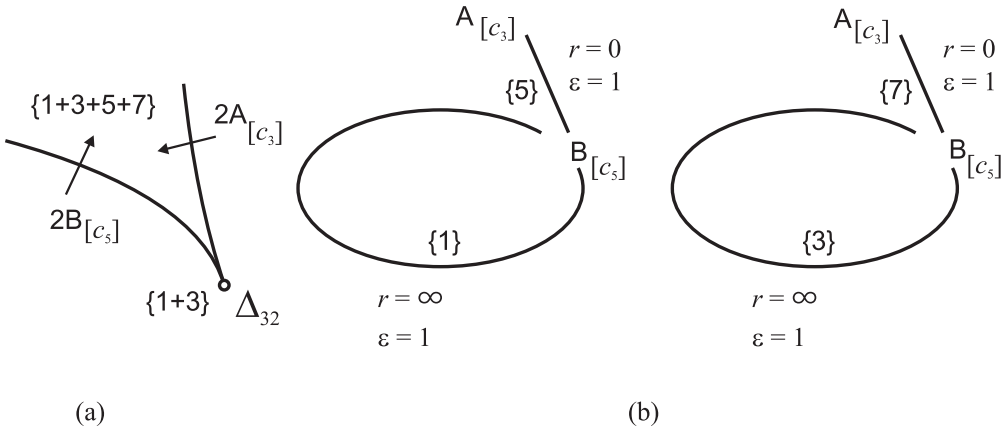

Fig. 49. Diagram and loop molecule for Δ_{34}

atom B of the edge c_9. This contradicts Proposition 22. Thus, the molecule of the point Δ_{32} consists of two components, and Proposition 22 determines the gluing rules for families. Marks are calculated in [8]. The result is shown in Fig. 48.

For the point Δ_{34} (the diagram $\Sigma_{HK}(\ell, \lambda)$ for the domain $2'$), the question on the number of components and the gluing rules for families is solved on the edge c_5 containing two atoms B. The endpoint of this is edge is the point δ_{26}, which is the image of a nondegenerate rank-0 critical point. At the same time, if we consider the diagram $\Sigma_{HK}(\ell, \lambda)$ for the domain $3'$, we can see that the edge c_5 also has an exit to the point δ'_{27}, which is the image of another nondegenerate rank-0 critical point. Thus, as was shown above, under the bifurcation of families in the two atoms $B_{[c_5]}$, a torus of the family $\{1\}$ is transformed into two tori in the families $\{1\}$ and $\{5\}$, whereas a torus of the family $\{3\}$ is transformed into two tori of the families $\{3\}$ and $\{7\}$. Since tori of the families $\{5\}$ and $\{7\}$ are generated on the edge c_3 and these tori come to distinct atoms B of the edge c_5, the molecule of the point Δ_{34} has two connected components. The gluing rules for families are stated uniquely. Having the proof of the existence of two components, we can take the marks from [20]. The result is shown in Fig. 49.

7. Isoenergetic Bifurcation Diagrams

7.1. Separating sets and isoenergetic diagrams. In this section, we classify bifurcation diagrams $\Sigma_{LK}(h,\lambda)$ of the mappings $L\times K$ restricted to isoenergetic levels $Q^4_h = H^{-1}(h)$ in the complete phase space P^5 (see [48]]). The topology of these levels can be obtained trivially. Since H on P^5 is a Morse function having exactly two critical points

$$\boldsymbol{\omega} = 0, \quad \boldsymbol{\alpha} = (\pm 1, 0, 0),$$

we have

$$Q^4_h = \begin{cases} \varnothing, & h < -1, \\ S^4, & -1 < h < 1, \\ S^2\times S^2, & h > 1. \end{cases}$$

We obtain the separating set Θ_H, or the H-atlas, immediately from Proposition 12, taking into account the results of all facts obtained above about critical subsystems: this set is the image on the (λ, h)-plane of the above-mentioned singular points (4.11), (4.16)–(4.21), (4.23)–(4.27), and (4.33) of the key sets of critical subsystems. Recall that the point D_4 is introduced in the classification of the diagrams $\Sigma_{HK}(\ell,\lambda)$ and does not cause surgeries of the diagrams on Q^4_h, but an additional point D_5 appears, which is substantial. As above, it suffices to consider $\lambda \geq 0$ to provide illustrations in the plane (h, λ^2).

Theorem 21 (M. P. Kharlamov, I. I. Kharlamova, and E. G. Shvedov)**.** *The separating set Θ_H in the classification of bifurcation diagrams $\Sigma_{LK}(h,\lambda)$ consists of the following* 13 *curves in the plane* (λ, h):

$$\begin{aligned}
&\xi_0 : h = -1, && \lambda \geq 0;\\
&\xi_1 : h = 1, && \lambda \geq 0;\\
&\xi_2 : h = \frac{3}{2}\sqrt{1+\lambda^4} - \lambda^2, && \lambda \geq 0;\\
&\xi_3 : h = \frac{1}{8}\left(\sqrt{4+\lambda^{4/3}} - \lambda^{2/3}\right)^2\left(2\sqrt{4+\lambda^{4/3}} + \lambda^{2/3}\right), && \lambda \geq 0;\\
&\xi_4 : \lambda = \frac{3x^4-4}{2x^3}, \quad h = \frac{3}{8}x^2 + \frac{2}{x^6}, && x \in \left(\sqrt[4]{4/3}, \sqrt{2}\right];\\
&\xi_5 : h = -\frac{\lambda^2}{2} + \lambda^{2/3} + \frac{1}{2\lambda^{2/3}}, && \lambda \in (0,1];\\
&\xi_6 : \lambda = \frac{1}{2}x + \frac{2}{x^3}, \quad h = \frac{1}{8}x^2 + \frac{2}{x^2} - \frac{2}{x^6}, && x \in \left[\sqrt{2}, \sqrt{2\sqrt{3}}\right];\\
&\xi_7 : \lambda = \frac{1}{2}x + \frac{2}{x^3}, \quad h = \frac{1}{8}x^2 + \frac{2}{x^2} - \frac{2}{x^6}, && x \in \left[\sqrt{2\sqrt{3}}, +\infty\right);\\
&\xi_8 : \lambda = \frac{3x^4-4}{2x^3}, \quad h = \frac{3}{8}x^2 + \frac{2}{x^6}, && x \in \left[-\sqrt[4]{4/3}, 0\right);\\
&\xi_9 : h = \frac{1+\lambda^4}{2\lambda^2}, && \lambda > 0;\\
&\xi_{10} : h = \frac{\lambda^2}{2}, && \lambda \geq 0;\\
&\xi_{11} : h = \sqrt{2} - \frac{\lambda^2}{2}, && \lambda^2 \leq \frac{1}{\sqrt{2}};\\
&\xi_{12} : h = \frac{\lambda^{2/3}}{2}(3 - \lambda^{4/3}), && \lambda^2 \in \left[0, \frac{8}{3\sqrt{3}}\right].
\end{aligned}$$

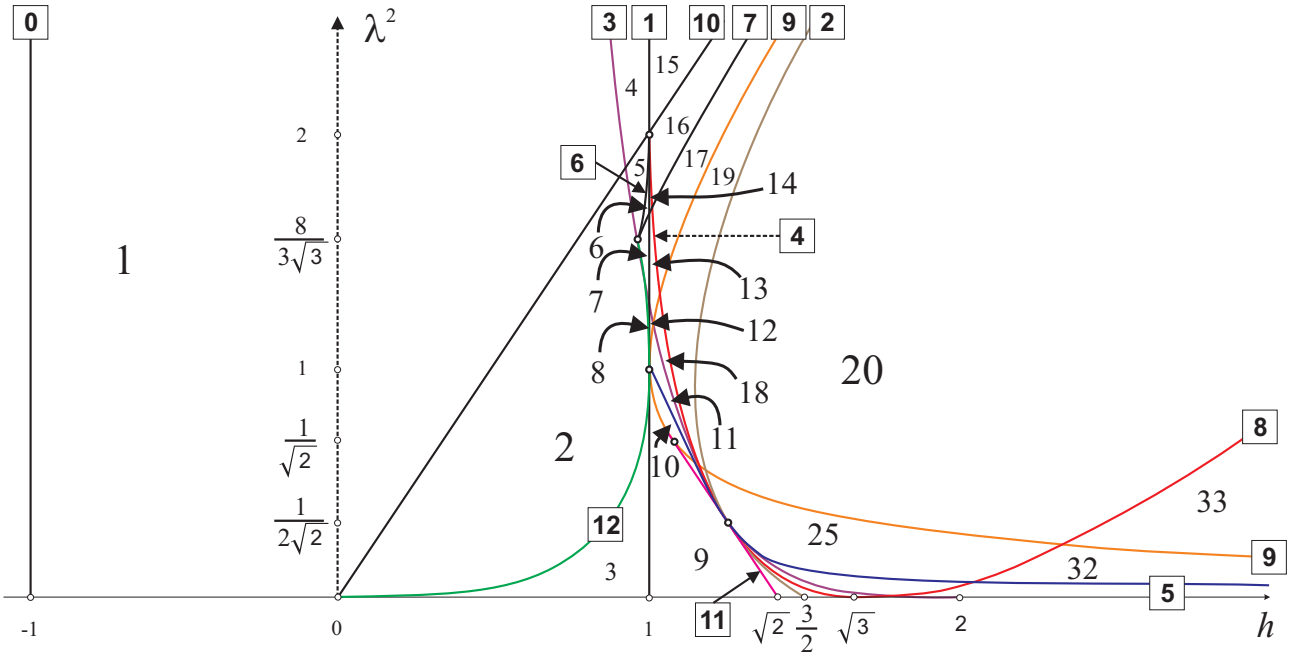

Fig. 50. Separating set Θ_H and generated domains

In this formulation, separating curves are listed in the sequence of the generating points A, B_1–B_7, C, D_1–D_3, and D_5. It is easy to see that ξ_4 and ξ_8 are combined into one smooth curve and ξ_6 and ξ_7 are combined into a curve with a cusp.

Separating curves with their numbers are shown in Fig. 50. In general, they divide the half-plane $\lambda \geq 0$ into 34 domains, one of which, namely, the domains where $h < -1$, corresponds to empty isoenergetic manifolds Q^4_h. The other domains are marked with the numbers 1–33. Due to the sufficiently complicated structure, fragments of the admissible set with complete enumeration of domains are presented in Fig. 51. For convenience, this is also done on the (h, λ^2)-plane.

Figure 52 shows the equipped isoenergetic diagrams. They are symmetric with respect to the axis $\ell = 0$, so it is possible to mark all smooth segments simultaneously (for which bifurcations and gluing rules for families have been previously established) on the right-hand side and indicate the chambers and bifurcations on the left-hand side explicitly. This yields a complete presentation of the isoenergetic two-dimensional invariant of the restriction of the system to the appropriate set Q^4_h; moreover, this is convenient for the construction of all isoenergetic one-dimensional invariants (Fomenko graphs) of reduces systems on P^4_ℓ.

The problem of computer visualization of "ultra small" domains in the construction of bifurcation diagrams is well known. Keeping in mind the the use of the diagrams $\Sigma_{LK}(h, \lambda)$ for the construction of Fomenko graphs (to do this, one must correctly see all sections of the admissible domain by vertical lines $\ell = \text{const}$ that differ by their structure), we try to keep these sections in the figures where possible, i.e., to use distortions of the diagrams by "fiberwise" diffeomorphisms. Obviously, this is not always possible without loss of clarity. In such cases, the requirement of clarity was of primary importance. Major deviations from fiberwise (i.e., preserving the sections $\ell = \text{const}$) diffeomorphisms are observed in the diagrams for the domains 27–33. For example, the edge c_4 actually lies on the curve, which is a continuation of the edge c_9 and, therefore, it should be "shorter" than a_5. As a result, the absolute value of the ℓ-coordinate of the point Δ_{02} is smaller than the ℓ-coordinate of the point Δ_{03}, but this is not so in figures. Moreover, the relation between the ℓ-coordinates for the pairs

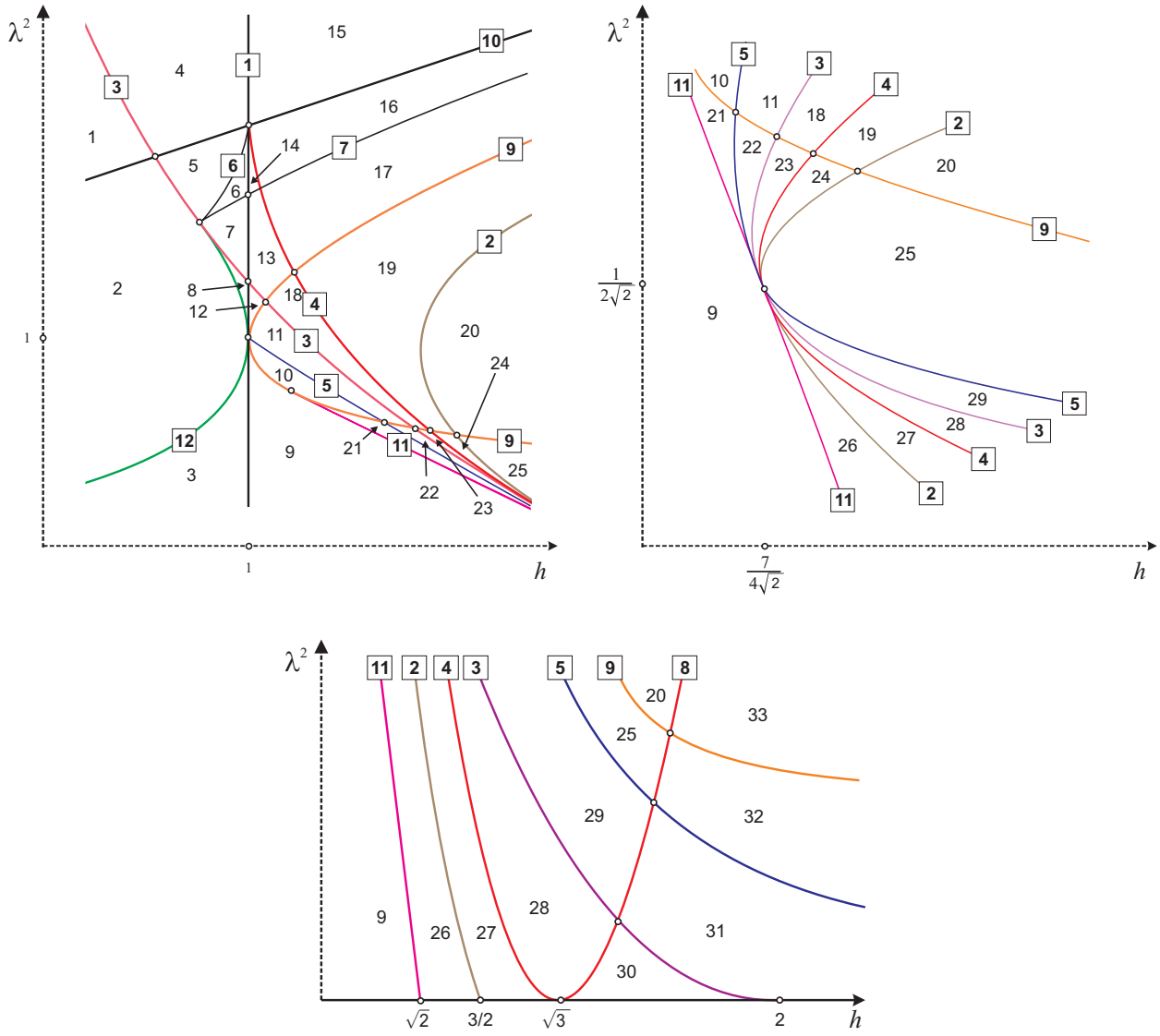

Fig. 51. Fragments of the set Θ_H and generated domains

of the "tails" $(\Delta_{31}, \Delta_{11})$ and $(\Delta_{31}, \Delta_{14})$ can be violated, and so on. At the same time, of course, the equipped isoenergetic diagram itself remains valid as a rough topological invariant.

For an accurate construction and analysis of all sections of the diagram Σ by fixed h and ℓ, software packages in the Wolfram Mathematica system were created (see [31]); they provide an opportunity to position the point (h, λ) in the interactive session with sufficient accuracy with respect to the separating set Θ_H, selection of the required value of ℓ, observing all relevant phenomena in the key sets of critical subsystems, and output the Morse–Bott indexes that define the bifurcation by information from the tables above for all singular points on the section $\ell = \text{const}$ of the diagram $\Sigma_{LK}(h, \lambda)$ in accordance with the formulas obtained above. A similar software package for the diagrams $\Sigma_{HK}(\ell, \lambda)$ was described in [50]. Of course, results of such computer simulations can only be considered as auxiliary; they provide an illustrative "constructor of topological invariants." All results on the classification of Fomenko graphs should be strictly justified analytically. This is done in the following section.

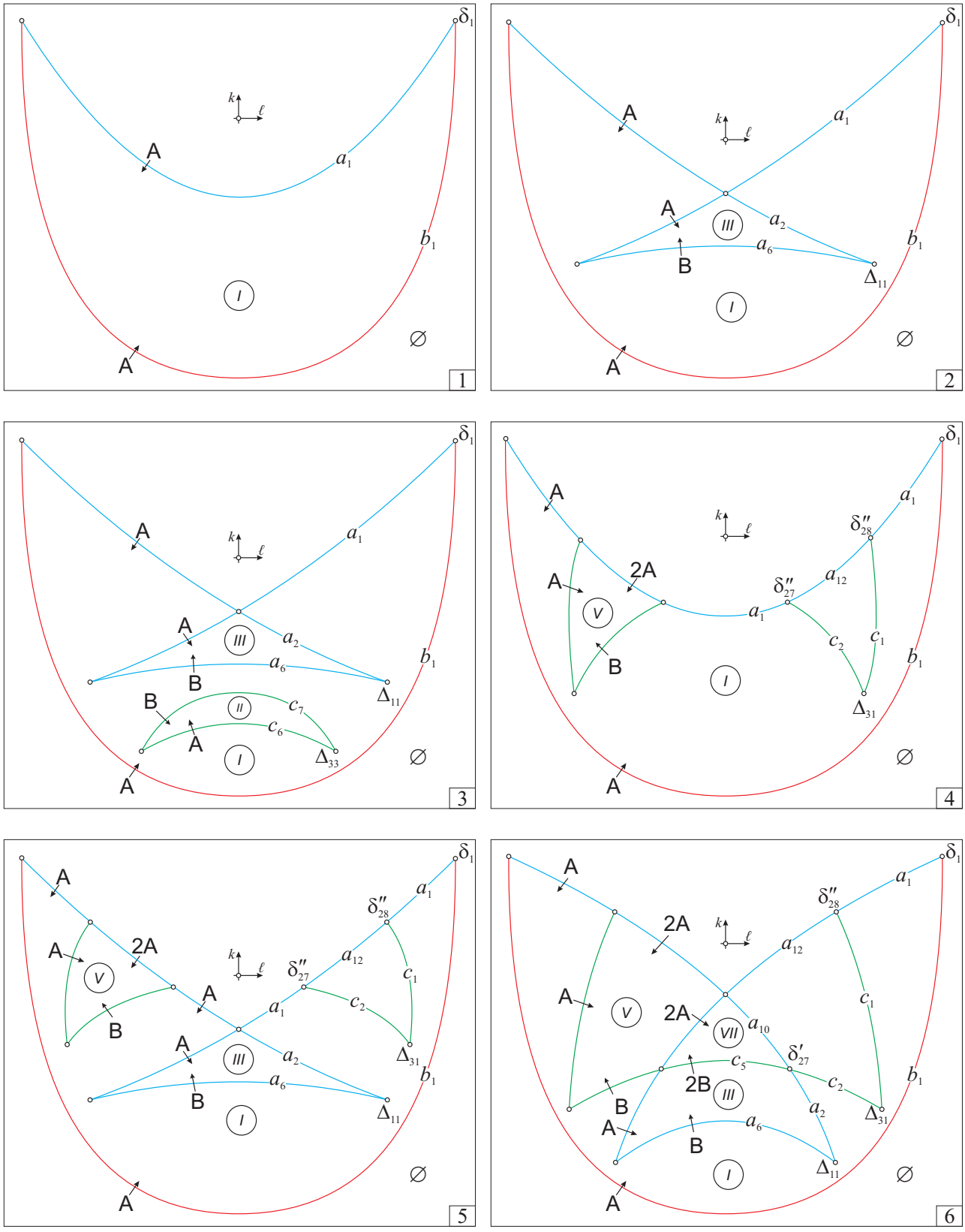

Fig. 52. Equipped diagrams $\Sigma_{LK}(h, \lambda)$

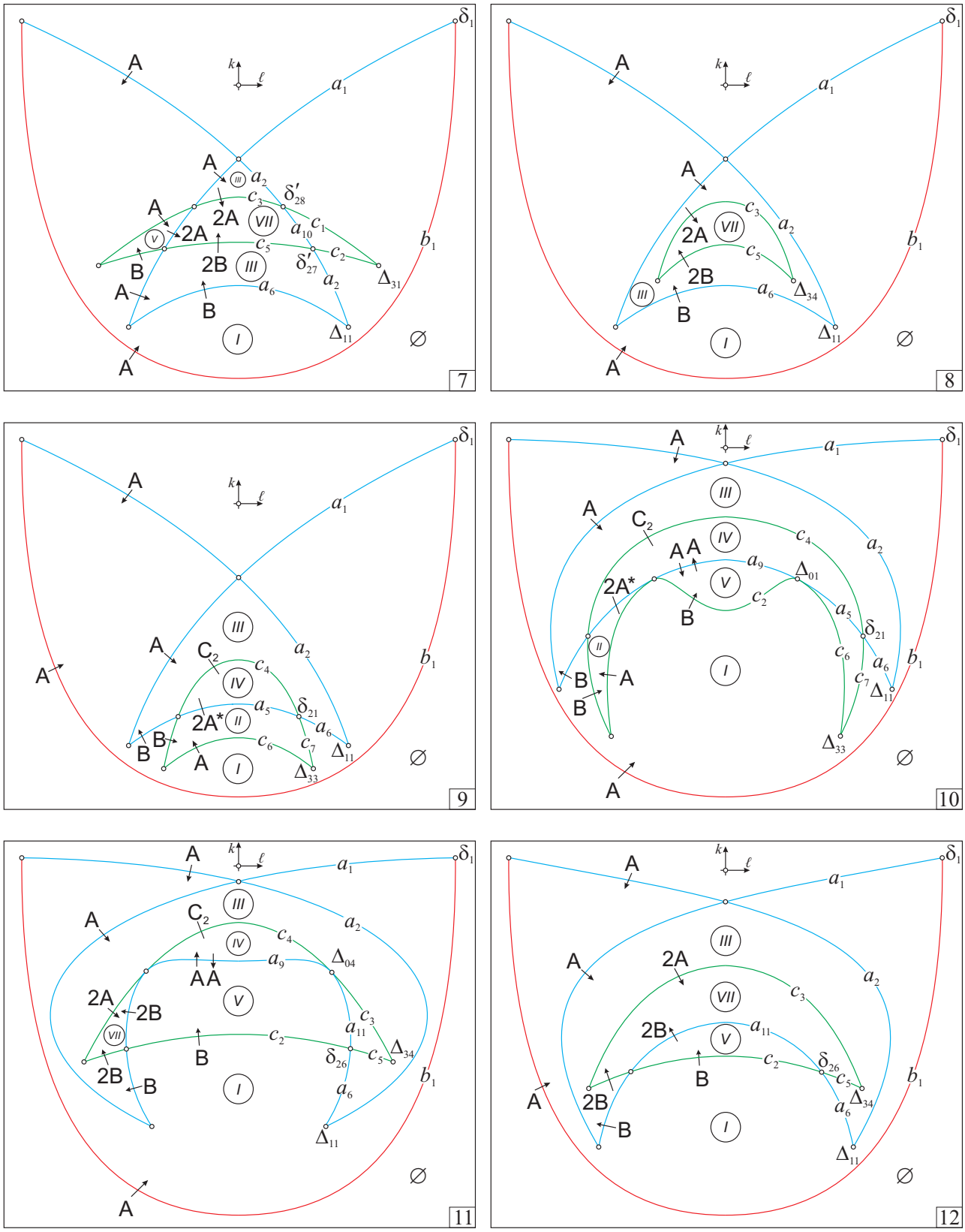

Fig. 52 (continued). Equipped diagrams $\Sigma_{LK}(h,\lambda)$

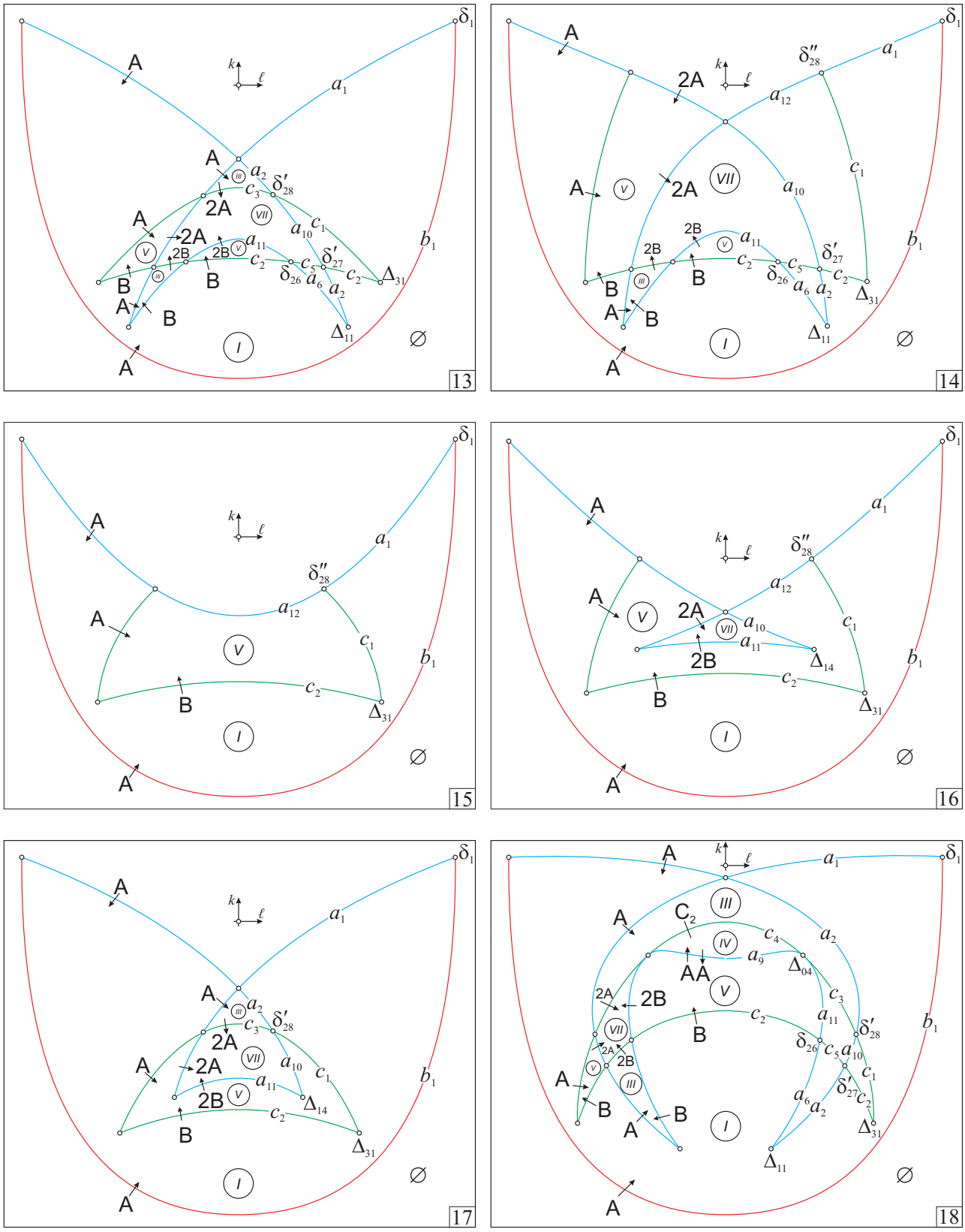

Fig. 52 (continued). Equipped diagrams $\Sigma_{LK}(h, \lambda)$

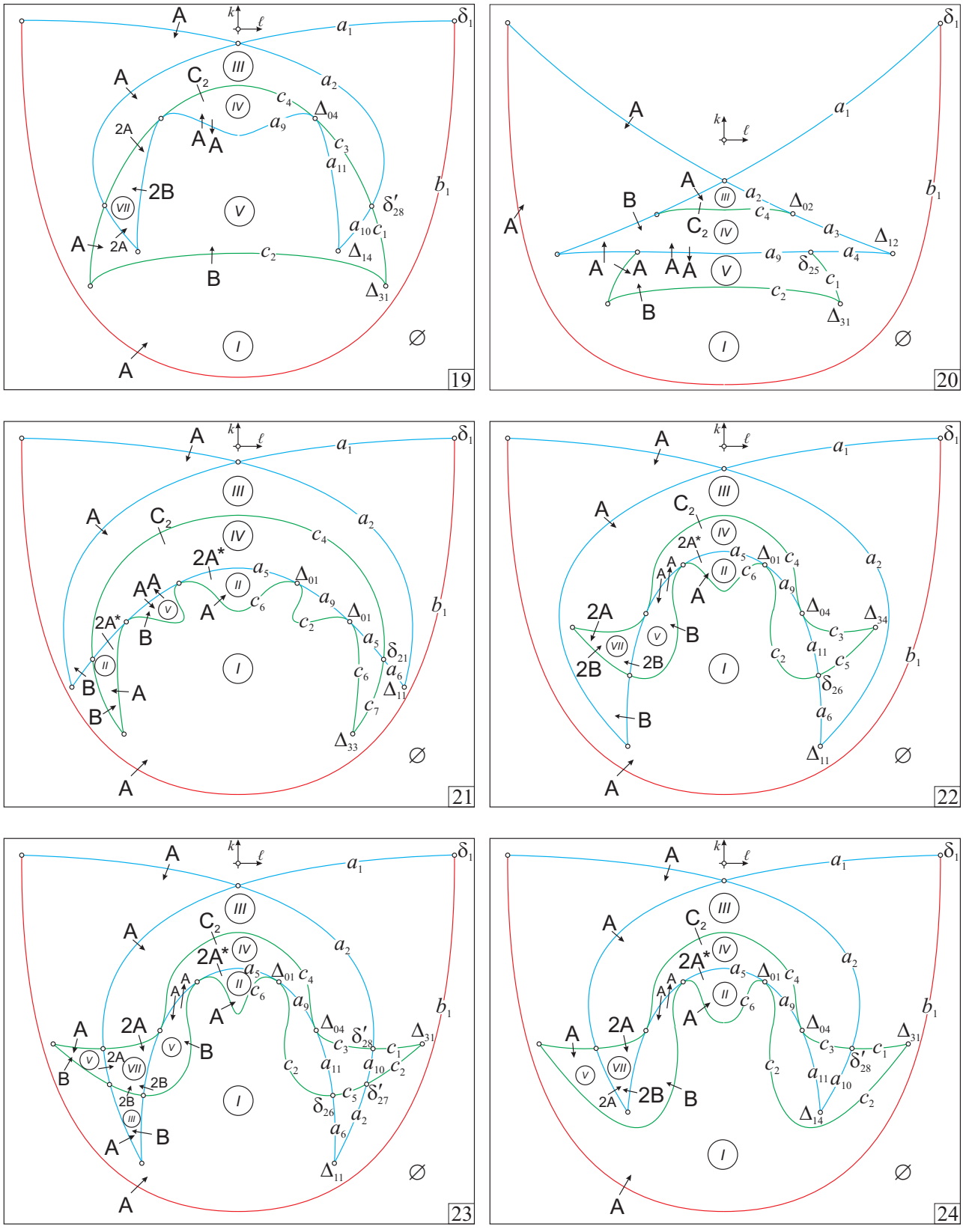

Fig. 52 (continued). Equipped diagrams $\Sigma_{LK}(h, \lambda)$

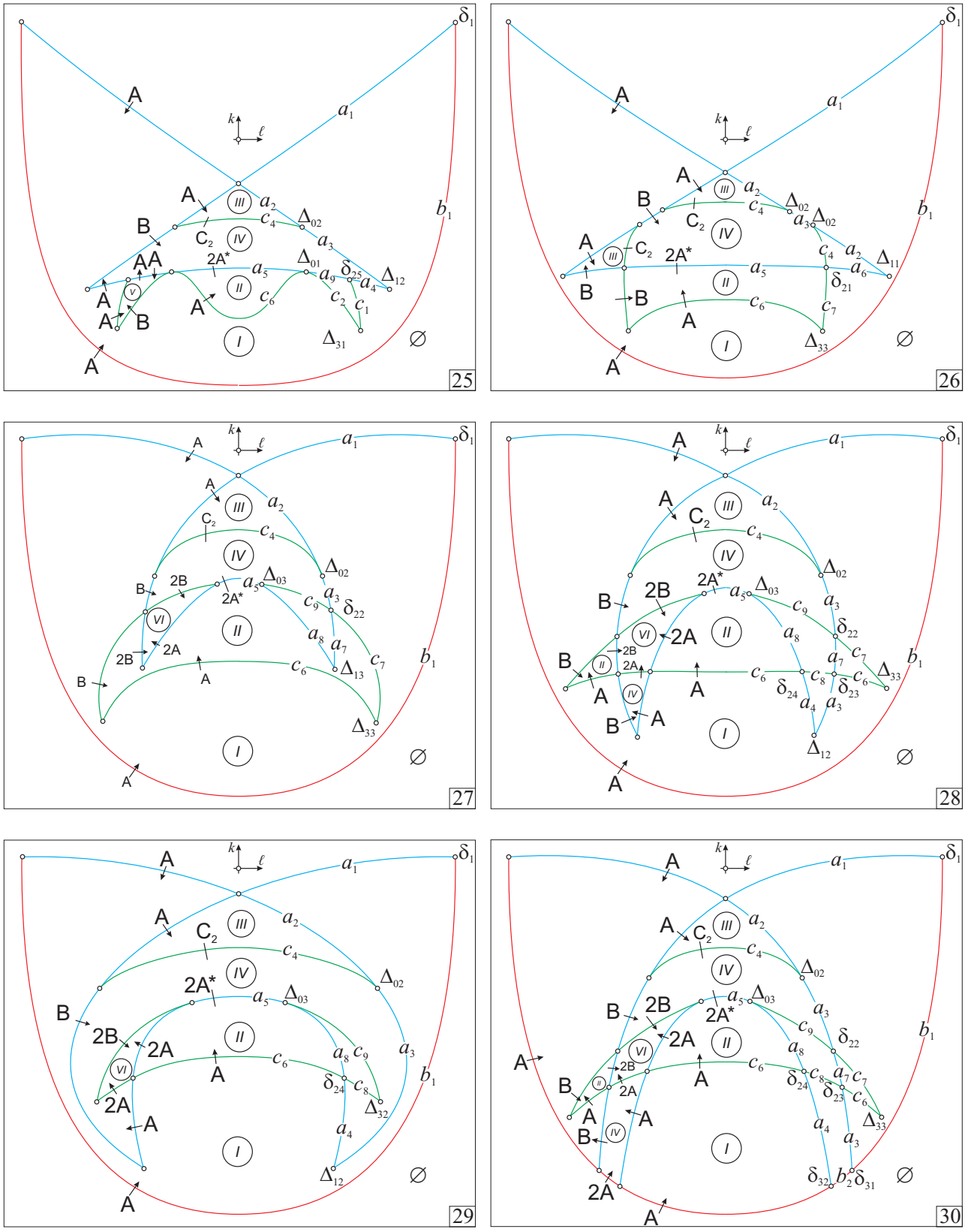

Fig. 52 (continued). Equipped diagrams $\Sigma_{LK}(h,\lambda)$

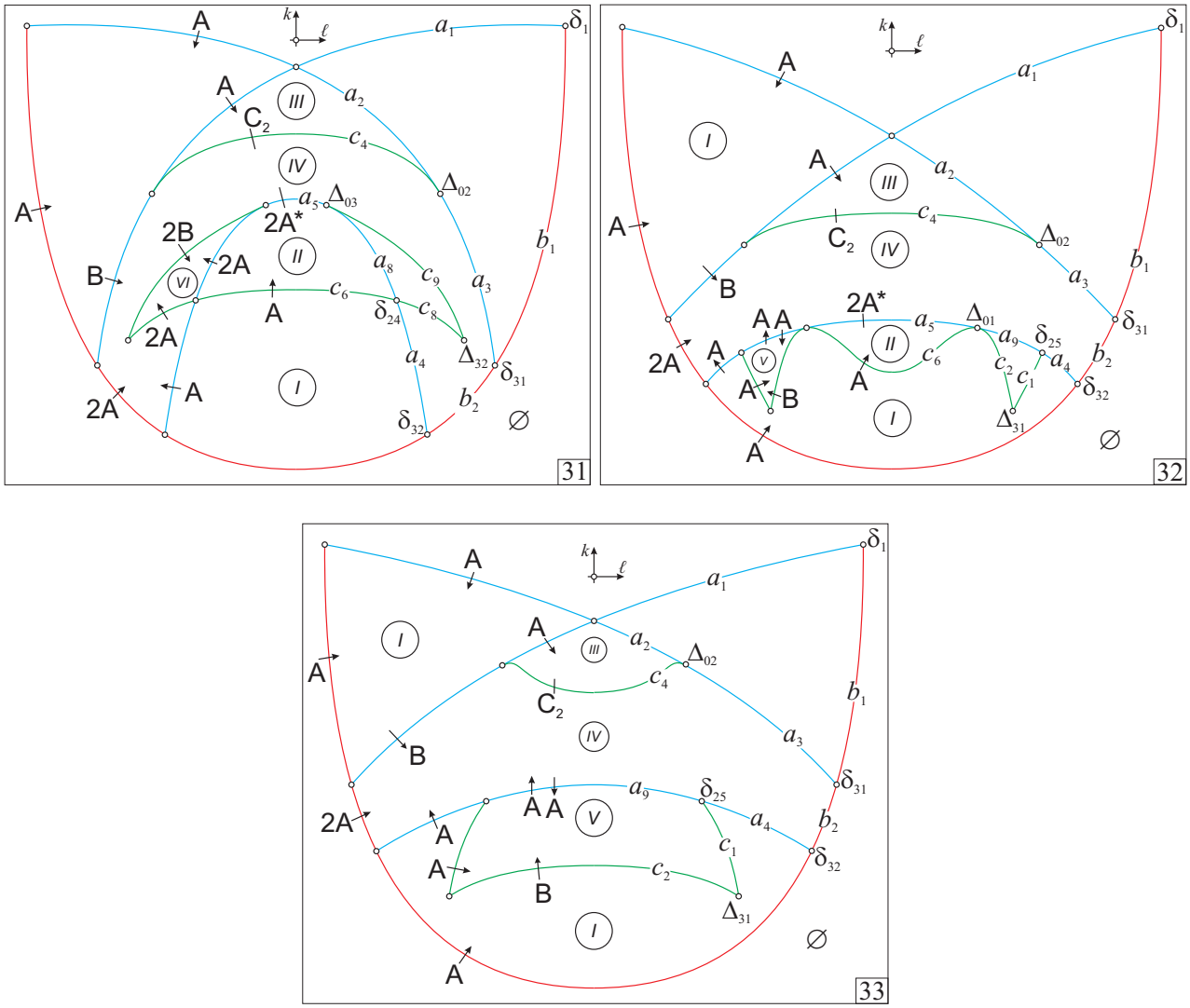

Fig. 52 (continued). Equipped diagrams $\Sigma_{LK}(h,\lambda)$

7.2. Classical Kovalevskaya case. Let us consider the limit case $\lambda = 0$ (the classic Kovalevskaya case). In Fig. 50, we see the separating values of h:

$$-1,\ 0,\ 1,\ \sqrt{2},\ \frac{3}{2},\ \sqrt{3},\ 2.$$

Initially, the (L,K)-diagrams for the Kovalevskaya case were considered by P. Richter and his disciples who used powerful graphic processors for visualization of diagrams, bifurcations, and Fomenko graphs in the 1990s. As a result, a movie was filmed in which the typical motion of bodies for various families of two-dimensional tori of the reduced system was shown. The mathematical description of backgrounds of this movie based on the results of [7, 39, 40] is presented in [67]. In particular, in [67], detailed isoenergetic diagrams were presented that were calculated on the $(\ell, \sqrt{k})$-plane. Separating values of h in the work were not explicitly listed, but they can be derived from the formulas provided there. These values were also obtained as limit values in the research on isoenergetic diagrams of the Kovalevskaya top in a dual field (see [49]). The diagrams $\Sigma_{LK}(h,\lambda)$ corresponding to nonseparating values of h (the exit to the axis $\lambda = 0$ from the domains 1, 3, 9, 26, 27, 30, and 31) are shown in

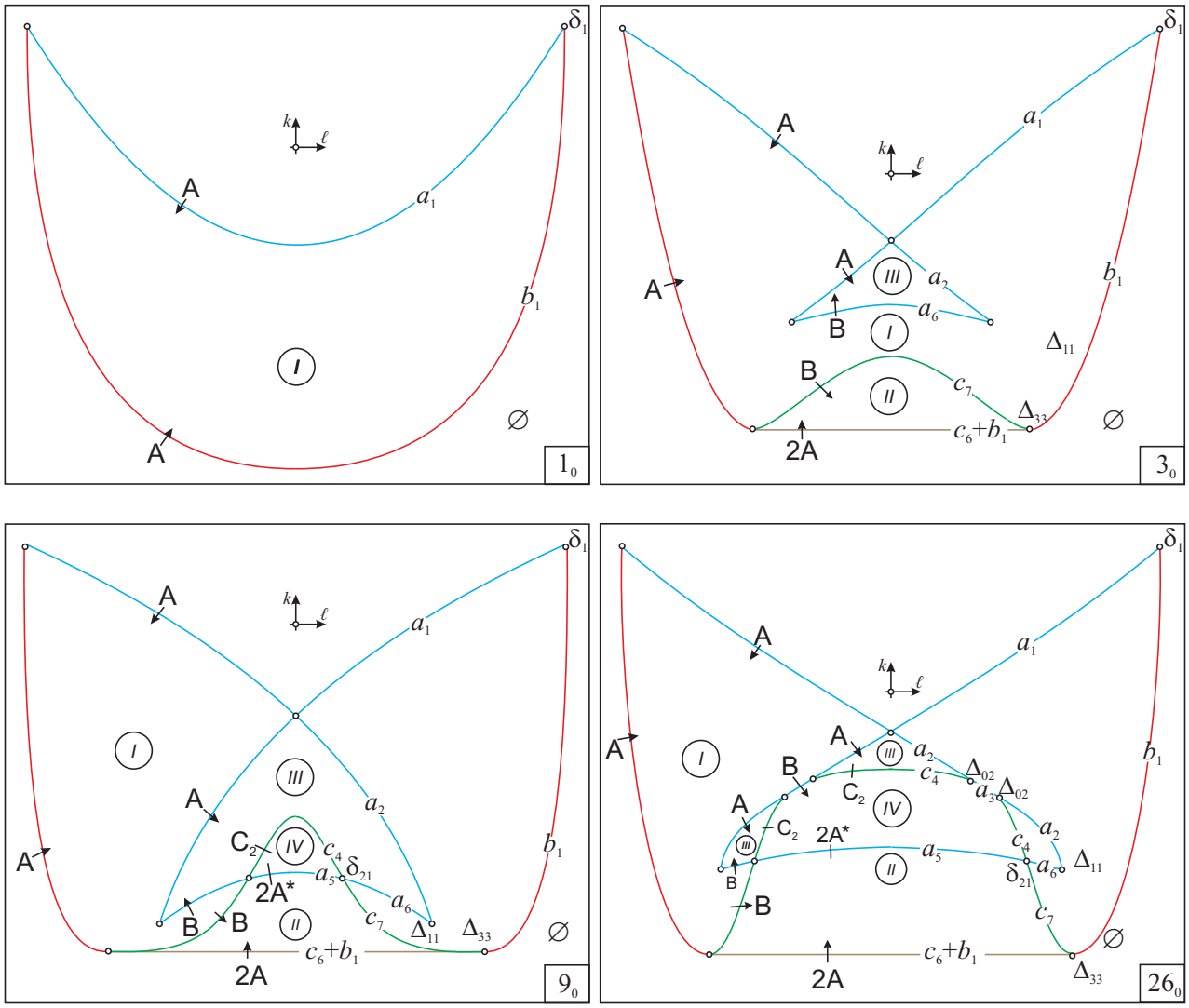

Fig. 53. Equipped diagrams $\Sigma_{LK}(h,0)$ (Kovalevskaya case)

Fig. 53. Here, due to the vertical distortion, the fiber-wise (i.e., preserving the sections $\ell = \text{const}$) diffeomorphism of the domain of the diagram is saved in sufficiently complex cases 27_0, 30_0, and 31_0.

We also note the following interesting feature. In [67], for the domain 30_0, two diagrams were presented. Obviously, the corresponding system on Q^4_h are Liouville equivalent, but they have different sets of Fomenko graphs since the projection of the point δ_{22} on the axis Oh can lie either on the edge $c_6 + b_1$ or on the edge $c_8 + b_2$.

8. Topological Invariants

8.1. Diagrams of Smale–Fomenko. In order to classify Fomenko graphs on $Q^3_{\ell,h}(\lambda)$, we must superpose the projection of the image of the set of degenerate rank-1 critical points on the plane of the Smale diagram. Indeed, the transition through such points determines surgeries in graphs that are not related with change of the topology of $Q^3_{\ell,h}(\lambda)$. Theoretically, splitting of certain atoms without appearing degenerate points is also possible (see [8]), but, as was shown above by listing all atoms appearing in this problem, this phenomenon does not occur here. We write the equations of the image

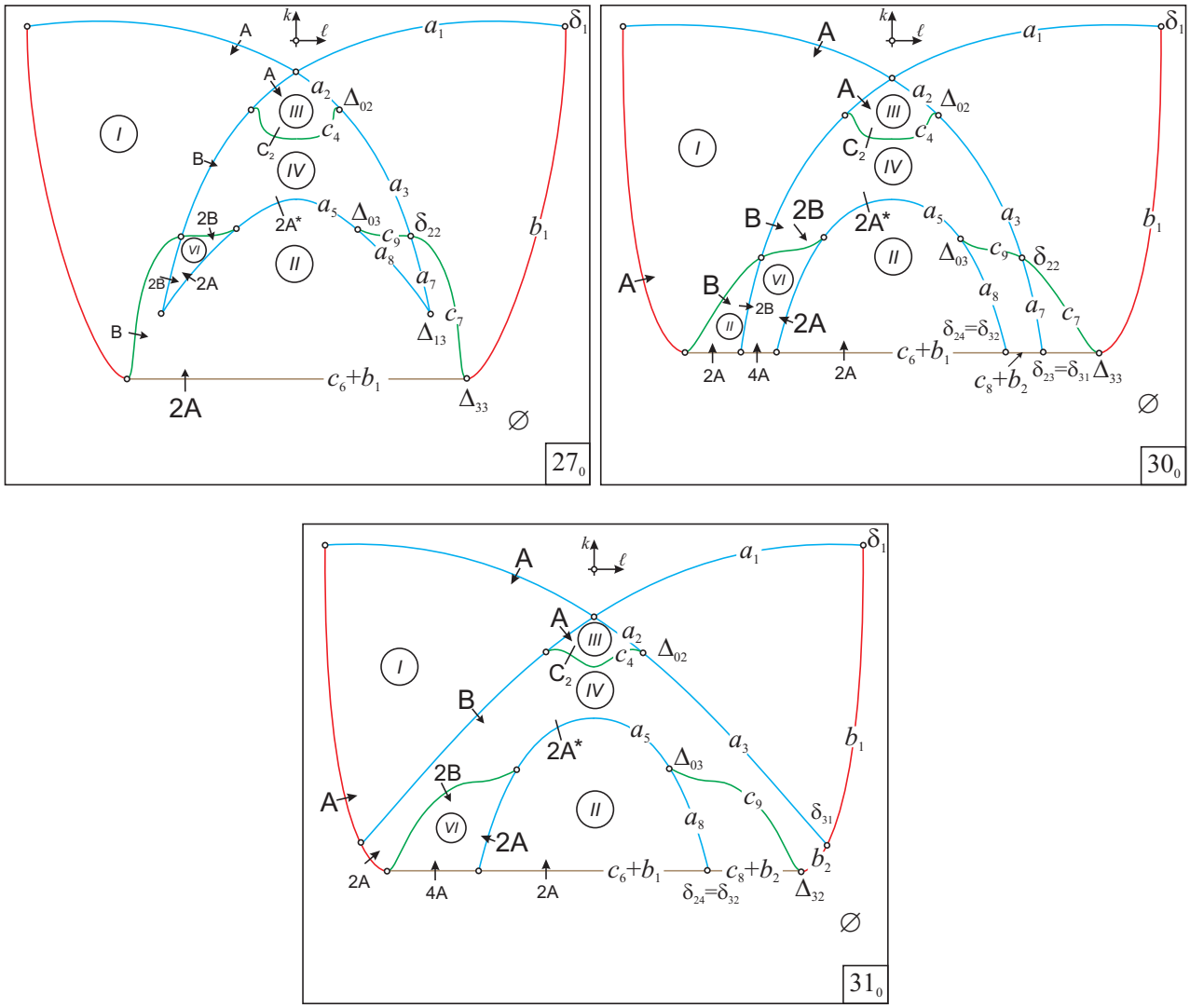

Fig. 53 (continued). Equipped diagrams $\Sigma_{LK}(h,0)$ (Kovalevskaya case)

of the set of degenerate rank-1 critical points taking into account conditions of the existence of motions of required types in accordance with Propositions 15 and 20.

Recall the notation (3.51) and information on the images of rank-1 degenerate points. The collection of curves that classify Fomenko graphs contains the following curves (see Theorem 13 and Proposition 20):

(1) the whole curve of touching of the surfaces Π_1 and Π_3:

$$\Delta_0: \quad \begin{cases} \ell = \pm\sqrt{\dfrac{s}{2}(1-2\lambda^2 s)}, \\ h = \dfrac{1-\lambda^2 s+2s^2}{2s}, \end{cases} \qquad 0 < s \le \frac{1}{2\lambda^2}; \tag{8.1}$$

(2) the cusp of the surface Π_1 between its intersections with the curve δ_3 (i.e., between the points that are the images of the class π_{31} of rank-0 degenerate points turning into the points B_3 on the

key sets):

$$\Delta_1: \quad \ell = \pm\frac{2}{3\sqrt{3}}\left(h - \frac{\lambda^2}{2}\right)^{3/2}, \quad \frac{\lambda^2}{2} \le h \le h_C(\lambda), \tag{8.2}$$

where the function $h_C(\lambda)$ is determined by (4.6);

(3) the cusp of the surface Π_3 within the following limits:

$$\Delta_3: \quad \ell = \pm\sqrt{\frac{h-h^*}{2}}, \qquad h \in \begin{cases} [h^*, +\infty) & \text{for } \lambda \le \lambda^*, \\ [h_{**}, +\infty) & \text{for } \lambda > \lambda^*, \end{cases} \tag{8.3}$$

where

$$h^* = \frac{\lambda^{2/3}}{2}\left(3 - \lambda^{4/3}\right),$$

$$h^{**} = \frac{1}{4}\left[\left(4 + \lambda^{4/3}\right)^{3/2} - \lambda^{2/3}\left(6 + \lambda^{4/3}\right)\right]$$

$$= \frac{1}{16}\left(\sqrt{4+\lambda^{4/3}} - \lambda^{2/3}\right)\left[\left(\sqrt{4+\lambda^{4/3}} - \lambda^{2/3}\right)^2 + 12\right].$$

Definition 13. The Smale–Fomenko diagram $\mathcal{S}'_{LH}$ is the union of $\mathcal{S}_{LH}$ with the image of the set of rank-1 degenerate points under the mapping $L\times H$.

Such diagrams were first considered by A. A. Oshemkov [23] for classical problems of rigid-body dynamics.

Since the set of intersection points of the curves Δ_i with the principal diagram consists of rank-0 degenerate points, its transformations with respect to λ are already taken into account. To classify extended diagrams, we need to consider the values of λ corresponding to surgeries of $\Delta_0 \cup \Delta_1 \cup \Delta_3$. Consider the evolution of self-intersections and double crossings of these curves (there are no triple intersection, $\Delta_0 \cap \Delta_1 \cap \Delta_3 = \varnothing$). The curves Δ_1 and Δ_3 are uniquely determined by the single-valued functions $h(\ell)$ and hence do not have self-intersections. The curve Δ_0 has a self-intersection corresponding to the values

$$s_\pm = \frac{1 \pm \sqrt{1-8\lambda^4}}{4\lambda^2}, \quad h = \frac{1-\lambda^4}{2\lambda^2}, \quad \ell = \pm\frac{\lambda}{\sqrt{2}}, \tag{8.4}$$

where $s_\pm$ belong to the interval $(0; 1/2\lambda^2)$ (if they exist, i.e., if $\lambda \le \lambda_* = 1/2^{3/4}$).

We represent the condition of intersection $\Delta_0 \cap \Delta_3$ in the form

$$2s(h - h^* - 2\ell^2) = 0,$$

where h and ℓ are defined by (8.1). Performing the substitution $Z = \lambda^{2/3}s$, we arrive at the equation $(Z+1)(2Z-1)^2 = 0$ whose unique positive root $Z = 1/2$ is double; so we obtain a tangent point with the coordinates

$$h = \frac{1}{2}\left[\lambda^{-2/3} + 2\lambda^{2/3} - \lambda^2\right], \quad \ell = \pm\frac{1}{2}\sqrt{\lambda^{-2/3} - \lambda^{2/3}}; \tag{8.5}$$

this point exists if $\lambda \le 1$. Since $1 < \lambda^*$, we must verify that $h \ge h^*$ at the point found. For $\lambda \le 1$ and h determined by (8.5) we have

$$h - h^* = \frac{1-\lambda^{4/3}}{2\lambda^{2/3}} \ge 0.$$

It is easy to see that the points (8.5) are the images of rank-0 degenerate points corresponding to the curve π_{21} (see Proposition 3).

We represent the condition of intersection $\Delta_0 \cap \Delta_1$ as follows:

$$2s^3\left[4\left(h - \frac{\lambda^2}{2}\right)^3 - 27\ell^2\right] = 0,$$

where h and ℓ are determined by (8.1). We have

$$\big(8s^2 - 2\lambda^2 s + 1\big)\big(s^2 - 2\lambda^2 s + 1\big)^2 = 0. \tag{8.6}$$

The roots of the first factor are

$$s = \frac{1}{8}\left[\lambda^2 \pm \sqrt{\lambda^4 - 8}\right];$$

then we have

$$\lambda^2 = -\frac{1}{128}\left[\lambda^2 \pm \sqrt{\lambda^4 - 8}\right]^3 < 0,$$

i.e., these solutions are extraneous. The second factor in (8.6) yields a tangent point and provides a positive root

$$s = \sqrt{\lambda^4 + 1} - \lambda^2,$$

for which the points

$$h = \frac{3}{2}\sqrt{\lambda^4 + 1} - \lambda^2, \quad \ell = \pm\sqrt{\frac{1}{2}\left(\sqrt{\lambda^4 + 1} - \lambda^2\right)^3}$$

exist for all λ; they are the images of rank-0 degenerate points corresponding to the curve π_{22} (see Proposition 5).

Consider the intersection $\Delta_1 \cap \Delta_3$. The system (8.2), (8.3) without restrictions has three solutions

$$h = \frac{1}{2}\left(3\lambda^{2/3} + \lambda^2\right), \quad \ell^2 = \frac{\lambda^2}{2}; \tag{8.7}$$

$$\begin{cases} h = \dfrac{1}{4}\left(-3\lambda^{2/3} + 2\lambda^2 + 3\sqrt{3(2 - \lambda^{4/3})}\right), \\ \ell^2 = \dfrac{1}{8}\left(-9\lambda^{2/3} + 4\lambda^2 + 3\sqrt{3(2 - \lambda^{4/3})}\right); \end{cases} \tag{8.8}$$

$$\begin{cases} h = \dfrac{1}{4}\left(-3\lambda^{2/3} + 2\lambda^2 - 3\sqrt{3(2 - \lambda^{4/3})}\right), \\ \ell^2 = \dfrac{1}{8}\left(-9\lambda^{2/3} + 4\lambda^2 - 3\sqrt{3(2 - \lambda^{4/3})}\right). \end{cases} \tag{8.9}$$

The pair of points (8.7) always exists. Obviously, at these points

$$h - h^* = \lambda^2 > 0, \quad h - h^{**} = \frac{1}{4}\big(4 + \lambda^{4/3}\big)\left[3\lambda^{2/3} - \sqrt{4 + \lambda^{4/3}}\right].$$

The last difference must be positive for $\lambda > \lambda^*$, but it is negative only if $\lambda < 1/2^{3/4} = \lambda_* < \lambda^*$. Therefore, these point satisfy all constraints. Note that, in accordance with (8.4), these points lie on the the same levels of ℓ as self-intersection points of the curve Δ_0 (if the latter exist).

At the points (8.9), under the realness condition $\lambda < 2^{4/3}$, the value of ℓ^2 is negative, so this solution is extraneous.

Consider the solution (8.8) for all real $\lambda < 2^{4/3}$. Let us verify the conditions for h on the curve Δ_1. Excluding x from (4.6) and setting $h = h_C$ in (8.8), we obtain the equation

$$1 + 48\lambda^{4/3} + 12\lambda^{8/3} - 8\lambda^4 - 6\sqrt{3(2 - \lambda^{4/3})}\big(\lambda^{2/3} + 4\lambda^2\big) = 0. \tag{8.10}$$

By the substitution $X = \lambda^{4/3}$ we reduce it to the equation

$$(2X - 1)^3\big(2X - 1 - 3\cdot 2^{1/3} + 3\cdot 2^{2/3}\big)\left[\left(2X + \frac{3}{2^{2/3}} - \frac{3}{2^{1/3}} - 1\right)^2 + \frac{27}{2^{2/3}}\left(1 + \frac{1}{2^{2/3}} + 2^{2/3}\right)\right] = 0.$$

We see that (8.10) has exactly two positive roots: a triple root $\lambda = \lambda_*$ and a simple root

$$\lambda_3 = \left(\frac{45}{2^{1/3}} - \frac{99}{4\cdot 2^{2/3}} - \frac{161}{8}\right)^{1/4} \approx 0.0287, \quad \lambda_1 < \lambda_3 < \lambda_*. \tag{8.11}$$

The condition $h < h_C$ holds for $\lambda > \lambda_3$. The root $\lambda = \lambda*$ is irrelevant to this inequality; its appearance is related to a singular point (3.37) defined by the same equation (4.6), but with positive x. We verify the conditions for h on the curve Δ_3 at the points (8.8). We have

$$h - h^* = \frac{1}{4}\left[\lambda^2 - 9\lambda^{2/3} + 3\sqrt{3\bigl(2-\lambda^{4/3}\bigr)}\right].$$

This value is nonnegative for $\lambda < (3/2)^{3/4} \approx 1.3554$ and hence for $\lambda < \lambda^* \approx 1.2408$. Let $\lambda > \lambda^*$. Then the difference

$$h - h^{**} = \frac{1}{4}\left[3\lambda^2 + 3\lambda^{2/3} + 3\sqrt{3\bigl(2-\lambda^{4/3}\bigr)} - \bigl(4+\lambda^{4/3}\bigr)^{3/2}\right]$$

must be nonnegative. The substitution $X = \bigl(\lambda^{2/3} + \sqrt{4+\lambda^{4/3}}\bigr)^2$ reduces the condition $h \ge h^{**}$ to the inequality

$$(X-8)^3(X^3 - 12X^2 - 32) \le 0,$$

whose solution is the interval

$$X \in \bigl[8,\ 2(2+2^{2/3}+2^{4/3})\bigr];$$

then $\lambda \in [\lambda_*, \lambda_4]$, where

$$\lambda_4 = \left[\frac{1}{2}\bigl(25 - 27\cdot 2^{1/3} + 9\cdot 2^{2/3}\bigr)\right]^{1/4} \approx 1.2740. \tag{8.12}$$

Thus, a pair of intersection points of the curves Δ_1 and Δ_3 defined by Eqs. (8.8) exists for $\lambda_3 < \lambda \le \lambda_4$.

Finally, we obtain the following assertion.

Theorem 22. *In the Kovalevskaya–Yehia case, there are ten structurally stable Smale–Fomenko diagrams $\mathcal{S}'_{LH}(\lambda)$. The separating values of the parameter λ are*

$$0,\ \lambda_1,\ \lambda_3,\ \lambda_*,\ 1,\ \lambda^*,\ \lambda_4,\ \lambda_5 = 2\sqrt{\sqrt{2}-1},\ \lambda_2,\ \sqrt{2}, \tag{8.13}$$

where λ_1, λ_2, λ_3, and λ_4 are defined by Eqs. (3.55), (3.56), (8.11), *and* (8.12).

The expanded diagram

$$\Lambda(\mathcal{S}'_{LH}) = \bigcup_{\lambda} (\mathcal{S}'_{LH}(\lambda)\times\{\lambda\}$$

generates 29 *chambers in the expanded space $\mathbb{R}^3(\ell, h, \lambda)$. Moreover, the Smale chambers $\mathbb{C}$, $\mathbb{D}$, $\mathbb{F}$, and $\mathbb{H}$ have no additional partitions whereas the Smale chambers $\mathbb{A}$, $\mathbb{B}$, $\mathbb{E}$, and $\mathbb{H}$ generate the Smale–Fomenko chambers $\mathbb{A}_1$–$\mathbb{A}_{13}$, $\mathbb{B}_1$–$\mathbb{B}_3$, $\mathbb{E}_1$–$\mathbb{E}_6$, and $\mathbb{H}_1$–$\mathbb{H}_3$.*

A Smale–Fomenko diagram for small λ ($0 < \lambda < \lambda_1$) is shown in Fig. 54 (with small smooth distortions of the picture). Recall that, as is seen on the diagrams of the third critical subsystem (see, e.g., Fig. 20), the sets Δ_3 and δ_2 have two common points in the domain $\ell > 0$ for small λ, namely, the points B_3 and B_5. The curve Δ_3 passes through the cusp δ_2 of the Smale–Fomenko diagram. This is the image of the singular point B_3; it has a finite limit as $\lambda \to 0$. According to (4.20), the h-coordinate of the image of the second point B_5 tends to ∞. Therefore, a large distortion is made on the curve Δ_3 for large h in order to show the distant common point of the curves Δ_3 and δ_2 (a tangent point) and the boundary between the chambers $\mathbb{A}_8$ and $\mathbb{A}_9$.

In Figs. 55 and 56, changes related to transitions through $\lambda = \lambda_1$ (the chambers $\mathbb{B}_3$ and $\mathbb{D}$ disappear) and through $\lambda = \lambda_3$ (the chamber $\mathbb{B}_2$ disappears) are shown. New chambers do not appear here.

Significant changes in the Smale–Fomenko diagram (as in all separating sets considered above) and in chambers occur when transitioning through the value $\lambda = \lambda_*$. At this value, the loop surrounding

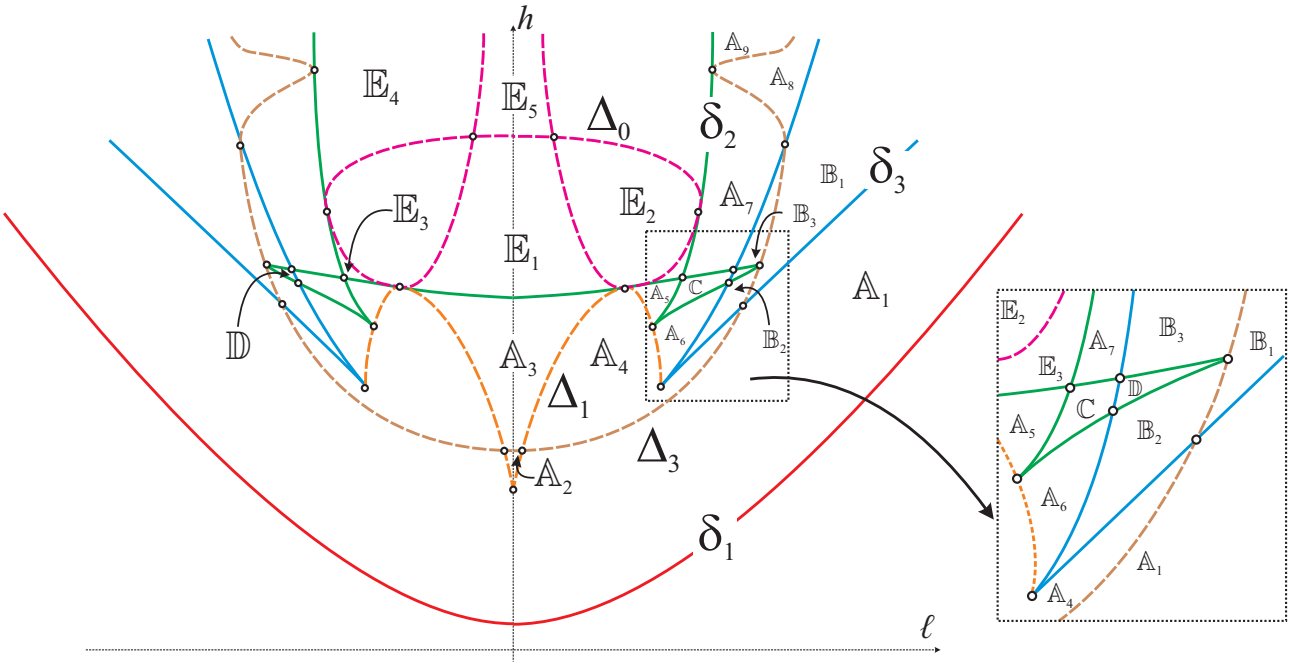

Fig. 54. Smale–Fomenko diagram for $\lambda < \lambda_1$

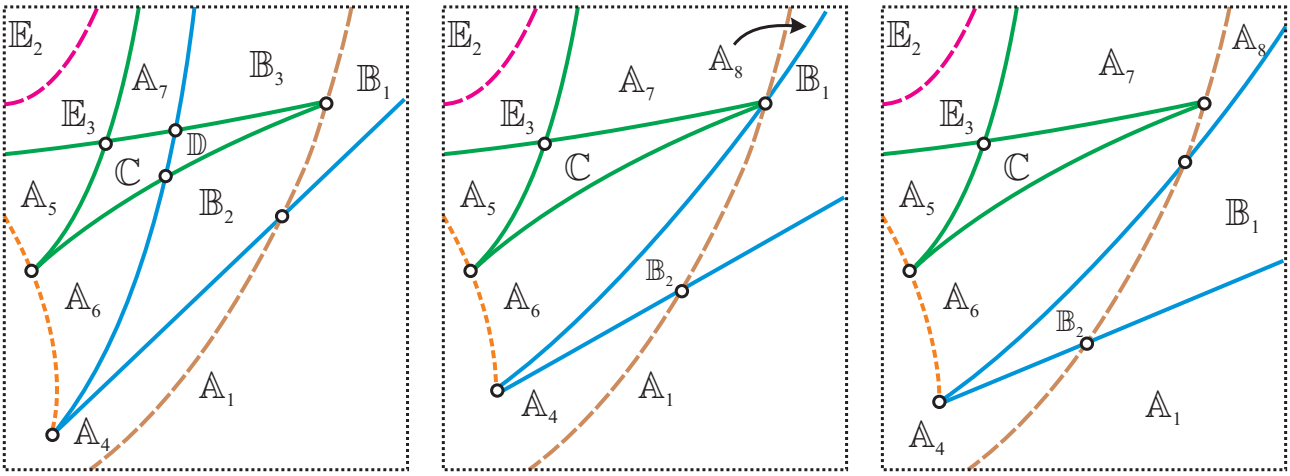

(*a*) $\lambda<\lambda_1$ (*b*) $\lambda=\lambda_1$ (*c*) $\lambda>\lambda_1$

Fig. 55. Transition through λ_1

the chamber $\mathbb{E}_2$, the chamber $\mathbb{E}_3$, the swallowtail of the curve δ_2 along with the chambers $\mathbb{A}_5$, $\mathbb{A}_6$, $\mathbb{A}_7$, and $\mathbb{C}$, and segments of the boundary of the chamber $\mathbb{A}_4$ are collapsed and then disappear. For $\lambda > \lambda_*$, a swallowtail appears again on the curve δ_2, but with other new chambers in its neighborhood, namely, the chambers $\mathbb{A}_{10}$, $\mathbb{A}_{11}$, $\mathbb{A}_{12}$, $\mathbb{A}_{13}$, $\mathbb{E}_6$, and $\mathbb{F}$. The tansition is shown in Fig. 57.

The transition through the value $\lambda = 1$ is quite simple: the common tangent point of Δ_2, Δ_0, and Δ_3 falls on the axis of symmetry $\ell = 0$ and then disappears; at the same time, the chambers $\mathbb{A}_3$ and $\mathbb{E}_1$ also disappear. The transition is shown in Fig. 58.

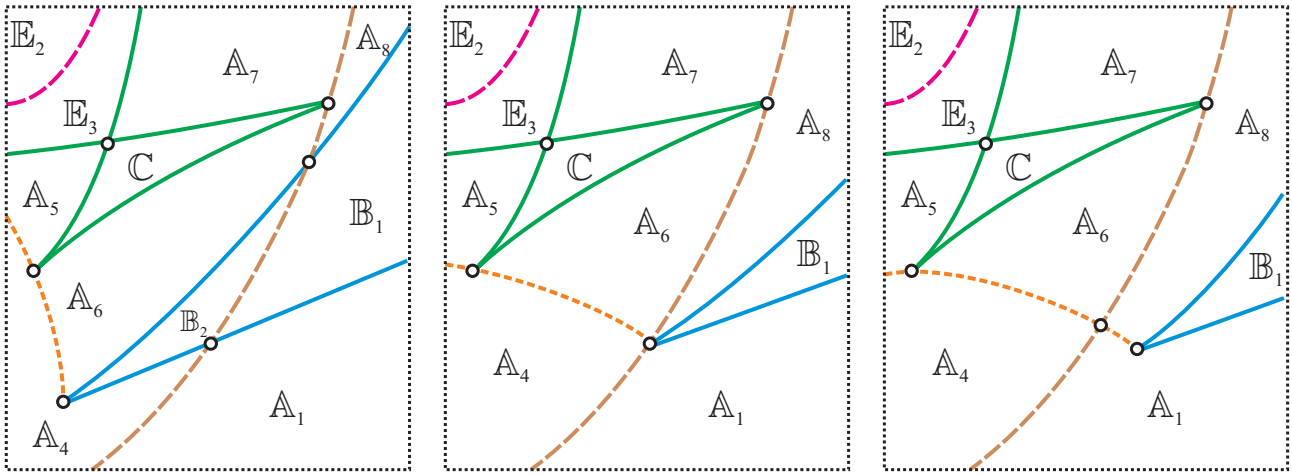

Fig. 56. Transition through λ_3

All further surgeries of the Smale–Fomenko diagrams are associated with points on the axis $\ell = 0$. The domain containing all these surgeries and the corresponding chambers is shown in Fig. 59.

The chambers $\mathbb{G}$ and $\mathbb{H}_1$ appear when transitioning through λ^*, while the chamber $\mathbb{H}_2$ appears when transitioning through λ_4. After the transition through λ_5 the chamber $\mathbb{A}_{13}$ disappears and the chamber $\mathbb{H}_3$ appears. After the transition through λ_2, the chamber $\mathbb{F}$ disappears, and after the transition through the last separating value $\sqrt{2}$, the chambers $\mathbb{G}$, $\mathbb{H}_1$, and $\mathbb{A}_2$ disappear. This information on the lifetime of chambers is presented in Table 8.1.

8.2. Fomenko graphs. For each chamber in the space $\mathbb{R}^3(\ell, h, \lambda)$ that is cut by the Smale–Fomenko diagram, we define a rough topological invariant, the Fomenko graph or the molecule $W_{\ell,h}(\lambda)$, i.e., the graph obtained by the retraction of each connected component of the integral manifold, with indication of the additional integral of the type K for each critical level and, if necessary, the orientation of the corresponding atom. Two Fomenko graphs are considered to be matching (identical) if there exists a graph homeomorphism that can be prolonged to atoms (for detail, see [8]).

All Fomenko graphs that appear in this problem on smooth isoenergetic levels $Q^3_{\ell,h}$ do not contain rank-0 critical points, and degenerate rank-1 critical points are described in [47] and are presented in Fig. 60. Here, graphs are collected in groups that are formally identical, but they cannot be converted one into another. The groups 1–6 correspond to graphs of the types W_1–W_6 found in [14]. The groups 7–9 are new. In contrast to the group 3 and the type W_3, in the groups 7 and 8 atoms B are not joined "head to head" (see [14]); in the group 9, in contrast to the graph W_7, the edge from the atom C_2 goes to the "foot," but not to the "head" of the atom B, which generates another Liouville foliation (see [14]).

Naturally, there exist coinciding Fomenko graphs even for different type of isoenergetic surfaces. To distinguish these graphs, it is necessary to apply a fine classification (see [8]). Using information on all arising chambers (see Table 8.1), we see that for most graphs, we can obtain marks directly from the analogs for the cases $\lambda = 0$ and $\ell = 0$. We note that in a similar table in [47], there is an inaccuracy: the lifetime of the chamber $\mathbb{A}_2$ is set as unlimited, although this chamber and the corresponding graph do not exist for $\lambda^2 > 2$.

Marks on graphs that have no analogs can be found by using loop molecules of nodal points of bifurcation diagrams found above. A possible representation of the result (with gluing matrices) is presented in [32]. This problem is discussed in the following section.

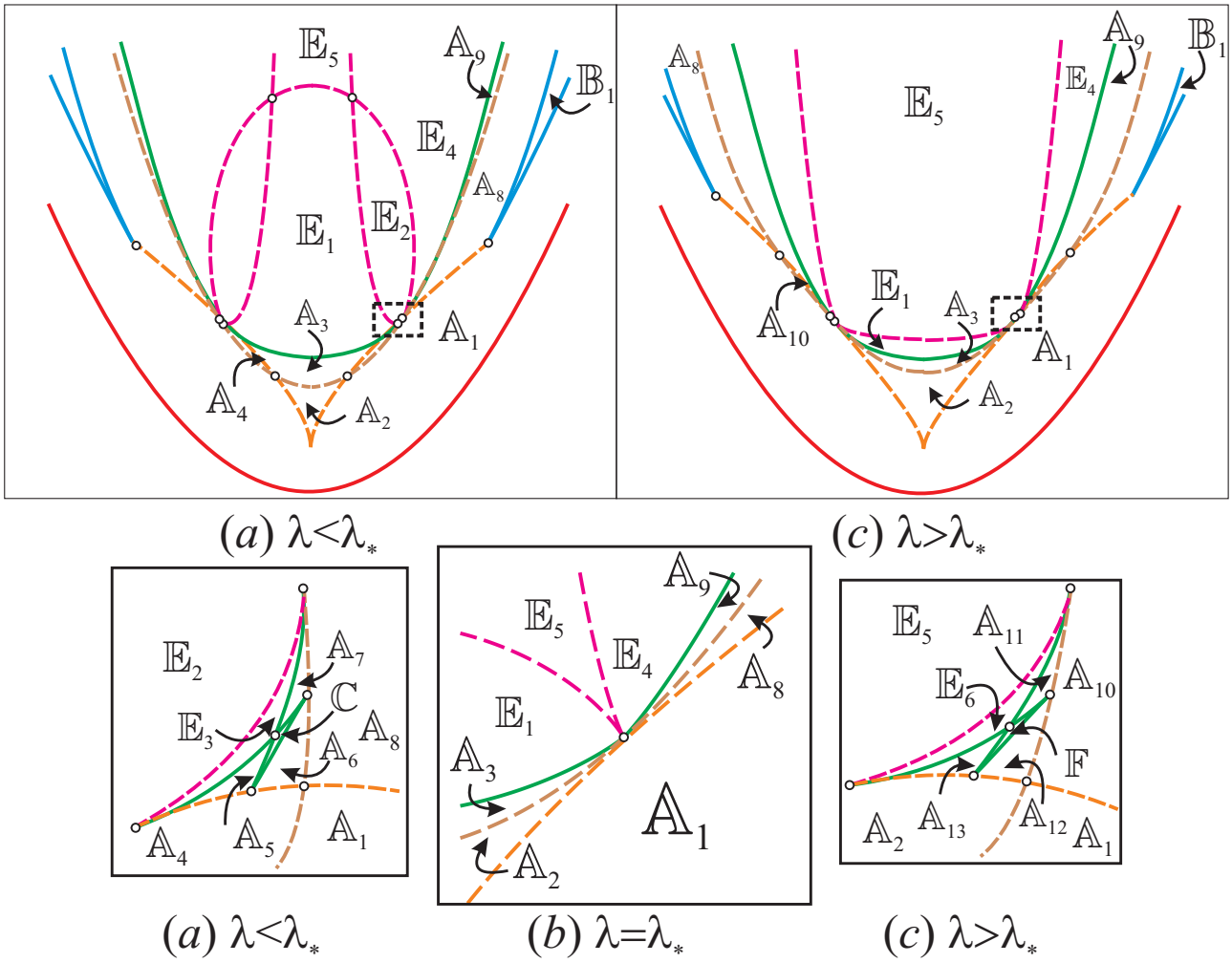

Fig. 57. Transition through λ_*

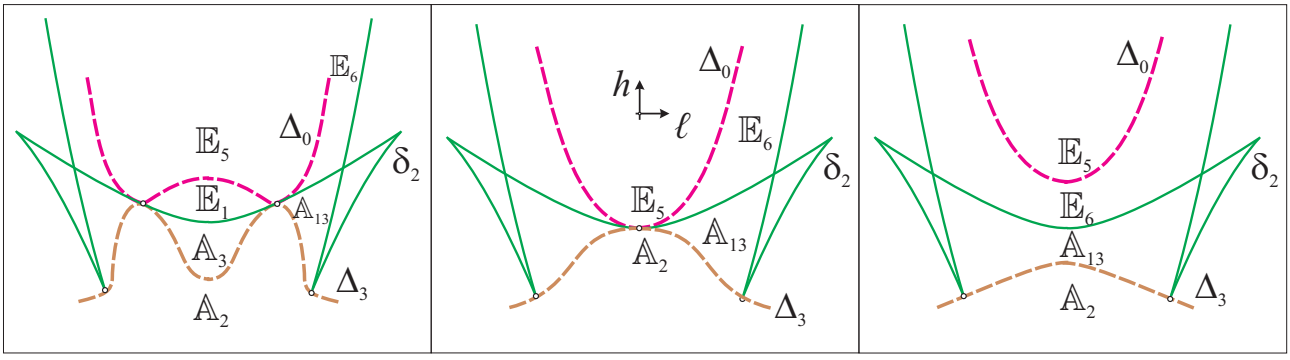

Fig. 58. Transition through $\lambda = 1$

Table 8.1

Chamber	Group of graph (number)	Lifetime on λ	Exit on $\lambda = 0/\ell = 0$	Marked molecule
$\mathbb{A}_1$	1(1)	$0 \leq \lambda < +\infty$	Yes/Yes	A [7, Table 3], [20, Table 8]
$\mathbb{A}_2$	2(2)	$0 < \lambda < \sqrt{2}$	No/Yes	B [20, Table 8]
$\mathbb{A}_3$	3(6)	$0 \leq \lambda < 1$	Yes/Yes	C [7, Table 3], [20, Table 8]
$\mathbb{A}_4$	2(3)	$0 \leq \lambda < \lambda_*$	Yes/No	B [7, Table 3]
$\mathbb{A}_5$	6(9)	$0 \leq \lambda < \lambda_*$	Yes/No	J [7, Table 3]
$\mathbb{A}_6$	7(16)	$0 < \lambda < \lambda_*$	No/No	
$\mathbb{A}_7$	6(9)	$0 < \lambda < \lambda_*$	No/No	
$\mathbb{A}_8$	2(3)	$0 < \lambda < +\infty$	No/No	
$\mathbb{A}_9$	8(20)	$0 < \lambda < +\infty$	No/No	
$\mathbb{A}_{10}$	2(2)	$\lambda > \lambda_*$	No/No	
$\mathbb{A}_{11}$	6(10)	$\lambda > \lambda_*$	No/No	
$\mathbb{A}_{12}$	7(17)	$\lambda_* < \lambda < \lambda_2$	No/No	
$\mathbb{A}_{13}$	6(11)	$\lambda_* < \lambda < \lambda_5$	No/Yes	F [20, Table. 8]
$\mathbb{B}_1$	2(4)	$0 \leq \lambda < +\infty$	Yes/No	F [7, Table 3]
$\mathbb{B}_2$	7(18)	$0 < \lambda < \lambda_3$	No/No	
$\mathbb{B}_3$	6(15)	$0 \leq \lambda < \lambda_1$	Yes/No	G [7, Table 3]
$\mathbb{C}$	6(12)	$0 < \lambda < \lambda_*$	No/No	
$\mathbb{D}$	6(13)	$0 \leq \lambda < \lambda_1$	Yes/No	I [7, Table 3]
$\mathbb{E}_1$	5(8)	$0 \leq \lambda < 1$	Yes/Yes	D [7, Table 3], [20, Table 8]
$\mathbb{E}_2$	4(7)	$0 \leq \lambda < \lambda_*$	Yes/No	E [7, Table 3]
$\mathbb{E}_3$	6(9)	$0 \leq \lambda < \lambda_*$	Yes/No	H [7, Table 3]
$\mathbb{E}_4$	8(21)	$0 < \lambda < +\infty$	No/No	
$\mathbb{E}_5$	9(22)	$0 < \lambda < +\infty$	No/Yes	E [20, Table 8]
$\mathbb{E}_6$	6(11)	$\lambda_* < \lambda < +\infty$	No/Yes	G [20, Table 8]
$\mathbb{F}$	6(10)	$\lambda_* < \lambda < \lambda_2$	No/No	
$\mathbb{G}$	6(14)	$\lambda^* < \lambda < \sqrt{2}$	No/Yes	H [20, Table 8]
$\mathbb{H}_1$	7(19)	$\lambda^* < \lambda < \sqrt{2}$	No/No	
$\mathbb{H}_2$	2(5)	$\lambda_4 < \lambda < +\infty$	No/Yes	J [20, Table 8]
$\mathbb{H}_3$	6(14)	$\lambda_5 < \lambda < +\infty$	No/Yes	I [20, Table 8]

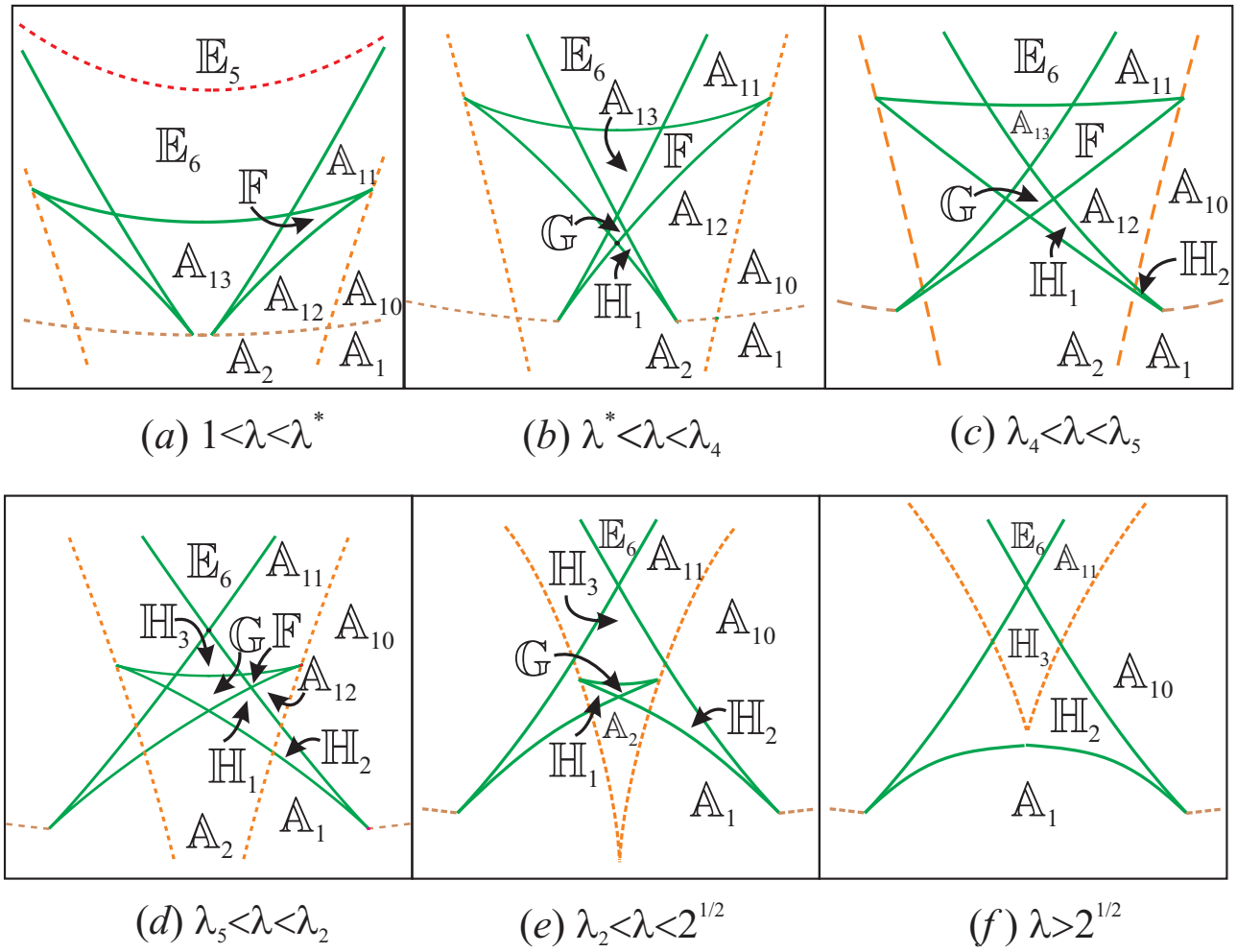

Fig. 59. Surgeries at large values of λ

Now we illustrate the operation of the "constructor" of Fomenko graphs by examples. We consider the Smale–Fomenko diagrams for average values λ (we take $\lambda = 0.8$). Let $h = 2.5$ (Fig. 61). If ℓ increases from zero, this level crosses five chambers $\mathbb{E}_5$, $\mathbb{E}_4$, $\mathbb{A}_9$, $\mathbb{A}_8$, $\mathbb{A}_1$ (the paths $\lambda = \text{const}$ on Fig. 61 are marked by the numbers $1, \dots, 5$). In the corresponding h-section of the diagram $\Sigma(\lambda)$, Fomenko graphs are determined by the bifurcations along the lines $\ell = \text{const}$ for increasing k (five broken arrows in Fig. 62). Another eight chambers can be observed on the same level of h at small values of λ. The Smale–Fomenko diagram for $\lambda = 0.1$ and the level $h = 1.8$ is shown in Fig. 63. The corresponding paths $\ell = \text{const}$ on the diagram $\Sigma(\lambda)$ are shown in Fig. 64. The crossed arcs correspond to domains determined by the diagrams of critical subsystems. The sequences of these intersections and the corresponding atoms for paths marked by the numbers $1, \dots, 13$ are shown in Table 8.2.

The following interesting phenomenon can occur (in the study of the coincidence of Fomenko graphs, this phenomenon is usually not discussed): some groups contain graphs that differ only in a pair of atoms on the same critical level. For example, in Fig. 60, all levels containing two critical circles possess the following property of "stability": for any sufficiently small perturbation (ℓ, h), the number of circles on such critical level is invariant. However, this is not so if the critical level contains multiple points, for example, the levels $\ell = 0$ and $k = 1+(h-\lambda^2/2)$, where $h \geq \lambda^2/2$, i.e., all levels whose images lie on the singular parabola (4.4). Such a level is contained in each Fomenko graph of the form $W_{0,h}$

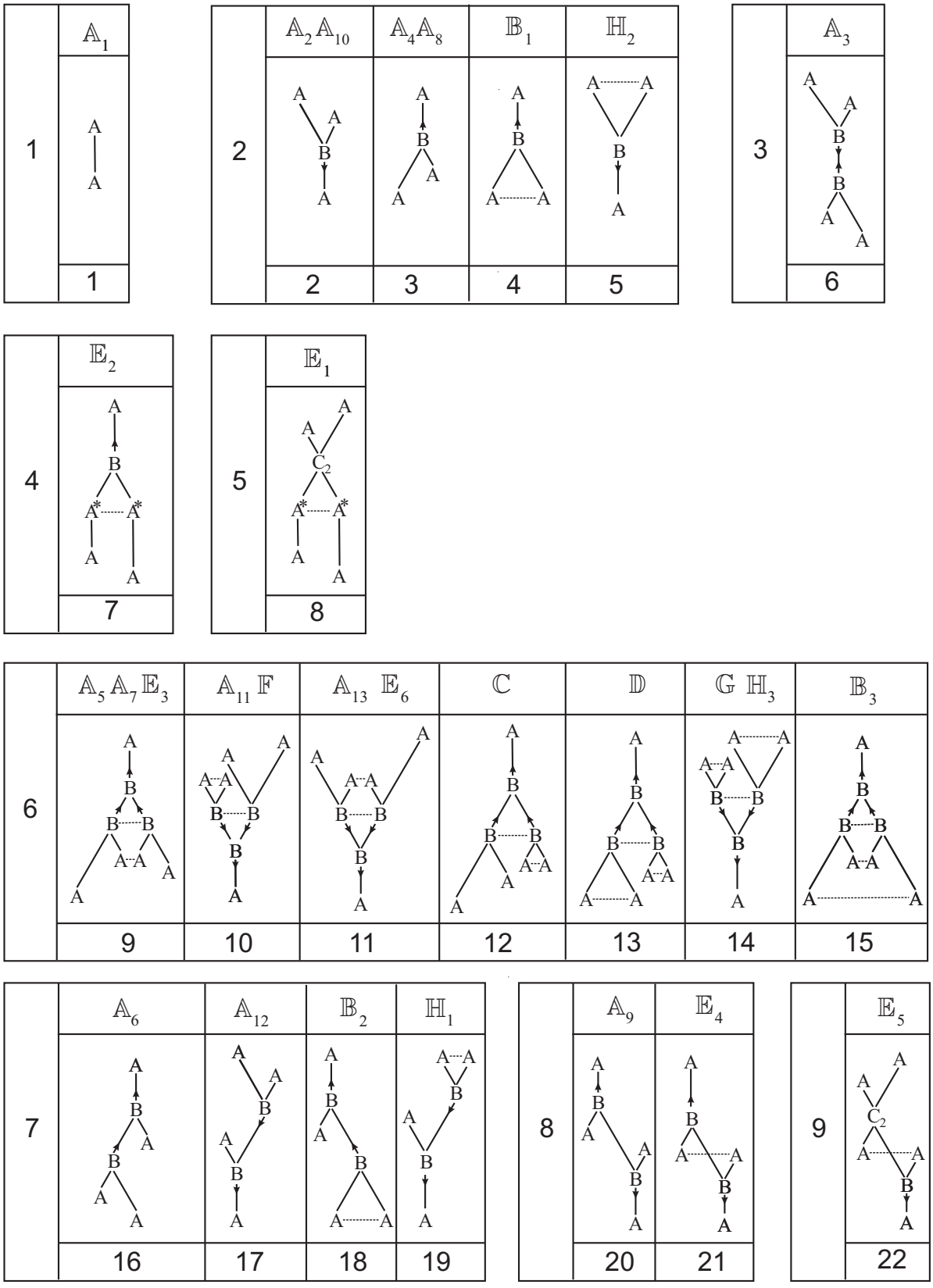

Fig. 60. Fomenko graphs

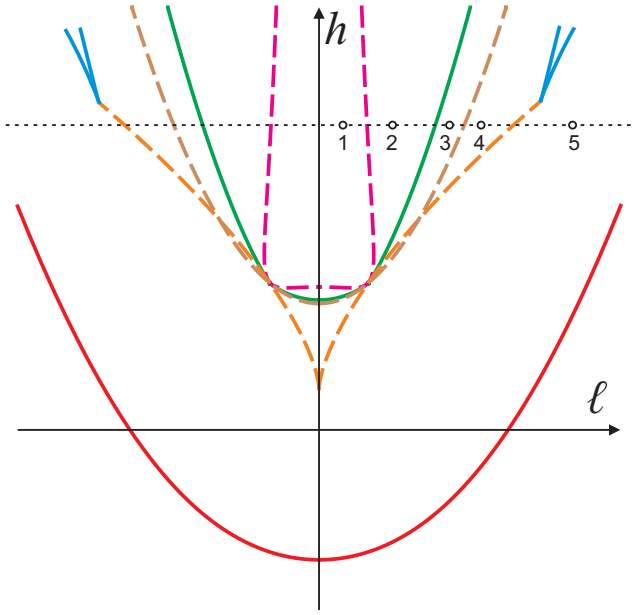

Fig. 61. Smale–Fomenko diagram for $\lambda = 0.8$

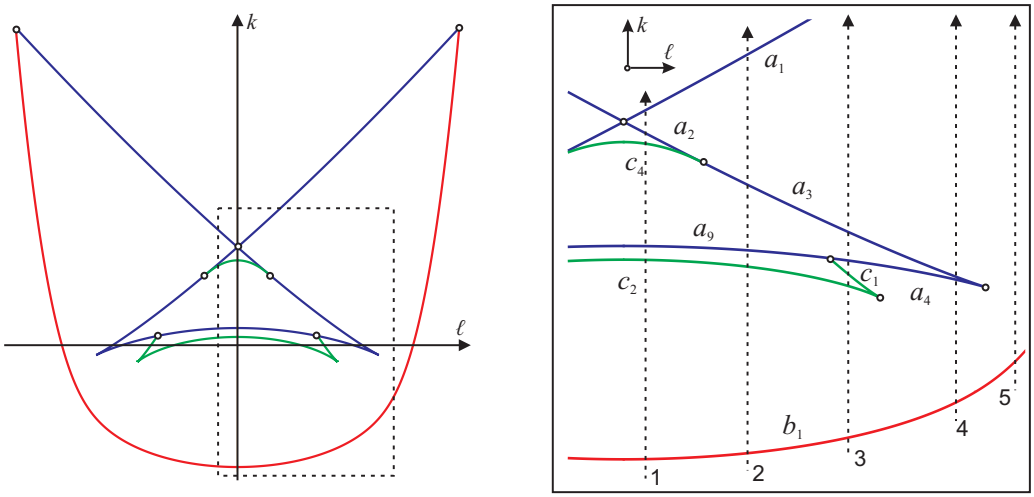

Fig. 62. Bifurcation diagram in the (ℓ, k)-plane for $\lambda = 0.8$ and $h = 2.5$

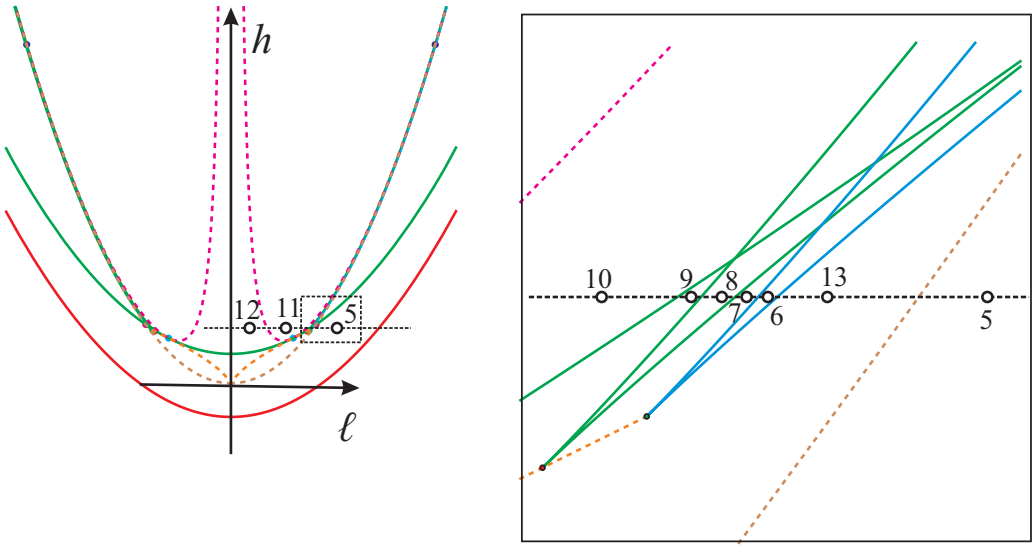

Fig. 63. Smale–Fomenko diagram for $\lambda = 0.1$

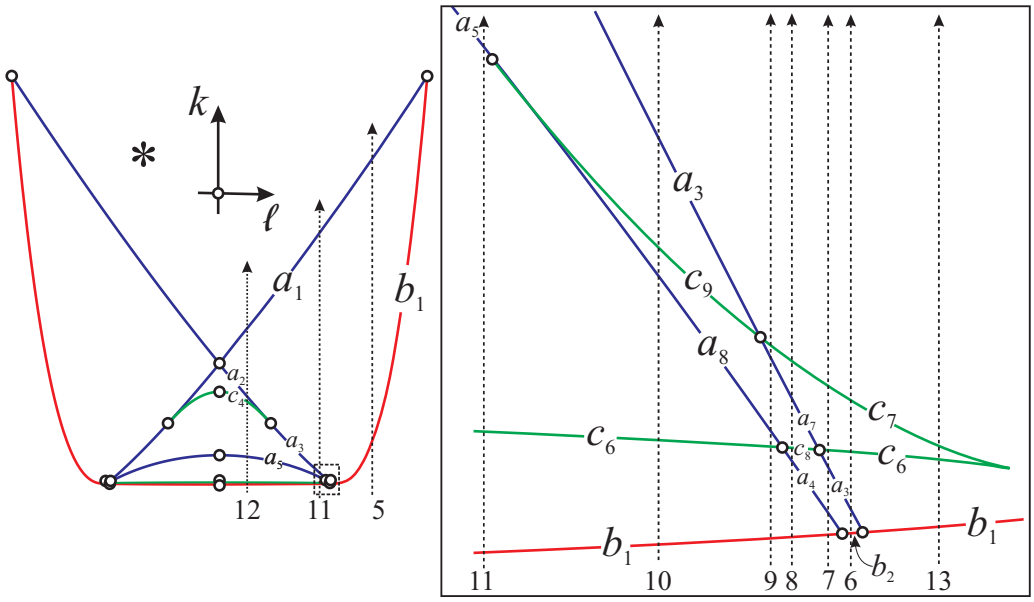

Fig. 64. Bifurcation diagram in the (ℓ, k)-plane for $\lambda = 0.1$ and $h = 1.8$

Table 8.2

Number of path	Chamber	Sequence of arcs	Sequence of atoms	Group of graph (number)
1	$\mathbb{E}_5$	$b_1 \to c_2 \to a_9 \to$ $\to c_4 \to a_2 \to a_1$	$A_+ \to B_+ \to (A_+, A_-) \to$ $\to C_2 \to A_- \to A_-$	9(22)
2	$\mathbb{E}_4$	$b_1 \to c_2 \to a_9 \to$ $\to a_3 \to a_1$	$A_+ \to B_+ \to (A_+, A_-) \to$ $\to B_- \to A_-$	8(21)
3	$\mathbb{A}_9$	$b_1 \to c_2 \to c_1 \to$ $\to a_4 \to a_3 \to a_1$	$A_+ \to B_+ \to A_- \to A_+ \to$ $\to B_- \to A_-$	8(20)
4	$\mathbb{A}_8$	$b_1 \to a_4 \to a_3 \to a_1$	$A_+ \to A_+ \to B_- \to A_-$	2(3)
5	$\mathbb{A}_1$	$b_1 \to a_1$	$A_+ \to A_-$	1(1)
6	$\mathbb{B}_2$	$b_2 \to a_3 \to c_6 \to$ $\to c_7 \to a_1$	$2A_+ \to B_- \to A_+ \to$ $\to B_- \to A_-$	7(18)
7	$\mathbb{A}_6$	$b_1 \to a_4 \to a_3 \to$ $\to c_6 \to c_7 \to a_1$	$A_+ \to A_+ \to B_- \to$ $\to A_+ \to B_- \to A_-$	7(16)
8	$\mathbb{C}$	$b_1 \to a_4 \to c_8 \to$ $\to a_7 \to c_7 \to a_1$	$A_+ \to A_+ \to 2A_+ \to 2B_- \to$ $\to B_- \to A_-$	6(12)
9	$\mathbb{A}_5$	$b_1 \to c_6 \to a_8 \to$ $\to a_7 \to c_7 \to a_1$	$A_+ \to A_+ \to 2A_+ \to 2B_- \to$ $\to B_- \to A_-$	6(9)
10	$\mathbb{E}_3$	$b_1 \to c_6 \to a_8 \to$ $\to c_9 \to a_3 \to a_1$	$A_+ \to A_+ \to 2A_+ \to 2B_- \to$ $\to B_- \to A_-$	6(9)
11	$\mathbb{E}_2$	$b_1 \to c_6 \to a_5 \to$ $\to a_3 \to a_1$	$A_+ \to A_+ \to 2A^* \to$ $\to B_- \to A_-$	4(7)
12	$\mathbb{E}_1$	$b_1 \to c_6 \to a_5 \to$ $\to c_4 \to a_2 \to a_1$	$A_+ \to A_+ \to 2A^* \to$ $\to C_2 \to A_- \to A_-$	5(8)
13	$\mathbb{A}_4$	$b_1 \to c_6 \to c_7 \to a_1$	$A_+ \to A_+ \to B_- \to A_-$	2(3)

Table 8.3

Chamber	Sequence of arcs	Sequence of atoms	Group of graph (number)
$\mathbb{A}_1(f_1)$	$b_1 \to a_1$	$A_+ \to A_-$	1(1)
$\mathbb{A}_2(f_2)$	$b_1 \to a_6 \to a_2 \to a_1$	$A_+ \to B_+ \to A_- \to A_-$	2(2)
$\mathbb{A}_3(f_3)$	$b_1 \to c_6 \to c_7 \to$ $\to a_6 \to a_2 \to a_1$	$A_+ \to A_+ \to B_- \to$ $\to B_+ \to A_- \to A_-$	3(6)
$\mathbb{A}_4(f_4)$	$b_1 \to c_6 \to c_7 \to a_1$	$A_+ \to A_+ \to B_- \to A_-$	2(3)
$\mathbb{A}_5(f_5)$	$b_1 \to c_6 \to a_8 \to$ $\to a_7 \to c_7 \to a_1$	$A_+ \to A_+ \to 2A_+ \to$ $\to 2B_- \to B_- \to A_-$	6(9)
$\mathbb{A}_6(f_6)$	$b_1 \to a_4 \to a_3 \to$ $\to c_6 \to c_7 \to a_1$	$A_+ \to A_+ \to B_- \to$ $\to A_+ \to B_- \to A_-$	7(16)
$\mathbb{A}_7(f_7)$	$b_1 \to a_4 \to c_8 \to$ $\to c_9 \to a_3 \to a_1$	$A_+ \to A_+ \to 2A_+ \to$ $\to 2B_- \to B_- \to A_-$	6(9)
$\mathbb{A}_8(f_8)$	$b_1 \to a_4 \to a_3 \to a_1$	$A_+ \to A_+ \to B_- \to A_-$	2(3)
$\mathbb{A}_9(f_9)$	$b_1 \to c_2 \to c_1 \to$ $\to a_4 \to a_3 \to a_1$	$A_+ \to B_+ \to A_- \to$ $\to A_+ \to B_- \to A_-$	8(20)
$\mathbb{A}_{10}(f_{10})$	$b_1 \to c_2 \to c_1 \to a_1$	$A_+ \to B_+ \to A_- \to A_-$	2(2)
$\mathbb{A}_{11}(f_{11})$	$b_1 \to c_2 \to a_{11} \to$ $\to a_{10} \to c_1 \to a_1$	$A_+ \to B_+ \to 2B_+ \to$ $\to 2A_- \to A_- \to A_-$	6(10)
$\mathbb{A}_{12}(f_{12})$	$b_1 \to a_6 \to a_2 \to$ $\to c_2 \to c_1 \to a_1$	$A_+ \to B_+ \to A_- \to$ $\to B_+ \to A_- \to A_-$	7(17)
$\mathbb{A}_{13}(f_{13})$	$b_1 \to a_6 \to c_5 \to$ $\to c_3 \to a_2 \to a_1$	$A_+ \to B_+ \to 2B_+ \to$ $\to 2A_- \to A_- \to A_-$	6(11)
$\mathbb{B}_1(f_{14})$	$b_2 \to a_3 \to a_1$	$2A_+ \to B_- \to A_-$	2(4)
$\mathbb{B}_2(f_{15})$	$b_2 \to a_3 \to c_6 \to$ $\to c_7 \to a_1$	$2A_+ \to B_- \to A_+ \to$ $\to B_- \to A_-$	7(18)
$\mathbb{B}_3(f_{16})$	$b_2 \to c_8 \to c_9 \to$ $\to a_3 \to a_1$	$2A_+ \to 2A_+ \to 2B_- \to$ $\to B_- \to A_-$	6(15)
$\mathbb{C}(f_{17})$	$b_1 \to a_4 \to c_8 \to$ $\to a_7 \to c_7 \to a_1$	$A_+ \to A_+ \to 2A_+ \to$ $\to 2B_- \to B_- \to A_-$	6(12)
$\mathbb{D}(f_{18})$	$b_2 \to c_8 \to a_7 \to$ $\to c_7 \to a_1$	$2A_+ \to 2A_+ \to 2B_- \to$ $\to B_- \to A_-$	6(13)
$\mathbb{E}_1(f_{19})$	$b_1 \to c_6 \to a_5 \to$ $\to c_4 \to a_2 \to a_1$	$A_+ \to A_+ \to 2A^* \to$ $\to C_2 \to A_- \to A_-$	5(8)
$\mathbb{E}_2(f_{20})$	$b_1 \to c_6 \to a_5 \to$ $\to a_3 \to a_1$	$A_+ \to A_+ \to 2A^* \to$ $\to B_- \to A_-$	4(7)
$\mathbb{E}_3(f_{21})$	$b_1 \to c_6 \to a_8 \to$ $\to c_9 \to a_3 \to a_1$	$A_+ \to A_+ \to 2A_+ \to$ $\to 2B_- \to B_- \to A_-$	6(9)
$\mathbb{E}_4(f_{22})$	$b_1 \to c_2 \to a_9 \to$ $\to a_3 \to a_1$	$A_+ \to B_+ \to (A_+, A_-) \to$ $\to B_- \to A_-$	8(21)
$\mathbb{E}_5(f_{23})$	$b_1 \to c_2 \to a_9 \to$ $\to c_4 \to a_2 \to a_1$	$A_+ \to B_+ \to (A_+, A_-) \to$ $\to C_2 \to A_- \to A_-$	9(22)
$\mathbb{E}_6(f_{24})$	$b_1 \to c_2 \to a_{11} \to$ $\to c_3 \to a_2 \to a_1$	$A_+ \to B_+ \to 2B_+ \to$ $\to 2A_- \to A_- \to A_-$	6(11)

Table 8.3 (continued)

Chamber	Sequence of arcs	Sequence of atoms	Group of graph (number)
$\mathbb{F}(f_{25})$	$b_1 \to a_6 \to c_5 \to$ $\to a_{10} \to c_1 \to a_1$	$A_+ \to B_+ \to 2B_+ \to$ $\to 2A_- \to A_- \to A_-$	6(10)
$\mathbb{G}(f_{26})$	$b_1 \to a_6 \to c_5 \to$ $\to a_{10} \to a_{12}$	$A_+ \to B_+ \to 2B_+ \to$ $\to 2A_- \to A_-$	6(14)
$\mathbb{H}_1(f_{27})$	$b_1 \to a_6 \to a_2 \to$ $\to c_2 \to a_{12}$	$A_+ \to B_+ \to A_- \to$ $\to B_+ \to 2A_-$	7(19)
$\mathbb{H}_2(f_{28})$	$b_1 \to c_2 \to a_{12}$	$A_+ \to B_+ \to 2A_-$	2(5)
$\mathbb{H}_3(f_{29})$	$b_1 \to c_2 \to a_{11} \to$ $\to a_{10} \to a_{12}$	$A_+ \to B_+ \to 2B_+ \to$ $\to 2A_- \to A_-$	6(14)

with $h > \lambda^2/2$ (recall that the boundary value $h = \lambda^2/2$ determines an isoenergetic manifold with a degenerate point; we do not consider this case in the present paper). It is easy to see that under a small perturbation of the zero level of ℓ within the chamber, the instable level splits into two levels and its atoms diverge. This phenomenon occurs in all chambers that have an exit on the axis $\ell = 0$ for $h > \lambda^2/2$. Unstable (in the above sense) Fomenko graphs are presented in Fig. 65, where the mark of the chamber equipped with the index 0 means the intersection of the chamber with the axis $\ell = 0$.

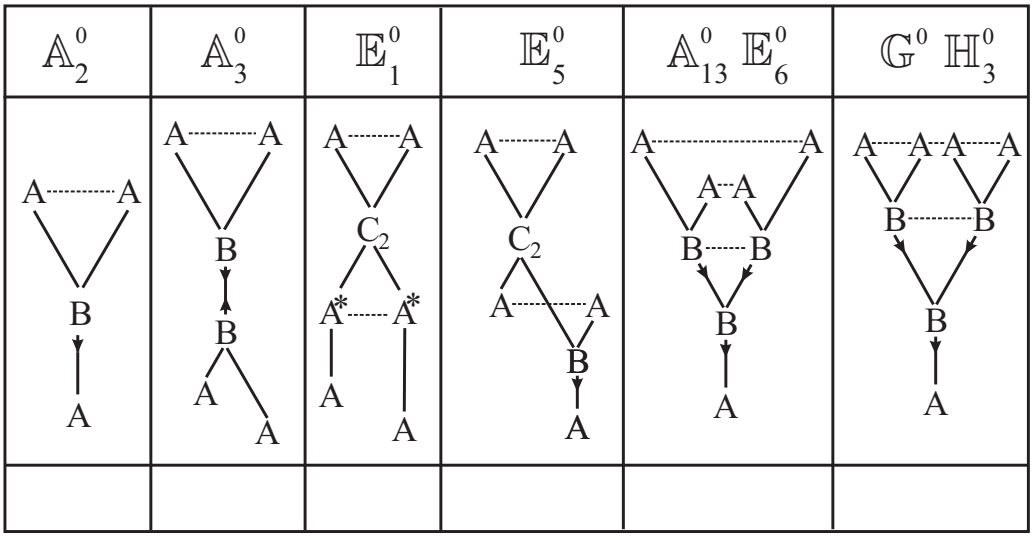

Fig. 65. Unstable Fomenko graphs

8.3. Fomenko–Zieschang invariants. To complete the description of topological invariants of isoenergetic levels of reduced systems, we must equip the Fomenko graphs found above with marks.

First, we write all transitions between atoms that can occur in Fomenko graphs into a table (see Table 8.4). Of course, here we mean atoms in which a wall of the bifurcation diagram (or, which is the same, a domain of the corresponding critical subsystem) is indicated. For each transition, we indicate all graphs in which this transition occurs. If at least one of these graphs is preserved in the limit cases $\lambda = 0$ and $\ell = 0$, we note this fact in the corresponding column of the table and then take r- and ε-marks from the results of [7] or [20], respectively. Missing marks are taken from loop molecules listed in the corresponding column of the table. In this case, necessary comments are given below.

Table 8.4

Number of edges	Edge	(r, ε)-labels	Graphs	Exit on $\lambda = 0/\ell = 0$	Loop molecule
1	$(A_{[b_1]}; A_{[a_1]})$	$r = 0$, $\varepsilon = 1$	$\mathbb{A}_1$	Yes/Yes	
2	$(A_{[b_1]}; B_{[a_6]})$	$r = 0$, $\varepsilon = 1$	$\mathbb{A}_2$, $\mathbb{A}_{12}$, $\mathbb{A}_{13}$, $\mathbb{F}$, $\mathbb{G}$, $\mathbb{H}_1$	No/Yes	
3	$(B_{[a_6]}; A_{[a_2]})$	$r = 0$, $\varepsilon = 1$	$\mathbb{A}_2$, $\mathbb{A}_3$, $\mathbb{A}_{12}$, $\mathbb{H}_1$	Yes/Yes	
4	$(B_{[a_6]}; A_{[a_1]})$	$r = 0$, $\varepsilon = 1$	$\mathbb{A}_2$, $\mathbb{A}_3$	Yes/Yes	
5	$(A_{[b_1]}; B_{[c_2]})$	$r = 0$, $\varepsilon = 1$	$\mathbb{A}_9$, $\mathbb{A}_{10}$, $\mathbb{A}_{11}$, $\mathbb{E}_4$, $\mathbb{E}_5$, $\mathbb{E}_6$, $\mathbb{H}_2$, $\mathbb{H}_3$	No/Yes	
6	$(B_{[c_2]}; A_{[c_1]})$	$r = 0$, $\varepsilon = 1$	$\mathbb{A}_9$, $\mathbb{A}_{10}$, $\mathbb{A}_{12}$	No/No	Δ_{31}
7	$(B_{[c_2]}; A_{[a_1]})$	$r = \infty$, $\varepsilon = 1$	$\mathbb{A}_{10}$, $\mathbb{A}_{12}$	No/No	δ''_{27}
8	$(B_{[c_7]}; A_{[a_1]})$	$r = \dfrac{1}{2}$, $\varepsilon = 1$	$\mathbb{A}_4$, $\mathbb{A}_5$, $\mathbb{A}_6$, $\mathbb{B}_2$, $\mathbb{C}$, $\mathbb{D}$	Yes/No	
9	$(A_{[c_6]}; B_{[c_7]})$	$r = 0$, $\varepsilon = 1$	$\mathbb{A}_3$, $\mathbb{A}_4$, $\mathbb{B}_2$	Yes/Yes	
10	$(A_{[b_1]}; B_{[c_7]})$	$r = 0$, $\varepsilon = 1$	$\mathbb{A}_3$, $\mathbb{A}_4$	Yes/Yes	
11	$(B_{[a_3]}; A_{[a_1]})$	$r = 0$, $\varepsilon = 1$	$\mathbb{A}_7$, $\mathbb{A}_8$, $\mathbb{A}_9$, $\mathbb{B}_1$, $\mathbb{B}_3$, $\mathbb{E}_2$, $\mathbb{E}_3$, $\mathbb{E}_4$	Yes/No	
12	$(A_{[a_4]}; B_{[a_3]})$	$r = 0$, $\varepsilon = 1$	$\mathbb{A}_6$, $\mathbb{A}_8$, $\mathbb{A}_9$	No/No	Δ_{12}
13	$(A_{[b_1]}; B_{[a_3]})$	$r = \infty$, $\varepsilon = 1$	$\mathbb{A}_6$, $\mathbb{A}_8$	No/No	δ_{31}
14	$(2A_{[b_2]}; B_{[a_3]})$	$r = \infty$, $\varepsilon = 1$	$\mathbb{B}_1$, $\mathbb{B}_2$	Yes/No	
15	$(B_{[c_2]}; 2A_{[a_{12}]})$	$r = \infty$, $\varepsilon = 1$	$\mathbb{H}_1$, $\mathbb{H}_2$	No/Yes	
16	$(B_{[c_7]}; B_{[a_6]})$	$r = 0$, $\varepsilon = 1$	$\mathbb{A}_3$	Yes/Yes	
17	$(2A^*_{[a_5]}; B_{[a_3]})$	$r = 0$, $\varepsilon = 1$	$\mathbb{E}_2$	Yes/No	
18	$(A_{[c_6]}; A^*_{[a_5]})$	$r = 0$, $\varepsilon = 1$	$\mathbb{E}_1$, $\mathbb{E}_2$	Yes/Yes	
19	$(A_{[b_1]}; A^*_{[a_5]})$	$r = 0$, $\varepsilon = 1$	$\mathbb{E}_1$, $\mathbb{E}_2$	Yes/Yes	
20	$(C_{2[c_4]}; A_{[a_1]})$	$r = 0$, $\varepsilon = 1$	$\mathbb{E}_1$, $\mathbb{E}_5$	Yes/Yes	
21	$(C_{2[c_4]}; A_{[a_2]})$	$r = 0$, $\varepsilon = 1$	$\mathbb{E}_1$, $\mathbb{E}_5$	Yes/Yes	
22	$(2A^*_{[a_5]}; C_{2[c_4]})$	$r = 0$, $\varepsilon = -1$	$\mathbb{E}_1$	Yes/Yes	
23	$(2B_{[a_7]}; B_{[c_7]})$	$r = 0$, $\varepsilon = 1$	$\mathbb{A}_5$, $\mathbb{C}$, $\mathbb{D}$	Yes/No	
24	$(A_{[a_8]}; B_{[a_7]})$	$r = 0$, $\varepsilon = 1$	$\mathbb{A}_5$	Yes/No	

Table 8.4 (continued)

Number of edges	Edge	(r, ε)-labels	Graphs	Exit on $\lambda = 0/\ell = 0$	Loop molecule
25	$(A_{[c_6]}; B_{[a_7]})$	$r = \infty$, $\varepsilon = 1$	$\mathbb{A}_5$	Yes/No	
26	$(A_{[b_1]}; B_{[a_7]})$	$r = \infty$, $\varepsilon = 1$	$\mathbb{A}_5$, $\mathbb{C}$	Yes/No	
27	$(2B_{[c_9]}; B_{[a_3]})$	$r = 0$, $\varepsilon = -1$	$\mathbb{A}_7$, $\mathbb{B}_3$, $\mathbb{E}_3$	Yes/No	
28	$(2A_{[c_8]}; 2B_{[c_9]})$	$r = 0$, $\varepsilon = 1$	$\mathbb{A}_7$, $\mathbb{B}_3$	Yes/No	
29	$(A_{[a_4]}; B_{[c_9]})$	$r = \frac{1}{2}$, $\varepsilon = 1$	$\mathbb{A}_7$	No/No	Δ_{03}
30	$(A_{[b_1]}; B_{[c_9]})$	$r = 0$, $\varepsilon = 1$	$\mathbb{A}_7$, $\mathbb{E}_3$	Yes/No	
31	$(2A_{[a_8]}; 2B_{[c_9]})$	$r = \frac{1}{2}$, $\varepsilon = 1$	$\mathbb{E}_3$	Yes/No	
32	$(A_{[c_6]}; B_{[c_9]})$	$r = 0$, $\varepsilon = 1$	$\mathbb{E}_3$	Yes/No	
33	$(B_{[a_{11}]}; A_{[a_1]})$	$r = 0$, $\varepsilon = 1$	$\mathbb{A}_{11}$, $\mathbb{E}_6$	No/Yes	
34	$(B_{[a_{11}]}; A_{[c_1]})$	$r = 0$, $\varepsilon = 1$	$\mathbb{A}_{11}$	No/No	Δ_{04}
35	$(B_{[a_{11}]}; 2A_{[a_{10}]})$	$r = 0$, $\varepsilon = 1$	$\mathbb{A}_{11}$, $\mathbb{H}_3$	No/Yes	
36	$(B_{[c_2]}; 2B_{[a_{11}]})$	$r = 0$, $\varepsilon = -1$	$\mathbb{A}_{11}$, $\mathbb{E}_6$, $\mathbb{H}_3$	No/Yes	
37	$(B_{[c_5]}; A_{[a_1]})$	$r = \infty$, $\varepsilon = 1$	$\mathbb{A}_{13}$, $\mathbb{F}$	No/Yes	
38	$(B_{[c_5]}; A_{[c_1]})$	$r = 0$, $\varepsilon = 1$	$\mathbb{F}$	No/No	Δ_{31}
39	$(B_{[c_5]}; 2A_{[a_{10}]})$	$r = \infty$, $\varepsilon = 1$	$\mathbb{G}$, $\mathbb{F}$	No/Yes	
40	$(B_{[a_6]}; 2B_{[c_5]})$	$r = 0$, $\varepsilon = 1$	$\mathbb{A}_{13}$, $\mathbb{G}$, $\mathbb{F}$	No/Yes	
41	$(B_{[c_5]}; A_{[a_2]})$	$r = \infty$, $\varepsilon = 1$	$\mathbb{A}_{13}$	No/Yes	
42	$(2B_{[c_5]}; 2A_{[a_3]})$	$r = 0$, $\varepsilon = 1$	$\mathbb{A}_{13}$	No/Yes	
43	$(B_{[a_{11}]}; A_{[a_2]})$	$r = 0$, $\varepsilon = 1$	$\mathbb{E}_6$	No/Yes	
44	$(B_{[a_{11}]}; 2A_{[c_3]})$	$r = 0$, $\varepsilon = 1$	$\mathbb{E}_6$	No/Yes	
45	$(2A_{[c_8]}; B_{[a_7]})$	$r = \infty$, $\varepsilon = 1$	$\mathbb{C}$, $\mathbb{D}$	Yes/No	
46	$(2A_{[b_2]}; B_{[a_7]})$	$r = \infty$, $\varepsilon = 1$	$\mathbb{D}$	Yes/No	
47	$(B_{[c_5]}; 2A_{[a_{12}]})$	$r = \infty$, $\varepsilon = 1$	$\mathbb{G}$	No/Yes	
48	$(B_{[a_{11}]}; 2A_{[a_{12}]})$	$r = 0$, $\varepsilon = 1$	$\mathbb{H}_3$	No/Yes	

Table 8.4 (continued)

Number of edges	Edge	(r,ε)-labels	Graphs	Exit on $\lambda=0/\ell=0$	Loop molecule
49	$(2A_{[b_2]};2B_{[c_9]})$	$r=0,\ \varepsilon=1$	$\mathbb{B}_3$	Yes/No	
50	$(B_{[c_6]};B_{[c_7]})$	$r=0,\ \varepsilon=1$	$\mathbb{A}_6$	No/No	Δ_{33}
51	$(B_{[a_3]};B_{[c_7]})$	$r=0,\ \varepsilon=1$	$\mathbb{A}_6$, $\mathbb{B}_2$	No/No	δ_{22}
52	$(B_{[a_6]};B_{[c_2]})$	$r=0,\ \varepsilon=1$	$\mathbb{A}_{12}$, $\mathbb{H}_1$	No/No	δ_{26}
53	$(B_{[c_2]};B_{[a_3]})$	$r=0,\ \varepsilon=-1$	$\mathbb{A}_9$, $\mathbb{E}_4$	No/No	$\delta_{31}+\dots$
54	$(A_{[a_9]};B_{[a_3]})$	$r=0,\ \varepsilon=1$	$\mathbb{E}_4$	No/No	$\delta_{31}+\delta_{32}$
55	$(B_{[c_2]};A_{[a_9]})$	$r=\dfrac{1}{2},\ \varepsilon=1$	$\mathbb{E}_4$, $\mathbb{E}_5$	No/Yes	
56	$(A_{[a_9]};C_{2[c_4]})$	$r=0,\ \varepsilon=1$	$\mathbb{E}_5$	No/Yes	
57	$(B_{[c_2]};C_{2[c_4]})$	$r=0,\ \varepsilon=-1$	$\mathbb{E}_5$	No/Yes	

Most of the marks on edges that are not present in the limit cases need no explanations. Thus, the edge No. 6 is explicitly present in the loop molecule of the point Δ_{31} (see Fig. 46), the edge No. 12 in the loop molecule of the point Δ_{12} (see Fig. 43), the edge No. 50 in the loop molecule of the point Δ_{33} (see Fig. 47), the edge No. 7 in the loop molecule of the point δ''_{27}, and the edge No. 13 in the loop molecule of the point δ_{31} (the last two molecules are shown in Table 6.2). The edge No. 51 is explicitly present in the loop molecule of the nondegenerate saddle point δ_{22} and the edge No. 52 in the loop molecule of the nondegenerate saddle point δ_{26} (both molecules are given in Table **??**).

Marks on some transition edges can be set immediately if we note that, in fact, these transitions are reduced to already known ones. So, consider the edge No. 54. On the diagrams $\Sigma_{HK}(\ell,\lambda)$, it joins the segments a_3 and a_9. Consider the diagram for the domain 9 (see Fig. 28). It contains the images of nondegenerate rank 0 critical points of the classes δ_{25} and δ_{32} (of the type "center-center") and δ_{31} (of the type "center-saddle"). If we slightly spread out the "double" edges (whose preimages contain the two critical circles), we obtain the picture shown in Fig. 66; then it becomes obvious that the transition discussed is actually a transition from a_3 to a part of a_9 marked by a''_9 in the figure: it is simply a prolongation of the segment a_4. Therefore, this transition coincides with the edge No. 12 whose mark has just been found. Note that in the proof of Proposition 15 (see above) this result for the transition along the edge No 12 was proved by using the addition rule for marks (Lemma 4) along two transitions $a''_9=a_4\to b''_2$ with $r=0$ from the loop molecule of the point δ_{32} and $b''_2\to a_3$ with $r=\infty$ from the loop molecule of the point δ_{31} (they are shown by broken arrows).

Similarly, we consider the edge No. 53 and, for example, find it on the diagram $\Sigma_{LK}(h,\lambda)$ for the domain 33 (see Fig. 52). As in the previous case, we spread out "double edges" (in this case, the same edges a_9 and b_2); the result is shown in Fig. 67. Obviously, the transition discussed $c_2\to a_3$ is the composition of two transitions: the transition from c_2 to the part of the chamber b_2 indicated in the figure by b'_2 (it is a prolongation of the segment b_1; this is the edge No. 5 with $r=0$) and the transition from b_1 to a_3 (the edge No. 1, which is a part of the loop molecule of the nongenerated point δ_{31} of the type "center-saddle" with the mark $r=\infty$). These two transitions are shown in the

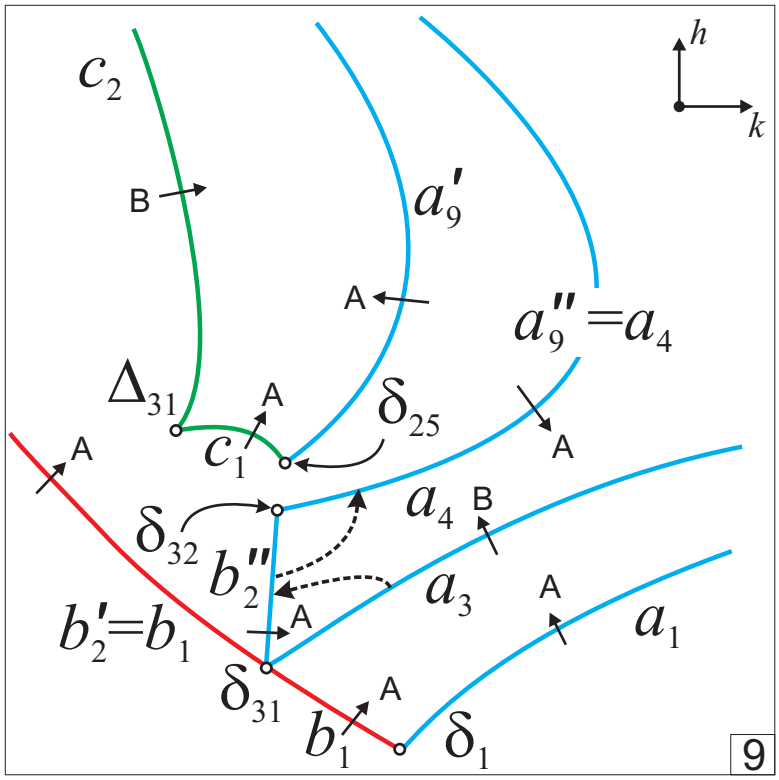

Fig. 66. Diagram $\Sigma_{HK}(\ell, \lambda)$ for the domain 9 with layers indicated

figure by broken arrows. Thus, we obtain that the r-mark on the transition discussed is equal to zero by Lemma 4.

Consider the edge No. 29. It is convenient to examine it on the diagram $\Sigma_{LK}(h, \lambda)$ for the domain 31 (see Fig. 52). Spreading out the double edges a_8 and c_9, we take into account that these edges start at a degenerate point Δ_{03}, and both edges c'_9 and c''_9 terminate at the corresponding points Δ_{32} and contain nondegenerate points of the type "center-center": δ_{24} (the end of one edge a_8, for example, a'_8) and δ_{32} (the end of the other edge a''_8, which coincides with a_4). Thus, the transition $a_4 \to c_9$ is one of the two transitions $a_8 \to c_9$, which, according to the loop molecule of the degenerated point Δ_{03} (see Fig. 39) have $r = 1/2$. The same result directly follows from the well-known mark of the "double" edge No. 31 in the graph $\mathbb{E}_3$, which exists for $\lambda = 0$ (see [7]).

Note that the analysis of the last two cases imply that $a_4 = a''_8$ and $a_4 = a''_9$. This fact is not casual: it can be clearly seen in the diagrams of the critical subsystem $\mathcal{M}_1$. For example, in Fig. 15, for small λ the domain a_4 is separated from a_8 by the curve consisting of the points δ_{24} and from a_9 by the curve consisting of the points δ_{25}. Both these curves correspond to points of the type "center-center" (so they generate a new critical circle), whereas the critical circle a_4 just passes through it without bifurcation.

On the edge No. 34, the behavior of transitions is determined by the loop molecule of the point Δ_{04} (see Figs. 40 and 41). Since the preimage of the point δ'_{28} contains a nondegenerate critical point of the type "center-center," the arc c_3 on the diagram $\Sigma_{LK}(h, \lambda)$ for the domain 24 splits into two arcs (see Fig. 52): the first arc c'_3 terminates at the point δ'_{28}, while the second can be prolonged to the arc $c''_3 = c_1$. Hence, the transition $a_{11} \to c_1$ is one of the two transitions $a_{11} \to c_3$ in the first component of the loop molecule of the point Δ_{04}, where $r = 0$.

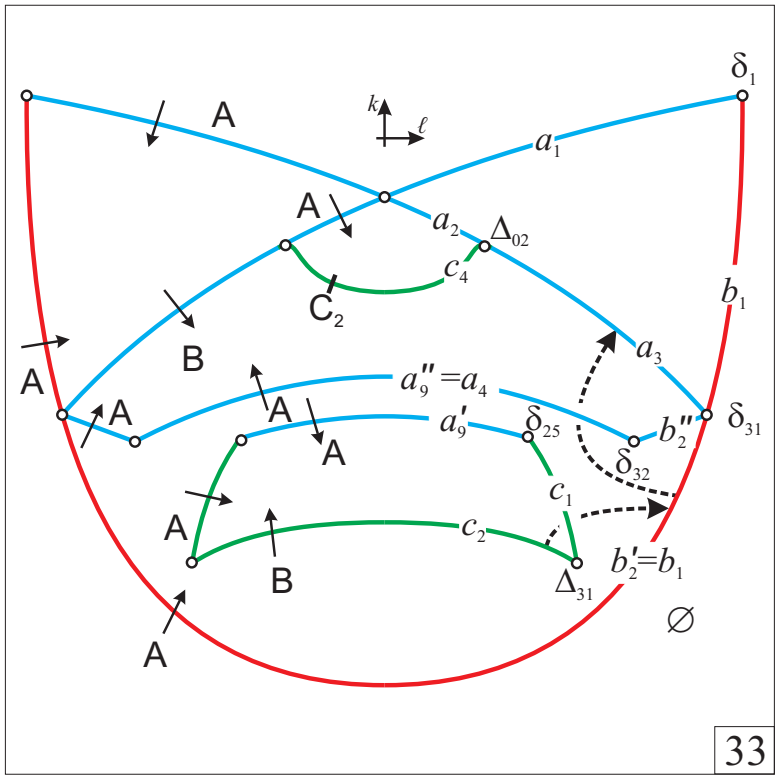

Fig. 67. Diagram $\Sigma_{LK}(h,\lambda)$ for 33 region with layers indicated

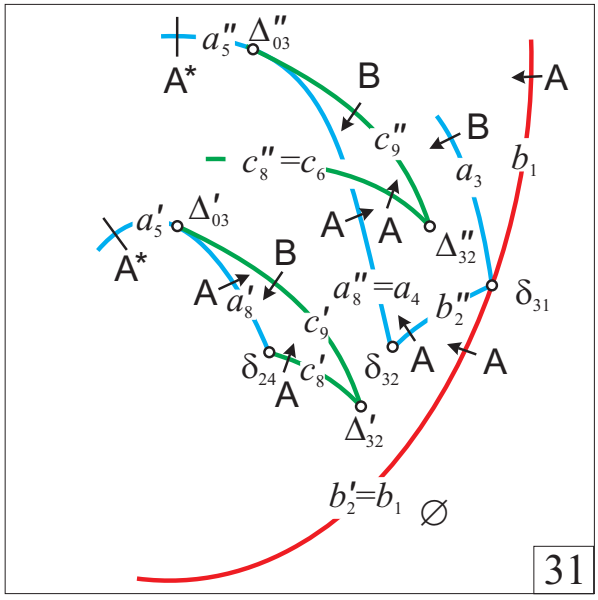

Fig. 68. Fragment of the diagram $\Sigma_{LK}(h,\lambda)$ for the domain 31 with layers indicated

Finally, another transition that has no direct analogs in the limit cases studied above is the edge No. 38. Consider the diagram $\Sigma_{LK}(h,\lambda)$ for the domain 7 (see Fig. 52) in a neighborhood of neighboring nodal points Δ_{31} and δ'_{27}. The latter point has the type "center-saddle" and attracts the part c'_5

of the double arc c_5 that terminates at this point. The transition to the arc c_1 is possible only from the arc c_5'', which, as a result, can be prolonged to c_2. Thus, the transition $c_5 \to c_1$ is the transition $c_2 \to c_1$, which is contained in the loop molecule of the point Δ_{31} (see Fig. 46). Hence, according to what was proved above, we obtain $r = 0$.

Here we have described the process of producing marks using either transitions in the special cases $\lambda = 0$ and $\ell = 0$ examined earlier, or loop molecules constructed above; for brevity, we have discussed only r-marks. In fact, the information used also contains all ε-marks. Thus, all data in Table 8.4 are completely justified.

Table 8.5 contains all Fomenko–Zieschang invariants for the Kovalevskaya–Yehia case. Each of them is supplied with the notation of the graph and the corresponding isoenergetic manifold. The complete list coincides with the list given in [32]; however, there is no correspondence between marked molecules and topological types $Q^3_{\ell,h}$ in [32] (although the notion of invariant requires such a correspondence).

After comparing invariants found (supplied with (r, ε)-marks defined above) with invariants listed in [32], we transferred all n-marks of families of hyperbolic atoms from [32]. Calculation of these marks requires considerable additional technical work. So, in [32], using one of the main procedures of the method of loop molecules, namely, the expression of all cycle bases on families of regular tori through λ-cycles of atoms of bifurcations, which are defined unambiguously (see [7]), a method of arrangement of glue matrices along edges of marked graphs is proposed. Then all n-marks of families are calculated by the corresponding definitions.

Table 8.5

Marked isoenergetic molecule	Marked isoenergetic molecule
$\mathbb{A}_1$ 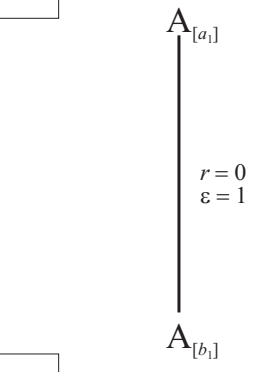 S^3	$\mathbb{A}_2$ 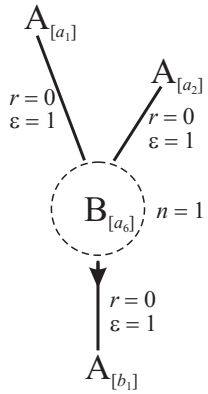 S^3

Table 8.5 (continued)

Marked isoenergetic molecule	Marked isoenergetic molecule
$\mathbb{A}_3$ 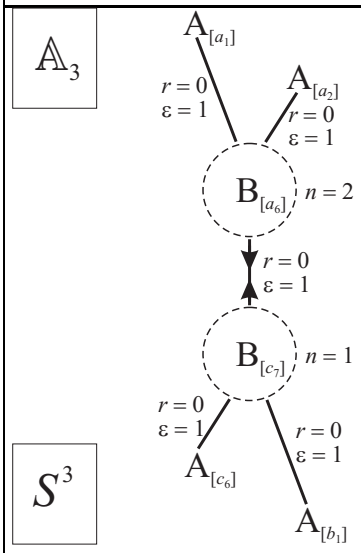 S^3	$\mathbb{A}_4$ 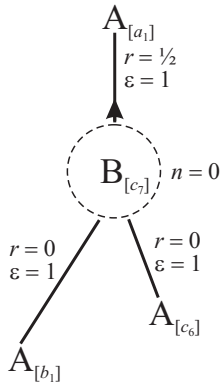 S^3
$\mathbb{A}_5$ 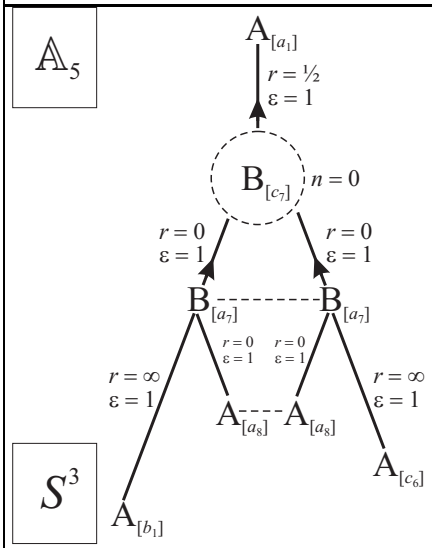 S^3	$\mathbb{A}_6$ 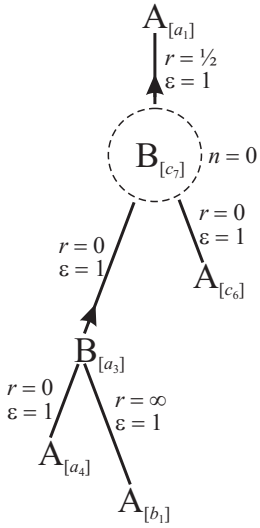 S^3

Table 8.5 (continued)

Marked isoenergetic molecule	Marked isoenergetic molecule
$\mathbb{A}_7$ 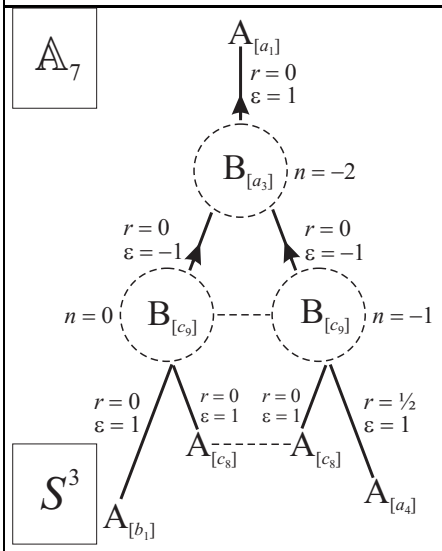 S^3	$\mathbb{A}_8$ 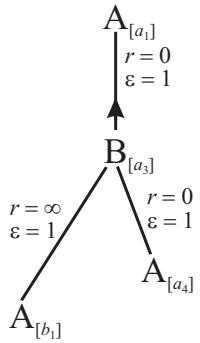 S^3
$\mathbb{A}_9$ 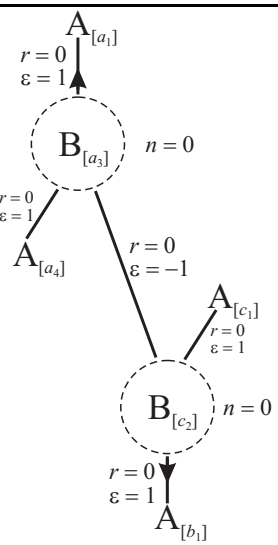 S^3	$\mathbb{A}_{10}$ 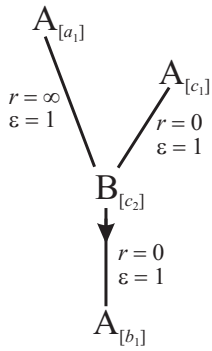 S^3

Table 8.5 (continued)

Marked isoenergetic molecule	Marked isoenergetic molecule
$\mathbb{A}_{11}$ 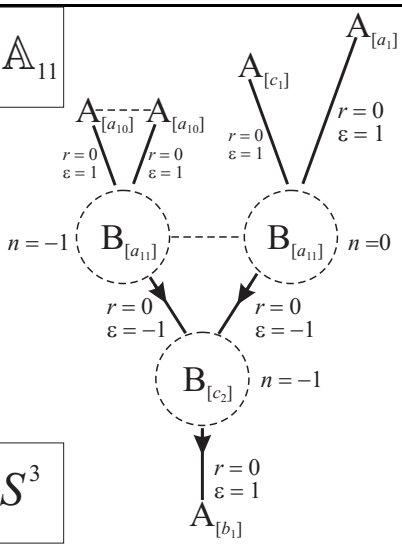	$\mathbb{A}_{12}$ 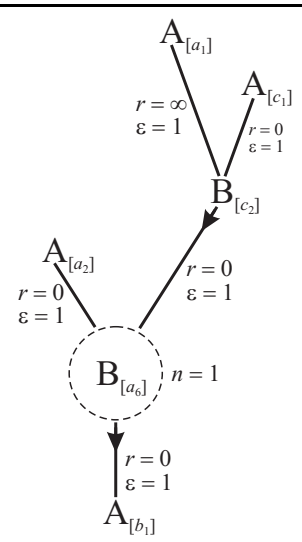
$\mathbb{A}_{13}$ 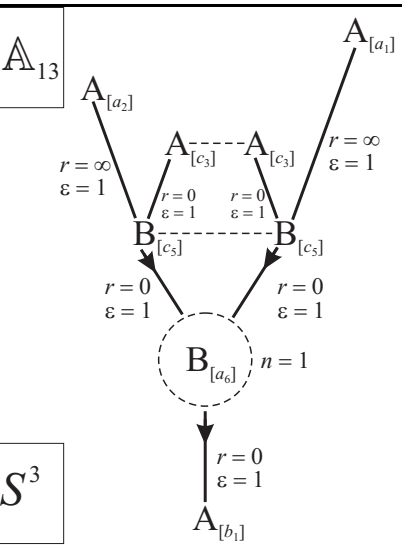	$\mathbb{B}_1$ 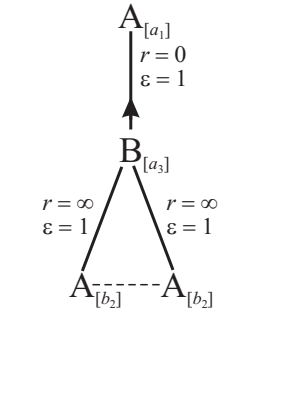

Table 8.5 (continued)

Marked isoenergetic molecule	Marked isoenergetic molecule
$\mathbb{B}_2$ 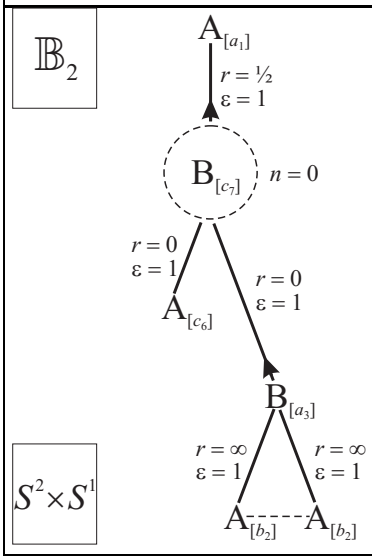 $S^2\times S^1$	$\mathbb{B}_3$ 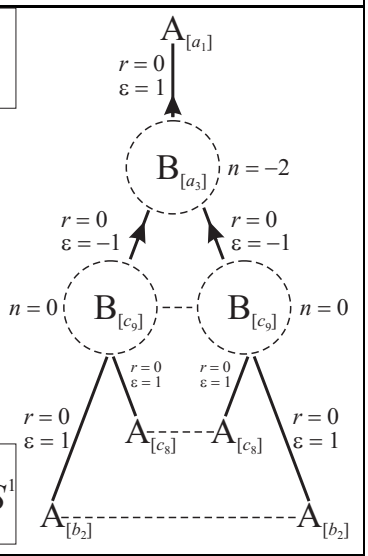 $S^2\times S^1$
$\mathbb{C}$ 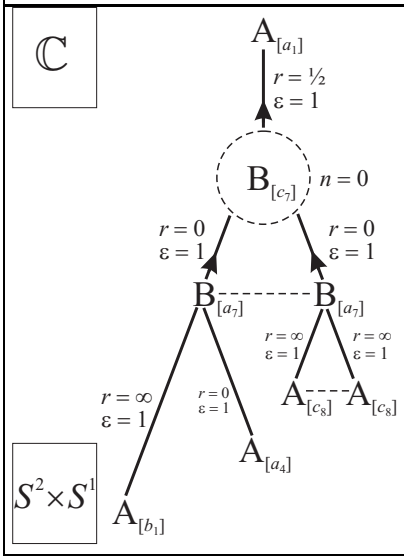 $S^2\times S^1$	$\mathbb{D}$ 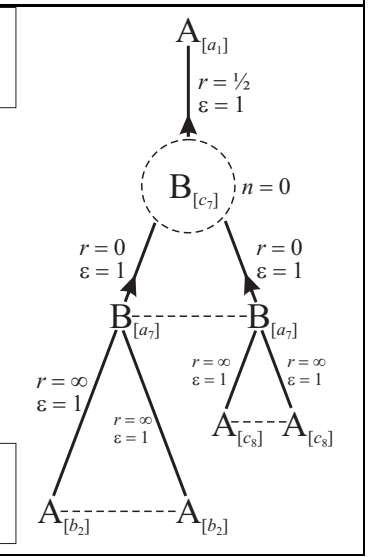 K^3

Table 8.5 (continued)

Marked isoenergetic molecule	Marked isoenergetic molecule
$\mathbb{E}_1$ 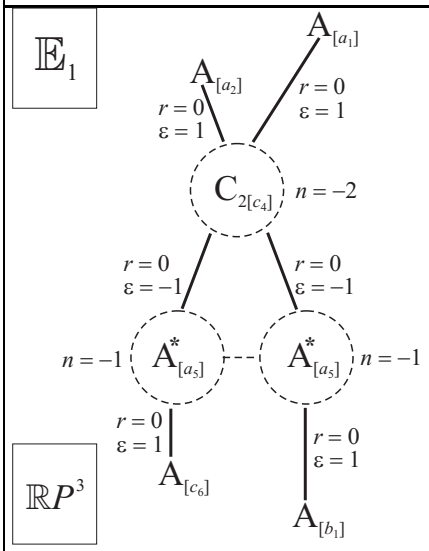 $\mathbb{R}P^3$	$\mathbb{E}_2$ 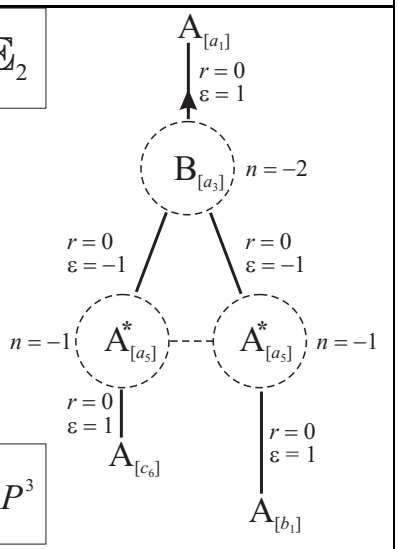 $\mathbb{R}P^3$
$\mathbb{E}_3$ 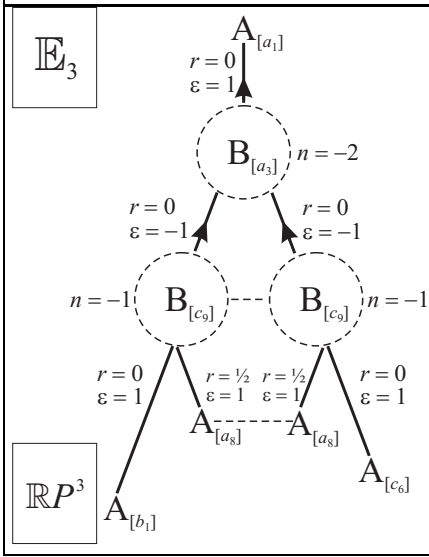 $\mathbb{R}P^3$	$\mathbb{E}_4$ 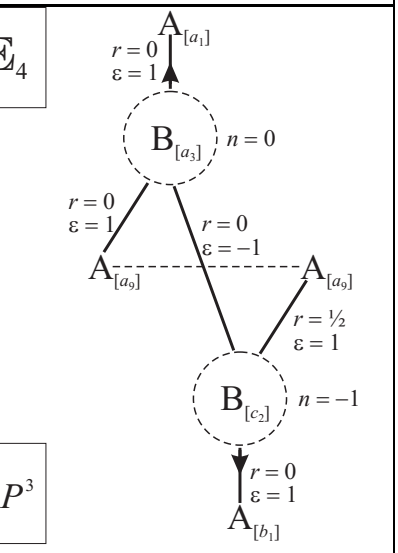 $\mathbb{R}P^3$

Table 8.5 (continued)

Marked isoenergetic molecule	Marked isoenergetic molecule
$\mathbb{E}_5$ 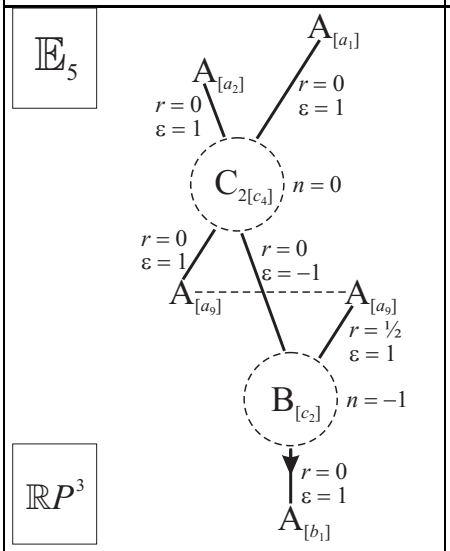 $\mathbb{R}P^3$	$\mathbb{E}_6$ 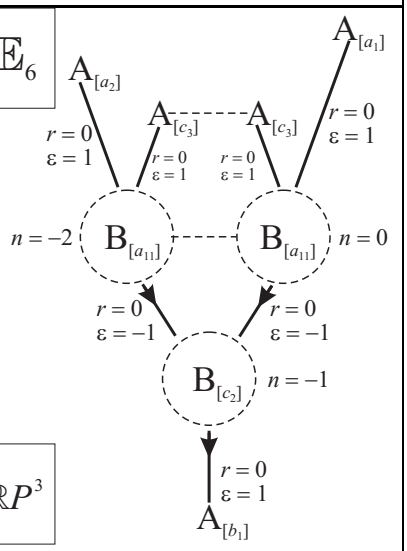 $\mathbb{R}P^3$
$\mathbb{F}$ 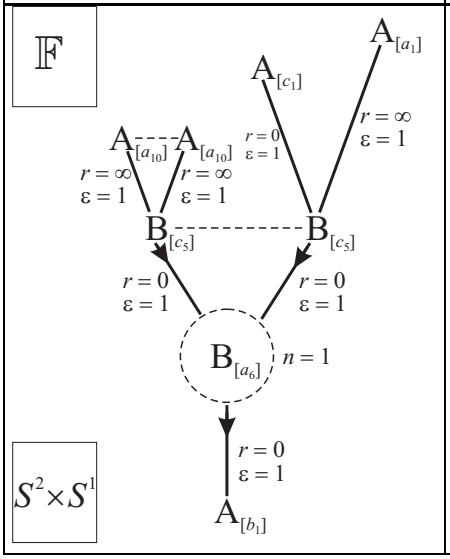 $S^2\times S^1$	$\mathbb{G}$ 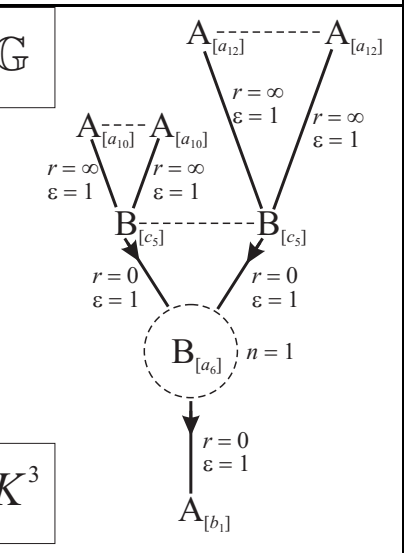 K^3

Table 8.5 (continued)

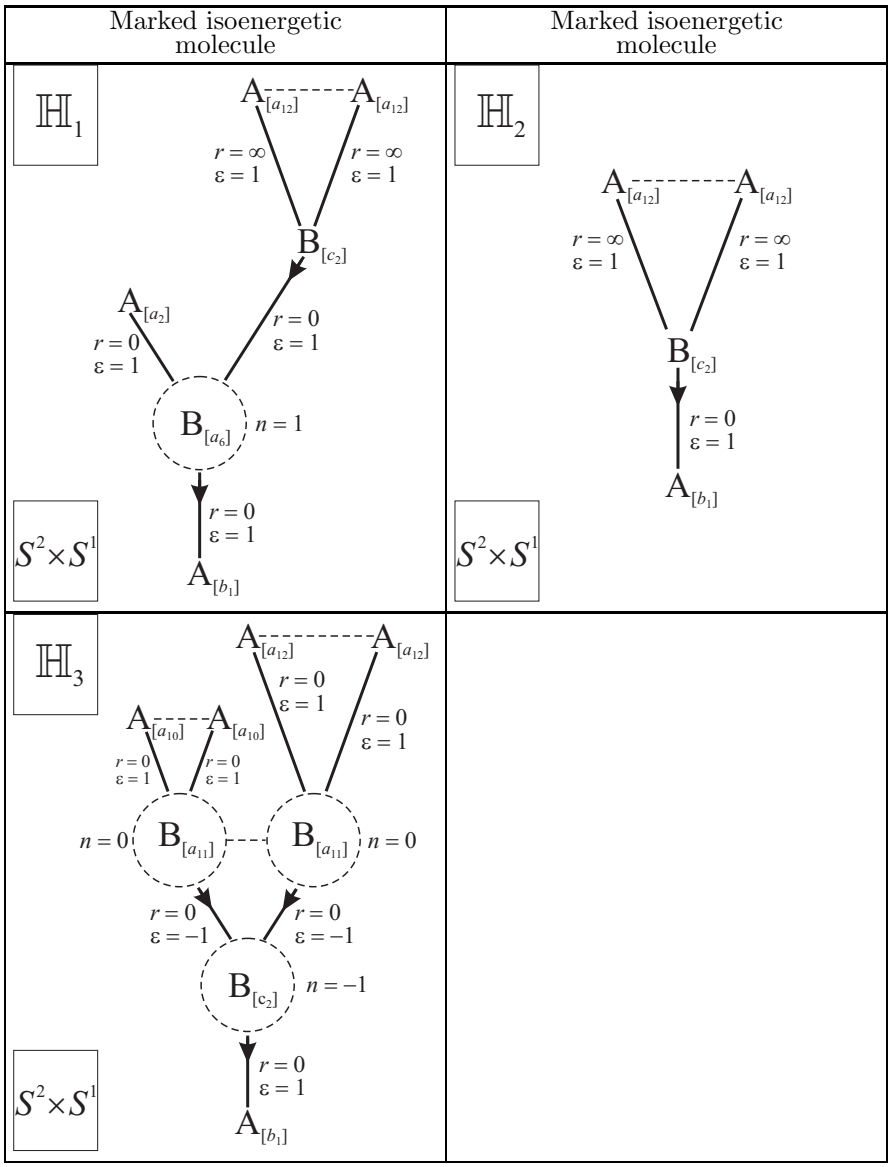

9. Conclusion

The study of the phase topology of the Kovalevskaya–Yehia case is complete. We have presented all results available today on analytical solutions and topological analysis of the Kovalevskaya–Yehia case. As was noted above, this work can be extended by a description of limit cases, namely, of the classical Kovalevskaya problem and a gyrostat with zero area constant. Here these results are assumed to be known and are used in the construction of fine topological invariants. The title of this paper contains the words "topological atlas"; we do not give any strict mathematical sense to this term. The authors want to emphasize that all objects studied are classified in the spaces of the corresponding parameters; separating sets and stability domains are constructed; the results of these studies resemble geographical atlases. We did not give a detailed explanation of the general theory

of integrable Hamiltonian systems (except for the very minimum necessary for definitions), since the volume of this work would substantially increase.

REFERENCES

1. V. M. Alekseev, V. M. Tikhomirov, and S. V. Fomin, *Optimal Control* [in Russian], Nauka, Moscow (1979).
2. P. P. Andreyanov and K. E. Dushin, "An approach to the study of bifurcation sets in the Kovalevskaya–Yehia problem," in: *Proc. XI Int. Conf. "Stability, Control, and Dynamics of Rigid Bodis," Donetsk* (2011), pp. 11–12.
3. P. P. Andreyanov and K. E. Dushin, "Bifurcation sets in the Kovalevskaya–Yehia problem," *Mat. Sb.*, **203**, No. 4, 3-46 (2012).
4. G. G. Appelrot, "Incompletely symmetric heavy gyroscopes," in: *Motion of a Rigid Body around a Fixed Point*, Moscow–Leningrad (1940), pp. 61–156.
5. O. I. Bogoyavlensky, "Integrable Euler equations on Lie algebras arising in problems of mathematical physics," *Izv. Akad. Nauk SSSR, Ser. Mat.*, **48**, No. 5, 883–938 (1984).
6. A. V. Bolsinov, S. V. Matveev, and A. T. Fomenko, "Topological classification of integrable Hamiltonian systems with two degrees of freedom. List of systems of low complexity," *Usp. Mat. Nauk*, **45**, No. 2 (272), 49–77 (1990).
7. A. V. Bolsinov, P. Richter, and A. T. Fomenko, "Method of loop molecules and topology of the Kovalevskaya top," *Mat. Sb.*, **191**, No. 2, 3–42 (2000).
8. A. V. Bolsinov and A. T. Fomenko, *Integrable Hamiltonian Systems. Geometry, Topology, Classification* [in Russian], Vols. 1, 2, Izhevsk (1999).
9. A. V. Borisov and I. S. Mamaev, *Modern Methods of the Theory of Integrable Systems* [in Russian], Regular and Chaotic Dynamics, Izhevsk (2003).
10. A. V. Borisov and I. S. Mamaev, *Dynamics of Rigid Bodies. Hamiltonian Methods, Integrability, Chaos* [in Russian], Regular and Chaotic Dynamics, Izhevsk (2005).
11. I. N. Gashenenko, "A new class of motions of a heavy gyrostat," *Dokl. Akad. Nauk SSSR*, **318**, No. 1, 66–68 (1991).
12. I. N. Gashenenko, "A new integrable case of equations of motion of a gyrostat," *Mekh. Tverd. Tela*, **24**, 1–4 (1992).
13. I. N. Gashenenko, "Bifurcation set in the problem of the motion of a gyrostat under the Kovalevskaya conditions," *Mekh. Tverd. Tela*, **27**, 31–35 (1995).
14. I. N. Gashenenko, "Integral manifolds and topological invariants of a case of the motion of a gyrostat," *Mekh. Tverd. Tela*, **29**, 1–7 (1997).
15. I. N. Gashenenko, "Bifurcation set in the problem of the motion of a heavy gyrostat under the Kovalevskaya conditions," *Dopov. Nats. Akad. Nauk Ukr.*, **2**, 60–62 (1997).
16. I. N. Gashenenko, *Invariant manifolds and sets of admissible velocities in the dynamics of a rigid body*, Doctoral thesis, Donetsk (2008).
17. A. F. Ipatov, "Motion of a Kovalevskaya gyrosrat on the boundary of an ultraelliptic domain," *Uch, Zap. Petrozavodsk. Univ.*, **18**, No. 2, 6–93 (1970).
18. N. S. Logacheva, "Classification of nondegenerate equilibria and degenerate one-dimensional orbits of an integrable Kovalevskaya–Yehia system," *Mat. Sb.*, **203**, No. 1, 31–60 (2012).
19. P. V. Morozov, "Topology of Liouville foliations in the Steklov and Sokolov integrable cases of the Kirchhoff equations," *Mat. Sb.*, **195**, No. 3, 69–114 (2004).
20. P. V. Morozov, "Calculation of the Fomenko-Zieschang invariants in the Kovalevkaya–Yehia integrable case," *Mat. Sb.*, **198**, No. 8, 59–82 (2007).
21. P. V. Morozov, "Fine Liouville classification of the Kovalevskaya–Yehia integrable case," *Vestn. Mosk. Univ. Ser. 1*, **2**, 11–19 (2008).
22. A. Y. Moskvin, "Topology of the Liouville foliation of the Dullin–Matveev integrable case on a two-dimensional sphere," *Mat. Sb.*, **199**, No. 3, 95–132 (2008).

23. A. A. Oshemkov, "Calculation of Fomenko invariants for the main integrable cases of the rigid-body dynamics," *Tr. Sem. Vect. Tenz. Anal.*, **25**, No. 2, 23–109 (1993).
24. A. G. Reiman and M. A. Semenov-Tyan-Shansky, "The Lax representation with a spectral parameter for the Kovalevskaya top and its generalizations," *Funkts. Anal. Prilozh.*, **22**, No. 2, 87–88 (1988).
25. P. E. Ryabov, *Some cases of degeneration of variables in one problem on the motion of a rigid body about a fixed point* [in Russian], deposited at the All-Russian Institute for Scientific and technical Information (VINITI), No. 3660-V91 (1991).
26. P. E. Ryabov, "On the calculation of bifurcation sets in the Kovalevskaya–Yehia case," *Mekh. Tverd. Tela*, **27**, 36–40 (1995).
27. P. E. Ryabov, "Bifurcation sets in the problem on the motion of a rigid body about a fixed point," *Vestn. Volgogradsk. Univ.*, **1**, 41–49 (1996).
28. P. E. Ryabov, *Surgeries of the bifurcation set in the generalized Kovalevskaya problem* [in Russian], deposited at the All-Russian Institute for Scientific and technical Information (VINITI), No. 884-B96 (1996).
29. P. E. Ryabov, *Bifurcation sets in the problem on the motion of a rigid body about a fixed point in the Kovalevskaya–Yehia case* [in Russian], thesis, Moscow State Univ. (1997).
30. P. E. Ryabov, "An analytic classification of singularities in the integrable Kovalevskaya–Yehia case," *Vestn. Udmurt. Univ., Ser. Mat. Mekh. Komput. Nauki*, **4**, 25–30 (2010).
31. A. Yu. Savushkin, I. I. Kharlamova, and E. G. Shvedov, "Electronic atlas of isoenergetic diagrams of the Kovalevskaya–Yehia gyrostat," *Izv. Volgogradsk. Tekh. Univ.*, **15** (102), 30–35 (2012).
32. N. S. Slavina, "Topological classification of systems of the Kovalevskaya–Yehia type," *Mat. Sb.*, **205**, No. 1, 105–160 (2014).
33. V. V. Sokolov and A. V. Tsyganov, "Lax pairs for deformed Kovalevskaya and Goryachev–Chaplygin tops," *Teor. Mat. Fiz.*, **131**, No. 1, 118–125 (2002).
34. P. Zh. Topalov, "Calculation of the fine Fomenko–Zieschang invariants for the main integrable cases of the motion of a rigid body," *Mat. Sb.*, **187**, No. 3, 143–160 (1996).
35. A. T. Fomenko amd H. Zieschang, "A topological invariant and an equivalence criterion for integrable Hamiltonian systems with two degrees of freedom," *Izv. Akad. Nauk SSSR, Ser. Mat.*, **54**, No. 3, 546–575 (1990).
36. P. V. Kharlamov, *Lectures In Dynamics od Rigid Bodies* [in Russian], Novosibirsk State Univ. (1965).
37. P. V. Kharlamov, "On a case of integrability of the equations of motion of a rigid body with a fixed point," *Mekh. Tverd. Tela*, **3**, 57–64 (1971).
38. M. P. Kharlamov, "Topological analysis of classical integrable systems in rigid-body dynamics," *Dokl. Akad. Nauk SSSR*, **273**, No. 6, 1322–1325 (1983).
39. M. P. Kharlamov, "Bifurcation of common levels of first integrals in the Kovalevskaya case," *Prikl. Mat. Mekh.*, **47**, No. 6, 922–930 (1983).
40. M. P. Kharlamov, *Topological Analysis of Classical Integrable Systems in Rigid Body Dynamics* [in Russian], Leningrad (1988).
41. M. P. Kharlamov, "Critical subsystems of the Kovalevskaya gyrostat in two constant fields," *Nonlin. Dynam.*, **3**, No. 3, 331–348 (2007).
42. M. P. Kharlamov, "Topological analysis and Boolean functions, I. Methods and application to classical systems," *Nonlin. Dynam.*, **6**, No. 4, 769–805 (2010).
43. M. P. Kharlamov, "Isoenergetic foliation of integrable systems with three degrees of freedom," in: *Modern Methods in the Theory of Boundary-Value Problems* [in Russian], Proc. Voronezh. Spring Math. School "Pontryagin Readings–XXII, Voronezh State Univ. (2011), pp. 199–200.
44. M. P. Kharlamov, "Analytic classification of uniform rotations of the Kovalevskaya–Yehia gyrostat," *Mekh. Tverd. Tela*, **42**, 47–61 (2012); `http://arxiv.org/abs/1310.0589`.

45. M. P. Kharlamov, "A complete topological atlas of integrable system with two or three degrees of freedom," in: *Modern Methods in the Theory of Boundary-Value Pproblems* [in Russian], Proc. Voronezh. Spring Math. School "Pontryagin Readings–XXIV," Voronezh State Univ. (2013), pp. 210-211; http://dx.doi.org/10.13140/RG.2.1.1119.6009.
46. M. P. Kharlamov and P. E. Ryabov, "Bifurcations of first integrals in the Kovalevskaya–Yehia case," *Regul. Khaot. Dinam.*, **2**, No. 2, 25–40 (1997).
47. M. P. Kharlamov and P. E. Ryabov, "Smale—Fomenko diagrams and rough invariants in the Kovalevskaya–Yehia case," *Vestn. Udmurt. Univ. Ser. Mat. Mekh. Komput. Nauki*, **4**, 40–59 (2011); http://arxiv.org/abs/1206.1413.
48. M. P. Kharlamov, E. I. Kharlamova, and E. G. Shvedov, "Bifurcation diagrams on isoenergetic levels of the Kovalevskaya–Yehia gyrostat," *Mekh. Tverd. Tela*, **40**, 77–90 (2010); http://arxiv.org/abs/1012.4071.
49. M. P. Kharlamov and E. G. Shvedov, "Bifurcation diagrams on isoenergetic levels of the Kovalevskaya top in a double field," *Mekh. Tverd. Tela*, **34**, 59–65 (2004).
50. I. I. Kharlamova and P. E. Ryabov, "Electronic atlas of bifurcation diagrams of the Kovalevskaya–Yehia gyrostat," *Vestn. Udmurt. Univ. Ser. Mat. Mekh. Komput. Nauki*, **2**, 147–162 (2011).
51. P. V. Kharlamov and E. I. Kharlamova, "A new solution of differential equations of motion of a body with a fixed point under the Kovalevskaya conditions," *Dokl. Akad. Nauk SSSR*, **189**, No. 5, 967–968 (1969).
52. A. V. Tsyganov, "Separation of variables in the Kovalevskaya–Goryachev–Chaplygin gyrostat," *Teor. Mat. Fiz.*, **135**, No. 2, 240–247 (2003).
53. C. Jacobi, *Lectures on Dynamics* [Russian translation], ONTI, Moscow–Leningrad (1936).
54. N. M. Yehia, "New integrable cases in the problem on the motion of a gyrostat," *Vestn. Mosk Univ. Ser. 1*, **4**, 88–90 (1987).
55. A. I. Bobenko, A. G. Reyman, and M. A. Semenov-Tyan-Shansky, "The Kowalewski top 99 years later: a Lax pair, generalizations, and explicit solutions," *Commun. Math. Phys.*, **122**, No. 2, 321–354(1989).
56. A. V. Bolsinov and V. S. Matveev, "Integrable Hamiltonian systems: Topological structure of saturated neighborhoods of nondegenerate singular points," in: *Tensor and Vector Analysis, Geometry, Mechanics, and Physics* [in Russian] (A. T. Fomenko et al., eds.), Gordon and Breach (1998), pp. 31–56.
57. H. R. Dullin, M. Juhnke, and P. H. Richter, "Action integrals and energy surfaces of the Kovalevskaya top," *Bifurcation Chaos*, **4**, 1535–1562 (1994).
58. H. R. Dullin and V. S. Matveev, "A new integrable system on the sphere," *Math. Res. Lett.*, **11**, Nos. 5-6, 715–722 (2004).
59. L. N. Gavrilov, "On the geometry of Gorjatchev–Tchaplygin top," *C. R. Acad. Bulg. Sci.*, **40**, 33–36 (1987).
60. A. Jacob, "Invariant manifolds in the motion of a rigid body about a fixed point," *Rev. Roum. Math. Pures Appl.*, **16**, No. 10, 1497–1521 (1971).
61. M. P. Kharlamov, "Bifurcation diagrams of the Kowalevski top in two constant fields," *Reg. Chaot. Dynam.*, **10**, No. 4, 381–398 (2005); http://arxiv.org/abs/0803.0893; http://dx.doi.org/10.1070/RD2005v010n04ABEH000321.
62. M. P. Kharlamov, "Extensions of the Appelrot classes for the generalized gyrostat in a double force field," *Reg. Chaot. Dynam.*, **19**, No. 2, 226–244 (2014); http://arxiv.org/abs/1312.5184; http://dx.doi.org/10.1134/S1560354714020063.
63. M. P. Kharlamov, "Phase topology of one system with separated variables and singularities of the symplectic structure," *J. Geom. Phys.*, **87**, 248–265 (2015); http://arxiv.org/abs/1312.5184; http://dx.doi.org/10.1016/j.geomphys.2014.07.004.
64. I. V. Komarov, "A generalization of the Kovalevskaya top," *Phys. Lett.*, **123**, No. 1, 14–15 (1987).

65. V. B. Kuznetsov, "Simultaneous separation for the Kowalevski and Goryachev–Chaplygin gyrostats," *J. Phys. A: Math. Gen.*, **35**, 6419–6430 (2002).
66. M. Radnović and V. Rom-Kedar, "Foliations of isoenergy surfaces and singularities of curves," *Reg. Chaot. Dynam.*, **13**, No. 6, 645–668 (2008).
67. P. H. Richter, H. R. Dullin, and A. Wittek, "Kovalevskaya top. Film C1961," *Publ. Wiss. Film., Sekt. Tech. Wiss./Naturwiss.*, No. 13, 33–96 (1997).
68. S. Smale, "Topology and mechanics," *Invent. Math.*, **10**, No. 4, 305–331 (1970).
69. H. M. Yehia, "New integrable cases in the dynamics of rigid bodies," *Mech. Res. Commun.*, **13**, No. 3, 169–172 (1986).
70. H. M. Yehia, "On certain two-dimensional conservative mechanical systems with a cubic second integral," *J. Phys. A: Math. Gen.*, **35**, 9469–9487 (2002).

M. P. Kharlamov
Russian Presidential Academy of National Economy
and Public Administration, Volgograd Branch, Volgograd, Russia
E-mail: mharlamov@vags.ru
P. E. Ryabov
Financial University under the Government of the Russian Federation, Moscow, Russia
E-mail: orelryabov@mail.ru
I. I. Kharlamova
Russian Presidential Academy of National Economy
and Public Administration, Volgograd Branch, Volgograd, Russia
E-mail: irinah@vags.ru